4/4/91

Indian J Chem

APRIL 1991

CODEN : IJOCAP 30A(4) 301-390 (1991)
ISSN : 0019-5103

वैज्ञानिक तथा औद्योगिक अनुसंधान परिषद का पुस्तकालय
SCIENTIFIC & RESEARCH LIBRARY
Accession No.....
- 4 APR 1991
सी.एफ.टी.आर.आई. क्षेत्रीय केन्द्र
C.F.T.R.I. REGIONAL CENTRE, LUDHIANA

C.F.T.R.I. REGIONAL CENTRE
डायरी नं./DIARY No. 28
दिनांक/DATE 4/4/91
लुधियाना/LUDHIANA-141 006

Indian Journal of CHEMISTRY

SECTION A

Inorganic, Bio-inorganic, Physical, Theoretical & Analytical Chemistry

Published by
PUBLICATIONS & INFORMATION DIRECTORATE, CSIR, NEW DELHI
in association with
THE INDIAN NATIONAL SCIENCE ACADEMY, NEW DELHI

AUTHOR INDEX

Aly A A M 379
Athappan P R 357

Banerjea D 347
Beg Mohd N 335

Chauhan R S 387

Das Asim K 347
Das M L 328
Dhas T Peter Amala 340

Garai S 375
Garg A N 350
Gupta A R 313
Gupta Y K 340

Inamdar Neeta C 313
Indrasenan P 382

Jangida B L 322

Kakkar L R 387
Kakkar Rita 308

Lanjewar R B 350

Mishra Dilip K 340
Mittal R K 340
Moulik S P 328
Mukherjee D C 328

Natarajan C 357

Osman A H 379

Paul B K 328
Pradhan Guru C 301

Raghava Naidu R 363
Raju J R 369
Ram Reddy M G 385

Sambrani M I 369
Sanyal G S 375
Sarala Devi Ch 385
Sarojini K R 382
Sarpal S K 313
Sheela C D 357
Siddiqi Fasih A 335
Singh Surendra P 335
Sreedhar Naidu G 363
Sundaresan M 322
Syamal A 390

Toteja R S D 322

Uzoukwu Bieluonwu Augustus 372

Venkata Ramana Reddy Ch 385

Walia Vibha 308

Indian Journal of Chemistry

Sect. A: Inorganic, Bio-inorganic, Physical, Theoretical & Analytical

VOL. 30A NUMBER 4 APRIL 1991

वैज्ञानिक तथा औद्यो... SCIENTIFIC & RESEARCH LIBRARY
- 4 APR 1991
C.S.I.R. T.R.L. REGIONAL CENTRE, LUDHIANA

CONTENTS

Symmetry consideration for the interpretation of isomeric product distribution in spontaneous aquation of octahedral cobalt(III) complexes 301
Guru C Pradhan

Methyl nitrene: Thermochemistry and kinetics of its rearrangement to methyleneimine . 308
Rita Kakkar* & Vibha Walia

Effect of temperature on hydrogen isotope effects in dehydration of ion-exchange resins: Alkali metal ionic (Li^+, K^+ and Cs^+) forms of Dowex-50W resins. 313
Neeta C Inamdar, S K Sarpal* & A R Gupta

Changes in thermodynamic parameters in the exchange of alkaline earth metals with sodium ions in Dowex-50WX8 and Amberlyst-15 resins in aqueous medium. 322
R S D Toteja, B L Jangida* & M Sundaresan

Phase behaviour and physicochemical properties of a microemulsion obtained from an edible oil (saffola) 328
B K Paul, M L Das, D C Mukherjee & S P Moulik*

Studies of L-α-phosphatidylcholine impregnated parchment paper model membrane . . 335
Fasih A Siddiqi*, Mohd N Beg & Surendra P Singh

Effect of iron(II), cerium(IV) and manganese(III) in the reaction between thallium(III) and hydrogen peroxide in aqueous perchloric acid 340
T Peter Amala Dhas, Dilip K Mishra, R K Mittal & Y K Gupta*

Kinetics and mechanism of dissociation of di-(2-pyridyl)amine complexes of copper(II), nickel(II) and cobalt(II) in aqueous acid media 347
Asim K Das & D Banerjea*

Synthesis, Mössbauer, infrared spectroscopic and thermal decomposition studies of some iron(III) carboxylate complexes. 350
R B Lanjewar & A N Garg*

Multidentate behaviour of 2-formylcyclohexanone schiff bases in the Co(II), Ni(II), Cu(II) and Zn(II) complexes 357
C Natarajan*, C D Sheela & P R Ahappan

Formation constants of Mn(II), Cu(II), Co(II), Zn(II), Fe(II), Ni(II) and Pd(II) complexes of peonolphenylhydrazone 363
G Sreedhar Naidu & R Raghava Naidu*

Notes

Osmium(VIII) mediated vanadium(V) oxidation of arsenic(III) in aqueous sulphuric acid. 369
M I Sambrani & J R Raju*

Continued overleaf

Physicochemical studies of 4-trifluoroacetyl and 4-trichloroacetyl derivatives of 3-methyl-1-phenylpyrazol-5-one and their U(VI), Fe(III) and Ca(II) complexes 372
Bieluonwu Augustus Uzoukwu

Studies on cobalt(II), nickel(II), copper(II) and zinc(II) complexes with glyoxal bis(2-pyrazinoyl hydrazone) 375
G S Sanyal* & S Garai

Reactions of dithizone with transition metal complexes of acetylacetone and oxine . . . 379
A A M Aly* & A H Osman

Some lanthanide(III) nitrate complexes of N-(4′-benzoylidene-3′-methyl-1′-phenylpyrazol-5′-one)isonicotinylhydrazine 382
P Indrasenan* & K R Sarojini

Formation constants of binary and ternary complexes of Cu(II) with ninhydrin and some O,O; N,O and N,N donor ligands in aqueous medium 385
Ch Venkata Ramana Reddy, Ch Sarala Devi & M G Ram Reddy*

An extractive spectrophotometric method for the determination of vanadium as V(II)-8-hydroxyquinoline complex into acetylacetone-chloroform 387
R S Chauhan & L R Kakkar*

Letter to the Editor

Comments on the paper "Synthesis and characterisation of model compounds: Part II – Complexes of iron(II), iron(III), cobalt(II), cobalt(III), nickel(II) and copper(II) with *o*-vanillin oxime 390
A Syamal

Authors for correspondence are indicated by (*)

Indian Journal of Chemistry
Vol. 30A, April 1991, pp. 301-307

Symmetry consideration for the interpretation of isomeric product distribution in spontaneous aquation of octahedral cobalt(III) complexes

Guru C Pradhan

Department of Chemistry, Utkal University, Bhubaneswar 751 004

Received 16 July 1990; accepted 15 November 1990

The stereochemical changes involved in the aquation of octahedral cobalt(III) complexes $[(N_4)Co(A)X]^{n+}$, where X is a leaving group, are related to the stereomobility of the transition state and/or the intermediate generated in the dissociative mode of reaction of the parent substrate. An attempt is made to explain the relative isomer distribution in the products of spontaneous aquation of such complexes applying a recently developed symmetry selection rule.

The octahedral cobalt(III) complexes are believed to undergo aquation via dissociative mode of activation[1] generating intermediates of reduced coordination number. Product distribution studies[2,3] in several such reactions, however, have indicated that there can be more than one intermediate in such reactions. Hence it is likely that the intermediate(s) can undergo isomerisation to give isomeric products.

Recently Schipper and Rodger[4] developed a symmetry selection scheme for spectroscopic processes which they have also extended to reaction mechanism[5]. The first stage of this scheme is called the classical selection rule (CSR) which they have applied to certain inversion reactions and metal ligand isomerisation[6].

In this paper we intend to apply the CSR procedure to these intermediates to provide an explanation of isomeric product distribution in the aquation of $[(N_4)M(A)X]^{n+}$ complex where M = cobalt(III), N_4 = the amine ligands (either monodentate or polydentate), A = an inert ligand (amine, aquo or anion) and X is the leaving group.

Stereochemical aquation of $[(N_4)CoAX]^{n+}$

The products of stereochemical aquation (both spontaneous and induced) of $[(N_4)Co^{III}AX]^{n+}$ have been reviewed in literature[7,8]. Presently the discussion is restricted to the stereochemical product distribution in the aquation of complexes $[Co(NH_3)_4AX]^{n+}$, $[Co(en)_2AX]^{n+}$ and $[Co(trien)AX]^{n+}$ by applying the CSR method. Extensive data are available on the stereochemical product distribution in the aquation for $[Co(en)_2AX]^{n+}$; however, those on $[Co(NH_3)_4AX]^{n+}$ and $[Co(trien)AX]^{n+}$ are rather scanty. Some selected experimental data on aquation of *cis* and *trans* complexes of the type mentioned above are collected in Table 1. It is usually observed that both *trans* and *cis* isomers on aquation yield a mixture of *cis* and *trans* aquo products, *trans* complexes yielding more of *trans* aquo product and the *cis* complexes yielding more of *cis* aquo products. The very fact that a given aquation reaction leads to the formation of isomeric products in more or less definite ratio suggests that the reaction must be stereomobile at least at the stage of formation of possible intermediate. Table 1 shows that the experimental product ratio is largely independent of the nature of the leaving group X and indicates that dissociation of X is well advanced towards penta coordination in the transition state. The dissociation of the complex may be spontaneous, induced or solvent assisted. Specific solvent effects have also been dealt with in several cases[18]. The role of π-bonding in dissociation mechanism to explain the complete stereoretent *cis* products has been discussed at length by Basolo and Pearson[19]. More recently the role of hetero ligand A in the isomeric product distribution in aquation of $[Co(en)_2AX]^{n+}$ has been discussed on the basis of ligand field calculations by Vanquickenborne and Pierloot[20]. The role of spin change acompanying a stereomobile reaction[21] is also dealt by the same authors. We intend to examine whether the symmetry considerations can provide certain guidelines in predicting the actual course of the stereomobile intermediate thus leading to a definite product distribution.

Reaction path in dissociation process

In a purely dissociative mechanism the five coordinated intermediate (*loc cit*) is likely to be a square pyramid (SP) if the dissociation process is not accompanied by simultaneous distortion. A stereore-

tent product would result if the square pyramid acquires a solvent molecule (H_2O) without further rearrangement. The square pyramid is more likely to rearrange to a trigonal bipyramid (TBP) as it involves no bond rupture and least amount of distortion. Such a rearrangement is in conformity with Pearson's concept of "least motion path"[22]. Thus the overall nonconcerted aquation process may be visualised to be consisting of the following three or four steps, each step being individually assumed to be concerted.

(i) Dissociation of hexacoordinated complex to generate a square pyramid

(ii) Rearrangement of square pyramid to trigonal bipyramid

(iii) Rearrangement of trigonal bipyramid to a more suitable square pyramid (if possible)

(iv) Acquisition of solvent molecule by the intermediates trigonal bipyramid/square pyramid to generate aquo products.

The most important steps which govern the production of isomeric products are the stereomobile steps (ii) and/or (iii). Depending upon the structure of the parent substrate the square pyramid and trigonal bipyramid intermediates may be regular or distorted and accordingly belong to different point symmetries. The CSR procedure may then be applied to the stereomobile step(s) to examine whether such step(s) (ii and iii) leading to isomeric progenies are allowed.

Application of CSR to aquation of $[(N_4)Co^{III}AX]^{n+}$

(a) $[Co(NH_3)_4AX]^{n+}$ $(A \neq NH_3)$

This complex exists as *cis* and *trans* isomers. The aquation of either of the complexes produces a mixture of isomeric *cis* and *trans* aquo products in varying proportions, (see Table 1). The aquation routes of each of the isomers can be traced as detailed below.

(i) *trans*-$[Co(NH_3)_4AX]^{n+}$

The *trans* complex after dissociation produces the pentacoordinated square pyramid intermediate $[Co(NH_3)_4A]^{m+}$ with ligand A in axial position so that it belongs to C_{4v} symmetry. The intermediate can take up a solvent molecule to give the stereoretent *trans* aquo complex. Further the square pyram-

Table 1—Stereochemical data on the spontaneous aquation of *cis* and *trans*-$Co(N_4)AX^{n+}$ complexes

Complexes	% *trans*	% *cis*	Ref.
	cis-complexes		
Λ-$Co(en)_2(CN)Cl^+$	0	100	9
Λ-$Co(en)_2(NO_2)Cl^+$	0	100	10
Λ-$Co(en)_2(N_3)Cl^+$	14 ± 4	82 ± 3	3
Λ-$Co(en)_2(N_3)Br^+$	15 ± 1	85 ± 1	3
Λ-$Co(en)_2(OH)Cl^+$	16 ± 1	84.5 ± 1	3
Λ-$Co(en)_2(OH)Br^+$	15 ± 1	85 ± 1	3
Λ-$Co(en)_2Cl_2^+$	25 ± 1.5	75 ± 1.5	3
Λ-$Co(en)_2Br_2^+$	26.5 ± 1.5	70 ± 2	3
β-*cis*-$Co(trien)(H_2O)Cl^{2+}$ (slow isomer)	*		11
β-*cis*-$Co(trien)(H_2O)Cl^{2+}$ (fast isomer)			
	trans-complexes		
trans-$Co(NH_3)_4Cl_2^+$	45 ± 10	—	12
trans-$Co(NH_3)_4(NCS)Cl^+$	100	—	13
trans-$Co(NH_2)_4(NO)_2Cl^+$	100	—	13
trans-$Co(en)_2(CN)Cl^+$	—	0	14
trans-$Co(en)_2(CN)Br^+$	—	0	15
trans-$Co(en)_2(NH_3)Cl^{2+}$	—	0	16
trans-$Co(en)_2(NH_3)Br^{2+}$	—	0	16
trans-$Co(en)_2(N_3)Cl^+$	—	9 ± 2	17
trans-$Co(en)_2(N_3)Br^+$	—	9 ± 2	17

*Retention of configuration and optical activity.

id rearranges to trigonal bipyramid species as depicted in Fig. 1 (a and b) by the so called rearrangement "hetero-conversion". In this hetero-conversion structure **1** denotes the reactant (R) and **2** and **3** refer to products (P) and T denotes the transition state. The conserved symmetry elements along the reaction path are given by $G_R \cap G_P = G_{RP} = \{E; C_2(1,3)(2,4); \sigma(1,3); \sigma(2,4)\} = C_{2v}$ for product **2**.

(Note that $R = R(i, j)(k, l, m)\ldots$ denotes that by operation R the ligands within a bracket are exchanged in a cyclic manner, i.e. operation R exchanges ligand i by j, j by i, k by l, l by m, m by k, ... etc). Obviously the symmetry of the transition state (same as G_{RP} in a hetero-conversion) is C_{2v} which is eventually the symmetry of the product **2** and also the symmetry at the nonstationary points $q \neq R, T, P$. The symmetry of the reaction coordinate is B_1 in R and A in P, T and q and, therefore, the rearrangement is symmetry allowed. This particular hetero-conversion path is two-fold degeneracy related as two distinct equivalent trigonal bipyramids **2** and **3** can be obtained from the same square pyramid **1** as shown in Fig. 1. Each of the two trigonal bipyramid intermediates has two equivalent edges and one non-equivalent edge at its equatorial trigonal plane. The addition of solvent (H_2O) molecule to an equivalent edge produces a *cis*-aquo product and to non-equivalent edge produces a *trans*-aquo product relative to A. The actual amount of each isomeric product would, however, depend upon the relative energies, relative stabilities and lifetimes of the intermediates **1**, **2** and **3**.

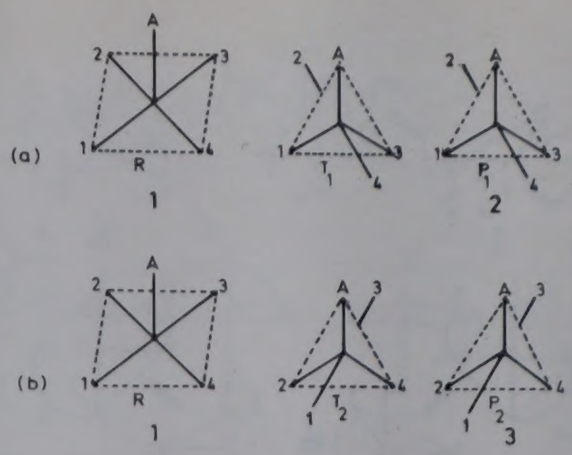

Fig. 1—R,T,P structures for square pyramid → trigonal bipyramid hetero-conversion of *trans*-$[Co(NH_3)_4A]^{m+}$ intermediates [symmetry specifications $C_{4v}(R)$, $C_{2v}(T_1, T_2, P_1$ and $P_2)$ and $C_{2v}(q)$]

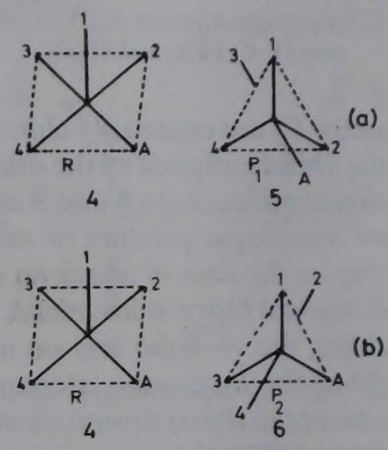

Fig. 2—R,P structure of the square pyramid → trigonal bipyramid hetero-conversion of *cis*-$[Co(NH_3)_4A]^{m+}$ intermediates [symmetry specification $C_s(R)$, $C_{3v}(P_1)$, $C_{2v}(P_2)$ and $C_s(q)$].

(ii) *cis*-$[Co(NH_3)_4AX]^{n+}$

The dissociation of X from the *cis*-complex generates a distorted square pyramid **4** with the ligand A situated at one of its basal vertices. The gross symmetry is C_s. The rearrangement of **4** to trigonal bipyramid would occur preserving the only $\sigma(2,4)$ present in the structure. Two types of non-equivalent trigonal bipyramid **5** (sym. C_{3v}) and **6** (sym. C_{2v}) are obtained as the products of the rearrangement (Fig. 2). In both the cases $G_{RP} = \{E; \sigma(2,4)\} = C_s = G_q = G_T = G_R$. The reaction coordinate is A' in R, T and q and E' in P (**5**) and B_1 in **6** and thus both the rearragements are symmetry allowed. The trigonal bipyramid **5** on aquisition of solvent molecule yields a totally *cis*-aquo product as all its equatorial edges on the trigonal plane are equivalent. The intermediate **6** can produce a mixture of *trans* and *cis* aquo isomers as is in the case of *trans* complex.

(b) (i) *trans*-$[Co(en)_2AX]^{n+}$

The complex $Co(en)_2AX^{n+}$ exists in total three isomeric forms i.e. one *trans* and two *cis* enantiomers. The *trans*-isomer has the gross symmetry of C_{2v} (while considering the symmetry, only the ethylenediamine skeleton is taken into consideration but not the indivisual C, H and N atoms). The two *cis*-enantiomers have no symmetry element and hence both belong to C_1. The dissociation of X leads to the formation of distorted square pyramids (Fig. 3); the *trans*-isomer producing **7** (symmetry, C_{2v}), one *cis*-isomer producing **10** and another **11** (both of symmetry C_1). The intermediate **7** can easily take up a solvent molecule prior to rearrangement to yield a stereoretent *trans*-aquo complex as the major product. It can also rearrange through a two-fold degeneracy related pathway into two distinctly equivalent approximate trigonal bipyramids **8** and **9**. This is the least motion possible to generate the trigonal bipyramids. For this hetero-conversion $G_{RP} = G_q = G_T = \{E; C_2(1,3)(2,4)\} = C_2 = G_P$.

The normal modes through which the rearrangement occurs are A_2 in **7** and A in both **8** and **9** and, therefore, the process is symmetry allowed. It is noteworthy that the trigonal bipyramids **8** and **9**

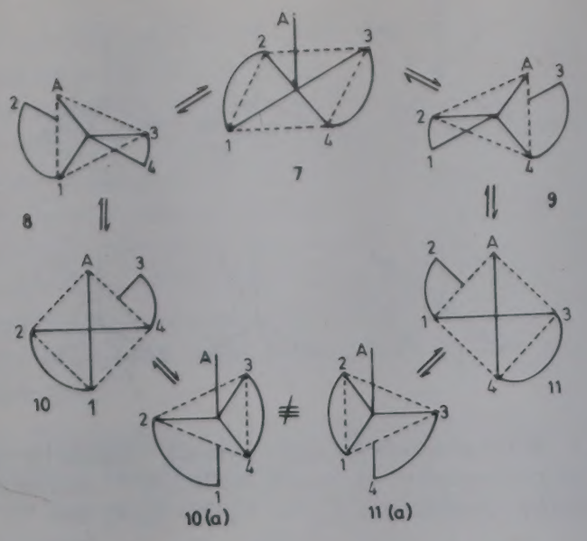

Fig. 3—Possible interconversions of intermediates of $[Co(en)_2A]^{m+}$ [symmetry specification C_{2v}(**7**) C_2 (**8** and **9**) C_1(**10** and **11**) C_s(**10(a)** and **11(a)**]

having symmetry C_2 are essentially chiral molecules and each is the chiral antipode of the other. The addition of a solvent molecule to **8** and **9** can generate a stereoretent *trans*-aquo product or *cis*-aquo product depending on the sites of attack on the equatorial planes of trigonal bipyramids; attack on equivalent sites yielding the *cis*-aquo and on non-equivalent sites yielding the *trans*-aquo (stereoretent) products. It is to be noted that only one *cis*-aquo isomer is obtained from either of the trigonal bipyramid **8** or **9** and both the *cis*-aquo isomers are mutual enantiomers of each other. If **8** and **9** are devoid of access to solvent addition[23] these can further rearrange into suitable square pyramids **10** and **11** (both of symmetry C_1) which are also chiral antipodes of each other. The rearrangements **8** → **10** and **9** → **11** may proceed via *B*-modes with the loss of C_2 axis in each case. The conversion **7** → **10** (or equivalent **7** → **11**) essentially becomes a two-step hetero-conversion with **7**, **8**, **10** (or equivalently **7**, **9**, **11**) as intermediates and is symmetry allowed. The resulting square pyramids **10** and **11** can now add up solvent molecules more conveniently to produce a pair of enantiomeric *cis*-aquo isomers leading to racemisation. Therefore, the complex *trans*-$[Co(en)_2AX]^{n+}$ on aquation via a dissociative interchange mechanism would yield a major stereoretent *trans*-product along with a racemic mixture of *cis*-product which is usually oberved.

(ii) *cis*-$[Co(en)_2AX]^{n+}$

The aquation of the *cis*-optical pairs via dissociative modes can be considered to begin with square pyramid intermediates **10** and **11** obtained from both the complexes. These can rearrange to trigonal bipyramids **8** and **9** (via *A*-modes) which on solvent addition generate the corresponding stereoretent *cis*-aquo products along with *trans*-aquo product. Again the original square pyramids **10** and **11** can add up solvent molecules to yield stereoretent product. Therefore, the stereoretent product would be the major one. The aquation of any of the enantiomers does not lead to optical inversion as can be seen from the following considerations. The skeletons **10** and **11** are interconvertible by a σ (representing the basal planes of both the square pyramids) which can be thought of as a product generating operation for the inversion (homo-conversion) of the species **10** and **11** (or their precursors) through a transition state **10(a)** or **11(a)**. The homo-conversion would be symmetry allowed provided the following two conditions are satisfied: (i) The structures **10(a)** and **11(a)** should represent a single transition state maximum and (ii) The product generating operation should be a point symmetry operation of the transition state. It may be noted that although the conversion **10** → **10(a)** or equivalently **11** → **11(a)** can be effected by an *A*-mode, the structures **10(a)** and **11(a)** are not identical. They are merely rotational isomers. Again the supposed product generating operation (σ) does not become a point symmetry operation of the assumed transition state as it is actually lost during the course of rearrangement instead a new $\sigma(1,2)(3,4)$ is generated. Therefore, the direct optical inversion is symmetry forbidden. The other indirect route for the inversion can be thought of via a multistep path (**10** → **8** → **7** → **9** → **11**). It has already been oberved that the conversions **8** → **10** and **9** → **11** are symmetry allowed. The intervening step of conversion **8** → **9** again corresponds to a chiral inversion (homo-conversion) since **8** and **9** are mutual chiral antipodes. Again the structures **8** and **9** are interconvertible by a point operation $\sigma(1,3)$ in **8** or $\sigma(2,4)$ in **9**. Therefore, the conversion can be thought of proceeding through **7**. This homo-conversion is symmetry allowed subject to the fact that the following conditions are satisfied: (i) Either $\sigma(1,3)$ or $\sigma(2,4)$ to become a product generating operation (combined with appropriate permutation operation) (a) must not be point-symmetry operation in **8** or **9** (b) must be a point symmetry stationary operation in **7** (ii) The structure **7** should then represent a transition state, i.e. it must correspond to a stationary point maxima on the potential energy surface. It can be seen that both the conditions (a) and (b) under (i) are clearly satisfied. Regarding condition (ii) the structure **7** actually corresponds to stationary minimum rather than a maximum since it is an intermediate obtained by the dissociation of *trans*-isomer. Therefore, the concerted homo-conversion **8** → **9** is forbidden. But this homo-conver-

sion may be thought of as a hetero-conversion consisting of two steps **8** → **7** and **7** → **9**; both steps being symmetry allowed as has been previously seen and in which case **7** need not be the transition maximum. Thus, summing up, we can presume that the overall indirect conversion **10** → **11** becomes a four step process (**10** → **8** → **7** → **9** → **11**). But the probability of occurrence of such a multistep process must be much less in comparison to direct aquation step. Nevertheless such an indirect multistep process may contribute to racemisation to a negligible extent. Clearly the rate of aquation is much larger than the rate of racemisation is consistent with the observation reported in the literature[3,24]. Therefore, we conclude that the aquation of either of the optical antipodes *cis*-$[Co(en)_2AX]^{n+}$ on aquation produces a major stereoretent *cis*-product, a lesser quantity (~5 to 35%) of inactive *trans*-aquo product accompanied by negligible quantity of racemic product.

(c) $[Co(trien)AX]^{n+}$

The trien complex is of still lower symmetry compared to the corresponding *bis*-ethylenediamine complex. Disregarding the stereochemistry at the secondary nitrogen atom of the trien ligand the complex will exist in a *trans*-form and three pairs of enantiomeric *cis*-forms (α, β_1 and β_2). The corresponding *trans*-isomer is well characterised for A=X=Cl. The *trans*-isomer has the only symmetry element σ and accordingly belongs to C_s. This *cis*-isomers are all chiral. The intermediates obtained after the dissociation of the leaving group X are square pyramids **12** for *trans*; **15** and **17** for *cis*-β_2, **16**, **18** for *cis*-β_1 and **19** and its minor image (not shown) for *cis*-α (see Fig. 4). The possible inter conversions, of square pyramid and trigonal bipyramid intermediates derived from possible isomers of trien complexes are shown in Fig. 4.

(i) *Trans*-$[Co(trien)AX]^{n+}$

The intermediate **12** (of the initial dissociation step of *trans*-isomer) can rearrange into chiral trigonal bipyramid antipodes **13** and **14** via two different *A*-modes. The access to solvent of **13** and **14** is further restricted as compared to that of the corresponding *bis*-ethylenediamine trigonal bipyramid intermediates because of extensive chelation. Therefore, the intermediate square pyramid **12** should preferentially in the initial state aquire a solvent molecule to yield a stereoretent *trans*-aquo complex as the major product. Again the intermediate **13** can further rearrange to square pyramids **15** and **16** and similarly **14** to **17** and **18** via different A-modes, which then add up solvent molecules to yield *cis*-aquo product β_1 and β_2. It is to be noted

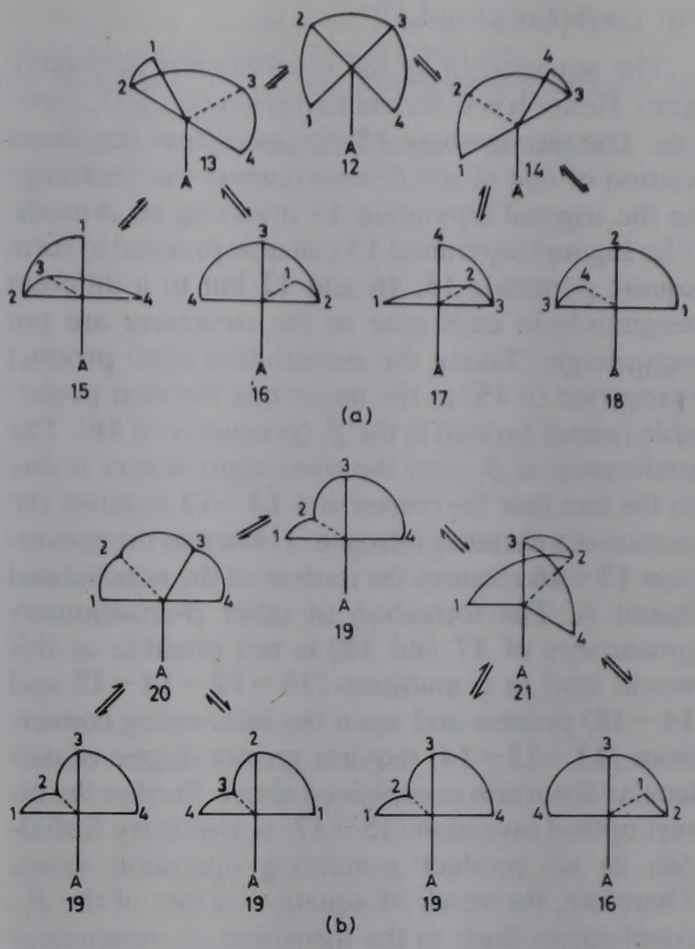

Fig. 4—Possible interconversion of some intermediates of $[Co(trien)A]^{m+}$ [symmetry specifications C_s(**12**) C_1(**13** to **19**, **21**) and C_2(**20**)]

that the conversions **13** → **15** and **14** → **17** leading to the formation of β_1 enantiomer pair are equienergic and require lesser distortion in the molecular frame than the equienergic conversions **13** → **16** and **14** → **18** forming β_2 enantiomer pair. This is because the former conversions require a larger displacement of the ligand A relative to chelated nitrogen(1). As a result, the formation of β_1 is expected to be favoured over β_2. Therefore, the aquation of the *trans* isomer is anticipated to yield a stereoretent *trans*-aquo product along with racemic *cis*-β_1 and racemic *cis*-β_2-aquo products where β_1 is predominated over β_2. The formation of β_1-aquo product in major proportion is consistent with the observation recorded in the aquation of *trans*-$[Co(trien)Cl_2]^+$ (ref. 25). However, experimentally the formation of *trans*-$[Co(trien)(OH_2)Cl]^{2+}$ has not been observed. This has been attributed to the associative interchange (S_N2) mode of aquation operating in this *trans*-dichlorocomplex[26]. However, Hg^{2+} induced aquation of *trans*-$[Co(trien)Cl_2]^+$ led predominantly to the formation of the *trans*-aquo product through formation of a penta-coordinated intermediate[27-29]

(ii) *cis*-β-$[Co(trien)AX]^{n+}$

The aquation of all the *cis*-β-isomers are analogous. Hence it is sufficient to discuss one such example. The intermediate **15** obtained from the dissociation of one of the β_1-enantiomers can rearrange to the trigonal bipyramid **13** involving an *A*-mode. The trigonal bipyramid **13** can now proceed to form square pyramids **15**, **16** and **12** but to a different magnitude in each case as the structures are not equienergic. Taking the stereoretent aquo product (precursor of **15**) as the major one the next preferable isomer formed is the β_2 (precursor of **16**). The preference of β_2 over the *trans*-aquo isomer is due to the fact that the conversion **13** → **12** requires the motion of a chelating nitrogen (1) whereas the conversion **13** → **16** requires the motion of the nonchelated ligand A. The formation of other β-enantiomers (precursors of **17** and **18**) is not possible as this would lead to a multistep (**15** → **12** → **14** → **17** and **14** → **18**) process and again the intervening conversions (**13** → **12** → **14**) requires greater degree of molecular distortion as explained above. Further the direct optical inversion (**15** → **17**) is symmetry forbidden as no product generating operation exists. Therefore, the result of aquation of one of the β_1-enantiomers leads to the formation of stereoretent β_1-aquo product (major product), β_2-aquo product (without inversion) and negligible quantity of inactive *trans*-aquo product. It is noteworthy to mention that β_1-dichloro ion on aquation gives 96% β_1 and 4% of β_2-chloro aquo product. The absence of *trans*-aquo product is consistent with this prediction[30]. The aquation of other β-isomers can be viewed in an analogous manner from Fig. 4(a).

(iii) *cis*-α-$[Co(trien)AX]^{n+}$

The aquation of one of the α-enantiomers can be traced from the square pyramid intermediate **19** which may rearrange to trigonal bipyramids **20** and **21**. The conversion **19** → **20** is favoured over the conversion **19** → **21** for the following reasons: (i) **20** is of higher symmetry (C_2) than that of **21** (sym. C_1), and (ii) **20** is obtained by the motion of the nonchelate ligand A whereas **21** requires the motion of the chelating ligand (4). Further trigonal bipyramid can only revert back to original square pyramid **19** as shown in Fig. 4(b) and **21** gives rise **19** and **16**. Therefore we always expect a stereoretent α-aquo product as the only major product with little of β_1. There is also no possibility of inversion since neither product generating operation exists (for a direct homo-conversion) nor a multistep process exists for indirect conversion. Sargeson *et al.*[30], reported that the aquation of the α-dichloro to chloro aquo complex in aqueous solution at $pH < 3$ occurred with retention of configuration and with no subsequent isomerisation of the chloro aquo ion.

In a similar manner the other α-enantiomer on aquation would produce a stereoretent *cis*-α-aquo product with lesser quantity of β_1-aquo product.

Conclusion

It is apparent from the above discussion that the isomeric product distribution in tune with experimental observation in the aquation of $[Co(N_4)AX]^{n+}$ [$N_4 = (NH_2)_4$, $(en)_2$, trien] can be explained on a more rational basis assuming the stereomobile rearrangement of the possible intermediates and as has been observed these rearrangements are symmetry allowed. Only the direct optical inversion of the complexes of the type *cis*-$[Co(N_4)AX]^{n+}$ ($N_4 = (en)_2$, trien) is symmetry forbidden. However, racemisation may occur to a limited extent via multistep paths, each step being symmetry allowed.

Acknowledgement

The author thanks Prof. R K Nanda and Prof. A C Dash, Utkal University, Bhubaneswar for their help and useful suggestions.

References

1 Basolo F & Pearson R G, *Mechanism of inorganic reactions*, (John Wiley) 1967, pp. 158.
2 Jackson W G, *Inorg Chim Acta*, 10 (1974) 51.
3 Sargeson A M & Jackson W G, *Inorg Chem*, 17 (1978) 1348.
4 Schipper P E & Rodger A, *Chem Phys*, 98 (1985) 29.
5 Schipper P E & Rodger A, *Chem Phys*, 107 (1986) 329.
6 Rodger A & Schipper P E, *Inorg Chem*, 27 (1988) 485.
7 Edwards J O, Monacelli F & Ortaggi G, *Inorg Chim Acta*, 11 (1974) 47.
8 House D A, *Coord chem Rev*, 23 (1977) 223.
9 Tobe M L & Williams C K, *Inorg Chem*, 15 (1976) 918.
10 Asperger S & Ingold C K, *J chem Soc*, (1956) 2862.
11 Sargeson A M & Searle G H, *Inorg Chem*, 6 (1967) 2171.
12 Link R G, *Inorg Chem*, 8 (1967) 1016.
13 Poon C K & Tong H W, *J chem Soc*, (A) (1971) 2151.
14 Chan S C & Tobe M L, *J chem Soc*, (1963) 514.
15 Chan S C; *J chem Soc*, (1964) 2716.
16 Tobe M L, *J chem Soc*, (1959) 3776.
17 Jackson W G & Begbie C M, *Inorg chim Acta*, 60 (1982) 115.
18 Poon C K, *Inorg Chim acta Rev*, (1970) 123.
19 Basolo F & Pearson R G, *Mechanism of inorganic reactions* (John Wiley) 1967, pp. 257.
20 Vanquickenborne L G & Pierloot K, *Inorg Chem*, 23 (1984) 1471.
21 Vanquickenborne L G & Pierloot K, *Inorg Chem*, 20 (1981) 3673.
22 Pearson R G, *Symmetry selection rules for chemical reactions*, (John Wiley) 1976, pp. 251.
23 Vanquickenborne L G & Ceulemans A, *Inorg Chem*, 17 (1978) 2730.

24 Kindred I J & House D A, *J inorg nucl Chem*, 37 (1975) 589.
25 Sargeson A M & Searle G H, *Nature*, 200 (1963) 356.
26 Buckingham D A, Marzilli P A & Sargeson A M, *Inorg Chem*, 6 (1967) 1032.
27 Posey F A & Taube H, *J Am chem Soc*, 76 (1957) 255.
28 Sargeson A M, *Aust J Chem*, 17 (1964) 385.
29 Buckingham D A, Olsen I I, Sargeson A M & Satrapa H, *Inorg Chem*, 6 (1967) 1027.
30 Sargeson A M & Searle G H, *Inorg Chem*, 4 (1965) 45.

Indian Journal of Chemistry
Vol. 30A, April 1991, pp. 308-312

Methyl nitrene: Thermochemistry and kinetics of its rearrangement to methyleneimine

Rita Kakkar* & Vibha Walia
Department of Chemistry, University of Delhi, Delhi 110 007

Received 13 July 1990; accepted 7 December 1990

The thermal unimolecular isomerisation of methylnitrene to methyleneimine has been studied, and the macroscopic thermodynamic and kinetic properties have been calculated using the vibrational frequencies and rotational constants evaluated theoretically. The high pressure rate constants have been calculated and the fall-off behaviour has been studied using the calculated reactant and transition state properties. Kinetic isotope effects on the reaction have also been studied. The effects of fluorine substitution on the thermochemical and kinetic parameters have also been investigated.

In our previous paper[1] on the isomerisation reaction of methyl nitrene, we had reported our calculations on the ground state potential energy surface for the reaction, and also reported the singlet and triplet state structures for the reactants, transition states and products, and the effect of fluorine as a substituent. In this paper, calculations of partition functions and thermodynamic properties derivable from the potential energy surfaces are presented.

Method of Calculation

We have used the optimized reactant, transition state and product structures from our earlier work[1] for all our calculations. The vibrational frequencies, calculated previously for confirming the transition state structures reported in our previous paper, and the calculated rotational constants were used in the calculation of partition functions and thermodynamic properties[2].

In these calculations, we have neglected the effects of rotation-vibration coupling, anharmonicity and centrifugal distortion. Since the molecules considered are rigid, no internal rotation has been considered.

The quantum statistical Rice-Ramsperger-Kassel-Marcus (RRKM) theory[3,4] was used to calculate the high pressure rate constants (k_∞) and the fall-off behaviour was also studied. Forst's approximation to $k(E)$ (see Eq. 1) was used in the calculations

$$k(E) = \frac{\alpha}{h}\frac{G^*(E-E_0)}{N(E)} \qquad \ldots(1)$$

where α is the reaction path degeneracy. $G^*(E-E_0)$ is the integrated density of states for the transition state at energy $E-E_0$ (E_0 is the activation energy for the reaction) and $N(E)$ is the density of states for the reactant. Both $G^*(E-E_0)$ and $N(E)$ were calculated by the method of steepest descents[5]. Hence k_∞ is given by Eq. (2)

$$k_\infty = \alpha \frac{kT}{h}\frac{Q^*}{Q}\exp(-E_0/RT) \qquad \ldots(2)$$

where Q^* and Q are, respectively, the partition functions for the transition state and reactant.

The unimolecular rate constant, k_{uni} is given by[4] Eq. (3)

$$k_{uni} = \frac{1}{Q}\int_{E_0}^{\infty}\frac{k(E)N(E)}{1+k(E)/\lambda Zp}\exp(-E/RT)\,dE \qquad \ldots(3)$$

Simpson's rule was used for the integration, with integration steps of 0.25 kcal/mol. The collisional deactivation efficiency (λ) was taken as 1, and Z, the collision frequency was calculated using a collision diameter of 4 Å.

The deuterium kinetic isotope effects on the reactions were also investigated. All calculations were carried out at various temperatures upto 298.15 K. Similar calculations were performed for the fluorine substituted compounds.

Results and Discussion

The calculated thermodynamic properties at 1 atmosphere pressure and 298.15 K for the singlet state stationary points of the three systems, viz. CH_3N, CH_2FN and CHF_2N, are given in Table 1. For the systems CH_3N, CH_2FN and CHF_2N, the en-

Table 1 – Calculated thermodynamic properties at 1 atmosphere pressure and 298.15 K for singlet states of CH_3N, CH_2FN and CHF_2N

System	Partition function (Q) $\times 10^{-37}$	Absolute entropy (S) (cal K^{-1} mol^{-1})
CH_3N		
Reactant	0.7085	68.06
Transition State	0.6281	67.73
Product	0.5225	67.34
CH_2FN		
Reactant	7.074	73.05
Transition State	6.521	72.67
Product	5.920	72.54
CHF_2N		
Reactant	41.27	77.20
Transition State	38.72	76.78
Product	40.45	77.17

Table 2 – Calculated thermodynamic properties at 1 atmosphere pressure and 298.15 K for triplet states of CH_3N, CH_2FN and CHF_2N

System	Partition function (Q) $\times 10^{-37}$	Absolute entropy (S) (cal K^{-1} mol^{-1})
CH_3N		
Reactant	0.2424	65.87
Transition State	0.2118	67.89
Product	0.6260	68.02
CH_2FN		
Reactant	7.849	73.22
Transition State	7.127	72.99
Product	7.631	73.66
CHF_2N		
Reactant	40.51	77.04
Transition State	46.00	77.68
Product	50.40	78.24

tropies of reaction have small negative values (-0.72, -0.51 and -0.03 cal K^{-1} mol^{-1}, respectively) and the activation entropies are also small and negative (-0.33, -0.38 and -0.42 cal K^{-1} mol^{-1}) respectively. This is to be expected as, the reactions being highly exothermic, the transition states resemble the reactants (according to Hammond's postulate[6]) and have similar vibrational frequencies. The only difference is that, in the transition state, one vibrational frequency for motion along the reaction coordinate becomes translational, and hence the vibrational contribution to the entropy decreases. The imaginary frequencies are 830, 838 and 802 cm^{-1}, respectively, for the transition states corresponding to the three reactions, and this accounts for a decrease of approximately 0.20 cal K^{-1} mol^{-1} in the vibrational contribution to the entropy.

The small negative entropies of reaction can also be explained on the basis that, in the product imines, the C – N bond has double bond character and this leads to an increase in the ν_{CN} mode, which in turn decreases its contribution to the vibrational entropy. In addition, the product is planar and has a lower rotational entropy.

In Table 2 are presented the thermodynamic properties for the triplet states. Here the situation is very different. For CH_3N, both the entropies of reaction and the activation entropy are larger (2.15 and 2.02 cal K^{-1} mol^{-1}, respectively). In this case, the increase is mainly due to an increase in the rotational contribution to the entropy. The reactant molecule has C_{3v} symmetry, and hence a symmetry factor of 3, which reduces its entropy.

Secondly, in contrast to singlet imines, triplet imines have nonplanar C_s geometries[1]. This suggests that they may have biradical character. An investigation of the highest occupied molecular orbitals in triplet CH_2NH indicates that the $^3A''$ state has a singly occupied a″ orbital mainly (86.4%) on nitrogen, and a singly occupied a′ orbital mainly (85.3%) on carbon. This biradical character accounts for the longer C – N bonds in triplet imines as compared to those in singlet imines, and the nonplanar CH_2 group in triplet imines. Both these factors lead to an increase in the entropy, and hence the entropy of reaction is positive.

Similarly, the transition states have biradical character with one electron localized on the nitrogen (89%), and the other electron shared equally by carbon and nitrogen. Hence, these reactions have loose biradical transition states, which account for the low vibrational frequencies in the transition states. Consequently, the vibrational contribution to the entropy is increased, leading to a positive entropy of activation.

For fluorine substituted compounds, too, the situation is similar. The only difference is that, in these cases, the reactants also have C_s geometry, and there is no contribution from the symmetry factor. Hence, although the entropies of reaction are again positive, the magnitudes are small.

We have performed RRKM calculations on the reactions. The calculated k_∞ values at various temperatures upto 298.15 K for all the reactions studied are given in Table 3. It is evident that, at low temperatures, e.g. 4 K, the rearrangement does not take

Table 3 – Calculated high pressure rate constants (k_∞) at different temperatures (K)

System	k_∞ at temp (K)				
	4	77	100	200	298.15
Singlet state					
CH_3N	0.0	2.55×10^{-4}	1.81×10	6.33×10^{6}	1.04×10^{9}
CH_2FN	0.0	3.99×10^{-3}	1.39×10	1.43×10^{7}	1.51×10^{9}
CHF_2N	0.0	9.74×10	2.85×10^{4}	4.56×10^{8}	1.02×10^{10}
Triplet state					
CH_3N	0.0	0.0	0.0	0.0	2.22×10^{-23}
CH_2FN	0.0	0.0	0.0	0.0	7.45×10^{-24}
CHF_2N	0.0	0.0	0.0	0.0	2.33×10^{-25}

Table 4 – Calculated high pressure Arrhenius parameters, A_∞ and E_∞

System	$A_\infty \times 10^{-13}$ (s^{-1})	E_∞ (kcal mol^{-1})
Singlet state		
CH_3N	2.909	5.7522
CH_2FN	1.940	5.3180
CHF_2N	0.967	3.6932
Triplet state		
CH_3N	9.824	52.375
CH_2FN	2.014	48.737
CHF_2N	1.428	49.086

Table 5 – Calculated log($p_{1/2}$) values for singlet rearrangements at various temperatures (K)

System	log $p_{1/2}$ (torr)			
	77	100	200	298.15
CH_3N	3.56	4.26	4.67	5.03
CH_2FN	3.93	4.08	4.55	4.89
CHF_2N	3.89	4.04	4.50	4.80

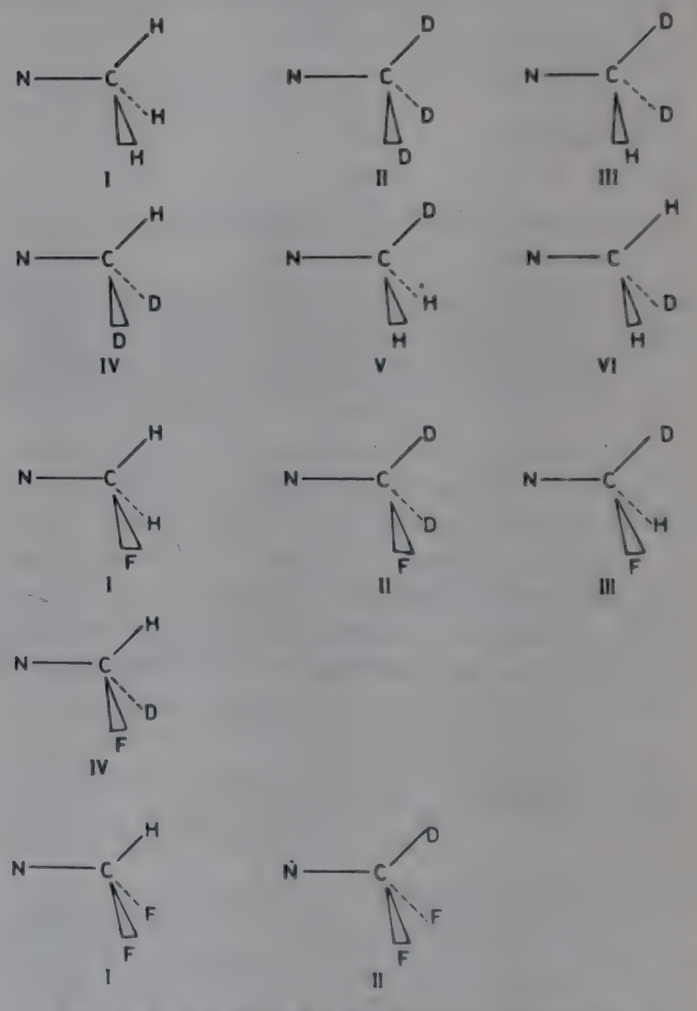

Fig. 1 – Structures of methylnitrene and substituted methylnitrenes.

place, and even the singlet state of CH_3N may be isolated. It has been experimentally established that alkylnitrenes cannot be observed[7] at 77 K, but are stable at 4 K (see ref. 8). Also, the rate of reaction increases with fluorine substitution. For the triplet states, even at 298.15 K, the reaction rate is very low. Accordingly, we did not calculate fall-off curves for the triplet reaction.

The high pressure Arrhenius frequency factor, A_∞ and the activation energy, E_∞, are given in Table 4. Both A_∞ and E_∞ decrease with increase in fluorine substitution, and A_∞ factors are typical of reactions involving rearrangements of carbenes.

The calculated log(k_{uni}/k_∞) values were subjected to polynomial fits with respect to log(p) and the resultant equations solved for $p_{1/2}$. The calculated log($p_{1/2}$/torr.) values for the various systems are reported in Table 5. The transition pressures, $p_{1/2}$, are an indication of the pressure below which the unimolecular rate constants k_{uni} begin to decline. The data in Table 5 indicate that the $p_{1/2}$ values are all in the range of 10^3-10^5 torr, and, as expected, increase with temperature. These values are quite high, and is indicative of the low activation energies of the reactions. There is a slight decrease in $p_{1/2}$ with increasing fluorine substitution.

We next calculated the deuterium kinetic isotope effects. Figure 1 shows the various deuterium labelled compounds used in our study. The effect on k_∞ is given by Eq. (4)

$$\frac{k_{\infty H}}{k_{\infty D}} = \frac{Q^*_H/Q_H}{Q^*_D/Q_D} \exp[(E_{0D} - E_{0H})/RT] \quad \ldots (4)$$

where Q_H and Q^*_H are, respectively, the partition functions of the reactant and transition states of the unlabelled compound, and Q_D and Q^*_D are those of the deuterium labelled isotopomers. E_{0H} and E_{0D} are, respectively, the zero-point energies of the unlabelled and labelled isotopomers. The calculated values of $k_{\infty H}/k_{\infty D}$ are greater than unity for isotopomers II, III and V of methylnitrene, i.e., the isotopomers II, III and V exhibit large normal isotope effects. However, for the other two isotopomers, viz. I and IV, the ratio is close to unity. This difference in isotope effects arises from the fact that the former (II, III and V) exhibit primary isotope effects, while the latter (I and IV) exhibit only secondary isotope effects.

Below the transition pressure, the reactions become bimolecular, and the low pressure limiting ratios were calculated from the formula (5)

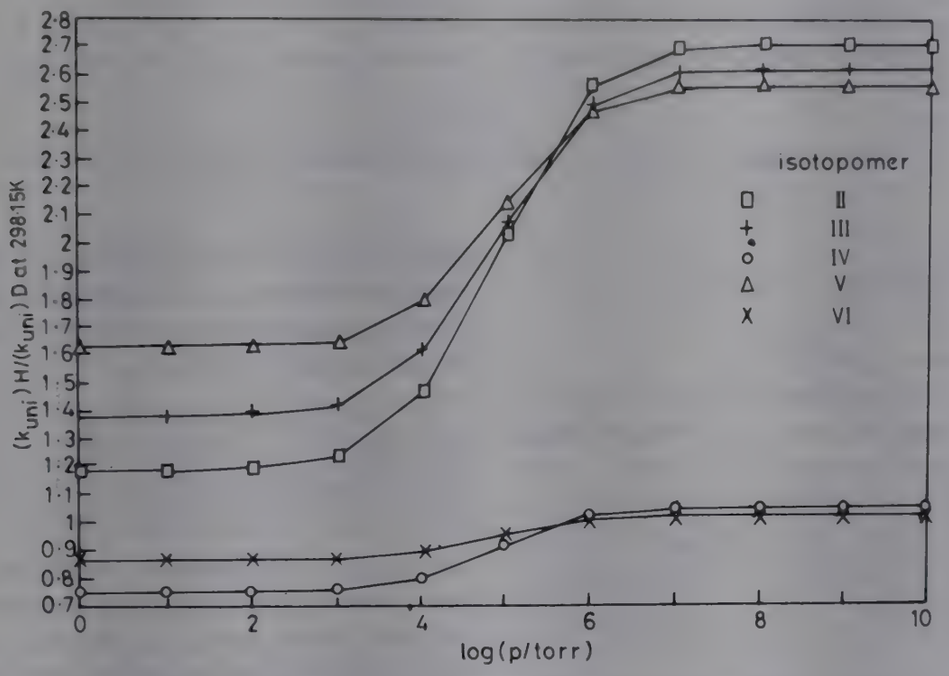

Fig. 2—Isotopic rate ratios for the deuterium labelled isotopomers of CH_3N.

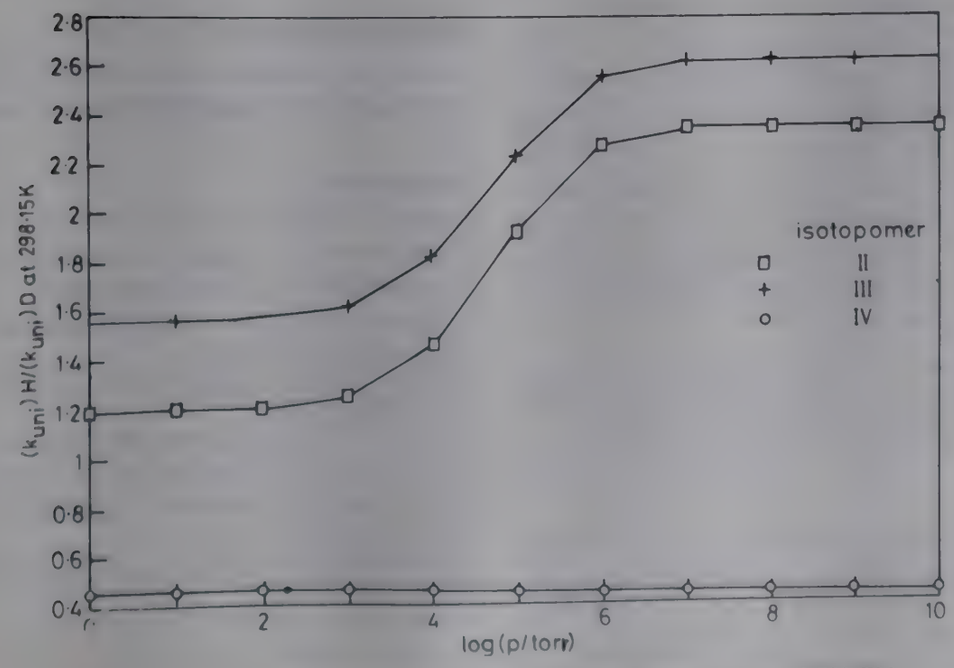

Fig. 3—Isotopic rate ratios for the deuterium labelled isotopomers of CH_2FN.

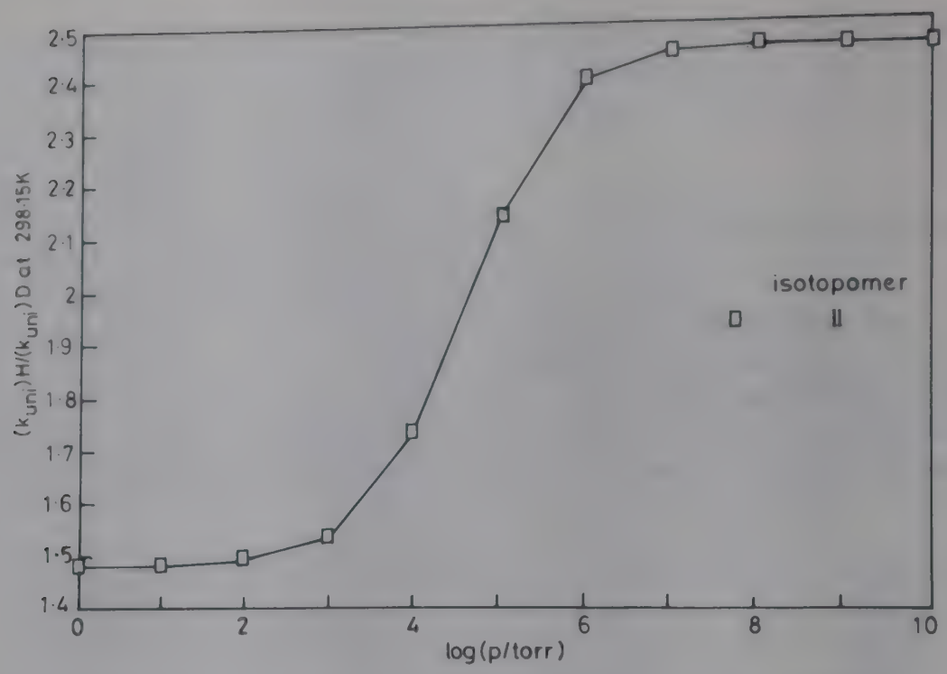

Fig. 4—Isotopic rate ratios for the deuterium labelled isotopomers of CHF_2N.

$$\frac{(k_{bim})_H}{(k_{bim})_D} = \frac{Q^*_H'/Q_H}{Q^*_D'/Q_D} \exp[(E_{0D} - E_{0H})/RT] \quad \ldots (5)$$

where $Q^{*\prime} = Q^* \exp(-E_0/RT)$

For the primary isotope effect, the ratio is greater than unity, but the isotopomers IV and VI exhibit inverse isotope effects. The ratios $(k_{uni})_H/(k_{uni})_D$ for methylnitrene are plotted against log(p/torr) in Fig. 2, where the above effects are apparent. The primary isotope effect is maximum for isotopomer II, while isotopomers III and V also exhibit large primary isotope effects. The three curves cross at log(p/torr) values between 5 and 6. Hence, the ratio $(k_{bim})_H/(k_{bim})_D$ is least for isotopomer II, but the ratio $k_{\infty H}/k_{\infty D}$ is maximum for this isotopomer.

For CH_2FN, the curves are given in Fig. 3. Here isotopomers II and III exhibit primary isotope effects, while isotopomer IV exhibits only a secondary isotope effect. For the isotopomers II and III, the curves are similar to those obtained for isotopomers II, III and V of methylnitrene, but now there is no crossing of the two curves. For isotopomer V, there is a large inverse secondary isotope effect at all pressures $[(k_{uni})_H/(k_{uni})_D \approx 0.45]$.

The only deuterated CHF_2N exhibits a normal primary isotope effect similar to the first two molecules. The curve is plotted in Fig. 4.

Conclusions

The thermodynamic parameters involved in the thermal unimolecular rearrangement of methylnitrene show that the activation entropies and entropies of reaction are small in magnitude and can be explained satisfactorily on the basis of the calculated transition state structures.

For the singlet states, based on the deuterium isotope effect, we have been able to predict that the primary isotope effects are normal, whereas there are inverse secondary isotope effects on the reactions.

Since it is difficult to experimentally obtain the low pressure bimolecular rate constants, particularly for reactions involving nitrenes and carbenes, the theoretical RRKM calculations should be useful for predicting $p_{1/2}$ values, etc.

Acknowledgement

The authors thank the staff of the Delhi University Computer Centre for their cooperation.

References

1 Walia V & Kakkar R, *Indian J Chem*, 29B (1990) 1007.
2 Fowler R H & Guggenheim E A, *Statistical thermodynamics*, (Cambridge University Press) 1939.
3 Robinson P J & Holbrook K A, *Unimolecular reactions*, (Wiley, London) 1972.
4 Forst W, *Theory of unimolecular reactions* (Academic Press, New York) 1973.
5 Forst W, *J phys Chem*, 76 (1972) 342.
6 Hammond G S, *J Am chem Soc*, 77 (1955) 334.
7 Smolinsky G, Wasserman E & Yager W A, *J Am chem Soc*, 84 (1962) 3220.
8 Wasserman E, Smolinsky G & Yager W A, *J Am chem Soc*, 86 (1964) 3166.

Indian Journal of Chemistry
Vol. 30A, April 1991, pp. 313-321

Effect of temperature on hydrogen isotope effects in dehydration of ion-exchange resins: Alkali metal ionic (Li^+, K^+ and Cs^+) forms of Dowex-50W resins

Neeta C Inamdar, S K Sarpal* & A R Gupta
Chemistry Division, Bhabha Atomic Research Centre, Bombay 400 085

Received 3 October 1990; accepted 12 December 1990

Hydrogen isotope effects in dehydration of alkali metal ionic (Li^+, K^+ and Cs^+) forms of Dowex-50W resins (with 2, 4, 8 and 12% divinylbenzene content), having n_w (number of moles of water per equivalent of resin) values of ~ 2 to ~ 27, have been determined at 303, 318 and 333K using a Rayleigh distillation type technique. For very low n_w values, the observed single stage separation factor, α_{obs}, for all the systems is independent of temperature and has a constant value of $\sim 1.025 \pm 0.004$, which is much lower than α_w, the single stage separation factor for pure water distillation at that temperature. In the case of Li^+ resins at all temperatures and K^+ and Cs^+ resins at higher temperatures only, the α_{obs} varies with n_w as follows: as n_w-value increases, α_{obs} increases gradually, reaches a maximum value, α_{max} (at n_{max}) which is greater than α_w. At still higher n_w-values the α_{obs} decreases gradually and finally approaches the α_w. In these systems where a maximum is observed in the $\varepsilon_{obs}[=\alpha_{obs}-1]$ versus n_w plots, the data have been analysed in terms of the three-water sub-system-model for cation hydration and the ε_1, ε_2 and ε_3, representing the separation factors for the water molecules in the primary shell, the secondary shell and the bulk water, respectively have been obtained. Analysis of the results for different temperatures shows that ε_1 and ε_2, originating from electrostatic interaction, are temperature independent. The fact that $\varepsilon_3 = \varepsilon_w$ (within the experimental error), shows that the effect of cationic charge does not extend beyond the second layer of water molecules. At lower temperature (303K), ε_{obs} versus n_w plots for K^+ and Cs^+ resins do not exhibit a maximum and ε_{obs} approaches ε_w at high n_w values. Further, ε_2 (353 or 303K) $< \varepsilon_w$ (303K) for these systems. These data show that water structure is preferentially formed at high n_w values at the expense of hydration shells, i.e., the hydration shells are destroyed by the more stable water structure at these temperatures. For any cationic form of the resin, the sharpness in the maximum of ε_{obs} versus n_w curve increases with increase in temperature, implying that with increasing temperature the bulk water structure is destroyed more rapidly than the hydration shell water structure. These observations are in consonance with the views reported in literature (see ref. 13) on electrolyte solutions.

Recent studies[1,2] on the hydrogen isotope effects in the dehydration of alkali metal ionic (Li^+, Na^+, K^+ and Cs^+) forms of Dowex-50W resins at 353K have emphasized that in the absence of strong interactions between counterions and the ionogenic groups, resin matrix provides a medium to study specifically the cation-water interactions without being influenced by the anions unlike in an electrolyte solution. The magnitudes of D/H isotope effects in these studies have revealed that water molecules in the secondary hydration shell are more strongly H-bonded to the water molecules in the primary hydration shell than the water molecules in the bulk water and that the effect of the cationic charge does not extend beyond the second hydration shell. The well defined characteristics of these hydration shells decrease with increase in size of the alkali metal ion, following the sequence $Li^+ > Na^+ > K^+ > Cs^+$, with Li^+ exhibiting the features associated with well defined first and second hydration shells and Cs^+ of very distorted first and second hydration shells. Similar studies on the electrolyte solutions have generally been made at ambient temperature. In order to correlate, directly, the information obtained from these studies with that from the studies on electrolyte solutions, we have extended the earlier investigations to lower temperatures, viz. 303, 318 and 333K.

Materials and Methods

All chemicals used were of AR or GR (E. Merck) grade. Hydrogen form of Dowex-50W resins (of 2, 4, 8 and 12% DVB contents and of 50-100 mesh), supplied by J.T. Baker & Co, USA, were treated in the usual manner[1,3-4] and finally converted into Li^+, K^+ or Cs^+ forms (see refs 1 & 2). Characterisation of the air-dried resin (ADR) samples was done by determining their moisture contents and ion-ex-

change capacities as described earlier[1-2]. The ion-exchange capacities were computed on the basis of oven dried resin (ODR), the moisture content of ADR being known. The maximum water uptake [obtained from moisture content of surface dried resin (SDR)], expressed in terms of n_w, the number of moles of water per equivalent of ODR and the ion-exchange capacities of the various resin samples are given in Table 1.

Resin samples of different n_w values (lower than the maximum attainable) were prepared as described earlier[3,4] by equilibrating isopiestically the ODR with LiCl or H_2SO_4 solution of appropriate water activity. For larger n_w values the SDR samples were used as such.

The equipment used for Rayleigh type distillations, has been described elsewhere[1,5]. Before doing the actual distillation experiment with a resin sample, its water content and the D/H composition of this water were determined by distillating, for ~1-2 hr, the entire water from a known weight of the resin in single step under running vacuum at 383K. The actual experiment involved multistep distillation of water from resin samples at the desired temperature (303, 318 or 333K) such that ~0.05 to ~0.25 g water was collected in each of the 3-4 fractions, the last fraction containing ~15-20% of the total water in the resin. A reasonable rate of distillation at a particular temperature was obtained by performing the experiment at an appropriate constant lower pressure. The last fraction was distilled at a raised temperature of 383K and under running vacuum for ~1-2 hr to ensure removal of last traces of water. Total weight of water in all the fractions (water collected) matched with the weight loss of the flask after distillation (water expected). Pure water was also distilled in an identical fashion at 303, 318 and 333K and the α_w (single stage separation factor for water distillation) values obtained (1.064 at 303K, 1.057 at 318K and 1.044 at 333K) were in good agreement with literature values[6] (1.070 at 303K, 1.057 at 318K and 1.046 at 333K).

The water fractions were analysed for their D-contents on a D/H ratio mass spectrometer model-660[7].

Table 1—Characteristics of the various samples of Dowex-50W (50-100) resins

Cross linking (% DVB)	Exchange capacity (meq/g ODR[a])	Max water uptake (n_w^b)
	Li^+-form	
2	4.90	35.0
4	4.91	22.0
8	4.87	11.5
12	5.03	9.5
	K^+-form	
2	4.34	27.5
4	4.25	18.6
	Cs^+-form	
2	3.03	27.1
4	3.21	17.8

a) Oven-dried resin
b) Number of moles of water per equivalent of ODR.

Results

The single stage separation factor, α, defined by Eq. (1)

$$\alpha = \frac{[D/H]_{(\text{liquid water/water in resin})}}{[D/H]_{(\text{water vapour})}} \quad \ldots (1)$$

is calculated using the Rayleigh formula[5] Eq. (2)

$$(N/N_0)^{\alpha/(\alpha-1)} = (W_0/W) \quad \ldots (2)$$

In Eq. (2) W and N are the weight and the D/H isotopic composition of the last fraction and W_0 and N_0 are the corresponding values for the total water initially present in the resin. The W_0 values, obtained from 'water collected' and 'water expected' were in excellent agreement with each other for all the experiments. N_0, the initial D/H composition, values obtained in the two ways, i.e. from the D/H isotopic analysis of water distilled in single step distillation and from the multistep distillation data by mass balance (the weights and the isotopic compositions of the individual fractions being known), were, likewise, in good agreement. For the computation of α, the W_0 and N_0 obtained from multistep distillation data were used, i.e. the value of W_0 used corresponded to 'water collected' and that of N_0 was obtained from the mass balance equation. The α-values obtained from these experimental data are labelled as α_{obs}.

The α_{obs}-values along with other relevant data for Li^+, K^+ and Cs^+ forms of Dowex-50W resins, are listed in Tables 2, 3 and 4, respectively. A good match between the values of the 'water collected' and 'water expected' indicates that the water losses during the experiments were negligible.

Variation of α_{obs} as a function of n_w for Li^+, K^+ and Cs^+ ionic forms of resins, at different temperatures, is shown in Figs 1 to 3, as plots of ε_{obs} [$= \alpha_{obs} - 1$] versus n_w. In Figs 1-3 the data for 353K (from refs 1 and 2) are also included for comparison. The general pattern of the curves is similar to that obtained earlier[1,2], for Li^+ resins at all temperatures and for K^+ resins at 333K. For K^+-form at 303K and for Cs^+-form at 303 and 333K, there are dis-

tinct differences, namely, ε_{obs} increases steadily for the lowest n_w-values and approaches $\varepsilon_w (= \alpha_w - 1)$ without exhibiting any maximum values.

Analysis of data

The hydration model for the alkali metal cations in the resin phase, used earlier[1,2], predicts that for systems having stable primary and secondary hydration shells, distinguishable from the bulk water, the ε_{obs} at very low n_w values is constant and very much lower than ε_w. Further, a well defined maximum is observed in the ε_{obs} versus n_w plots. The ε_{obs} at any n_w value is given in terms of individual contributions of ε_1, ε_2 and ε_3 from the three-water sub-systems (primary hydration shell, secondary hydration shell and the bulk water, respectively), by Eq. (3)

$$\varepsilon_{obs} \cdot n_w = \varepsilon_1 \cdot n_1 + \varepsilon_2 \cdot n_2 + \varepsilon_3 \cdot n_3 \quad \ldots (3)$$

where $n_w [= n_1 + n_2 + n_3]$ is the total number of moles of water per equivalent resin; n_1 and n_2 are the number of moles of water in primary and secondary hydration shells, respectively; and n_3 $(= n_w - n_1 - n_2)$ represents the bulk water. In ref. 1, fixed values of $n_1 (= 4)$ and $n_2 (= 2n_1$, i.e. 8) were used for Li^+ ions with the following boundary conditions:

$$n_w \leqslant 4 \quad : n_1 = n_w, n_2 = 0, \quad n_3 = 0$$
$$4 < n_w \leqslant 12 \quad : n_1 = 4, n_2 = n_w - n_1, n_3 = 0$$
$$n_w > 12 \quad : n_1 = 4, n_2 = 8, \quad n_3 = n_w - 12$$

As the number of water molecules in the first and second hydration shells vary from cation to cation and are expected to be temperature dependent, the present data have been analysed without assigning any value for n_1 and n_2. For this purpose a computer

Table 2 – Hydrogen isotope effects in dehydration of Li^+ ionic forms of Dowex-50W resins at different temperatures

Resin sample	n_w	Water (g)		Initial D-content (N_0) (ppm)	Water in last fr. (W) (gm)	D-content last fr. (N) (ppm)	α_{obs} (±.004)
		Expected	Collected (W_0)				
			A: 303K				
1.	3.7	0.5224	0.5218	154.8	0.1500	160.2	1.028
2.	3.8	0.5249	0.5314	154.5	0.1671	159.7	1.029
3.	5.0	0.2507	0.2552	154.0	0.0735	159.9	1.031
4.	6.1	0.9070	0.9065	153.4	0.1851	165.3	1.049
5.	7.4	0.8262	0.8290	153.4	0.2608	162.9	1.055
6.	9.4	0.7076	0.7096	154.4	0.2501	164.2	1.063
7.	10.2	0.4439	0.4503	153.7	0.1382	165.4	1.066
8.	12.7	0.2659	0.2655	153.2	0.0638	169.8	1.078
9.	14.6	0.2546	0.2690	158.4	0.0653	175.1	1.076
10.	15.0	0.6210	0.6286	152.4	0.2048	165.0	1.076
11.	20.0	0.5024	0.5082	155.4	0.1656	167.1	1.069
12.	27.0	0.2433	0.2373	155.8	0.0276	178.6	1.067
			B: 318K				
1.	2.4	0.3711	0.3703	150.5	0.1383	153.6	1.021
2.	5.5	0.3615	0.3601	151.6	0.0915	159.8	1.040
3.	6.0	0.3725	0.3709	154.0	0.0837	163.5	1.042
4.	11.5	0.2665	0.2627	153.9	0.0833	165.6	1.068
5.	12.3	0.2446	0.2455	152.9	0.0736	165.6	1.071
6.	15.0	0.3969	0.3999	155.4	0.0854	170.3	1.063
7.	22.6	0.5123	0.5163	154.7	0.1213	167.3	1.057
			C: 333K				
1.	3.4	0.5250	0.5202	149.0	0.1347	153.2	1.021
2.	6.0	0.3225	0.3205	154.6	0.0853	161.5	1.034
3.	10.5	0.4426	0.4395	153.9	0.0987	166.4	1.055
4.	11.0	0.4839	0.4812	155.4	0.1012	169.4	1.058
5.	12.0	0.4854	0.4877	154.0	0.1029	169.3	1.065
6.	15.0	0.3661	0.3639	153.9	0.1003	164.9	1.057
7.	23.2	0.5501	0.5511	155.5	0.1122	168.5	1.053

program based on pattern search method was developed in which the values of n_1 and n_2 were not assumed. If n_{max} is the number of water molecules at the maximum in the ε_{obs} versus n_w curve, tne boundary conditions then become:

$n_w < n_1$: $n_1 = n_w, n_2 = 0, \quad n_3 = 0$

$n_1 < n_w \leqslant n_{max}$: $n_1 = n_1, n_2 = n_w - n_1, \quad n_3 = 0$

$n_w > n_{max}$: $n_1 = n_1, n_2 = n_{max} - n_1, n_3 = n_w - n_{max}$

The ε_{obs} values for each experimental point, i, (i = 1 to k), were calculated giving a range of values for ε_1, ε_2, ε_3, n_1 and n_{max}. The error sum square defined by Eq. (4)

$$S = \sum_{i=1}^{k} [\varepsilon_{i(obs)} - \varepsilon_{i(cal)}]^2 \qquad \ldots (4)$$

was minimised. The program was executed on ND computer. The optimised values of the various parameters for different temperatures, where this model

Table 3 – Hydrogen isotope effects in dehydration of K^+ ionic form of Dowex-50W resins at different temperatures

Resin sample	n_w	Water (g)		Initial D-content (N_0) (ppm)	Water in last fr. (W) (g)	D-content last fr. (N) (ppm)	α_{obs} (±.004)
		Expected	Collected (W_0)				
			A: 303K				
1.	2.8	0.2461	0.2473	154.1	0.0988	157.9	1.027
2.	3.8	0.2948	0.2950	155.1	0.0520	164.7	1.036
3.	4.8	0.3848	0.3850	151.7	0.1201	160.2	1.049
4.	6.7	0.4454	0.4432	156.4	0.0980	169.2	1.055
5.	10.0	0.4101	0.4154	156.5	0.1717	165.0	1.064
6.	11.7	0.3673	0.3680	151.5	0.0950	165.3	1.069
7.	18.0	0.6304	0.6375	155.2	0.2428	165.3	1.070
			B: 333K				
1.	2.9	0.3310	0.3340	153.1	0.1366	156.2	1.023
2.	3.6	0.3119	0.3108	150.5	0.1040	156.7	1.038
3.	4.9	0.3807	0.3832	152.5	0.0520	164.7	1.040
4.	11.3	0.3324	0.3396	153.4	0.0655	166.2	1.051
5.	14.2	0.3069	0.3077	150.6	0.0838	159.8	1.048
6.	18.5	0.5525	0.5583	152.4	0.0745	166.5	1.046

Table 4 – Hydrogen isotope effects in dehydration of Cs^+ ionic form of Dowex-50W resins at different temperatures

Resin sample	n_w	Water (g)		Initial D-content (N_0) (ppm)	Water in last fr. (W) (g)	D-content last fr. (N) (ppm)	α_{obs} (±.004)
		Expected	Collected (W_0)				
			A: 303K				
1.	2.6	0.2662	0.2679	144.7	0.1120	147.6	1.023
2.	2.8	0.2144	0.2197	150.0	0.0720	154.5	1.027
3.	4.7	0.3318	0.3322	153.9	0.0889	164.3	1.052
4.	5.4	0.2239	0.2261	155.3	0.0570	166.1	1.051
5.	6.0	0.3312	0.3352	156.0	0.0830	167.4	1.053
6.	15.4	0.7731	0.7709	156.1	0.3240	165.1	1.069
7.	17.5	0.5639	0.5649	156.0	0.2876	163.0	1.070
			B: 333K				
1.	2.0	0.2130	0.2131	154.9	0.1031	157.2	1.021
2.	2.6	0.2311	0.2364	153.2	0.1182	155.6	1.023
3.	4.7	0.3145	0.3172	152.3	0.0946	158.3	1.033
4.	8.3	0.3668	0.3627	156.6	0.1304	163.1	1.041
5.	11.2	0.3103	0.3006	152.3	0.0650	162.0	1.042
6.	16.0	0.4110	0.4105	155.2	0.0833	166.5	1.046
7.	17.0	0.5755	0.5756	155.4	0.0912	168.5	1.046

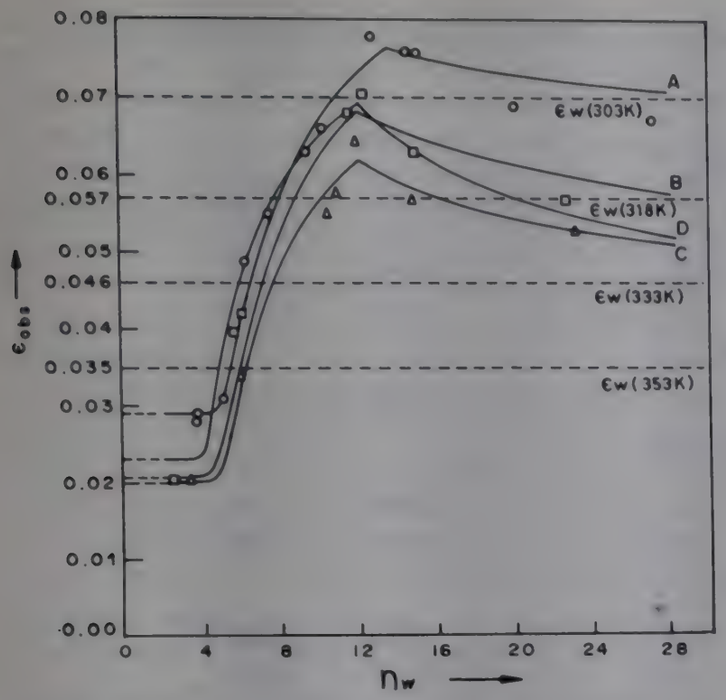

Fig. 1 – Variation of ε_{obs} with n_w for Li^+ form of Dowex-50W resins. [Solid lines: Calculated from optimised parameters in Table 5, A: 303K (○, exptl.); B: 318K (□, exptl.); C: 333K (Δ, exptl.) and D: 353K (ref. 1)].

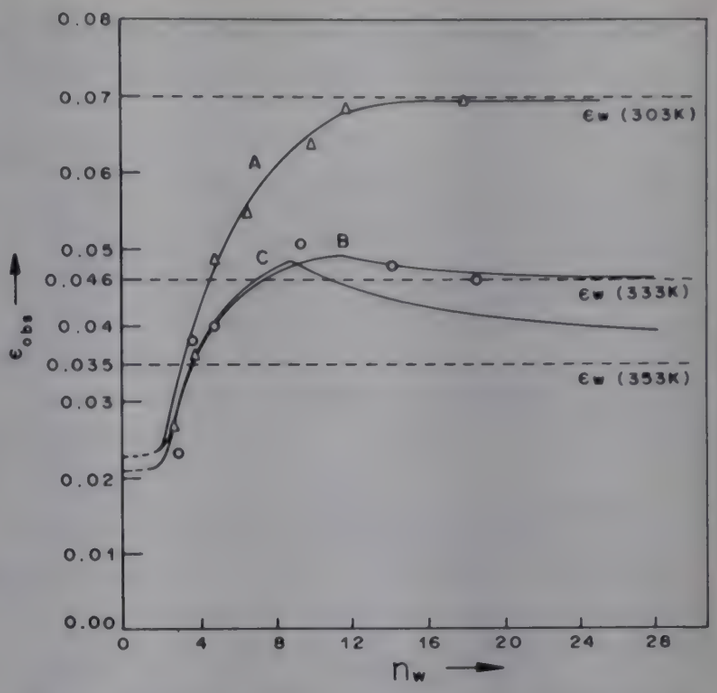

Fig. 2 – Variation of ε_{obs} with n_w for K^+ form of Dowex-50W resins. [A: 303K (Δ); B: 333K (○, exptl.; –, calcd. from optimised parameters in Table 5) and C: 353K (ref. 2) (—, calcd. from optimised parameters in Table 5)].

is applicable, were obtained. The data for the various alkali metal ionic resins at 353K[1,2] were also analysed using the same program.

Discussion

(i) *Lithium ion*

The optimised values of the various parameters (ε's and n's) for Li^+ resins at different temperatures are given in Table 5. The values for the parameters at 353K are in good agreement with those reported earlier[1]. The primary hydration number for Li^+ ion in the resin (n_1 in Table 5) is 4.9 ± 0.4 at 303, 318 and 333K. This is in agreement with the hydration number for Li^+ ion in aqueous electrolyte solution which vary from 4 ± 1 (determined by X-ray diffraction[8-11]) to 5.7 (from molecular dynamics (MD) simulation studies[12]) at temperature close to 303K. The hydration numbers reported in the present study are for lithium ion in the resin phase where disturbing effect of the anions, which are invariably present in aqueous electrolyte solutions, are absent. This implies that the Li^+-water interactions are so strong that the effect of the anions even in moderately concentrated electrolyte solutions (as in X-ray diffraction or MD simulation) do not affect them. The hydration number of lithium ions in the resin obtained by this technique is 4.0 ± 0.4 at 353K as reported in Table 5 and is lower than that at 303K. Busleava and Samoilov[13] have also observed that hydration number of Li^+ decreases as temperature increases and have reported a value of the temperature coefficient for hydration number of Li^+ as -0.005 deg^{-1}. This would lead to a change in hydration number by about 0.3 for Li^+. This is within the limits of accuracy of the present data (± 0.4). As such no quantitative conclusions regarding the effect of temperature on hydration numbers can be drawn. However, qualitatively one can say that hydration number does decrease when the tempera-

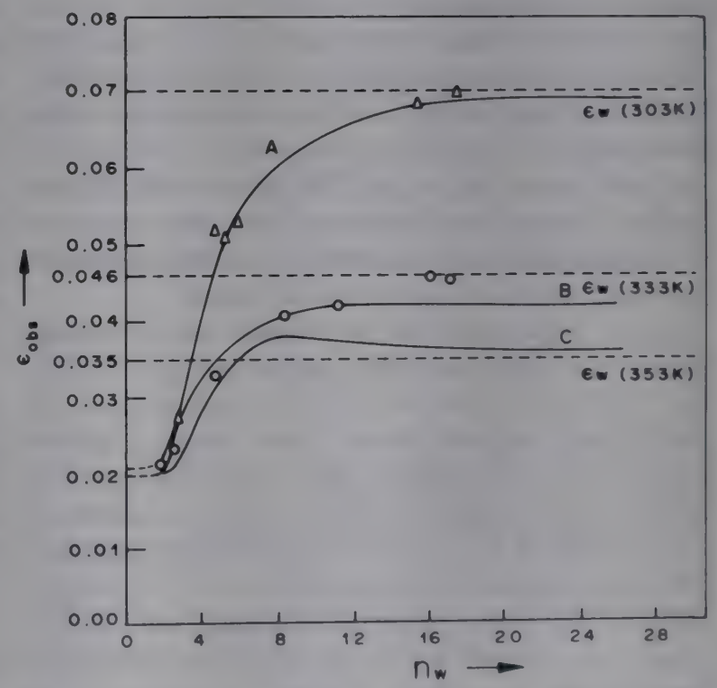

Fig. 3 – Variation of ε_{obs} with n_w for Cs^+ form of Dowex-50W resins. [A: 303K (Δ); B: 333K), ○: explt, –: calcd. from optimised parameters in Table 5) and C: 353K (ref. 2) (–: calcd. from optimised parameters in Table 5)].

Table 5 – Optimised parameters (ε's and n's) at different temperatures for alkali metal ionic forms of Dowex-50W resins

Temp (K)	ε_1 (±.004)	n_1 (±.4)	ε_2 (±.004)	n_{max} (±.2)	n_2 (±.4)	ε_3 (±.004)	ε_w^5
			A: Li^+ ionic resin				
303.0	0.029	4.9	0.103	13.6	8.7	0.066	0.070
318.0	0.021	4.8	0.100	12.0	7.2	0.050	0.057
333.0	0.020	4.9	0.091	12.0	7.1	0.043	0.046
353.0	0.023	4.0	0.092	12.0	8.0	0.039	0.035
			B: Na^+ ionic resin				
353.0	0.025	3.0	0.070	9.0	6.0	0.037	0.035
			C: K^+ ionic resin				
333.0	0.023	2.2	0.055	11.4	9.2	0.044	0.046
353.0	0.021	2.3	0.058	9.0	6.7	0.035	0.035
			D: Cs^+ ionic resin				
333.0	0.021	2.3	0.048	10.5	8.2	0.043	0.046
353.0	0.020	2.8	0.048	8.0	5.2	0.035	0.035

ture increases from 303 to 353K. These features can also be seen in the variation of n_{max} with temperature, i.e. n_{max} qualitatively increases when the temperature decreases, e.g. from 353 to 303K. However, the well-defined maximum at 353K, indicative of a very stable second hydration shell, gradually becomes less sharp as temperature decreases. Besides, the number of water molecules in the second hydration shell (equal to $2n_1$ at 353K) becomes less than $2n_1$ as temperature decreases. Both these observations suggest that the stability of second hydration shell decreases as temperature decreases.

The ε_1 represents the magnitude of H-bonding among the water molecules within primary hydration shell. Table 5 shows that it is independent of temperature and very much lower than ε_w at any temperature. This implies that water molecules in this shell are strongly oriented under the effect of electric field of the cation with very little possibility of H-bonding among themselves as in the crystal hydrates[14]. The ε_2 represents the strength of H-bonds formed by water molecules in the second hydration shell with the water molecules in the primary hydration shell. Data in Table 5 show that ε_2 is independent of temperature, within the limits of experimental error, and has an average value of 0.096 ± 0.005. The ε_3 is equal to ε_w, within experimental error, at all temperatures, i.e. it increases in the same way as does ε_w, with decreasing temperature. As ε_1 and ε_2 are independent of temperature, ε_{max} should be the same at all temperatures. The distinctly larger value of ε_{max} at 303K arises because n_{max} is larger and the contribution of $\varepsilon_2 n_2$ term to the ε_{obs} becomes greater. This supports the above conclusion that the number of water molecules in the first and second hydration shells of Li^+ ions are greater at 303K than at 353K.

The sharpness of the maximum in the ε_{obs} versus n_w curves is governed by the difference in the ε_{max} and ε_w. As ε_{max} is in turn determined by ε_2, the sharpness of the maximum is controlled by $\varepsilon_2 - \varepsilon_w$ at any temperature. As ε_2 is constant at all temperatures and ε_w increases with decrease in temperature, it follows that the maximum in the ε_{obs} versus n_w curve becomes progressively less sharp with decreasing temperature, as is actually observed. For the same reason the approach of ε_{obs} to ε_w at high n_w values becomes progressively slower as the temperature increases, e.g. at $n_w = 24$, the difference $\varepsilon_{obs} - \varepsilon_w$ at various temperatures is: 303K (0.0018), 318K (0.0020), 333K (0.0065) and 353K (0.0190). It implies that the H-bonded structure of water become stronger with decreasing temperature but the hydration shell remains unaffected, or in other words, hydration shell gets more structured relative to the bulk water as temperature increases. The same conclusion was reached by Samoilov and coworkers in their study on the effect of temperature on ionic hydration in aqueous solutions.

As ε_2 depends upon the nature of cations, a situation can arise when, for a given cation at some temperature, ε_2 may become smaller than ε_w. The consequence of this on the nature of the ε_{obs} versus n_w curves and (cation) hydration will be discussed as and when such situations arise.

(ii) *Sodium ion*

A sharp maximum was obtained in the ε_{obs} versus n_w plots and the ε_{obs}, for very low n_w values, was constant and very much lower than ε_w at 353K (see

ref. 2). Thus, the three-water sub-system-model for ionic hydration, applicable for Li^+ ions, can be applied to this system also. Using the computer program described in an earlier section, optimised values of ε_1, n_1, ε_2, n_{max}, n_2 and ε_3 were obtained and are listed in Table 5. As discussed for Li^+ ions, ε_1 and ε_2 are independent of temperature and n_1 and n_2 values increase slightly at 303K as compared to those at 353K. As $\varepsilon_2 > \varepsilon_w$ at 303K, one would expect that the same model would apply to Na^+ resins at 303K. Thus the behaviour of Na^+ in resin phase would be very similar to that of Li^+ resins. No detailed study of Na^+ resins at different temperatures was carried out. All the same, ε_{obs} for the Na^+ resin at 303K was determined at one n_w value (= 20.3) and was found to be 0.069. The ε_{obs} at 303K for this n_w value was computed using Eq. (3) with $\varepsilon_1 = 3.0$, $\varepsilon_2 = 0.074$, $n_2 = 7.0$ and $\varepsilon_3 = 0.070$. Computed value of ε_{obs} (= 0.065) agrees well with the observed value within the limits of experimental error, confirming that Na^+ resins behave like Li^+ resins at 303K. In particular this establishes that Na^+ ions are able to retain their primary and secondary hydration shells in the resin even at 303K.

(iii) *Potassium ion*

The ε_{obs} versus n_w plots for K^+ ions at 353K and 333K show a maximum and a flat portion at very low n_w values where $\varepsilon_{obs} < \varepsilon_w$ and has a constant value. These are the features required for the application of the three-water sub-system-model (Eq. 3). The data for K^+ resins at these temperatures were analysed using the computer program described above and the values of the optimised parameters are listed in Table 5.

It was pointed out while discussing K^+ resin data at 353K (ref. 2), that due to weaker electrostatic interaction between K^+ and water dipoles, even before the primary hydration shell gets completed, water molecules start forming the H-bonds amongst themselves. Thus the distinction between the first and second hydration shells is lost. The maximum in the ε_{obs} versus n_w plots marks the completion of this composite hydration shell. Therefore, n_1 is not the primary hydration number but refers to the nearest neighbour water molecules which do not form H-bonds amongst themselves and n_2 refers to the number of water molecules in the composite hydration shell which forms H-bonds. So far as the ε_2, which is a measure of the H-bond strength formed by these n_2 water molecules, is greater than ε_w, stable hydration shell is formed (a situation realised at 353K and 333K). At 303K, the ε_{obs} versus n_w plot for K^+ resin does not show a maximum and there is no indication of a flat portion at very low n_w values indicating that the three-water sub-system-model is not applicable. Also, at 303K, $\varepsilon_2 < \varepsilon_w$ (303K). If the three-water sub-system-model is applied to the data at 303K, it is found that ε_2 (303K) > ε_2 (353 or 333K), as well as ε_2 becomes equal to ε_w at 303K. This clearly shows that the model breaks down at this temperature. The fact that $\varepsilon_w > \varepsilon_2$ at 303K suggests that water structure is more stable than the hydration shell structure. All the same, at low n_w values ($< n_{max}$ at 353 or 333K) where normal water structure cannot be formed, a composite hydration shell around K^+ in the resin will exist at 303K as in the cases at 353 or 333K.

To ascertain whether the hydration shell structure at high n_w values is retained and only the extra water molecules [$= n_w - n_{max}$ (353K)] form the normal water structure, ε_{obs} at 303K was computed using ε_1, n_1, ε_2, and n_2 (353K) and ε_3[$= \varepsilon_w$ (303K)]. The computed values are much lower than the observed values (Table 6). It means that at $n_w > n_{max}$ (353K), the number of water molecules contributing to ε_{obs} with individual contribution of ε_w is greater than $n_w - n_{max}$ (353K), i.e. the composite hydration shell has less than n_{max} (353K) water molecules. This implies that the hydration shells which are stable at 353K and 333K, are being destroyed at 303K and normal water structure is progressively formed at their expense. This means that n_{max} value observed at 353K (the overall hydration number, n_h) progressively decreases. To test this hypothesis, n_h values for $n_w > n_{max}$ (353K) were computed using Eq. (5)

$$\varepsilon_{obs} \cdot n_w = \varepsilon_1 \cdot n_1 + \varepsilon_2 \cdot n_2 + \varepsilon_3 \cdot (n_w - n_2 - n_1)$$
$$= \varepsilon_{max} \cdot n_h + \varepsilon_3 \cdot (n_w - n_h) \qquad \ldots (5)$$

In Eq. (5) ε_1, n_1, ε_2 and n_2 are taken from Table 5 and $\varepsilon_3 = \varepsilon_w$ (303K). These computed values for n_h at $n_w > n_{max}$ (353K) are given in Table 6 which clearly demonstrates that hydration shell of K^+ ion is destroyed as bulk water structure is progressively formed, i.e. the bulk water structure is formed at the expense of hydration shells structure.

(iv) *Caesium ion*

The ε_{obs} versus n_w plots for Cs^+ resins at 353K show a maximum and conform to the system where the three-water sub-system-model can be applied. The calculated values for n_1, ε_1, n_{max}, ε_2 and ε_3 are given in Table 5. Though the ε_{obs} versus n_w plots for Cs^+ resins at 333K do not show a clear maximum, it is observed that $\varepsilon_2 = \varepsilon_w$ (333K), indicating that the model could be applicable. The values of ε's and n's at 333K for Cs^+ resins (Table 5) show that n_1, ε_1, n_2 and ε_2 are the same as observed for 353K and ε_3 is equal to ε_w (333K), confirming that the model is in-

deed applicable. However, at 303K, the ε_2 obtained from data at higher temperatures is much less than ε_w (303K). Also there is no maximum in ε_{obs} versus n_w plot at 303K. Thus this system behaves like K^+ resins at 303K and the same arguments apply. As n_w value increases beyond n_{max} (obtained from data at 353 and 333K), hydration shell structure is progressively destroyted and bulk water structure is increasingly formed at their expense. The n_h values which satisfy ε_{obs} at higher n_w (Eq. 5) are listed in Table 6, confirming the above conclusions.

(v) *Comparison of results for various ionic resins at different temperatures*

The overall ε-value at any temperature is the smallest for Cs^+ system and the largest for Li^+ system, that for K^+ falling in between the two. The ε_{max}, which is largely composed of ε_2-value is, likewise, the highest for Li^+ system and the lowest for Cs^+ system. The magnitude of ε-value reflects the strength and/or number of H-bonds between the water molecules. In other words the ε-value is a measure of the extent of H-bonded structure formed amongst the water molecules, more the structuring the greater is the ε-value and vice-versa. The $\Delta\varepsilon (= \varepsilon_{max} - \varepsilon_w)$, which is a measure of the enhanced structuring of water in the hydration shells as compared to the bulk water, follows the sequence: $\Delta\varepsilon_{(Li^+)} > \Delta\varepsilon_{(K^+)} > \Delta\varepsilon_{(Cs^+)}$ for all temperatures.

The influence of temperature on the degree of structuring of water molecules in the hydration shells around any alkali metal ion and the bulk water can, similarly, be expressed in terms of the $\Delta\varepsilon$, and it is observed that the relative structuring of water in the hydration shells (as compared to the bulk water) is larger at higher temperature than at the lower, i.e. for any metal ionic system: $\Delta\varepsilon_{(353K)} > \Delta\varepsilon_{(333K)} > \Delta\varepsilon_{(318K)} > \Delta\varepsilon_{(303K)}$. This observation is in consonance with the conclusions of Busleava and Samoilov[13] that with the increase in temperature the bulk water structure is destroyed more rapidly than the hydration shelled water structure.

Table 6 – Variation in overall hydration numbers (n_h) of K^+ and Cs^+ ions in Dowex-50W resins at 303K at high n_w values

n_w	ε_{obs}	ε_{cal}	n_h
	K^+ Resin		
10.0	0.0650	0.051	4.20
12.0	0.0680	0.054	2.00
14.0	0.0685	0.056	1.75
16.0	0.0690	0.058	1.33
18.0	0.0695	0.059	0.75
	Cs^+ Resin		
9.0	0.0625	0.042	3.10
10.0	0.0640	0.045	2.70
12.0	0.0665	0.049	1.91
14.0	0.0675	0.052	1.59
16.0	0.0690	0.054	0.73
18.0	0.0695	0.056	0.41

Conclusion

Hydrogen isotope effects in liquid-vapour equilibrium in any water system, which are a measure of their H-bonded structure, have been effectively used to get an insight of the delicate balance between alkali metal cation-water interactions (ion hydration) and water-water interactions (H-bonded water structure). Ion-water interactions being electrostatic in character are insensitive to temperature changes (separation factors ε_1 and ε_2 for primary and secondary hydration shell water molecules are independent of temperature, within the experimental errors) and depend primarily on the nature of the cation. However, the bulk water structure is very sensitive to temperature (ε_w decreases with increasing temperature). At high ionic concentrations (low n_w values) and at all temperatures where normal water structure is not present, all cations form their hydration shells in the resin phase where the anionic effects, which destroy the hydration shells at high concentrations in aqueous electrolyte solutions, are absent. Small cations, like Li^+ or Na^+, interact very strongly with water molecules and their hydration shells have stronger H-bonded structure than liquid water in the temperature range 303K to 353K ($\varepsilon_2 > \varepsilon_w$ in this temperature range). Thus they retain their hydration shells at all temperatures even at low ionic concentrations, i.e. at high n_w values (maxima are observed in the ε_{obs} vs n_w curves). K^+ and Cs^+ ions are able to form only distorted hydration shells where the distinction between the primary and the secondary shells is lost due to weak electrostatic interactions between these cations and water molecules. For these cations $\varepsilon_2 > \varepsilon_w$ at 353 and 333K but $< \varepsilon_w$ at 303K. Thus these cations retain hydration shells at low ionic concentrations or at high n_w values (where bulk water structure can be formed) only at 353 and 333K temperatures. At 303K, for K^+ and Cs^+ at low ionic concentration (high n_w values), water structure is preferentially formed at the expense of hydration shells, i.e. their hydration shells are progressively destroyed. In general, hydration shells get more structured relative to the bulk water structure as temperature increases because water structure is more rapidly destroyed with increasing temperature whereas hydration shells are relatively insensitive to temperature. Qualitatively, these studies support the observation that primary or overall

hydration number of cations decreases with increasing temperature.

Acknowledgement

The authors wish to express their sincere thanks to Dr J P Mittal, for his interest in these investigations.

References

1 Gupta A R, Nandan D & Sarpal S K, *J phys Chem*, 86 (1982) 3257.
2 Gupta A R & Nandan D, *J phys Chem*, 89 (1985) 4329.
3 Nandan D & Gupta A R, *Indian J Chem*, 12 (1974) 808.
4 Hellferich F, *Ion exchange*, (McGraw Hill, New York) 1962.
5 Wahl W H & Urey H C, *J chem Phys*, 3 (1935) 411.
6 Pupezin J, Jakli G, Jansco G & VanHook W A, *J phys Chem*, 76 (1972) 743.
7 Murthy M S, Prahallad Rao B S, Handu V K & Satam J V, *Report BARC*-1026 (1979).
8 Narten A H, Vaslow F & Levy H A, *J chem Phys*, 58 (1973) 5017.
9 Maeda M & Ohtaki H, *Bull chem Soc Japan*, 48 (1975) 3755.
10 Terekhova D S, Ryss A I & Radchenko I V, *Zh struk Khim*, 10 (1969) 923.
11 Lawrence R M & Kruh R F, *J chem Phys*, 47 (1967) 4758.
12 Heinzinger K & Vogel P C, *Z Naturforsch*, 31A (1976) 463.
13 Busleava M N & Samoilov O Ya, *Zh struk Khim*, 2 (1961) 551.
14 Manche E P & Carrol B J, *J phys Chem*, 81 (1977) 2637.

Indian Journal of Chemistry
Vol. 30A, April 1991, pp. 322-327

Changes in thermodynamic parameters in the exchange of alkaline earth metals with sodium ions in Dowex-50W × 8 and Amberlyst-15 resins in aqueous medium

R S D Toteja, B L Jangida* & M Sundaresan

Analytical Chemistry Division, Bhabha Atomic Research Centre, Bombay 400 085

Received 29 May 1990; accepted 31 July 1990

Standard free energy, ΔG^0, enthalpy, ΔH^0 and entropy, ΔS^0, changes have been evaluated for Mg^{2+}/Na^+, Ca^{2+}/Na^+, Sr^{2+}/Na^+, Ba^{2+}/Na^+ exchange systems on strong polystyrenesulfonic (PSS) acid type cation exchange resins, Dowex-50W × 8 and Amberlyst-15 (macroreticular) in dilute aqueous solutions from equilibrium ionic distribution and heat of exchange measurements calorimetrically at 298K. The alkaline earth metals are preferred by both the resins and the preference increases from magnesium through barium. The selectivity is lower for all the metals on Amberlyst-15 resin. The exchanges take place with absorption of heat. The endothermicity is more on Amberlyst-15 and it decreases with increasing size of the metal ion on both the exchangers. The uptake of divalent ions is governed by increase in entropy. The difference in entropies of hydration of alkaline earth metal and sodium ions is considered to be a major factor responsible for increase in standard entropy. The lower selectivity of alkaline earth metals on Amberlyst-15 is attributed to decrease in the hydration numbers of the cations in the resin since it imbibes more water than Dowex-50W × 8.

Considerable amount of work has been done on ion-exchange equilibria involving organic cation exchange resins but very less work has been reported on enthalpy changes involving heterovalent ions. Further, no systematic study has been made on the dependence of the heat of exchange of unequally charged cations on the ionic composition of the exchanger. Boyd *et al.*[1] reported for the first time such a dependence for Zn^{2+}/Na^+ exchange reaction. Later Jangida and Sundaresan[2] reported this type of dependence for Al^{3+}/H^+ exchange system. Recently, Boyd[3] has reported the changes in the thermodynamic properties for the heterovalent ion exchange reaction of lanthanum with sodium ions. The present work is a part of an on-going programme in our laboratory on the thermodynamics of heterovalent cation exchange reactions, and presents the equilibrium and thermochemical measurements on strong polystyrenesulphonate (PSS) type resins, Dowex-50W × 8 (8% DVB nominally crosslinked gel type) and Amberlyst-15 (macroreticular type of unknown cross-linking). The standard free energy change, ΔG^0 and the enthalpy change, ΔH^0 were estimated for four heterovalent cation exchange systems, Mg^{2+}/Na^+, Ca^{2+}/Na^+, Sr^{2+}/Na^+ and Ba^{2+}/Na^+ on these two resins and the entropy changes, ΔS^0 were derived.

It is important to note that Bonner and coworkers[4-9] reported equilibrium constants for several cation exchange systems involving uni-, bi- and tri-valent ions on various crosslinked Dowex-50 resins. But the activity coefficient ratios were not determined for most of the ion pairs. Flett and Meares[10] estimated activity coefficient ratios by using the theory of mixed electrolytes and calculated the thermodynamic equilibrium constant (K) and hence free energy changes, by combining the data of Bonner and coworkers[4-9] and the activity coefficient ratios. However, there was an error[11] in the calculation of K and the results reported by them[10] need re-evaluation. This has been explained later in the text.

Materials and Methods

Dowex-50W × 8 (J.T. Baker) and Amberlyst-15 (Rohm and Haas) resins were reagent grade preparations with 100-200 and 20-25 mesh sizes respectively. The resins were converted into sodium, magnesium, calcium, strontium and barium forms, air dried and stored. Their moisture contents were determined after drying at 383K in a vacuum oven and the exchange capacities were determined by the conventional method. The isopiestic method was used for determining the equivalent water contents of the fully swollen resins at unit water activity. The capacities on dry basis and equivalent water contents are presented in Table 1.

Equilibrium procedure

Air-dried resin (Na^+ form) (0.5g) was equilibrat-

Table 1—Capacities and equivalent water contents of Dowex-50W × 8 and Amberlyst-15

Resin form	Dowex-50W × 8		Amberlyst-15	
	Capacity meq/g dry resin	n_w (mole of H_2O/equiv)	Capacity meq/g dry resin	n_w (mole of H_2O equiv)
HR	4.95	10.80	4.84	11.64
NaR	4.52	8.72	4.26	11.11
MgR	4.86	8.27	4.27	11.60
CaR	4.49	7.88	4.23	11.54
SrR	4.27	7.49	3.83	11.27
BaR	3.82	5.77	3.25	11.23

ed with the total electrolyte mixture (50ml) containing 0.1 *N* NaCl and 0.1 *N* MCl_2 (where M was Mg^{2+}, Ca^{2+}, Sr^{2+} or Ba^{2+}). The volumes of NaCl and MCl_2 were adjusted so as to give the desired equivalent fraction of M^{2+} in the resin after equilibration.

The equilibrated solution was analysed for M^{2+} ions only by EDTA titration at *p*H 10 using EBT as an indicator. A known amount of magnesium was added while titrating Ca^{2+}, Sr^{2+} or Ba^{2+} ions to get a sharper end point.

The equilibrium compositions of the resin and solution phases were obtained from the amount of resin taken, its capacity, the concentration of M^{2+} ion at equilibrium and the initial composition of the solution. The concentrations of M^{2+} and Na^+ in the resin phase were calculated by difference.

Calorimetric measurements

The isoperibol calorimeter set-up, described elsewhere[2,12] was used with some modifications. The dewar flask was enclosed in a thick (~ 5 mm) cylindrical brass vessel complete with a flange and an O ring and nuts and bolts arrangement to make the vessel water tight. It was immersed completely below the surface of water in the thermostat for a better control of temperature. A potentiometric strip-chart recorder, Omniscribe (0 to 5 V) (Digital Electronics, Bombay) was used for recording imbalance in the Wheatstone bridge potential. A digital d.c. source (Zenith Electronics, model DPML 200) was used to supply a constant voltage (upto 6 V) to the heater. A digital electronic quartz timer (APLAB) having a range from 1 ms to 999.9 s and time base accuracy of ± 0.1 was used to measure the time of passage of current through the heater.

The procedure followed for the measurement of heat of exchange was the same as described earlier[2]. The electrolyte mixture (100 ml) filled in the dewar flask consisted of 0.1 *N* NaCl and 0.1 *N* MCl_2 as the case may be. The electrolyte solution in the calorimeter was analysed for M^{2+} ions after attainment of equilibrium. The equivalent fraction and the milliequivalents of M^{2+} ions in the exchanger corresponding to the measured heat exchange were calculated.

Treatment of Experimental Data

Evaluation of ΔG^0

The standard state reaction for the M^{2+}/Na^+ exchange system in the resin has been described by Boyd *et al.*[1] and is represented by Eq. (1).

$$2NaR\,(a = 1, \text{equil with } 0.1\ N\ NaCl) + MCl_2\,(aq, a = 1) = MR_2\,(a = 1, \text{equil with } 0.1\ N\ MCl_2) + 2NaCl\,(aq, a = 1) \quad \ldots (1)$$

The thermodynamic equilibrium constant, *K* for the above reaction was estimated following Gaines and Thomas[13] equation (2) (contributions from the solvent terms were neglected)

$$\ln K = -1 + \int_0^1 \ln K_c\, dN_M \quad \ldots (2)$$

where

$$K_c = \frac{N_M m_{Na}^2 \gamma_{Na}^2}{N_{Na}^2 m_M \gamma_M} = K_c' \frac{\gamma_{\pm\,NaCl}^4}{\gamma_{\pm\,MCl_2}^3} \quad \ldots (3)$$

In Eq. (3) K_c' is the experimental stoichiometric concentration product, N_M and N_{Na} are the equivalent fractions of the resinates, MR_2 and NaR in the exchanger, m_M and m_{Na} are the molalities of MCl_2 and NaCl respectively in solution, γ_M and γ_{Na} are the respective activity coefficients of M^{2+} and Na^+ ions in the electrolyte mixture and $\gamma_{\pm\,MCl_2}$ and $\gamma_{\pm\,NaCl}$ are the mean molal activity coefficients for the salts MCl_2 and NaCl respectively in the aqueous electrolyte mixture.

Activity coefficient of MCl_2 *and NaCl mixture*

The activity coefficient ratio, $\gamma_{\pm\,NaCl}^4 / \gamma_{\pm\,MCl_2}^3$ varied with the relative concentration of NaCl and MCl_2 in external solution since the ionic strength changed from 0.1 to 0.13. The method suggested by Boyd *et al*[1] for the sodium-zinc nitrate aqueous mixture has been used for the calculation of $\log[\gamma_{\pm\,NaCl}^4 / \gamma_{\pm\,MCl_2}^3]$.

Thus $B = 2B_{NaCl} - B_{MCl_2}$

The values of $B_{NaCl} = 0.005$, $B_{MgCl_2} = 0.2295$, $B_{CaCl_2} = 0.1605$, $B_{SrCl_2} = 0.1418$ and $B_{BaCl_2} = 0.0975$ were calculated as per the Eqs (5) and (6) of Boyd *et*

al[1] using the literature[14] values of $\gamma^{0}_{\pm\,NaCl}$ and $\gamma^{0}_{\pm\,MCl_2}$ for 0.1 *m* pure NaCl and MCl_2 solutions respectively. The B-values were then obtained from the above and are as follows:

Mixture	B
1. $MgCl_2$ + NaCl	0.2195
2. $CaCl_2$ + NaCl	0.1505
3. $SrCl_2$ + NaCl	0.1318
4. $BaCl_2$ + NaCl	0.0875

The $\log [\gamma^{4}_{\pm\,NaCl}/\gamma^{3}_{\pm\,MCl_2}]$ values were calculated for each set of experiment from a knowledge of the concentrations of NaCl and MCl_2 at equilibrium. This ratio varied from 0.1972 to 0.2193 for Mg^{2+}/Na^{+}; from 0.2042 to 0.2261 for Ca^{2+}/Na^{+}; from 0.2059 to 0.2279 for Sr^{2+}/Na^{+} and from 0.2103 to 0.2320 for Ba^{2+}/Na^{+} system.

The validity of the above method was verified by comparing the data with the published work. Platford[15] has reported the activity coefficients for a ternary system, H_2O-NaCl-$MgCl_2$ at 298K. Considering a case of a mixed electrolyte at a total ionic strength of unity ($\mu = 1$) where $m_{NaCl} = 0.4$ and $m_{MgCl_2} = 0.2$ the reported values for $\log \gamma_{\pm\,NaCl}$ and $\log \gamma_{\pm\,MgCl_2}$ are -0.173 and -0.326 respectively in the mixed electrolyte thus giving $\log [\gamma^{4}_{\pm\,NaCl}/\gamma^{3}_{\pm\,MgCl_2}] = 0.280$ which compares well with the value of 0.297 calculated by the above method by obtaining the B_{NaCl} and B_{MgCl_2} values at 1 *N* pure electrolytes of NaCl and $MgCl_2$ respectively. The agreement can be considered satisfactory since the comparison has been done for an electrolyte mixture of high ($\mu = 1$) concentration while the equations (5) and (6) used by Boyd *et al*[1] are best suited for dilute solutions.

The $\log K_c$ values were obtained from Eq. (3) and were plotted versus the equivalent fraction N_M (Figs 1 and 2). The curves were extrapolated on both sides to $N_M = 0$ and $N_M = 1$ and the areas under them were determined graphically.

The thermodynamic equilibrium constant was calculated using Eq. (2) and ΔG^0 was obtained from the expression (4)

$$\Delta G^0 \text{ (kJ/equiv.)} = -\tfrac{1}{2} RT \ln K \qquad \ldots (4)$$

Evaluation of ΔH^0

The quantity ΔH^0 is defined as the standard enthalpy change which accompanies the complete conversion of homoionic exchanger NaR to MR_2, each in their respective standard states. To find ΔH^0, the integral enthalpy of exchange per equivalent, ΔH, for the complete reaction must be derived from the experimental heats corrected for the enthalpy changes which occur in an electrolyte solution. Thus

$$\Delta H^0 = \Delta H + \tfrac{1}{2}\,\phi_L(MCl_2) - \phi_L(NaCl) \qquad \ldots (5)$$

where ϕ_L is the apparent molar heat content. The ΔH of total exchange was determined by numerical integration of the composition dependent differential heat of exchange, $(\delta \Delta H/\delta N_M)$.

$$\Delta H = \int_0^1 (\partial \Delta H/\partial N_M)\, dN_M \qquad \ldots (6)$$

The chord area technique[16] was applied for deriving the dependence of $(\partial \Delta H/\partial N_M)$ on the equivalent fraction, N_M in which the measured heats of partial exchange per equivalent were plotted as chords. A smooth curve defining $(\partial \Delta H/\partial N_M)$ as a function of N_M was drawn through the mid-points of the chords (Figs 3 and 4 where only midpoints have been plotted) such that the area above and below any given chord was equal. The area under the curve within the limits as per Eq. (5) was determined to obtain ΔH value.

The ϕ_L values were obtained from literature[17] and the $\Delta\phi_L$ values for Mg^{2+}/Na^{+}, Ca^{2+}/Na^{+}, Sr^{2+}/Na^{+} and Ba^{2+}/Na^{+} exchange systems were calcu-

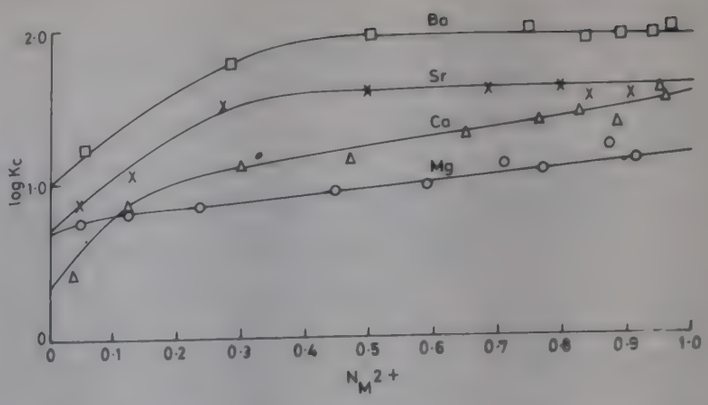

Fig. 1—M^{2+}/Na^{+} exchange on Dowex-50W×8 (aqueous)

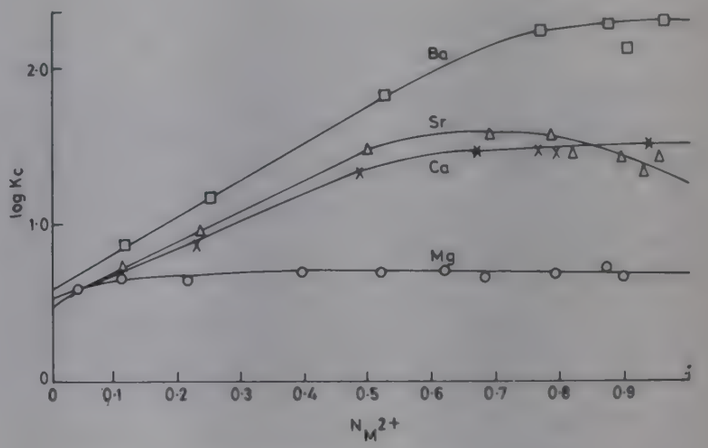

Fig. 2—M^{2+}/Na^{+} exchange on Amberlyst-15 (aqueous)

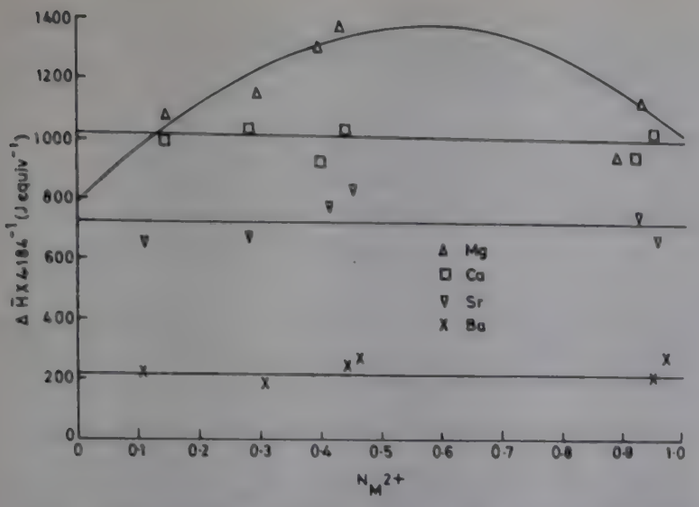

Fig. 3—Heats of partial exchange of M^{2+}/Na^{+} system as a function of $N_{M^{2+}}$ on Dowex-50W×8 (aqueous)

lated as 640, 586, 531, 515 J/equiv respectively by obtaining ϕ_L values for 0.1 *N* solutions.

Results and Discussion

The reliability of the equilibrium data was tested by conducting the equilibrium measurements for four exchange systems under investigation on Dowex-50×8 resin in duplicate. The duplicate results agreed within ± 5%.

The dependence of log K_c on ionic composition (loading) of the resins is shown in Figs 1 and 2 where log K_c increased with the equivalent fraction of the preferred ion for all the exchange systems except for Sr^{2+}/Na^{+} system on Amberlyst-15 where a decrease was observed at higher loading.

As mentioned earlier, Flett and Meares[10] have obtained equilibrium data of Bonner and coworkers[4-9] and substituted them for K_c in their Eq. (13) (see ref. 10) to calculate K which was not correct[11]. While the latter have used mole fraction of the resinate in their equation for the calculation of equilibrium constant, the former have used Gaines and Thomas[13] equation where equivalent fraction of the resinate has been used. For the counter ions of the same charge the mole fraction and equivalent fraction become equal but in the case of heterovalent system it is not so. The equation using mole fraction scale for the calculation of K differs from that based on equivalent fraction by a factor which is equal to the difference in the valences of the counter ions involved. Jangida[18] has explained this effectively by an illustrative example. Thus K values calculated by Flett and Meares[10] are in error by a factor of $(Z_B - Z_A)$ and in turn the free energy change, ΔG^x (cal/equiv) is in error by a factor of $-RT(Z_B - Z_A)/Z_A Z_B$.

The dependence of the differential heat of exchange, $\Delta \bar{H}$ on N_M is shown in Figs 3 and 4. $\Delta \bar{H}$ for

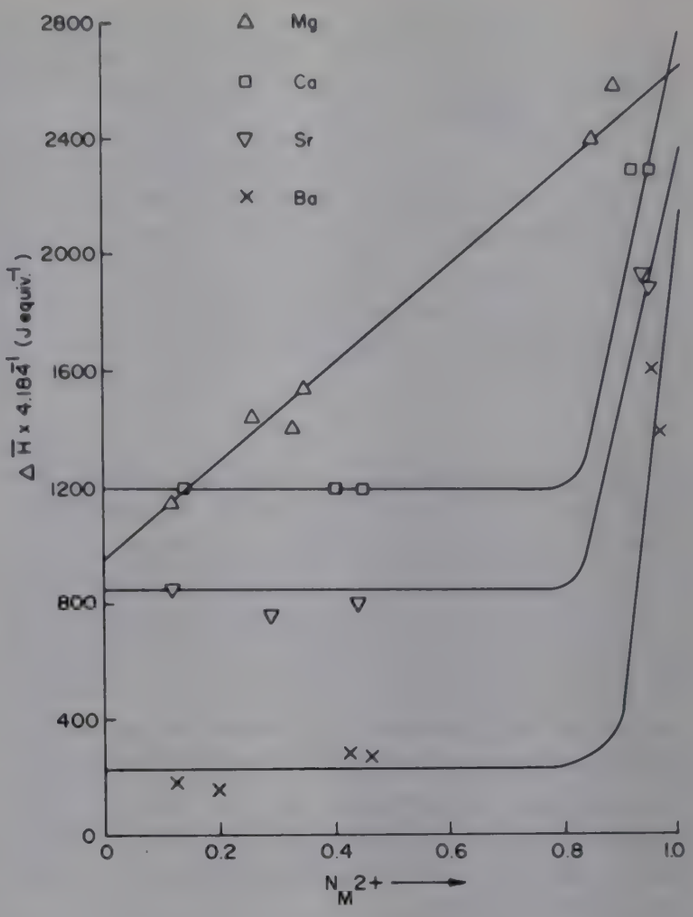

Fig. 4—Heats of partial exchange of M^{2+}/Na^{+} system as a function of $N_{M^{2+}}$ on Amberlyst-15 (aqueous)

Dowex-50×8 resin (Fig. 3) did not change with composition of resin except for Mg^{2+}/Na^{+} system where a maximum was observed and then a decrease at higher loadings. In the case of Amberlyst-15 resin (Fig. 4) $\Delta \bar{H}$ increased continuously with composition for Mg^{2+}/Na^{+} system but it remained constant for the rest three systems upto $N_M \simeq 0.8$ and then increased at higher loadings.

The ΔH^0 values reported here for Dowex-50W×8 have been compared with those calculated from the reported[10,19] values using the triangular rule. The values obtained were 6.81, 4.74, 3.74 and 2.02 kJ/equiv for Mg^{2+}/Na^{+}, Ca^{2+}/Na^{+}, Sr^{2+}/Na^{+} and Ba^{2+}/Na^{+} exchange systems respectively. All the ΔH^0 values for Dowex-50W×8 estimated in the present work were lower than the calculated ones[10,19] except for Ca^{2+}/Na^{+} system where the reverse was observed. The differences could be due to the fact that a different approach (dependence on composition) has been used in the present work for the evaluation of ΔH^0.

The four exchange reactions in both the resins were endothermic and the endothermicity decreased from magnesium through barium. The endothermicity was higher for the macroreticular resin, Amberlyst-15.

The endothermicity could be due to the fact that

Table 2—Standard free energies, enthalpies, and entropies of ion exchange reactions at 298 K on Dowex-50 × 8 and Amberlyst-15 in aqueous medium

Exchange system	Dowex-50W × 8			Amberlyst-15		
	$-\Delta G^0$ kJ/equiv	ΔH^0 kJ/equiv	ΔS^0 J/deg/equiv	$-\Delta G^0$ kJ/equiv	ΔH^0 kJ/equiv	ΔS^0 J/equiv/deg
Mg^{2+}-Na^+	1.54	5.66	24.2	0.77	8.21	30.1
Ca^{2+}-Na^+	2.09	4.89	23.5	2.15	6.16	27.9
Sr^{2+}-Na^+	2.84	3.54	21.4	2.46	4.69	24.0
Ba^{2+}-Na^+	3.95	1.52	18.4	3.44	1.99	18.2

the enthalpy change of an exchange reaction depends on the difference in energy of interacting counter ions with resin functional groups and on relative energy contributions due to the dehydrations of a counter ion entering the resin and hydration of a counter ion originally present in the ion exchanger. The heats of hydrations of M^{2+} ions are more exothermic relative to that of Na^+ ions. The amount of heat absorbed to remove M^{2+} ions from solution is only partially compensated by the heat evolved when two sodium ions enter the aqueous solution. This can be illustrated from the following hypothetical exchange reaction.

$$2Na^+(g) + M^{2+}(aq) \rightleftharpoons M^{2+}(g) + 2Na^+(g) \quad \ldots (7)$$

The ΔH^0 values were calculated for the above hypothetical reaction using the thermodynamic data from NBS Circular[20] 500 and were found to be 1113, 782, 636 and 494 kJ/mol for Mg^{2+}/Na^+, Ca^{2+}/Na^+, Sr^{2+}/Na^+ and Ba^{2+}/Na^+ systems respectively. These high values require complete dehydration of the ions. Since ΔH^0 obtained in Table 2 were of the order of 3-17 kJ/mol only, partial dehydration must have occurred during the exchange process. This partial dehydration must be proportional to the heats of hydration of the ions so that endothermic reactions can be expected for M^{2+}/Na^+ exchange systems. The decreasing endothermicity while going from magnesium through barium was also evident from ΔH^0 calculated for Eq. (7).

The standard enthalpy changes opposed the ion exchange reactions studied in the present work. It was thus purely entropy effect which was responsible for making ΔG^0 negative.

It is significant to note that the relative magnitudes of standard free energies of hydration[21] of Na^+ and M^{2+} ions are such that a large positive ΔG^0 of the hypothetical ion exchange reaction (Eq. 7) might be expected if these cations were completely dehydrated on entering the exchanger. However, the exchange systems reported in this work showed small negative ΔG^0 (Table 2) indicating, as suggested by Boyd *et al*,[1] that a balance must have occurred between the net enthalpy change (to partially dehydrate M^{2+} ion and to fully hydrate two Na^+ ions) and the net gain in entropy for the same process. The water contents of the resinates (Table 1) suggested that these ions retained their primary hydration shells so the observed ΔH^0 and ΔS^0 (shown in Table 2)) must have been governed by enthalpy and entropy effects associated with secondary hydration shells. The gain in entropy on removing this secondary water shell was thus sufficient to overcome the enthalpy change which opposed the ion exchange reaction in the first place.

The selective uptake of M^{2+} ions was accompanied by relatively large increase in standard entropy changes as is evident from Table 2. This suggested that extensive dehydration of M^{2+} ions must have taken place when they entered the exchanger since the values approached the entropy increase for the release of water by crystalline hydrates[22] (i.e. ca 39.3 J/mol deg). The sizeable increase in entropy suggested that transfer of water molecules from the exchanger to the dilute aqueous electrolyte mixture involved the release of bound water.

The measured values of ΔS^0 are the net result of two factors—contributions due to increased hydration of Na^+ ions when they enter aqueous phase and contributions due to decreased hydration of M^{2+} ions when they get exchanged. The contribution to the net ΔS^0 arising due to change in swelling, say in the case of Dowex-50W × 8, when Na^+ form of the resin is changed into M^{2+} form and the increased configurational[23] entropy (5.9 J/deg/equiv) when two Na^+ ions are replaced by one doubly charged M^{2+} ion may be considered small. Thus, increase in ΔS^0 is largely contributed by the difference in the entropies of hydration of the exchanging ions.

The increase in ΔS^0 could be explained due to higher negative entropies of hydration of M^{2+} ions as against that of the univalent Na^+ ions. The magnitude of increase in entropy due to differences in hydrations can be generalised if ΔS^0 for the hypotheti-

cal reaction (Eq. 7) can be calculated. In the absence of entropy data on gaseous ions ΔS^0 for Eq. 2 could not be calculated. The sodium and alkaline earth metal ions were not completely dehydrated in the resinates as may be seen from the water contents of the ionic forms of the resins.

The selectivity of the alkaline earth metal ions was found to be less on Amberlyst-15 compared to that on Dowex-50W × 8. This may be due to the effect of crosslinking. Gupta[24] has interpreted the effect of crosslinking on the selectivity of alkali metals in Dowex-50W resins in terms of various molecular interactions involved. A similar interpretation for the selectivity of alkaline earth metals cannot be given because the hydration numbers for these cations in solution as well as resin phases are not available. However, an attempt has been made to explain it qualitatively.

The macroreticular Amberlyst-15 resin can be considered to behave like a low cross-linked (< 8% DVB) resin compared to Dowex-50W × 8 resin since it imbibes more water (Table 1) due to its rigid structure and large pore sizes. The alkaline earth metals are able to form their hydration shells in the moderately crosslinked Dowex-50W × 8 resin where the disturbing effects of the normal water structure as well as anions are absent. With decrease in crosslinking as in the case of Amberlyst-15, Dowex-50W resin imbibes more water, and the hydration shells of the preferred cations are destroyed to a greater extent by the normal water structure formed by the free water present in the resin. When alkaline earth metals are transferred from solution to the resin phase, the change in hydration numbers in Amberlyst-15 will be less than that in Dowex-50W × 8. Similarly, when Na^+ ions are transferred from resin to solution, the change in its hydration number will be less in the former resin than that in the latter. Therefore, the total change in hydration numbers due to the above two steps is less in Amberlyst-15 than in Dowex-50W × 8. When the hydration number of a cation increases a negative contribution[24] or a positive contribution if it decreases, to ΔG would result. Thus the decrease in the hydration numbers of the cation in Amberlyst-15 will have positive contributions to ΔG^0 (Table 2) causing lower selectivities in the resin. The changes in hydration numbers account for the observed enthalpy changes as well. There is a positive contribution to ΔH^0 (Table 2) for Amberlyst-15 thus making them more endothermic than that for Dowex-50W × 8.

References

1 Boyd G E, Vaslow F & Lindenbaum S, *J phys Chem*, 71 (1967) 2114.
2 Jangida B L & Sundaresan M, *Indian J Chem*, 9 (1971) 1119.
3 Boyd G E, *J phys Chem*, 84 (1980) 2752.
4 Bonner O D & Payne W H, *J phys Chem*, 58 (1954) 183.
5 Bonner O D, *J phys Chem*, 58 (1954) 318.
6 Bonner O D & Livingstone F L, *J phys Chem*, 60 (1956) 530.
7 Bonner O D & Smith L L, *J phys Chem*, 61 (1957) 326.
8 Bonner O D, Jumper C P & Rogers C C, *J phys Chem*, 62 (1958) 250.
9 Bonner O D & Pruett R R, *J phys Chem*, 63 (1959) 1420.
10 Flett D S & Meares P, *Trans Faraday Soc*, 61 (1965) 1469.
11 Verified from Prof. P Meares (Private communication to one of the authors, BLJ).
12 Nandan D, Gupta A R & Shankar J, *Indian J Chem*, 10 (1972) 1172.
13 Gaines G L & Thomas H C, *J chem Phys*, 21 (1953) 714.
14 Robinson R A & Stokes R H, *Electrolyte solutions* (Butterworths, London) 1955, pp 497.
15 Platford R F, *J phys Chem*, 72 (1968) 4053.
16 Young T F & Vogel O G, *J Am chem Soc*, 54 (1932) 3030.
17 Harned H S & Owen B B, *Physical chemistry of electrolyte solutions*, (Reinhold, USA) 1950, pp 707.
18 Jangida B L, *Indian Agriculture (Spl Vol)* (1982) 27.
19 Boyd G E, Vaslow F & Lindenbaum S, *J phys Chem*, 68 (1964) 590.
20 Rossini F D, Wayman D D, Evans W H, Levine S & Jaffe I, *Selected values of chemical thermodynamic properties* (Circular of the National Bureau of Standards 500) 1952.
21 Latimer W M, *J chem Phys*, 23 (1955) 90.
22 Latimer W M, *Oxidation potentials* (Prentice-Hall, New Jersey) 1952, pp 364.
23 Cruickshank E H & Meares P, *Trans Faraday Soc*, 53 (1957) 1289.
24 Gupta A R, *Indian J Chem*, 29A (1990) 409.

Indian Journal of Chemistry
Vol. 30A, April 1991, pp. 328-334

Phase behaviour and physicochemical properties of a microemulsion obtained from an edible oil (saffola)

B K Paul†, M L Das, D C Mukherjee† & S P Moulik*
Department of Chemistry, Jadavpur University, Calcutta 700 032

Received 28 March 1990; revised and accepted 16 November 1990

A microemulsion obtained from edible oil saffola, Triton × 100, *n*-butanol and water (or brine) has been prepared and its phase behaviour and physicochemical properties have been studied. The ternary phase diagram shows an unusually large three-phase region. The single phase (1ϕ) microemulsion zone increases with increase in temperature and decreases in presence of brine, urea and cholesterol. The effect of the additives on the 1ϕ microemulsion zone varies in the order: urea ~ cholesterol < brine, upto 50% (w/w) oil as per phase diagram; thereafter, the order is cholesterol < brine < urea. The viscosity of the microemulsion (S + CoS 85%, oil 7.5% and brine 7.5% w/w) at different temperatures in presence of additives, viz., cholesterol, esters of cholesterol (acetate, benzoate and stearate), a crown ether (18 crown 6) and urea exhibits a systematic decrease, whereas the conductance varies non-systematically. Three distinct trends in conductance are witnessed in the range 10°-60°C at higher ratios of brine/oil. At lower ratios as well as in presence of additives two distinct zones are exhibited. A mild percolation phenomenon is observed at temperatures above 20°C which turns into a moderate phenomenon at 50°C. While increase in temperature imparts fluidity to the microemulsions, the conductance behaviour advocates stage wise changes in their internal (microscopic) structure.

Microemulsions for industrial use and fundamental studies primarily contain hydrocarbons (C_7-C_{12}), benzene, toluene, xylene, carbon tetrachloride, etc., as the oil constituent, whereas the pharmaceutical preparations are based on paraffin and vegetable oils. Fundamental studies[1-4] regarding the structure and dynamics have been much more numerous on the former class. In recent years, microemulsions have been used as liquid membranes, and transport of both electrolytes and non-electrolytes across them has been studied[5-7]. Microemulsions thus can mimic biological membranes as regards the transport of proteins and steroid bodies in the lipid matrix. Investigations on the formation and characterisation of such microemulsions are, therefore, of great importance. Recently, we have initiated studies on such systems, termed as 'biological microemulsions'[8,9], using cholesterol, esters of cholesterol, proteins and polymers as the constituents. The hydrocarbon oils so far used in the emulsion preparations are biologically noncompatible.

In the present paper we report the preparation, phase behaviour and physical properties of an emulsion system obtained from saffola (an edible oil and excellent source of pure linoleic acid), Triton × 100, *n*-butanol and brine. The effects of temperature and additives, viz., cholesterol, esters of cholesterol (acetate, benzoate and stearate), a crown ether (18 crown 6) and urea on the phase behaviour, viscosity and conductance of the system are reported. It is hoped that results of the present study will be useful in assessing the potential of vegetable oils as the base of biological microemulsions. Cholesterol and several of its esters have been used as additives in the system studied since sterol and its derivatives occur in cell membrane and blood[10]. The choice of crown ether and urea is arbitrary; the latter compound, of course, affects the lipid association and membrane structure.

Materials and Methods

The oil used, saffola, containing 73.3% linoleic acid, was a purified product obtained from M/s Bombay Oil Industries Pvt. Ltd., Bombay. Its estimated acid value was 0.40 mg of KOH per g of oil. Triton × 100 was a Sigma (USA) product with polydispersity in the ethylene oxide group (9.5 EO groups per molecule on the average). *n*-Butanol was a BDH (England) product (b.p. 117.3°C). These materials were used without further purification. The additives cholesterol (C), cholesteryl acetate (CA), cholesteryl benzoate (CB) and cholesteryl stearate (CS) had the specifications and quality reported

†Geological Studies Unit, Indian Statistical Institute, Calcutta 700 035
‡Department of Chemistry, Calcutta University, Calcutta 700 009

elsewhere[11]. The crown ether (18 crown 6) was obtained from Aldrich (USA). Sodium chloride (G R, S. Merck, India) and urea (ExcelaR grade, BDH, India) were used as received. Doubly distilled conductivity water of specific conductance 1-2 $\mu s\ cm^{-1}$ at 303 K was used for all the preparations.

Conductance of the microemulsions was measured with a Jenway (England) conductometer in a cell of cell constant 0.75 cm^{-1}. Viscosity measurements were made using a calibrated Ostwald viscometer of flowtime 54.6 sec for water at 30°C assuming newtonian behaviour of the microemulsions. Densities were measured with a calibrated pycnometer. Phase changes of microemulsions were studied with a SICO (India) polarising microscope.

All the measurements were made in a constant temperature water bath accurate to ± 0.1°C.

Preparation of microemulsion

Microemulsions were prepared by taking known amounts (by weight) of saffola, Triton × 100 and *n*-butanol in a series of stoppered and graduated glass test tubes which were placed in the thermostated bath at the desired temperature. Water was then progressively added from a microburette with constant stirring until each of the mixtures became just biphasic when viewed against crossed polarised light. Two ratios of the surfactant/co-surfactant (S/CoS), 1:5 and 1:8 (w/w), were used. The solutions with 1ϕ microemulsion were allowed to stand for considerable length of time for stability testing. Random check of samples stored for several weeks to several months revealed excellent stability. They neither became turbid nor separated into oil and water phases. We did not check the chemical stability of the polyunsaturated oil, saffola. It may be mentioned that its chemical instability did not affect the time dependent stability of the prepared microemulsions. The prepared microemulsions used for physicochemical studies at the temperatures 10°, 20° 30°, 40°, 50° and 60°C, fell inside the single phase zones and were, therefore, of Winsor IV type[12]. Unless mentioned otherwise, the preparations had S/CoS ratio of 1:5, but proportions of saffola and water varied. Addition of either extra oil or water yielded biphasic and triphasic preparations. In the triphasic system, the bottom phase was normally aqueous micellar solution of T × 100 with a low concentration of butanol followed by the middle isotropic microemulsion phase and the top phase of mainly oil with low concentrations of the surfactant and co-surfactant. To study the effects of the additives (brine, urea, cholesterol) on the phase behaviour, aqueous solutions of the first two and oil solution of the third were used as titrants.

Results and Discussion

Phase diagram

The pseudo-ternary phase diagrams of the saffola/T × 100/butanol/water system under different conditions were constructed. A representative diagram is depicted in Fig. 1. At 20°C and at S/CoS = 1:5, the single phase and the three phase zones are larger in comparison to those at S/CoS = 1:8. Such a large three phase zone is unusual. The extent of a phase was affected by the temperature. With increase in temperature from 30°C to 50°C, the single phase microemulsion zone (Winsor IV) increased; a larger three phase zone was observed at 40°C. The additives, NaCl (0.2 equiv. dm^{-3}), cholesterol (2.5% w/v) and urea (3 mol. dm^{-3}) at S/CoS = 1:5 decreased the single phase microemulsion zone as well as the three phase zone as per the phase diagram. The efficacy in decreasing the Winsor IV microemulsion zone followed the order: urea ~ cholesterol < NaCl upto 50% (w/w) oil content; thereafter, the order was: cholesterol < NaCl < urea.

In the quaternary multiphasic system usually it is very difficult to estimate the actual compositions of the different phases; only an overall estimate of their types is possible. For the present system, in the two phase region, the water rich samples were Winsor I (o/w) type and the oil rich samples were Winsor II (w/o) type. The middle phase of the triphasic samples was bicontinuous; the top and bottom phases were dilute solutions of Triton × 100 and *n*-butanol in oil and water respectively. The proportions of the individual phases varied with the concentrations of the components. The middle region of the triphasic compositions contained more of the bicontinuous phase than the end regions. It is noteworthy that in the phase diagrams a triphasic area is not centrally flanked touching three single phase regions; instead, it is touched by two single phase regions. The former pattern is the ideal situation, which is hardly (if ever) achieved in practice, particularly with multicomponent systems containing amphiphiles[13,14].

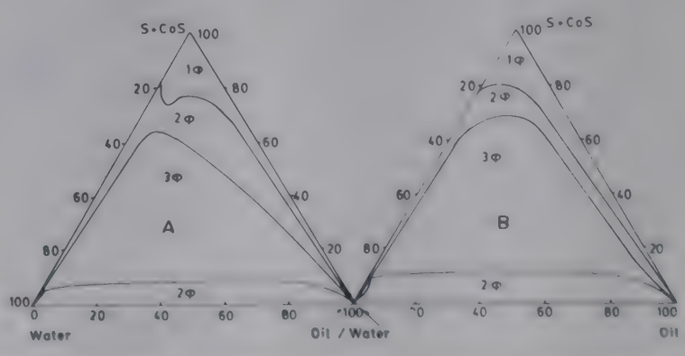

Fig. 1—Triangular phase diagram of saffola/T × 100/butanol/water system at 20°C [A, S/CoS = 1:8; B, S/CoS = 1:5].

Trials to produce the ideal situation were unsuccessful.

Viscosity behaviour

The viscosity of the microemulsion system was measured at different compositions with S + CoS varying in the range 48%-85% (w/w), oil in the range 2%-50% (w/w) and NaCl in the range 2%-15% (w/w). The viscosity was found to decrease as the brine/oil ratio and temperature increased (Fig. 2). The viscosity of the system at brine/oil ratio = 1 in presence of different additives, e.g., cholesterol (C, 0.5%-2.5%, w/v), cholesteryl acetate (CA, 2.5%, w/v), cholesteryl benzoate (CB, 1.60%, w/v), cholesteryl stearate (CS, 0.8%, w/v), urea (3 mol. dm^{-3}), crown ether (CE, 3%, w/v), crown ether + cholesterol (CE 3% + C 2.5%, w/v) was found to decrease gradually with increasing temperature. The curves for the additives are close together (Figs 2B & C). At brine/oil ratio 1 and above the viscosity remained unchagned at all temperatures. The plots of log η vs T^{-1} were fairly linear and yielded the energy of activation, ΔE^{*}_{vis} for the viscous flow of the microemulsions. The ΔE^{*}_{vis} values are presented in Tables 1 and 2. The values remain practically unaffected in presence of the additives as well as for the varying brine/oil ratios. Only 2.5% C and 1.6% CB lowered ΔE^{*}_{vis}; the flowing microemulsion crossed a lower barrier during transport. This was in contrast to the behaviour in presence of 3% CE, where the barrier was higher.

Conductance behaviour

The conductance-temperature profiles of the microemulsions at different brine/oil ratios without additives exhibited three distinct regions at higher ratios (Fig. 3). In the lower temperature range (10°-20°C), the conductance sharply declined. In the middle range (20°-50°C), there was a mild increase, whereas a rapid increase was observed in the upper

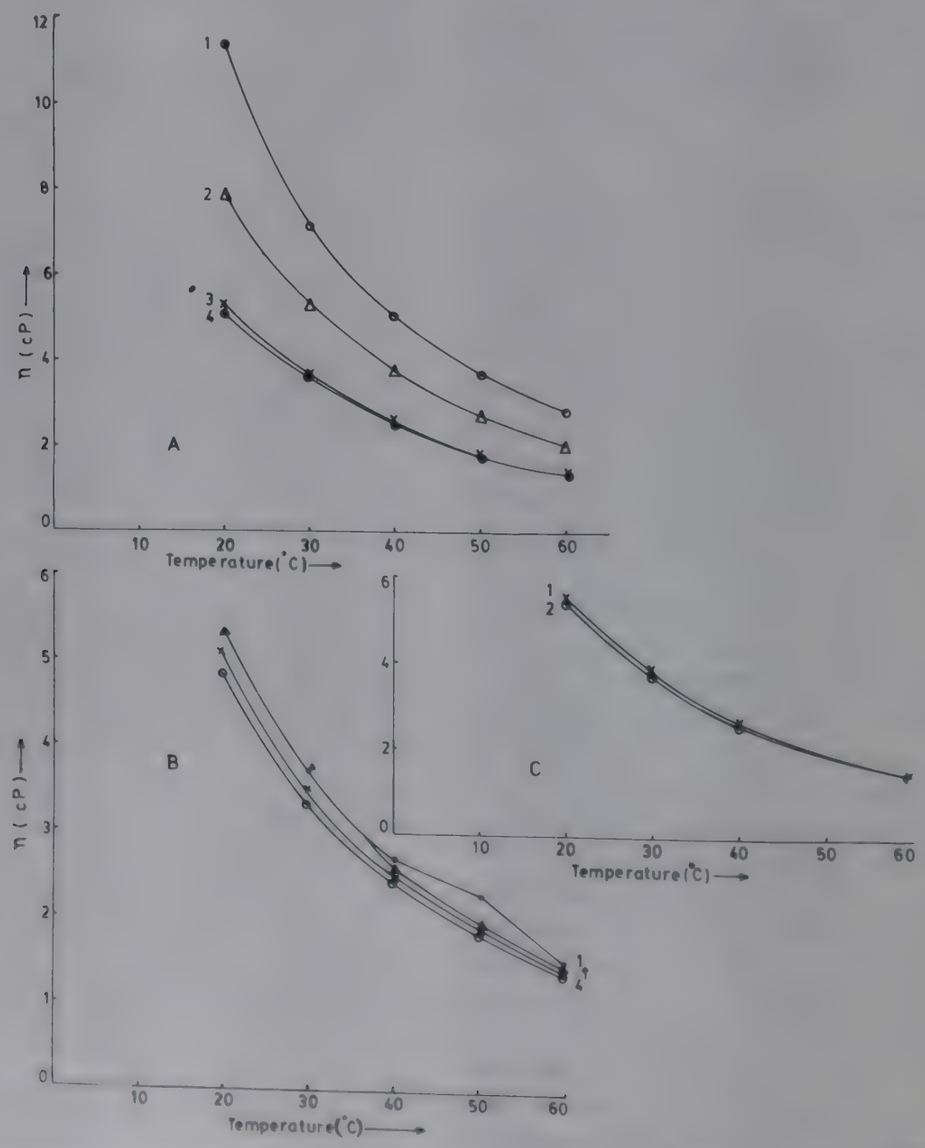

Fig. 2—Temperature dependent viscosity of microemulsion [A: curves 1-4, brine/oil ratio, 0.05, 0.2, 1.0, 7.5; B: brine/oil = 1, curves 1-4, 2.5% C, 2.5% CA, 1.6% CB, 0.8% CS w/v; C: brine/oil = 1, curves 1-2, (2.5% C + 3% CE), (2.5% C + 3 mol dm^{-3} urea].

Table 1—Activation energies for ionic conduction and viscous flow of saffola/T × 100/butanol/brine (0.2 equiv. dm^{-3}) microemulsion)

Composition (S + CoS/oil/brine)	B/O	ΔE^*_{cond} (kJ mol^{-1})			ΔE^*_{vis} (kJ mol^{-1})
		Slope 1	Slope 2	Slope 3	
55/43/2	(0.047)	—	—	—	27.4
48/50/2	(0.04)	—	—	+ 2.3	—
70/25/5	(0.2)	—	3.74	−35.1	27.1
80/15/5	(0.33)	—	8.74	−34.96	—
85/7.5/7.5	(1.0)	55.9	1.3	−42.9	26.1
85/5/10	(2.0)	49.9	6.8	−44.5	—
83/2/15	(7.5)	17.7	3.5	−46.0	26.6

Table 2—Activation energies for ionic conduction and viscous flow of saffola/T × 100/butanol/brine (0.2 equiv. dm^{-3}) microemulsion of composition (85/7.5/7.5 as (S + CoS/oil/brine) in presence of additives

Additives (0%, w/w)	ΔE^*_{cond} (kJ mol^{-1})			ΔE^*_{vis} (kJ mol^{-1})
	Slope 1	Slope 2	Slope 3	
0	55.9	1.3	−42.9	26.1
C (0.5)	—	4.0	1.1	—
C (1.0)	—	3.6	2.2	—
C (2.5)	—	3.6	0	24.5
CA (2.5)	—	3.9	1.3	25.9
CB (1.6)	—	3.1	1.8	25.4
CS (0.8)	—	2.9	−31.7	26.0
C (2.5) + urea (3 mol dm^{-3})	7.4	21.6	−21.89	25.6
CE (3.0)	—	2.7	−28.6	27.5
C (2.5) + CE (3.0)	—	0.94	−29.7	26.9

range (50°-60°C). At brine/oil ratios of 0.33 and 0.2, the third stage was absent.

The conductance of w/o microemulsion may increase with temperature and may undergo a rapid change after a threshold value; this phenomenon is called percolation[15-20]. Above this threshold, the micro water droplets suffer sticky collisions forming clusters through which ions in the water pools efficiently migrate[21-25]. In the present system, a moderate percolation appeared above 50°C. The rapid decline in conductance between 10° and 20°C is very unusual. In certain systems, only a mild initial decrease in conductance has been observed[25]. The additive cholesterol removed the first stage of decrease in conductance and shifted the initial percolation transition to higher temperature. A similar effect was exhibited by CA and CB; CS, however, retained the features of the lower temperature range and removed the second transition (Fig. 4). Both C and CE in combination, and CE alone exhibited effects parallel to that of CS. In combination with C, urea showed the normal features with lowering of the second transition (results are not presented). The above phenomena are striking. The internal structure of microemulsion, controlling the conductance behaviour, seems to be significantly susceptible to environmental modification. This was not at all reflected in the viscosity behaviour.

The activation energy for conduction was determined from the log σ versus T^{-1} plots; the estimated ΔE^*_{cond} values are presented in Tables 1 and 2. Three stages of variation of conductance resulted in three values of ΔE^*_{cond} for sets having brine/oil ratios 7.5, 2.0 and 1.0. Two other ratios (0.33 and 0.2) yielded two ΔE^*_{cond} values, and the lowest ratio (0.04) exhibited a single value. Graphical presentations are not shown to save space. The ΔE^*_{cond} values obtained from slope 1 in log σ vs T^{-1} plot corresponded to the phenomenon of second percolation. The values derived from slope 2 corresponded to the first stage of percolation and those from slope 3 represented the initial stage of conduction. For the additives C, CA, CB, CS and CE, the second percolation was absent and, therefore, the

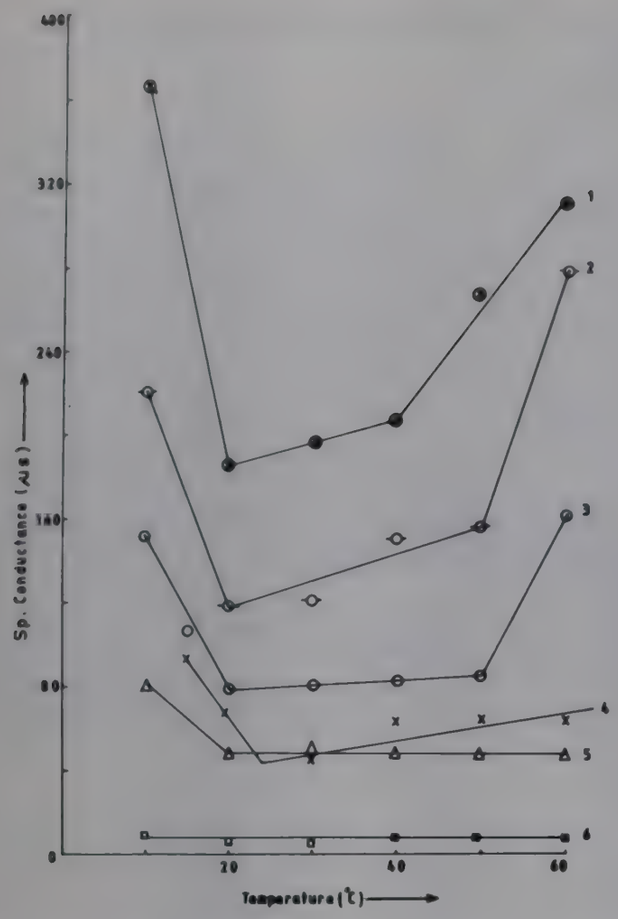

Fig. 3—Specific conductance of microemulsions as a function of temperature [Curves 1-6, brine/oil ratio 7.5, 2.0, 1.0, 0.33, 0.2 & 0.04 respectively].

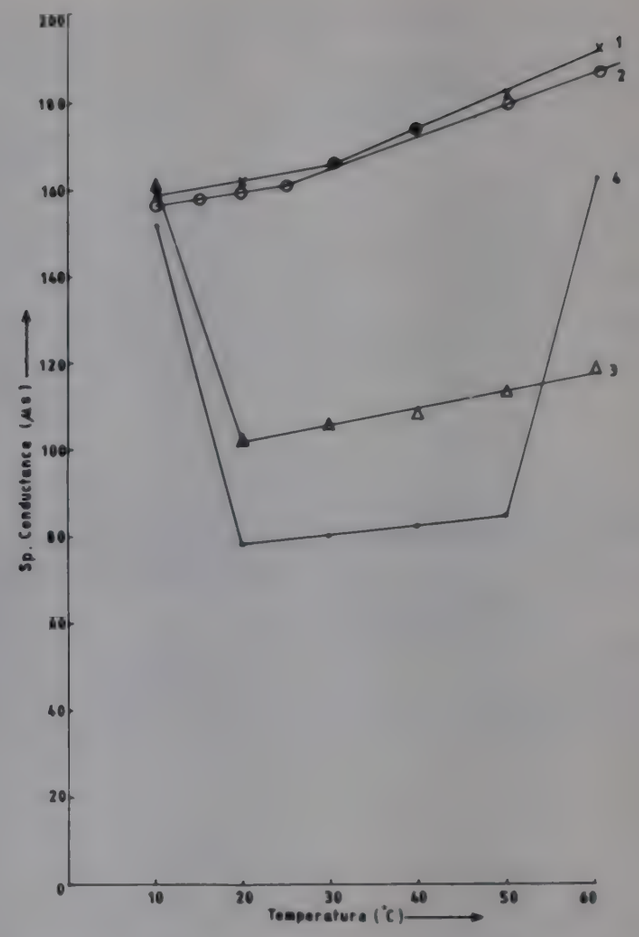

Fig. 4—Specific conductance of microemulsions as a function of temperature at brine/oil = 1 [Curves 1-4, 2.5% CA, 1.6% CB, 0.8% CS & 0% additive w/v].

results under slopes 2 and 3 are presented. Only urea in combination with C offered three distinct values of ΔE^*_{cond}. It must be noted that in both the lower and upper stages, the evaluation of ΔE^*_{cond} was mainly based on two data points; the results, therefore, were less accurate. But since the transitions were sharp, their locations might be close to those shown in the figures. Since the differences in the slopes relative to the middle range were appreciable, they could be indicative of the trend in the energetics of conductance. The long time required for completion of duplicate sets of measurements (usually 8-10 hr for a set) was a constraint and the study could be carried out at a limited number of temperatures only.

The earlier reported[25,26] activation energies for hydrocarbon oils are in the range 500-750 kJ mol^{-1} in comparison to the present values of 2-50 kJ mol^{-1}. The additives C, CA, CB and CS decreased the ΔE^*_{cond} for the first stage (slope 3) by nearly 50 units (Table 2). The transport of ions, upon sticky collisions[22,23] among the micro brine droplets, became easier in presence of the additives. The threshold percolation temperatures increased in the additive environments as was also observed with hydrocarbon oils[25,27]. The effects of urea and crown ether alone and in combination were distinct. Urea increased the ΔE^*_{cond} for the second percolation process, which was absent in presence of crown ether. The activation energy for conduction for the first percolation in presence of CE was, however, comparable to that in presence of other additives. The higher positive ΔE^*_{cond} in presence of urea may be ascribed to the hindrance offered by urea to the clustering of water droplets by interaction (urea reduces water structure or its association[28-30]).

The plot of conductance (σ) versus weight per cent of surfactant plus brine (S + B) revealed occurrence of conductance maximum and minimum at 14% and 16% (w/w) of (S + B) respectively in the temperature range 10°-60°C (Fig. 5). Except at 10°C, the trends at other temperatures were systematic; the conductance maximum decreased with decreasing temperature whereas all the minima crowded in a narrow region. The above phenomena suggested transitions in the internal structure of the microemulsion occurring at 14% and 16% (S + B). The viscosity decreased upto 19% (S + B) and remained unchanged thereafter. The higher the temperature, the lower was the effect. The weight per

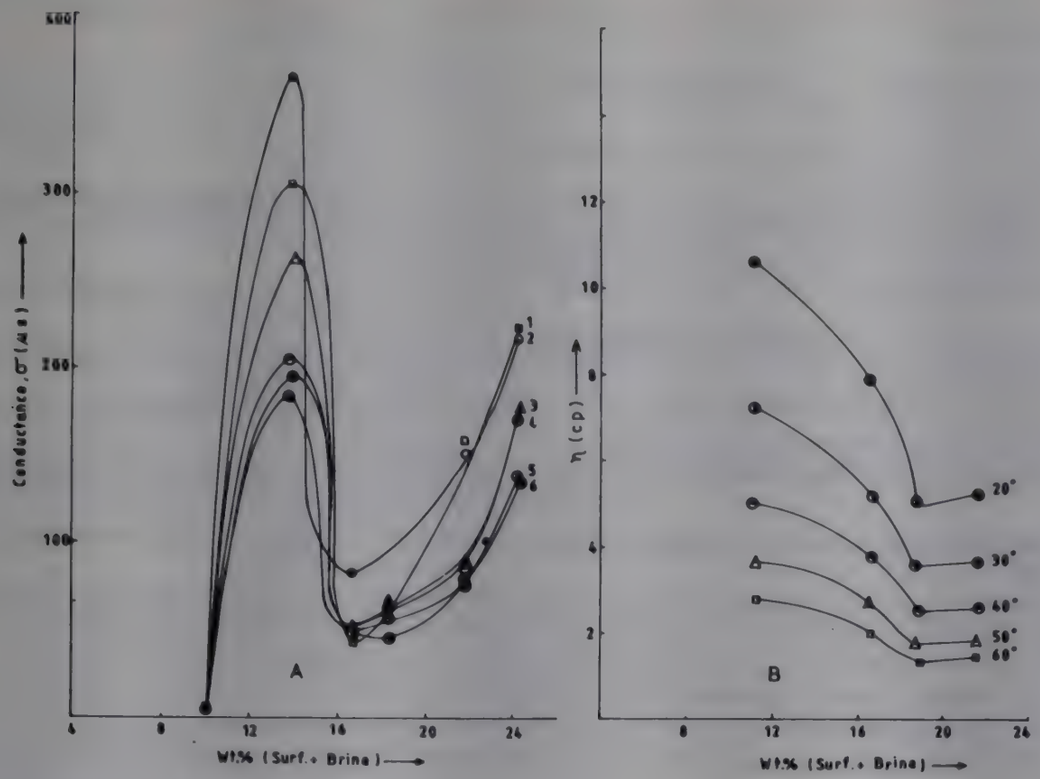

Fig. 5—(A) Specific conductance & (B) viscosity of microemulsions as a function of weight % of surfactant + brine at different temperatures [A: curves 1-6, 60°, 10°, 50°, 40°, 30° & 20°C respectively].

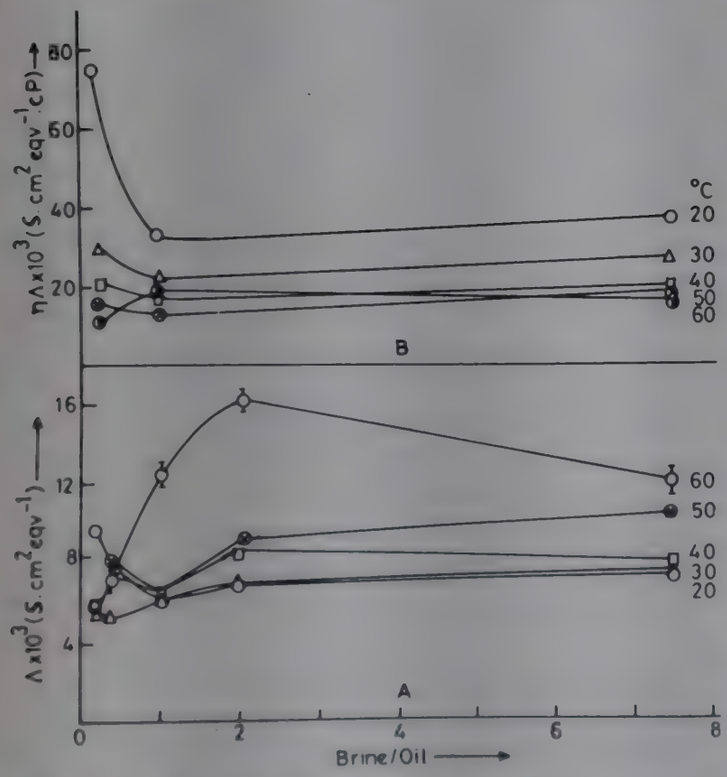

Fig. 6—(A) Equivalent conductance & (B) Walden product of microemulsion as a function of brine/oil ratio at different temperatures.

cents of (S+B) for conductance minima more or less corresponded to the viscosity minima. The equivalent conductance (Λ) varied nonsystematically with increase in the brine/oil ratio (Fig. 6). The effect was pronounced upto the brine/oil ratio 2. At 60°C, there was a systematic increase, and a decline thereafter. The Walden product Λη sharply decreased upto brine/oil = 1, beyond which (upto 7.5) it remained almost constant. An initial increase was observed at 60°C. The Walden product, on the whole, decreased with temperature, the change in conductance was not compensated by the change in viscosity upto brine/oil = 1; afterwards it was exact. Variable Walden products of microemulsions have been observed earlier also[18].

Acknowledgement

Partial financial support for this work was rendered by the Indian Statistical Institute, Calcutta. Thanks are due to Mr A K Das (G S U) for preparing illustrations and to Mr D K Saha (G S U) for typing the manuscript.

References

1 Gueruif P & Lindman B, *Langmuir*, 1 (1985) 464.

2 Stilbs P & Lindman B, *Progr Colloid Polym Sci*, 69 (1984) 39.

3 Friberg S, *Colloids & Surfaces*, 4 (1982) 201.

4 Kahlweit M, Lessuer E & Stray R, *J phys Chem*, 87 (1983) 5032.

5 Wong K H, Yagi K & Smid J, *J membr Biol*, 18 (1974) 379.

6 Xenakis A & Tondre C, *J phys Chem*, 87 (1983) 4737.

7 Tondre C & Xenakis A, *Faraday Discuss chem Soc*, 77 (1984) 771.

8 Das M L, Bhattacharya P K & Moulik S P, *Indian J Biochem Biophys*, 26 (1989) 24.

9 Das M L, Bhattacharya P K & Moulik S P, *Langmuir* (in press).
10 Parkar W E, Koos l E & Sw n D, in *Biochemical preparations* (Wiley, New ork) Vol , 1955.
11 Mukhopadhyay L, Bhattach ya P K & Moulik S P, *Indian J Biochem Biophys*, 26 (1989) 178.
12 Winsor P A, *Trans Faraday Soc*, 44 (1984) 376.
13 Bourrel M & Schechter R S, in *Microemulsions & related systems* (Marcel Dekker Inc, New York & Basel) 1988, Ch 4, pp 130-152.
14 Das M L, Bhattacharya P K & Moulik S P, *Langmuir* (in press).
15 Lagues M, *J Phys Lett (Orsay, Fr)*, 40 (1979) L33.
16 Robb I D, *Microemulsion*, (Plenum, New York) 1982.
17 Bisal S R, Bhattacharya P K & Moulik S P, *J phys Chem*, 94 (1990) 350.
18 Bisal S R, Bhattacharya P K & Moulik S P, *Indian J Chem*, 28A (1989) 550.
19 Lagues M, Ober R & Taupin C J, *J Phys Lett (Orsey, Fr)*, 39 (1978) L487.
20 Geiger S, Eicke H F & Spielmann, *Z Phys B, Condensed Matter*, 68 (1987) 175.
21 Kim M W & Huang J S, *Phys Rev A*, 34 (1986) 719.
22 Safran S A, Grest G S & Bug A L R, in *Microemulsion systems*, edited by H L Rosano & M Clausse (Marcel Dekker, New York) 1987.
23 Jada A, Lang J & Zana R, *J phys Chem*, 93 (1989) 10.
24 Jada A, Lang J, Candau S J & Zana R, *Colloids & Surfaces*, 38 (1989) 251.
25 Jada A, Lang J, Zana R, Makhlonfi R, Hirsch E & Candau S J, *J phys Chem*, 94 (1990) 387.
26 Mathew C, Patanjali P K, Nabi A & Maitra A N, *Colloids & Surfaces*, 30 (1988) 253.
27 Dutkiewicz E & Robinson B H, *J electroanal Chem*, 251 (1988) 11.
28 MacDonald J C, Ser Phillips J & Guerrera J J, *J phys Chem*, 77 (1973) 370.
29 Franks F, *Water, A comprehensive treatise* (Plenum, New York), Vol. 4, 1978.
30 Kresheck G C & Scheraga H A, *J phys Chem*, 69 (1965) 1704.

Indian Journal of Chemistry
Vol. 30A, April 1991, pp. 335-339

Studies of L-α-phosphatidylcholine impregnated parchment paper model membrane

Fasih A Siddiqi*, Mohd N Beg & Surendra P Singh
Membrane Research Laboratory, Chemistry Department, Aligarh Muslim University, Aligarh 202 002, India

Received 12 July 1990; revised 1 October 1990; accepted 8 November 1990

Measurements of bi-ionic potential (BIP) across L-α-phosphatidylcholine impregnated parchment paper model membrane have been carried out in a cell of the type,

$$\underset{C_1}{SCE\,|A^+M^-|}\ membrane\ \underset{C_1}{|B^+M^-|\,SCE}$$

The magnitude of the BIP depends upon the concentration and nature of the cations. Theories based on the principles of irreversible thermodynamics as proposed by Tasaka *et al.* [*J memb Sci*, 24 (1985) 29] and Toyoshima *et al.* [*J phys Chem*, 74 (1970) 2704] have been compared to obtain a relationship which has been used for the evaluation of theoretical values of bi-ionic potentials. The close agreement between the theoretical and the observed values confirms the applicability of the derived relationship to the membrane-electrolyte systems used in these investigations.

A potential difference is observed between the two sides of a membrane when the membrane separates two electrolyte solutions of the same molar concentrations with a common co-ion but different counter ions. The membrane potential is called the bi-ionic potential (BIP)[1-3]. Extensive studies have been initiated to understand the complex behaviour of biological membranes by developing various artificial membranes such as parchment supported or cellophane supported systems, which may mimic some properties of biological membranes[4-9]. However, investigation of the physiochemical processes occurring in biological membranes is frequently discouraged by the complex structure and multicomponent nature of these membranes. This fact is responsible for the great interest in the study of properties of simple model systems, among which bilayer lipid membranes (BLMs) and liposomes have been most commonly studied[10-12].

Some authors have studied model membranes in the form of porous substrates, such as ultrafilters impregenated with organic solvents[13] and lipid dissolved therein[14,15]. In the present study, we have prepared L-α-phosphatidylcholine (L-α-lecithin) parchment supported membrane and measured the BIP across the membrane. The conductance behaviour of this lipid membrane with respect to some common electrolytes has been studied at different temperatures.

Materials and Methods

L-α-Phosphatidylcholine was purified as described earlier and kept *in vacuo*. Chloroform and methanol were twice distilled. Doubly distilled water (over potassium permanganate) was used in the present experiments. The lipid solution was prepared by dissolving the pure lipid in chloroform-methanol mixtures (2:1, v/v) to which *n*-decane (20% of the lipid amount) was added so as to prevent solidification of the lipid. One milliliter of this solution was used to form a thin lipid layer on parchment paper. For doing this, the cell containing the parchment paper was clamped vertically and the lipid solution was added dropwise onto the parchment paper with a pipette. After the addition of a drop, the solvent mixture was quickly evaporated vigorously before the addition of the next drop. This resulted in the complete evaporation of the liquid, leaving a thin layer of the lipid covering the whole of parchment paper in the cell.

The potential developed by setting up a concentration cell (A) was measured using a potentiometer at 25°C ± 1°C and saturated calomal electrode (SCE). The cell potential was taken as a measure of BIP.

SCE	Solution A^+M^- I (C_1)	L-α-phosphatidylcholine model membrane (A)	Solution B^+M^- II (C_1)	SCE

For conductometric measurements, the membrane was first equilibrated with an electrolyte solution. The latter was then replaced by purified mercury without removing the adhering surface liquid. Platinum electrodes dipping in mercury were used to es-

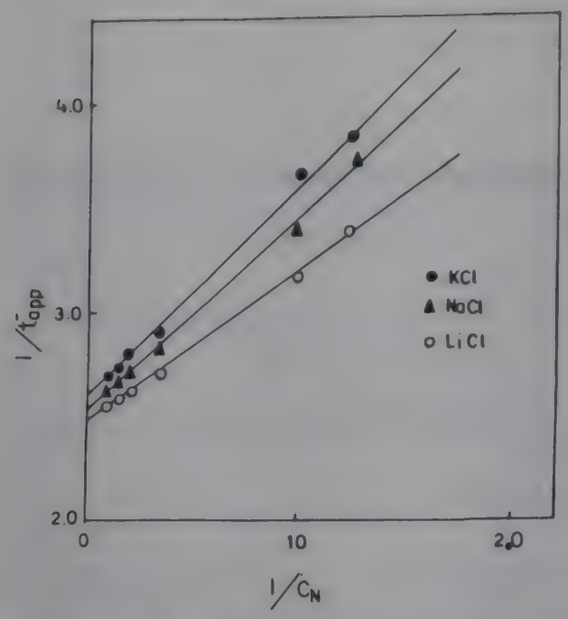

Fig. 1—Plots of $1/t_{app}$ versus $1/C_N$ for various electrolytes for L-α-phosphatidylcholine model membrane.

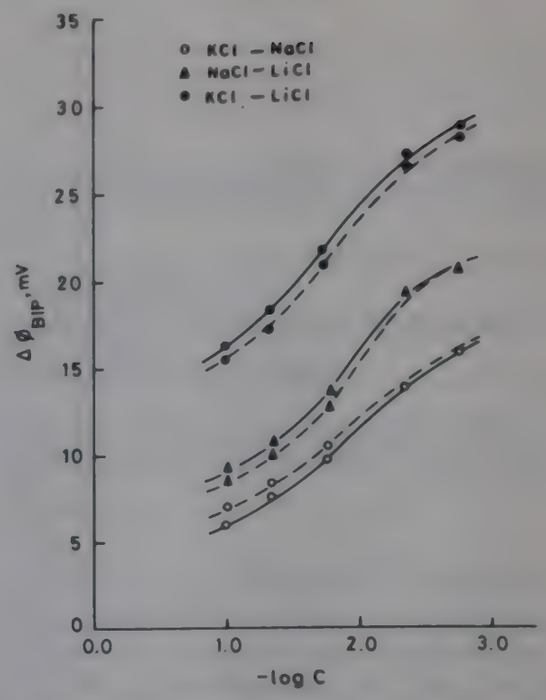

Fig. 2—Plots of calculated (—) and observed (—) values of $\Delta\phi_{BIP}$ versus $-\log C$ for L-α-phosphatidylcholine model membrane.

tablish electrical contact for conductance measurements.

The electrolyte solutions were prepared by dissolving analytical grade reagents in doubly distilled water.

Results and Discussion

By definition[16] the BIP is the algebraic sum of the two potentials arising at the two solution-membrane interfaces and the liquid junction potential arising because of the membrane.

On the basis of flow equations based on the thermodynamics of irreversible processes, Toyoshima and Nozaki[1] derived the following equation for the steady electromotive force, called the bi-ionic potential, of a bi-ionic cell, containing two electrolytes (with a common anion but different cations) separated by a membrane,

$$\Delta\phi_{BIP} = \left[2 \ln \left(\frac{K_{A^+}}{K_{B^+}}\right) + \ln (JV_{A^+} + 1)/(JV_{B^+} + 1)\right] \times (F/RT) \quad \ldots (1)$$

where K_{A^+}/K_{B^+} is the selectivity constant of a membrane for positive ions A^+ and B^+ and the terms V_N and J are defined as,

$$V_N = 1 + \frac{u_+^0}{u_-^0} (N = A^+, B^+) \quad \ldots (2)$$

$$(2J + 1) \ln (g_{A^+} + 2J)/(g_{B^+} + 2J) - \ln (JV_{A^+} + 1)/(JV_{B^+} + 1) = g_{A^+}/g_{B^+} \quad \ldots (3)$$

where $g_N = 1 + [1 + (2 K_N C/X)^2]^{1/2}$ ... (4)

In order to evaluate V_N and X/K_N with the help of data of apparent transferable number of anion (t_{app}) and thermodynamically effective fixed charge density (X) of the membrane, the following expression has been proposed,

$$1/t_{app} = V_N + (V_N - 1)(\gamma - 1)/\gamma \ln \gamma \left(\frac{X}{K_N}\right)\left(\frac{1}{C_N}\right) + \quad \ldots (5)$$

Equation (5) indicates that the intercept and slope of a straight line plot of $1/t_{app}$ against $1/C_N$ at fixed γ (Fig. 1) will give the values of V_N and X/K_N respectively. The values of V_N were found to be 2.60, 2.54 and 2.48 for KCl, NaCl and LiCl respectively, while the X/K_N values were 0.16, 0.15 and 0.12 respectively for these salts. These values may then be utilized to evaluate g_N with the help of Eq. (1). With the help of these parameters for a membrane-electrolyte system, the values of J and $\Delta\phi_{BIP}$ can be calculated using Eqs (3) and (1), respectively.

The observed and calculated values of bi-ionic potentials for the L-α-phosphatidylcholine (L-α-lecithin) model membrane in contact with different pairs of electrolytes are plotted against log C in Fig. 2. It is apparent from the figure that there is a good agreement between the observed and theoretical values of bi-ionic potentials and it may be concluded that the theory of Toyoshima and Nozaki[1] is fairly well applicable to L-α-phosphatidylcholine model membrane.

Table 1—Values of mobility ratio of various alkali metal ion pairs for the L-α-phosphatidylcholine membrane

Concentration (*M*)	U_{K^+}/U_{Na^+}	U_{Na^+}/U_{Li^+}	U_{K^+}/U_{Li^+}
0.1/0.1	1.31	1.41	1.84
0.05/0.05	1.37	1.47	1.95
0.02/0.02	1.49	1.62	2.25
0.005/0.005	1.72	2.08	2.76
0.002/0.002	1.86	2.21	2.95

Table 2—Values of selectivity constant (K_{ij}) of various alkali metal ion pairs for the L-α-phosphatidylcholine model membrane

Concentration (*M*)	$K_{K^+}/_{Na^+}$	K_{Na^+}/Li^+	K_{K^+}/Li^+
0.1/0.1	1.01	1.01	0.96
0.05/0.05	1.02	1.04	1.00
0.02/0.02	1.03	1.05	1.08
0.005/0.005	1.04	1.07	1.16
0.002/0.002	1.05	1.08	1.18

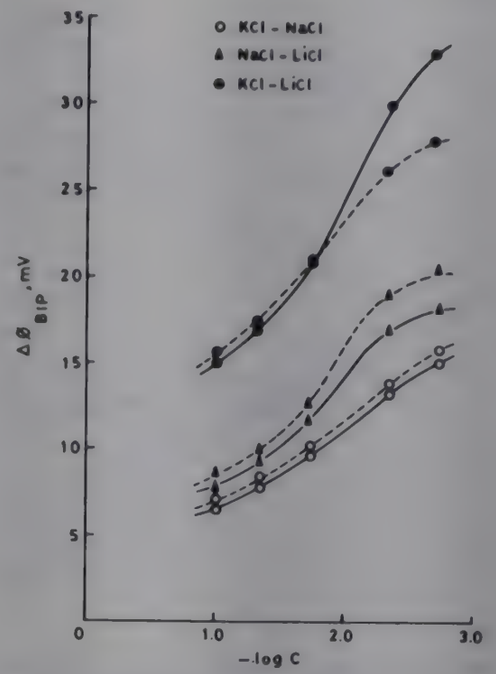

Fig. 3—Plots of calculated (—) and observed (---) values of $\Delta\phi_{BIP}$ versus $-\log C$ for L-α-phosphatidylcholine model membrane.

Theoretical values of $\Delta\phi_{BIP}$ can also be obtained with the help of Eq. (6), derived on the basis of a recent theory of Tasaka *et al.*[8] using the principle of irreversible thermodynamics as,

$$\Delta\phi_{BIP}=\frac{RT}{Z_{A^+}F}\ln\frac{l_{A^+}\bar{C}_{A^+}(1)+l_{\bar{m}}\bar{X}_{\bar{m}}(1)}{l_{B^+}\bar{C}_{B^+}(2)+l_{\bar{m}}\bar{X}_{\bar{m}}(2)} \quad \ldots (6)$$

where $l_{A^+}=l_{A^+A^+}+l_{B^+A^+}-l_{\bar{m}A^+}$

$l_{B^+}=l_{A^+B^+}+l_{B^+B^+}-l_{\bar{m}B^+}$

$l_{\bar{m}}=-l_{A^+\bar{m}}-l_{B^+\bar{m}}-l_{\bar{m}\bar{m}}$

$\bar{C}$ represents the concentration of counter ions (A^+, B^+) or co-ion ($\bar{m}$) in the membrane phase and (1) and (2) refer to the two surfaces of the membrane. At the limit of low electrolyte concentration, Eq. (6) reduces to,

$$\Delta\phi_{BIP}=\frac{RT}{Z_{A^+}F}\ln l_{A^+}/l_{B^+} \quad \ldots (7)$$

while at the limit of high electrolyte concentration Eq. (6) gives,

$$\Delta\phi_{BIP}=\frac{RT}{Z_{A^+}F}\ln\left(\frac{l_{A^+}+l_{\bar{m}}}{l_{B^+}+l_{\bar{m}}}\right) \quad \ldots (8)$$

Comparison of this equation with that of Nozaki[1] for uni-univalent electrolytes gives,

$$\Delta\phi_{BIP}=\frac{RT}{F}\left[2\ln\frac{S_{A^+\bar{m}}}{S_{B^+\bar{m}}}+\ln\frac{(jV_{A^+}-1)}{(jV_{B^+}-1)}\right] \quad \ldots (9)$$

where $S^2_{N\bar{m}}=\exp(1-/RT)(\bar{\mu}^0_N-\mu^0_N)$

$+(\bar{\mu}^0_m-\mu^0_m)(N=A^+,B^+)$ ... (10)

$j=(j_{A^+}+j_{B^+})(V_{A^+}j_{A^+}+V_{B^+}j_{B^+})$ ... (11)

$j_N=-J_N/RT\ln X$ ... (12)

$V_N=1+l_{A^+}/l_{B^+}$ ... (13)

μ^0_N and $\mu_{\bar{m}}$ are the standard chemical potentials of counter ions and co-ions, respectively, and symbols with an overbar indicate the membrane phase.

As at the limit of low electrolyte concentration the solute flux through a charged membrane, J_N, is governed only by the co-ion species[9], we obtain

$-j_{A^+}/j_{B^+}=l_{A^+}/l_{B^+}$ ... (14)

On the other hand, at the limit of high electrolyte concentration, we get

$-j_{A^+}/j_{B^+}=(1_{B^+}+l_{\bar{m}})/(l_{A^+}+l_{\bar{m}})$ ... (15)

Comparison of Eqs (2) and (13) gives

$l_{A^+}/l_{\bar{m}}=U^0_{A^+}/U^0_{\bar{m}}$ ... (16)

and

$l_{B^+}/l_{\bar{m}}=U^0_{B^+}/U^0_{\bar{m}}$ ... (17)

On dividing Eq. (16) by (17), we get

$l_{A^+}/l_{B^+}=U^0_{A^+}/U^0_{B^+}$

Hence, in terms of mobility ratio, Eq. (7) becomes

$$\Delta\phi_{BIP}=\frac{RT}{Z_{A^+}F}\ln U^0_{A^+}/U^0_{B^+} \quad \ldots (18)$$

Equation (18) affords the calculation of theoretical

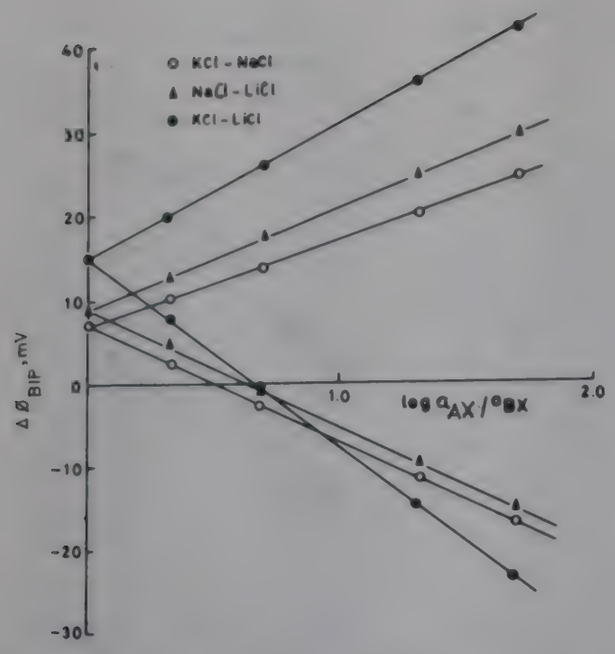

Fig. 4—Plots of $\Delta\phi_{BIP}$ versus log a_{AX}/a_{BX} for L-α-phosphatidylcholine model membrane.

value of bi-ionic potential, if the value of the mobility ratio is known. The mobility ratio, $\bar{U}_{A^+}/\bar{U}_{B^+}$, has been expressed[17] as

$$\bar{U}_{A^+}/\bar{U}_{B^+} = \bar{m}_{A^+}\bar{\lambda}_{A^+}/\bar{m}_{B^+}\bar{\lambda}_{B^+} \quad \ldots (19)$$

where $\bar{m}_{A^+}$ and $\bar{m}_{B^+}$ represent the steady state equilibrium concentrations of ions A^+ and B^+ in the respective junction zones and λ_i and λ_j represent the conductivities of the membrane when wholly in the A^+ and B^+ forms respectively. It has also been shown that $\bar{m}_{A^+}/\bar{m}_{B^+}$ is nearly equal to $K_{B^+A^+}$, the selectivity constant or the ion-exchange equilibrium constant. In terms of $K_{B^+A^+}$, Eq. (19) becomes,

$$\bar{U}_{A^+}/\bar{U}_{B^+} = K_{B^+A^+}(\bar{\lambda}_{A^+}/\bar{\lambda}_{B^+}) \quad \ldots (20)$$

The selectivity constant is also related to the permeability ratio P_{A^+}/P_{B^+} as

$$P_{A^+}/P_{B^+} = K_{B^+A^+}(U_{A^+}/U_{B^+}) \quad \ldots (21)$$

The mobility ratio values (Table 1) evaluated with the help of conductance data and Eq. (19) have been used to calculate (a) the theoretical values of bi-ionic potentials from Eq. (18), (b) the selectivity constant (Table 2) from Eq. (20) and (c) the permeability ratio (Table 3) from Eq. (21). These theoretical as well as observed values of bi-ionic potential have been plotted as a function of log C in Fig. 3. The very close agreement between the theoretical and observed bi-ionic potentials proves the applicability of the derived equation to the L-α-phosphatidylcholine model membrane system.

For checking selectivity of the membrane, the bi-ionic potentials were also measured by keeping the concentration of one of the electrolytes, say A^+M^-, constant and varying the concentration of the other electrolyte say B^+M^-, and again by keeping the concentration of B^+M^- constant and varying the concentration of A^+M^-. These data are represented in the form of plots of bi-ionic potential against log $a_{A^+M^-}/a_{B^+M^-}$ (Fig. 4). The point of intersection of the straight lines, demanded by the equation,

$$\Delta\phi_{BIP} = \frac{RT}{F}\ln t_{A^+}/t_{B^+} \quad \ldots (22)$$

at the same activity gave the values of transport ratio. The transport ratios thus obtained for different 1:1 electrolyte pairs are:

$t_{K^+}/t_{Li^+} = 1.820$, $t_{Na^+}/t_{Li^+} = 1.413$, and

$t_{K^+}/t_{Na^+} = 1.312$

The observed data on membrane potential, bi-ionic potential, transport ratio, mobility ratio (Table 1) and permeability ratio (Table 3) of cations show that phosphatidylcholine model membrane behave as a cation selective membrane[18,19].

Table 3—Values of permeability ratio of various alkali metal ion pairs for the L-α-phosphatidylcholine model membrane

Concentration (*M*)	P_{K^+}/P_{Na^+}	P_{Na^+}/P_{Li^+}	P_{K^+}/P_{Li^+}
0.1/0.1	1.32	1.42	1.86
0.05/0.05	1.39	1.49	1.96
0.02/0.02	1.53	1.66	2.32
0.005/0.005	1.78	2.14	2.90
0.002/0.002	1.91	2.30	3.48

Acknowledgement

The authors are grateful to Prof. S A A Zaidi, Chairman, Department of Chemistry, A M U, Aligarh for providing necessary facilities. The financial assistance from CSIR, New Delhi to one of the authors is gratefully acknowledged.

References

1 Toyoshima Y & Nozaki H, *J phys Chem*, 74 (1970) 2704.
2 Siddiqi F A, Singh S P, Beg M N, Gupta V & Parakash P, *Bull chem Soc Jpn*, 52 (1979) 1337.
3 Siddiqi F A & Alvi N I, J memb Sci, 46 (1989) 185.
4 Siddiqi F A & Tien H Ti, *Bioelectrochem Bioenerg*, 5 (1983) 157.
5 O'Boyle K P, Siddiqi F A & Tien H Ti, *Immunol Commun*, 13 (1984) 85.
6 Kimura Y, Lim H J & Iyima T, *J memb Sci*, 18 (1984) 285.
7 Peppas N A & Meadows D L, *J memb Sci*, 16 (1983) 361.
8 Tasaka M, Iwaaka S, Yamagishi K & Ikeda Y, *J memb Sci*, 24 (1985) 29.
9 Tasaka M, Aoki N, Kondo Y & Nagasawa N, *J phys Chem*, 79 (1975) 1307.

10 Tien H T, *Bilayer lipid membranes: Theory and practice* (Marcel Dekker, New York) 1974.
11 Geogoriadis G & Alison A, *Liposomes in biological system* (John Wiley and Sons, Chichester) 1980, 384.
12 Ploeg V, *J chem Phys*, 76 (1982) 3271.
13 Ilani A, *Biochim Biophys Acta*, 94 (1965) 405.
14 Nash H A & Tobias J M, *Proc Natl Acad Sci USA*, 51 (1964) 476.
15 Tokertomi S, Ohki K & Ohnishi S, *Biochem Biophys Acta*, 192 (1986) 596.
16 Sollner K J, *Phys colloid Chem*, 53 (1969) 1211.
17 Wylli M R J & Kannan S L, *J phys Chem*, 58 (1954) 73.
18 Shiratori M, Mizuno H, Taguhi H & Takeuchi Y, *J Tokyo Univ Fish*, 55 (1968) 45.
19 Shiratori M, Mizuno H & Kobayashi Y, *J Kobyo Univ Fish*, 55 (1968) 53.

Indian Journal of Chemistry
Vol. 30A, April 1991, pp. 340-346

Effect of iron(II), cerium(IV) and manganese(III) in the reaction between thallium(III) and hydrogen peroxide in aqueous perchloric acid

T Peter Amala Dhas, Dilip K Mishra, R K Mittal & Y K Gupta*
Department of Chemistry, University of Rajasthan, Jaipur 302 004

Received 19 June 1990; revised 3 September 1990; accepted 10 December 1990

The otherwise slow reaction between Tl(III) and H_2O_2 goes to completion in a few seconds in the presence of 10^{-6} mol dm^{-3} Fe(II). The reaction involves a cycle of steps with reactive intermediates such as Tl(II) and $H\dot{O}_2$. [Fe(III)] > 1×10^{-4} mol dm^{-3} is very effective and [Fe(III)] < 1×10^{-5} mol dm^{-3} has no effect at all on the reaction. Cerium(IV) and Mn(III) induce Tl(III) – H_2O_2 reaction and the extent of reduction of Tl(III) depends on the absolute and relative concentrations of the reactants. Ag(II) and Cr(III) are without any effect, but vanadium(IV) induces the reaction.

Small amounts (~ 10^{-6} mol dm^{-3}) of iron(II) have been employed as initiator or pre-reductor for the determination[1] of H_2O_2 with Tl(III). The reaction, $Tl(III) + Fe(II) \rightleftharpoons Tl(II) + Fe(III)$ is said to initiate[2,3] the oxidation of H_2O_2, but the forward reaction[4] is slow and has a second order rate constant of 4.6×10^{-2} mol^{-1} dm^3 s^{-1} at 25° (or 1.39×10^{-2} mol^{-1} dm^3 s^{-1} at 23° found by Dodson and coworkers[5]) and hence initiation by this step seems to be less likely. An alternative initiating reaction[6] could be $Fe(II) + H_2O_2 \rightarrow Fe(III) + OH^{\cdot} + OH^-$ which has a second order rate constant of 53 mol^{-1} dm^3 s^{-1} (see ref. 6). Such conflicting reports necessitate a thorough kinetic study of Tl(III)-H_2O_2 reaction in the presence of Fe(II). Further the effect of various metal ions, e.g. Ce(IV), Mn(III), Ag(II) etc. which could oxidize H_2O_2, and of Cr(III), VO^{2+} etc. which could reduce H_2O_2, has also been investigated.

Materials and Methods

Thallium(III) solutions were prepared as described earlier[7] and standardised iodometrically. Stock solutions of H_2O_2 were always prepared afresh by dilution of 30% H_2O_2 (E. Merck) and standardised cerimetrically using ferroin as indicator. Lithium perchlorate was prepared by dissolving Li_2CO_3 (AR Sisco) in 70% $HClO_4$. CO_2 was removed by gentle heating and *p*H of the solution adjusted to 6.7-7.0. Solutions of ceric sulphate were prepared by dissolving ammonium Ce(IV) pentanitrate in 1.0 mol dm^{-3} H_2SO_4. Ceric perchlorate was prepared by precipitating Ce(IV) as hydroxide by the addition of dilute ammonia and then dissolving the precipitate in 1.0 mol dm^{-3} $HClO_4$. Mn(III) sulphate solution was prepared[8] by dissolving Mn(III) acetate (Aldrich) in 6.0 mol dm^{-3} H_2SO_4 in the presence of 0.1 mol dm^{-3} Mn(II) sulphate (E. Merck). Ag(II) solution was prepared[9,10] by dissolving AgO (Aldrich) in 4.0 mol dm^{-3} $HClO_4$ in the presence of 0.2 mol dm^{-3} $AgClO_4$. Vanadium(IV) solution was prepared by dissolving $VOSO_4$ (AR, BDH) in water and standardised iodometrically. Ferric perchlorate (E. Merck) was employed for Fe(III) and Fluka chromium(III) nitrate for Cr(III).

Kinetic Procedure

Experiments were conducted in stoppered conical flasks immersed in a thermostated water bath at (20 ± 0.1)° unless mentioned otherwise. The reaction was initiated by adding a known volume of Fe(II) solution to a temperature pre-equilibrated (20 ± 0.1°) mixture containing required amounts of Tl(III), H_2O_2 and $HClO_4$. Since the reaction goes to completion within 1-2 minutes, the usual kinetic procedure of sampling was not adopted. For each experiment, 7-8 identical reaction mixtures were prepared and allowed to react for different predetermined times. Ice cold 5% KI solutions (10ml) was added to each flask and liberated iodine was titrated below 5° (see ref. 11) against standard thiosulphate while shaking continuously. Separate experiments with mixtures of H_2O_2 and KI without Tl(III) showed that no iodine is liberated in about 3 min. If [$HClO_4$] < 1.0 mol dm^{-3}. Initial rates (ir) were determined by the plane mirror method[12] and these were reproducible within ± 15%. Larger concentrations of reactants could not be employed since the reaction becomes too fast for conventional method of analysis.

Concentrations of metal ions employed were of the order 10^{-5} mol dm^{-3} and hence did not matter

in iodometric estimation of Tl(III). Even otherwise metal ions are rapidly reduced by H_2O_2 and there is no interference from them in the iodometric estimation of Tl(III). [V(IV)] employed was of the order of $\sim 10^{-4}$ mol dm^{-3} and this interfered with the iodometric estimation of Tl(III), and hence the latter was determined by ascorbic acid. A known excess of ascorbic acid was added to the reaction mixture. The reaction[13] of ascorbic acid and Tl(III) is fast and unreacted ascorbic acid was determined iodimetrically. Vanadium(V) also reacts[14] with ascorbic acid and hence an amount of iodine equivalent to V(V) was substracted from the total titre of iodine.

Results

Stoichiometry of Tl(III) – H_2O_2 reaction

Several mixtures with different concentrations of reactants at constant $[HClO_4] = 0.5$ mol dm^{-3} and at $I = 1.0$ mol dm^{-3} and temp = 30° were allowed to react. Excess of Tl(III) was determined iodometrically and excess H_2O_2 was determined cerimetrically[15]. From several experiments an average value of $\Delta[Tl(III)]/\Delta[H_2O_2]$ was found to be 0.99 ± 0.01.

Order of mixing the reactants and kinetic results

There are two ways of initiating the reaction. Tl(III) and H_2O_2 can be mixed and reaction may be initiated by the addition of Fe(II) in the end. Alternatively Tl(III) and Fe(II) may be mixed and then H_2O_2 added to initiate the reaction. The rates under identical conditions are about two times larger in the latter case. Reaction, however, cannot be initiated by adding Tl(III) in the end since Fe(II) is completely oxidised to Fe(III) which in small amounts has no effect. In the second way of initiation, Fe(II) and Fe(III) are in equilibrium(I) and Fe(II) is not oxidised completely.

$$Tl(III) + Fe(II) \rightleftharpoons Tl(II) + Fe(III) \qquad \ldots (1)$$

Reaction initiated by Fe(II): Thallium(III) and H_2O_2 dependences

The [Tl(III)] was varied in the range (3.0×10^{-4}-11.8×10^{-4}) mol dm^{-3} at two different $[H_2O_2]$, other conditions being as shown in Fig. 1. The order in Tl(III) is thus one. The first order rate constants for $[H_2O_2] = 3.6 \times 10^{-4}$ mol dm^{-3} and 5.5×10^{-4} mol dm^{-3} were found to be 0.714×10^{-2} s^{-1} and 1.66×10^{-2} s^{-1} respectively. The third order rate constants of 5.51×10^4 and 5.48×10^4 mol^{-2} dm^6 s^{-1} obtained by dividing the first order rate constants by $[H_2O_2]^2$ show that order in H_2O_2 is two. This is further supported by a plot of rate versus $[H_2O_2]^2$ (Fig. 1).

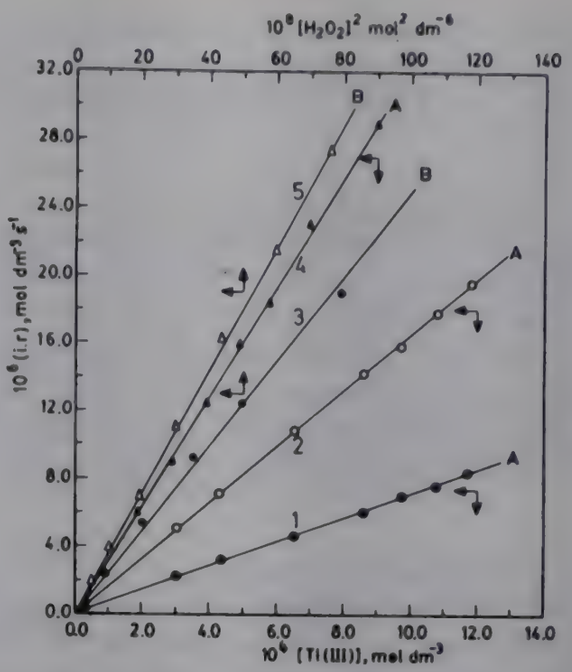

Fig. 1 – Tl(III) (A) and H_2O_2 (B) dependences at 20°C {$[HClO_4] = 0.5$ mol dm^{-3}; $[LiClO_4] = 1.0$ mol dm^{-3}; (1), $[H_2O_2] = 3.60 \times 10^{-4}$ mol dm^{-3}; (2), $[H_2O_2] = 5.50 \times 10^{-4}$ mol dm^{-3}; (3), $[Tl(III)] = 4.875 \times 10^{-4}$ mol dm^{-3}; (4), $[H_2O_2] = 5.85 \times 10^{-4}$ mol dm^{-3} and (5); $[Tl(III)] = 3.90 \times 10^{-4}$ mol dm^{-3}; Curves 1, 2, 3, reactions initiated by Fe(II); Curves 4, 5, reaction initiated by H_2O_2}

Iron(II) dependence

The initial rates versus [Fe(II)] plot shows increase in rate which tends to be limiting with increase in [Fe(III)]. The third order rate constant under limiting conditions was found to be 1.4×10^5 mol^{-2} dm^6 s^{-1} at 20°. The order in [Tl(III)] and $[H_2O_2]$, and dependence on [Fe(II)] suggest a rate law of the following type.

$$-d[Tl(III)]/dt = \frac{A[Tl(III)][H_2O_2]^2[Fe(II)]}{B + C[Fe(II)]} \qquad \ldots (2)$$

where A, B and C are constants.

Reaction initiated by H_2O_2

The variations of [Tl(III)] and $[H_2O_2]$ have been shown in Fig. 1. Again the order in Tl(III) and H_2O_2 were one and two respectively and the third order rate constants for $[Fe(II)] = 5.0 \times 10^{-6}$ mol dm^{-3} were found to be 9.4×10^4 mol^{-2} dm^6 s^{-1} and 9.3×10^4 mol^{-2} dm^6 s^{-1} in the two cases respectively. The effect of varying [Fe(II)] at three different $[H_2O_2]$ is shown in Fig. 2. The third order rate constants (mol^{-2} dm^6 s^{-1}) under limiting conditions were 2.85×10^5, 2.80×10^5 and 2.90×10^5 for $[H_2O_2] = 3.0 \times 10^{-4}$ mol dm^{-3}, 4.5×10^{-4} mol dm^{-3} and 6.0×10^{-4} mol dm^{-3} respectively. Thus the nature of the results under the two conditions of order of mixing is similar, but the rates are about

two times high in the case H_2O_2 is added in the end. It is appropriate to study the kinetics by the addition of Fe(II) since Tl(III) – H_2O_2 reaction is extremely slow.

Effect of $[H^+]$ and ionic strength

Variation in $[H^+]$ (0.2 to 1.0) mol dm^{-3} keeping $[Tl(III)] = 4.0 \times 10^{-4}$ mol dm^{-3}, $[H_2O_2] = 5.0 \times 10^{-4}$ mol dm^{-3}, $[Fe(II)] = 1.0 \times 10^{-5}$ mol dm^{-3} and $I = 1.0$ mol dm^{-3} did not affect the rate. Similarly variation in ionic strength ($LiClO_4$) at $[H^+] = 0.5$ mol dm^{-3} keeping the other concentrations as above (except ionic strength) does not affect the rate.

Effect of Fe(III) and Tl(I) on the rate

Added Tl(I) has no effect on the rate of reaction and Fe(III) alone at a concentration of 1.0×10^{-5} mol dm^{-3} or less has no effect (Table 1). However, in the presence of iron(II), 1×10^{-5} mol dm^{-3} Fe(III) had some effect on the rate. Fe(III) at a concentration of 1×10^{-4} mol dm^{-3} in the presence or absence of Fe(II) made the reaction to go to completion instantaneously. The previous finding[16] that

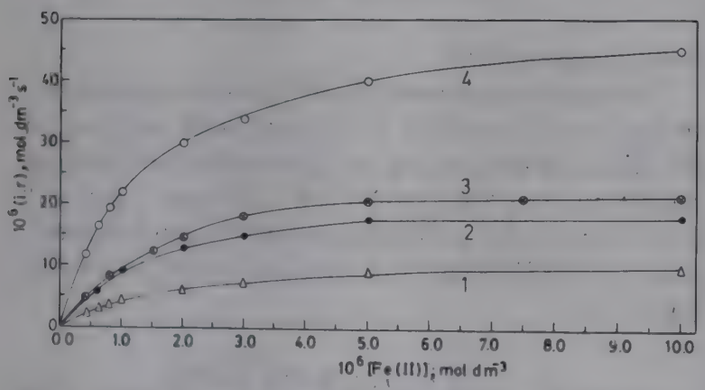

Fig. 2 – Fe(II) dependence at 20°C {$[HClO_4] = 0.5$ mol dm^{-3}; $[LiClO_4] = 1.0$ mol dm^{-3}; $[Tl(III)] = 3.90 \times 10^{-4}$ mol dm^{-3}; $[H_2O_2] = 3.0 \times 10^{-4}$ mol dm^{-3} (1), 5.25×10^{-4} mol dm^{-3} (2), 4.36×10^{-4} mol dm^{-3} (3), 6.0×10^{-4} mol dm^{-3} (4); Curves 1, 3, 4, reaction initiated by H_2O_2 and Curve 2, reaction initiated by Fe(II)}

Fe(III) is without any effect on the rate, is a sweeping statement and is valid if $[Fe(III)] < 1.0 \times 10^{-5}$ mol dm^{-3}. Thus Fe(III) may not be effective for the reaction when present in low concentrations, but it is as effective as Fe(II) if the concentrations is 1×10^{-4} mol dm^{-3} or more.

Reaction of Tl(III) with UV irradiated H_2O_2

Since the reaction is said to be accompanied by the formation of intermediate free radicals[3,16] from H_2O_2, it is likely that irradiation of H_2O_2 solution might generate these radicals and initiate the otherwise slow reaction. H_2O_2 was irradiated with UV lamp in a box for 5 min and then added to Tl(III) solution. The third order rate constant with irradiated H_2O_2 was found to be 4×10^4 mol^{-2} dm^6 s^{-1} at 29.5°, and $[HClO_4] = 0.5$ mol dm^{-3}. This rate constant with unirradiated H_2O_2 was found to be about 12 mol^{-2} dm^6 s^{-1} at 30° and $[HClO_4] = 0.5$ mol dm^{-3}. The value found earlier[2] was between 10-15 mol^{-2} dm^6 s^{-1} under the same conditions. Thus there is more than thousand fold increase in the rate for the irradiated H_2O_2.

Tl(III) – H_2O_2 reaction in the presence of Ce(IV)

The reaction of Ce(IV) and H_2O_2 is quite fast[17-19] and it is over within the time of mixing. The first iodometric analysis for Tl(III) could be done only after 5 seconds and thereafter no change occurred if the concentration of reactants is of the order of $\sim 10^{-4}$ mol dm^{-3}. This gave an estimate of reduction of Tl(III) on account of induced reaction. It may also be noted that at $[Ce(IV)] < 1 \times 10^{-4}$ mol dm^{-3} the induced reaction is a little slower. The previous works[14,17] have shown the reduction on account of induced reaction to be equivalent (or half molar) to Ce(IV). Our results show that this is partly true, and that for smaller concentrations ($\sim 10^{-5}$ mol dm^{-3}) of Ce(IV) employed, there is always larger reduction of Tl(III) than expected and that at large ($> [H_2O_2]$)

Table 1 – Effect of Tl(I) and Fe(III) on the rate of Tl(III) – H_2O_2 reaction
$[Tl(III)] = 4.1 \times 10^{-4}$ mol dm^{-3}; $[H_2O_2] = 6.25 \times 10^{-4}$ mol dm^{-3}; $[HClO_4] = 0.5$ mol dm^{-3} $[LiClO_4] = 1.0$ mol dm^{-3}; $[Fe(II)] = 4.0 \times 10^{-6}$ mol dm^{-3}; 25°

Time sec.	10^4[Tl(III)]/mol dm^{-3}						
	[Tl(I)] = 0.0 [Fe(III)] = 0.0	[Tl(I)]/mol dm^{-3}		[Fe(III)]/mol dm^{-3}			
		1.0×10^{-3}	5.0×10^{-3}	4×10^{-6} [a]	1×10^{-5}	1×10^{-4}	1×10^{-4} [a]
0	4.1	4.1	4.1	4.1	4.1	4.1	4.1
5.5	3.5	3.4	3.35	4.1	3.2	0.0	0.0
10	2.9	2.9	3.0	4.05	2.6	0.0	0.0
20	2.1	2.0	2.0	4.1	1.6	0.0	0.0
30	1.0	1.0	1.0	4.05[b]	0.80	0.0	0.0

[a]No Fe(II) added, only in the presence of Fe(III). [b]No reaction even after six hr.

Ce(IV), the amount of Tl(III) reduced is always much less than the expected amount. The results are quite complicated and depend on the relative and absolute [Tl(III)], [H_2O_2] and [Ce(IV)]. As a matter of fact if [Tl(III)] > [H_2O_2] > [Ce(IV)], the reduction of Tl(III) is always more than that on the basis mentioned above. Table 2 shows such results. For certain [Ce(IV)], the whole of H_2O_2 is oxidised and the amount of Tl(III) reduced is equal to $\{\frac{1}{2}[Ce(IV)] + [H_2O_2] - [Ce(IV)]\}$.

Tl(III) – H_2O_2 reaction in the presence of Mn(III)

The reaction of Mn(III) with H_2O_2 is also known to be fast[20] and the free radicals $H\dot{O}_2$ are formed which are likely to induce Tl(III) – H_2O_2 reaction. The results are more or less similar to the reaction in the presence of Ce(IV).

Silver(II)[21] is another oxidant similar to Ce(V) and Mn(III) that reacts with H_2O_2 and yields $H\dot{O}_2$ radicals and which is expected to initiate or induce Tl(III) – H_2O_2 reaction. However, Ag(II) is not at all effective for promoting Tl(III) – H_2O_2 reaction.

Tl(III) and H_2O_2 reaction in the presence of V(IV) and Cr(III)

Vanadium(IV) was employed in view of the fact that it is oxidised with H_2O_2. These results show that vanadium(IV) does induce the slow reaction of Tl(III) – H_2O_2. Estimation of Tl(III) in the presence of vanadium(IV) is complicated and hence it was not pursued. Chromium(III) has no effect on the Tl(III) – H_2O_2 reaction.

Spectrophotometric results

These measurements were made on Hitachi model U2000. $H\dot{O}_2$ radical is known to have an absorption maximum[22] at 230 nm. Tl(III) and Fe(II) do not absorb, and H_2O_2 absorbs little at 230 nm. Tl(I) has molar extinction coefficient of about 54 mol^{-1} cm^{-1} and hence 0.001 mol dm^{-3} Tl(III) on reduction would give an absorption of only 0.054 due to Tl(I). An absorption of 0.5 of the reaction mixture ($[Tl(III)] = 4.8 \times 10^{-4}$ mol dm^{-3}, $[H_2O_2] = 1.0 \times 10^{-3}$ mol dm^{-3}; $[Fe(II)] = 1.0 \times 10^{-5}$ mol dm^{-3}, $[HClO_4] = 1.0$ mol dm^{-3}) must be due to some intermediate, most probably $H\dot{O}_2$.

Discussion

The empirical rate law (2) can be explained on the basis of the reactions (3) and (4).

$$Tl^{3} + 2\,H_2O_2 \underset{k_2}{\overset{k_1}{\rightleftharpoons}} Tl(H_2O_2)_2^{3+} \qquad \ldots (3)$$

$$Tl(H_2O_2)_2^{3+} + Fe^{2+} \xrightarrow{k_3} Tl(II) + Fe(III) + 2\,H_2O_2 \qquad \ldots (4)$$

As a matter of fact step (4) is followed by several fast steps involving reactive intermediates like Tl(II), $H\dot{O}_2$ and $O\dot{H}$ radicals. Based on steps (3) and (4), rate law (5) can be derived.

$$-d[Tl(III)]/dt = \frac{k_1 k_3 [Tl(III)][H_2O_2]^2[Fe(II)]}{k_2 + k_3[Fe(II)]} \qquad \ldots (5)$$

This is identical with (2) with $A = k_1k_3$, $B = k_2$ and $C = k_3$. From a plot of $(ir)^{-1}$ versus $[Fe(II)]^{-1}$ (Figs 3 and 4). k_1 and k_2/k_3 have been calculated and these

Table 2 – Reduction of Tl(III) by H_2O_2 induced and triggered by Ce(IV)

$[Tl(III)] = 2.632 \times 10^{-3}$ mol dm^{-3}; $[H_2O_2] = 1.935 \times 10^{-3}$ mol dm^{-3}, $[HClO_4] = 0.5$ mol dm^{-3}; temp = 30°

A 10^4[Ce(IV)]/mol dm^{-3} taken	B 10^4[Tl(III)]/mol dm^{-3} expected to be reduced by induction (½ A)	C $10^4[H_2O_2]$/mol dm^{-3} expected after oxidation with Ce(IV)·$[H_2O_2]$ – A	D 10^4[Tl(III)]/mol dm^{-3} expected to be reduced after induction and reaction with H_2O_2·(B + C)	E 10^4[Tl(III)]/mol dm^{-3} reduced
0.267	0.1335	–	–	–
0.890	0.445	18.46	18.905	1.22
1.78	0.890	17.57	18.46	2.12
3.56	1.78	15.79	17.57	2.82
5.34	2.67	14.01	16.68	5.02
7.12	3.56	12.23	15.789	8.32
8.90	4.45	10.45	14.90	8.82
12.46	6.23	6.89	13.12	11.37
13.34	6.67	6.01	12.68	12.50
14.24	7.12	5.11	12.23	12.30
16.02	8.01	3.34	11.34	10.97

are given in Table 3. The experimentally found k_0 (third order rate constant) is in good agreement with the calculated value (see Table 3). It is not possible to separate k_2 and k_3. The value of k_1k_3/k is 5×10^9. It will be seen later that k_3 cannot be less than $\sim 10^4$ (100 times the rate constant for reaction 6) and it cannot be more than $\sim 10^8$ since it cannot be diffusion controlled. k_1/k_2 would then be between 10^5 and unity and since k_1 is $\sim 10^5$, k_2 would be between unity and 10^5. There is no kinetic evidence for complex $Tl(H_2O_2)_2^{3+}$ and since [Tl(III)] and $[H_2O_2]$ employed are of the order of $\sim 10^{-4}$ mol dm^{-3}, the equilibrium constant (k_1/k_2) could have any value from 10^6 downwards. This is in line with the conclusion drawn above. Unfortunately $[H_2O_2]$ larger than $\sim 10^{-3}$ mol dm^{-3} could not be employed to obtain kinetic evidence for the complex since the reaction is too fast for conventional method of analysis.

Complex formation between Tl(III) and H_2O_2 which has been discussed at length in the previous paper[14], is quite possible even though there is no direct evidence. However, more important is the fact that the order in H_2O_2 is two and in no case less than two for even the lower concentration range of H_2O_2 and this fact points to the existence of a dimer of H_2O_2 in the system. Such dimerization of H_2O_2 by hydrogen bonding in concentrated solutions, has been indicated from NMR[23] and Raman[24] studies in the past. It is possible that this dimer may complex with Tl(III). The facts that a kinetic study of the reaction by conventional method was possible only with low ($\sim 10^{-4}$ mol dm^{-3}) concentrations of H_2O_2 and the determination[1] of H_2O_2 (immediate reaction with Tl(III) can be made only if $[H_2O_2] > 10^{-3}$ mol dm^{-3}, show how effective is the concentration for dimerization and the redox reaction between Tl(III) and H_2O_2.

The two reactants, Tl(III) and H_2O_2 involve two reactive radical intermediates, Tl(II) and $H\dot{O}_2$ and the role of iron(II) can be explained by generating one of them through one of the following reactions (i-iv).

$$Tl(III) + Fe(II) \rightleftharpoons Tl(II) + Fe(III) \quad \ldots (i)$$

The rate constant[4,5] for the forward reaction is $\sim 10^{-2}$ mol^{-1} dm^3 s^{-1} and the equilibrium constant is 3×10^{-8} at 25°.

$$Fe^{2+} + H_2O_2 \rightarrow Fe^{3+} + O\dot{H} + OH^- \quad \ldots (ii)$$

The second order rate constant[6] for this reaction is reported to be 53 mol^{-1} dm^3 s^{-1} at 25°. The subsequent reaction produces radicals $H\dot{O}_2$.

$$OH + H_2O_2 \rightarrow H\dot{O}_2 + H_2O \quad \ldots (iii)$$

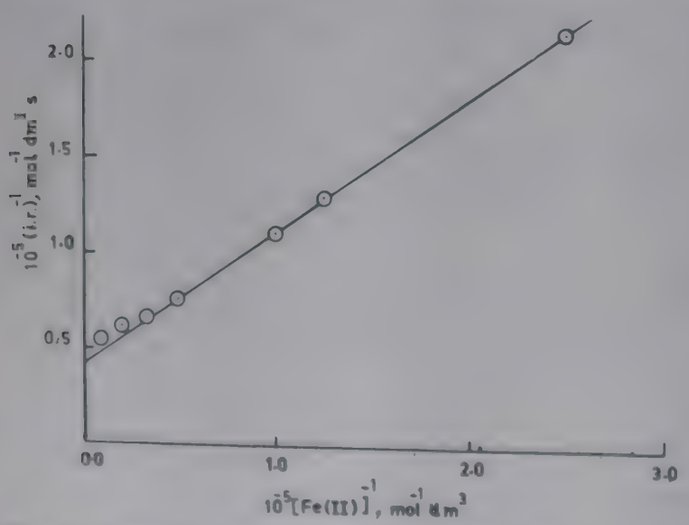

Fig. 3 – Plot of (i.r.)$^{-1}$ versus Fe(II)$^{-1}$ {[Tl(III)] = 4.90×10^{-4} mol dm^{-3}; $[H_2O_2] = 5.25 \times 10^{-4}$ mol dm^{-3}; $[HClO_4] = 0.50$ mol dm^{-3}; $I = 1.0$ mol dm^{-3}; temp = 20°C; reaction initiated by Fe(II)}

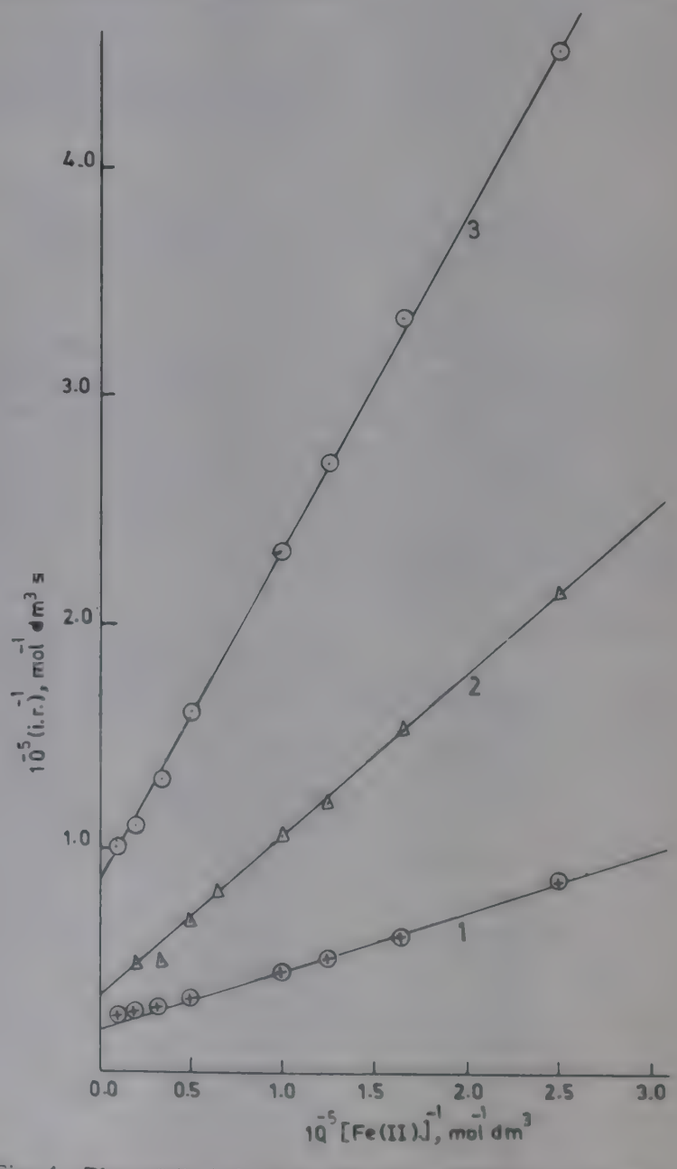

Fig. 4 – Plot of (i.r.)$^{-1}$ versus [Fe(II)]$^{-1}$ {[Tl(III)] = 3.90×10^{-4} mol dm^{-3}; $[HClO_4] = 0.5$ mol dm^{-3}; $I = 1.0$ mol dm^{-3}; temp = 20°C; $[H_2O_2] = 6.0 \times 10^{-4}$ mol dm^{-3} (1), 4.356×10^{-4} mol dm^{-3} (2), and 3.0×10^{-4} mol dm^{-3} (3); reaction initiated by H_2O_2}

Table 3—Rate constants for Tl(III) – H_2O_2 reaction in the presence of iron(II) at 20° from the variation of different concentration parameters

10^4[Tl(III)] (mol dm^{-3})	10^4[H_2O_2] (mol dm^{-3})	10^6[Fe(II)] (mol dm^{-3})	$10^{-5}\,k_1$ ($mol^{-2}\,dm^6\,s^{-1}$)	$10^5\,(k_2/k_3)$	$10^{-4}\,k_0$ ($mol^{-2}\,dm^6\,s^{-1}$)
3.0-11.8	5.50	5.0[d]	—	—	5.5[a,d]
3.0-11.8	3.60	5.0[d]	—	—	5.5[a,d]
4.875	1.48-8.88	5.0[d]	—	—	5.6[b,d]
3.90	5.25	4.0-100[d]	2.21	1.62	5.2[c,d]
1.95-9.0	5.88[e]	5.0	—	—	9.4[a,e]
3.90	2.18-8.71[e]	5.0	—	—	9.3[b,e]
3.90	3.0[e]	4.0-100	3.95	1.55	9.6[c,e]
3.90	4.36[e]	4.0-100	3.85	1.81	8.3[c,e]
3.90	6.0[e]	4.0-100	3.75	1.71	9.6[c,e]

[a]Slope/[H_2O_2]^2; [b]Slope/[Tl(III)]; [c]k_1[Fe(II)]/(k_2/k_3 + [Fe(II)]) = 5.0×10^{-6} mol dm^{-3}; [d]Reaction initiated by adding Fe(II) in the end; [e]Reaction initiated by adding H_2O_2 in the end.

This reaction is reported[25] to be rapid. The reaction of Fe(II) and OH is also rapid, but this does not seem to occur as compared to reaction (iii), since otherwise the main reaction between Tl(III) and H_2O_2 would not occur.

$$Tl(H_2O_2)_2^{3+} + Fe^{2+} \xrightarrow{k_3} Tl(II) \text{ or } H\dot{O}_2 + \text{other products} \quad \ldots (iv)$$

The rate constant for this reaction is not known, but one can compare the rate of this reaction with those of other two reactions under similar conditions. For [Tl(III)] = 4×10^{-4} mol dm^{-3}, [H_2O_2] = 4×10^{-4} mol dm^{-3} and [Fe(II)] = 5×10^{-6} mol dm^{-3}, the rate for Tl(III) – Fe(II) reaction would be 10^{-10} mol dm^{-3} s^{-1} and the rate for H_2O_2 – Fe(II) reaction would be 10^{-7} mol dm^{-3} s^{-1}. The overall rate for the present reaction is 10^{-5} mol dm^{-3} s^{-1}. Thus it is obvious that the present reaction is initiated by reaction(iv) which can be regarded as a combination of steps (i) and (ii). Optimum concentrations of $H\dot{O}_2$ and Tl(II) generate a cycle of following reactions till one of the reactants is exhausted.

$$Tl(II) + H_2O_2 \rightarrow Tl(I) + H\dot{O}_2 + H^+ \quad \ldots (v)$$

$$Tl(III) + H\dot{O}_2 \rightarrow Tl(II) + H^+ + O_2 \quad \ldots (vi)$$

The possible reactions that may occur in the solvent cage are (ii), (iii) and (v) in that order. The second order rate constant for reaction (v) has been reported[24] to be 3.0×10^7 mol^{-1} dm^3 s^{-1} at 25°. The rate constant for reaction (vi) is not known, but immediate reduction of Tl(III) (possibly by $H\dot{O}_2$) in the presence of Ce(IV), shows that this is rapid.

Cerium(IV) and manganese(II) have limited role in promoting Tl(III) – H_2O_2 reaction and $H\dot{O}_2$ radicals are responsible for initiating the reaction as shown below

$$Ce(IV)/Mn(III) + H_2O_2 \rightleftharpoons Ce(III)/Mn(II) + H\dot{O}_2 + H^+ \quad \ldots (6)$$

$$Ce(IV)/Mn(III) + H\dot{O}_2 \rightarrow Ce(III)/Mn(II) + H^+ + O_2 \quad \ldots (7)$$

$$Tl(III) + H\dot{O}_2 \rightarrow Tl(II) + H^+ + O_2 \quad \ldots (8)$$

There is computation between Ce(IV)/Mn(III) and Tl(III) and hence [Tl(II)] would depend on the relative concentrations of Tl(III) and the other oxidant. Unless an optimum concentration of Tl(II) is formed, the main cycle of reactions would not be triggered. Our results show that Mn(III) is not so effective as an inductor as Ce(IV). The second order rate constant for reaction (6) is ~ 1×10^6 mol^{-1} dm^3 s^{-1} (for Ce^{IV})[26] and 5.0×10^4 mol^{-1} dm^3 s^{-1} (for Mn^{III})[27] at 25° and hence equilibrium concentration of $H\dot{O}_2$ is likely to be smaller in case of Mn(III). Then the induction would also depend on the relative reactivities of Ce(IV) and Mn(III) towards $H\dot{O}_2$. These are not known presently.

Ag(II) is not effective for induction. Though reaction (6) is fast[19] (first order rate constant is 80 s^{-1} at 20°), reaction (7) appears to be much faster than (8) and hence no $H\dot{O}_2$ is available for induction. Cr(III) does not induce Tl(III) – H_2O_2 reaction at all. It is also obvious by the relative reactivities of several of the oxidants towards H_2O_2 lying in the following order[20], and Tl(III) would probably occupy a position between Fe(III) and Cr(III).

$$Ce(IV) > Mn(III) > Ag(II) \gg Co(III) > Fe(III) \gg Cr(III)$$

The role of Fe(III) requires a special mention. Large concentrations of Fe(III) ($> 1 \times 10^{-4}$ mol dm^{-3}) affect the reaction significantly. The mechan-

ism involves a reaction (9) similar to (6) producing $H\dot{O}_2$ radicals, but this is a slow process[28].

$$Fe(III) + H_2O_2 \rightarrow Fe^{2+} + H\dot{O}_2 + H^+ \quad \ldots (9)$$

with a rate constant[29] of less than $\sim 10^{-3}$ mol^{-1} dm^3 s^{-1} at 25°, the optimum concentration of $H\dot{O}_2$ to induce cycle of reactions, is not generated. It is Fe(II), however, which is formed as a product which can participate in reaction (iv) to generate [Tl(II)] to induce the cycle of reactions (v) and (vi). A reaction (10) with a rate constant[6] of 1.2×10^5 mol^{-1} dm^3 s^{-1} has not been considered since both $[H\dot{O}_2]$ and [Fe(III)] would be small.

$$H\dot{O}_2 + Fe(III) \rightarrow Fe(II) + H^+ + O_2 \quad \ldots (10)$$

All the oxidants mentioned above are similar in their action in producing first $H\dot{O}_2$ radical, but Fe(II) is different in that it first generates $O\dot{H}$ and then $H\dot{O}_2$. Vanadium(IV) was employed to support this mechanism. The results do show an induction of $Tl(III) - H_2O_2$ reaction and it should be through $O\dot{H}$ radicals since $V(IV) - H_2O_2$ reaction yields $O\dot{H}$ radical.

We could not verify the order between two and three with respect to H_2O_2 as found by Csanyi and co-workers[3] since we could not employ $[H_2O_2]$ larger than 1×10^{-3} mol dm^{-3} to avoid interference in iodometric determination. However, we did not observe the slightest trend for increase in the order even at the largest concentration of H_2O_2 employed.

References

1 Sharma P D & Gupta Y K, *Talanta*, 20 (1973) 903.
2 Csanyi L J, Cseh F, Szil Zs & Boti Zs, *Acta Chim Acad Sci Hung*, 75 (1972) 1.
3 Boti Zs, Horvath I & Csanyi L J, *J chem Soc Dalton Trans*, (1978) 1013.
4 Ashurst K G & Higginson W C E, *J chem Soc*, (1953) 3044.
5 Schwarz H A, Comstock D, Yandell J K & Dodson R W, *J phys Chem*, 78 (1974) 488.
6 Barb W G, Baxendale J H, George P & Hargrave K R, *Trans Farad Soc*, 47 (1951) 591.
7 Gupta K S & Gupta Y K, *J chem Soc (A)*, (1970) 256.
8 Rosseinsky D R, *J chem Soc*, (1963) 1181.
9 Kirwin J B, Peat P D, Proll P S & Sutcliffe L H, *J phys Chem*, 67 (1963) 1617.
10 Rechnitz G A & Zammovick S B, *Talanta*, 11 (1964) 713.
11 Liebhafsky H A & Mohammad S B, *J Am chem Soc*, 55 (1933) 3977.
12 Latshaw M, *J Am chem Soc*, 47 (1925) 793.
13 Gupta D, Sharma P D & Gupta Y K, *Talanta*, 22 (1975) 913.
14 Kustin K & Toppen D L, *Inorg Chem*, 12 (1973) 1404.
15 Kolthoff I M & Belcher R, *Volumetric analysis* (Interscience, New York) Vol. 3 (1957) 650.
16 Sharma P D & Gupta Y K, *J chem Soc Dalton Trans*, (1975) 81.
17 Sharma P D & Gupta Y K, *Indian J Chem*, 14A (1977) 243.
18 Mahlman H A, Methews R W & Sworski T J, *J phys Chem*, 75 (1971) 250.
19 Wells C F & Hussain M, *J chem Soc (A)*, (1970) 1013.
20 Wells C F & Mays D, *J chem Soc (A)*, (1968) 665.
21 Wells C F & Mays D, *Inorg nucl Chem Letters*, (1969) 59.
22 Czepski G & Dorfman L M, *J phys Chem*, 68 (1964) 1169.
23 Anbar M, Lowenstein S & Meiboom S, *J Am Chem Soc*, 80 (1958) 2630.
24 Taylor R C & Cross P C, *J chem Phys*, 24 (1956) 41; Luft N M, *Disc Faraday Soc*, 12 (1952) 266.
25 Weiss J, *Adv Catalysis*, 4 (1952) 343.
26 Sigler P B & Masters B J, *J Am chem Soc*, 79 (1957) 6353; Czapski G, Bielski B H J & Sutin N, *J phys Chem*, 67 (1963) 201.
27 Davies G, Kirschenbaum L & Kustin K, *Inorg Chem*, 7 (1968) 146.
28 Hoggeth M L, Jones P & Wynne-Jones W F K, *Disc Faraday Soc*, 29 (1960) 153; Jones P, Kelching R, Tobe M L & Wynne-Jones W F K, *Trans Faraday Soc*, 55 (1959) 79.
29 Kremer M L, *Trans Faraday Soc*, 59 (1963) 2535.

Indian Journal of Chemistry
Vol. 30A, April 1991, pp. 347-349

Kinetics and mechanism of dissociation of di-(2-pyridyl)amine complexes of copper (II), nickel (II) and cobalt (II) in aqueous acid media

Asim K Das & D Banerjea*
Department of Chemistry, University College of Science, 92, Acharya Prafulla Chandra Road, Calcutta 700009

Received 12 July 1990; accepted 8 November 1990

Kinetics of dissociation of ML_2^{3+} (M = Cu(II), Ni(II)) and CoL^{2+} [L = di-(2-pyridyl)amine] complexes in acid media forming aqua-metal ions and the protonated ligand as the ultimate products have been studied by stopped-flow spectrophotometry. Dissociation of the bis-complexes occurs in two consecutive steps through formation of the mono complexes in the first step, which is faster than the second. For each of the steps of the different complexes the observed rate constant k_x shows acid dependence. Arguments have been put forth in favour of chelate ring-opening as the rate-determining step. These complexes are much more labile to dissociation than the corresponding complexes of 2,2′-bipyridyl.

Thermodynamic studies[1] on complex formation by di-(2-pyridyl)amine with different metal ions of the transition series have been reported and results compared with those of 2,2′-bipyridyl (bipy). Kinetics of dissociation of cobalt (II), nickel (II) and copper (II) complexes of 2,2′-bipyridyl and 1,10-phenanthroline (phen) have been reported[2]. Di-(2-pyridyl) amine differs from bipy and phen in having a free basic site, imino group (−NH−), in the metal bound ligand and forms a six-membered chelate ring as against the five-membered one formed by bipy and phen. Due to presence of free basic sites many thermodynamically stable complexes dissociate fairly easily[3] in acid media. Chelate ring size also has an effect on rate of dissociation. Hence, results of the present investigations afford useful comparison with those of the bipy and phen complexes.

Materials and Methods

The complexes $[Cu(C_{10}H_9N_3)_2]Cl_2$ (ref. 4), $[Cu(C_{10}H_9N_3)Cl_2]$ (ref. 4) and $[Co(C_{10}H_9N_3)Cl_2]$ (ref. 5) were prepared by known methods using di-(2-pyridyl)amine ($C_{10}H_9N_3$) obtained from Reilly Tar & Chemical Corp., USA; $[Ni(C_{10}H_9N_3)_2]Cl_2$ was prepared in the same way as the copper (II) complex. Purities of the complexes were checked by elemental analyses. All other chemicals used were of reagent grade or else purified by known methods. Solutions were freshly prepared before use in doubly distilled water.

Apparatus and procedure

The spectra of freshly prepared aqueous solutions of the complexes were recorded using VSU-2P (Carl-Zeiss, Jena, East Germany) spectrophotometer. The rates of dissociation of the complexes in aqueous solution (0.001 mol dm^{-3} for cobalt and copper complexes, and 0.002 mol dm^{-3} for nickel complex) containing varying amounts of HCl (0.01-0.04 mol dm^{-3} for cobalt and copper complexes, and 0.025-0.08 for nickel complex) and KCl (to adjust the ionic strength to 0.10 mol dm^{-3}) were followed spectrophotometrically at appropriate wavelengths (at λ_{max} of the complexes; 640 nm for CuL_2^{3+}, 670 nm for CuL^{2+}, 555 nm for NiL_2^{3+} and 490 nm for CoL^{2+}; at these wavelengths the reaction products are virtually non-absorbing in the concentration ranges used) using a stopped-flow spectrophotometer (SF-3A, Hi-Tech, England) coupled with a fast recorder system. The reacting solutions and the cell were thermostated at the desired temperature (±0.05°C). The observed changes in absorbance with time for the bis-complexes of copper and nickel were in conformity with pathways having two consecutive steps; a fast step followed by a slow step. The pseudo-first order rate constants (k_{fast} and k_{slow}) for these steps were evaluated using known graphical procedure[6]. Multiple runs carried out in a few cases indicated good reproducibility of the results.

Results and Discussion

In the cases of CuL_2^{3+} and NiL_2^{3+} analysis of absorbance-time profiles indicated two consecutive steps, initial faster step (k_{fast}) followed by a relatively slower step (k_{slow}). Each of these observed pseudo-first order rate constants showed acid dependence, which could be expressed by Eq. (1)

$$k_x = k'_x + k''_x [H^+] \quad \ldots (1)$$

In Eq. (1) x = 'fast' or 'slow' as the case may be. The results are in accord with the changes shown in Scheme 1 (illustrated with the mono complexes):

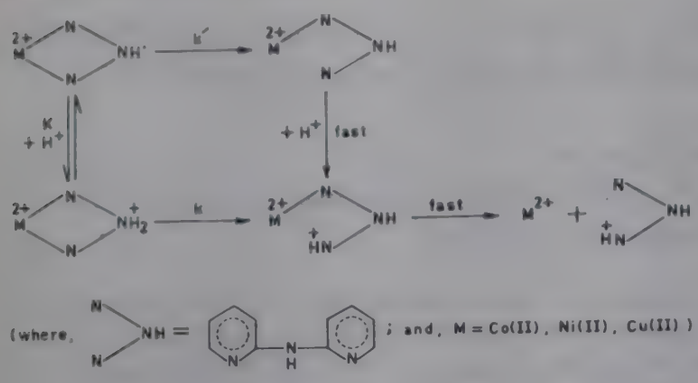

Mechanism in Scheme 1 leads to $k'' = k.K$. The specific rate constants k'_x (acid independent path) and k''_x (acid dependent path) were evaluated in each case from the k_x values at different acid concentrations making use of Eq. (1) and least-squares procedure. In the case of CoL^{2+}, a one-step corresponding to the second (slow) step in the dissociation of the bis-complexes of Cu(II) and Ni(II) was observed. The mono complex CuL^{2+} showed a similar behaviour. In the case of bis-complexes the first step corresponds to dissociation of the bis-complex to the mono-complex, and second step corresponds to dissociation of the mono-complex to the aqua-metal ion and a protonated ligand in each case. This is proved by the fact that the observed value of k_{slow} for the second step dissociation of CuL_2^{2+} is identical under the same set of experimental conditions with that observed with CuL^{2+} present in $Cu(L)Cl_2$. In the cases of bis-complexes of Cu(II) and Ni(II), the first step is faster then the second as usual. Activation parameters ($\Delta H^{\ddagger}$ and $\Delta S^{\ddagger}$) corresponding to k'_x and k''_x in each case were evaluated using Eyring equation[7] and the results are given in Table 1.

For the six-coordinate complexes of Co(II), Ni(II) and Cu(II) which are d^7, d^8 and d^9 systems respectively, the values of ligand field activation energy for dissociation of their complexes by a dissociative mechanism are zero, 2Dq and zero respectively[2]. Hence, such Cu(II) and Co(II) complexes are exceptionally labile to ligand replacement processes while the corresponding Ni(II) complexes are far less labile.

Comparison of the kinetic behaviour of these di-(2-pyridyl) amine metal complexes with those of the corresponding complexes of bipy and phen is

Table 1—Kinetic parameters for dissociation of di-(2-pyridyl) amine complexes of Cu(II), Ni(II) and Co(II) in aqueous acid medium (I = 0.1 mol dm^{-3} (KCl + HCl) if not stated otherwise)

Complex	Temp. (°C)	k'_{fast} (s^{-1})	K''_{fast} ($dm^3mol^{-1}s^{-1}$)	k'_{slow} (s^{-1})	k''_{slow} ($dm^3mol^{-1}s^{-1}$)
CuL_2^{2+}	20	3.00±0.02	(8.25±0.01)×10²	2.10±0.01	(6.55±0.03)×10²
	25	5.01±0.02	(10.60±0.03)×10²	3.40±0.02	(8.30±0.04)×10²
	25[a]	4.96±0.03	(8.90±0.02)×10²	3.42±0.02	(7.02±0.03)×10²
	30	8.00±0.03	(13.50±0.03)×10²	5.15±0.02	(10.35±0.04)×10²
$\Delta H^{\ddagger}$ (kJ mol^{-1})		68.9±2.1	33.8±1.0	66.9±2.4	32.1±1.3
$\Delta S^{\ddagger}$ (JK^{-1}mol^{-1})		−2.3±0.8	−75.3±4.8	−12.9±1.0	−82.9±3.8
NiL_2^{2+}	40	0.31±0.02	27.80±0.02	0.10±0.01	3.30±0.01
	45	0.50±0.02	42.00±0.03	0.18±0.01	5.20±0.02
	45[b]	0.48±0.01	49.20±0.02	0.17±0.02	6.04±0.02
	50	0.78±0.02	62.50±0.04	0.30±0.02	8.00±0.03
	25[c]	0.08±0.02	7.65±0.06	0.02±0.01	0.87±0.02
$\Delta H^{\ddagger}$ (kJ mol^{-1})		72.7±2.5	65.4±1.2	82.8±3.6	69.1±2.8
$\Delta S^{\ddagger}$ (JK^{-1}mol^{-1})		−24.8±1.4	−10.7±1.0	−1.7±0.4	−16.6±1.4
CoL^{2+}	20			7.0±0.04	(2.40±0.01)×10²
	25			11.00±0.04	(3.20±0.02)×10²
	25[a]			10.90±0.02	(2.65±0.02)×10²
	30			16.90±0.03	(4.20±0.01)×10²
$\Delta H^{\ddagger}$ (kJ mol^{-1})				62.9±1.9	39.1±1.6
$\Delta S^{\ddagger}$ (JK^{-1}mol^{-1})				−15.9±1.0	−67.3±2.7

(a) I = 0.05 mol dm^{-3} (KCl + HCl); (b) I = 0.15 mol dm^{-3} (KCl + HCl); (c) values calculated, for comparison with those of Cu(II) and Co(II), using the $\Delta H^{\ddagger}$ and $\Delta S^{\ddagger}$ values.

interesting. For dissociation[2,8], $k_{Cu(bipy)}/k_{Ni(bipy)} \approx 61$ and $k_{Cu(phen)}/k_{Ni(phen)} \approx 5.5 \times 10^6$, at 25°C. The high value for phen complex has been explained[8] as due to the rigid nature of the 1,10-phenanthroline ring, which prohibits one-ended dissociation while such a process is feasible in the case of bipy complexes. It is likely that the fairly low ratio of the rate constant, observed for the mono-bipyridyl complexes is due to the fact that the rate-determining step for dissociation of the mono-complexes of bipyridyl is the one-ended dissociation of chelate ring, leading to chelate ring opening, followed by a fast dissociation of the second metal-ligand bond leading to loss of the bipyridyl from the inner coordination sphere of the metal. In the case of phen complexes such an one-ended dissociation is not possible due to rigidity of the phenanthroline ring, and hence the rate-determining step involves complete dissociation and a high ratio of the rate constants has been observed in this case due to inherent greater lability of Cu(II) complexes. In the present investigation, at 25°C (I = 0.1 mol dm^{-3}) $k'_{CuL_2}/k'_{NiL_2} = 62.6$ and $k'_{CuL}/k'_{NiL} = 170$; these ratios are better comparable to those of the the bipy complexes hence chelate ring-opening can be argued as the rate-determing step in these cases also. However, for any metal these complexes are much more labile than the corresponding bipy complexes.

Results show $k''_{CuL_2}/k''_{NiL_2} = 138.6$ and $k''_{CuL}/k''_{NiL} = 954$, at 25°C, which are much higher than the corresponding ratios for the k'-path. According to the proposed mechanism, k'' is a composite constant being product of the protonation constant (K) of free $-NH-$ group in the bound ligand and rate constant (k) leading to chelate ring-opening. The increased ratio for k''-path ($k'' = K.k$) arises probably due to higher K value because of higher basicity of $-NH-$ group in the case of Cu(II) complex than that of the Ni(II) complex. This is possibly due to a better metal to ligand back bonding in the case of d^9 copper(II) system than that in the case of d^8 nickel (II) system.

For the mono-complexes the following relative labilities have been found (at 25°C, I × 0.1 mol dm^{-3}): for k'_{slow}, Co(II) : Cu(II) : Ni(II) = 550 : 170 : 1 and for k''_{slow}, Co(II) : Cu(II) : Ni(II) = 368 : 954 : 1. The observed sequence for k'_{slow} is what is generally observed; but the sequence observed in k''_{slow} is also known[8] in some cases. Increase in ionic strength hardly affects k'_x but causes increase in k''_x presumably due to increase in K.

References

1 Basak A K & Banerjea D, *Indian J Chem*, 14A (1976) 184.

2 cf. Banerjea D, in *Fundamental principles of inorganic chemistry*, (Sultan Chand & Sons, New Delhi) 1984, p 362.

3 (a) Banerjea D & Chakraborty B, *J inorg nucl Chem*, 26 (1964) 1235.
(b) Banerjea D, *Trans Met Chem*, 12 (1987) 97.

4 Kirschner S, *Inorganic synthesis*, Vol 5, edited by T Moeller (McGraw-Hill, New York) 1957, p 14.

5 Bailar J C (Jr) & Kirschner S, *Inorganic synthesis*, Vol 5, edited by T Moeller (McGraw-Hill, New York), 1957, p 184.

6 Banerjee R N & Banerjea D, *Indian J Chem*, 17A (1979) 246.

7 Wynne-Jones W F K & Eyring H, *J chem Phys*, 3 (1935) 492.

8 Gangopadhyay S, Banerjee R N & Banerjea D, *Trans Met Chem*, 10 (1985) 310.

Indian Journal of Chemistry
Vol. 30A, April 1991, pp. 350-356

Synthesis, Mössbauer, infrared spectroscopic and thermal decomposition studies of some iron(III) carboxylate complexes

R B Lanjewar & A N Garg*
Department of Chemistry, Nagpur University, Nagpur 440 010

Received 7 May 1990; revised 23 July 1990; rerevised and accepted 1 October 1990

Several new iron(III) carboxylate complexes with the general formula $Na_3[Fe(OCOR)_6]$ where $R=(CH_3)_3C-$, $CH_3(CH_2)_5-$, $CH_3(CH_2)_{10}-$, 2,5-$Cl_2C_6H_3-$, 2,5-$(CH_3)_2C_6H_3-$, 2-$MeOC_6H_4-$ and 3-$MeOC_6H_4-$ have been synthesized. Also, iron(III) complexes with pyridine 2,6-dicarboxylic acid and quinic acid have been synthesized. Infrared data suggest unidentate nature of the carboxylate ligands in all cases. Mössbauer spectra of all the complexes exhibit quadrupole doublet except for quinic acid complex where a triplet has been observed. Isomer shift (δ) values are in the range 0.58-0.74 mm s^{-1} (with respect to sodium nitroprusside as a standard) suggesting iron(III) in high spin state. Quadrupole splitting (ΔE_Q) values are in the range of 0.30-2.71 mm s^{-1} and its variation is attributed to varying distortions in octahedral geometry. Thermogravimetric (TGA) studies show a single stage, but slow decomposition yielding a mixed sodium iron oxide or sodium ferrate ($3Na_2O.Fe_2O_3$). Magnetic moment and reflectance spectral data have also been reported.

Carboxylate ion ($-\overset{O}{\overset{\|}{C}}-O^-$) is a unique ligand which can act as a unidentate, bidentate or bridging ligand depending on the nature of metal ion, carboxylic acid and the reaction conditions[1-3]. Iron is known to form simple and some basic salts with formic and acetic acids[4-7]. Earlier we have studied several iron(III) carboxylate complexes[8-10] of mono- and di-carboxylic acids by Mössbauer and infrared spectroscopy. In order to further study the effect of more bulky groups on the octahedral geometry, we report here synthesis and structural investigations on some new carboxylate complexes with the general formula $Na_3[Fe(OCOR)_6]$ where $R=(CH_3)_3C-$, $CH_3(CH_2)_5-$, $CH_3(CH_2)_{10}-$, 2,5-$Cl_2C_6H_3-$, $(CH_3)_2C_6H_3-$, 2-$MeOC_6H_4-$ and 3-$MeOC_6H_4-$. Also iron(III) complexes with pyridine 2,6-dicarboxylic acid and quinic acid have been synthesized and their spectral studies carried out. We have also studied the thermal decomposition behaviour of the complexes.

Materials and Methods

All the chemicals used were of AR, GR or high purity grade. Quinic acid (1,3,4,5-tetrahydroxycyclohexane 1-carboxylic acid), pyridine 2,6-dicarboxylic acid and heptanoic acid were Fluka AG (puram) reagents. Sodium salts of the acids were prepared by mixing equimolar (0.1 *M*) aqueous solutions of the acids and sodium hydroxide. In case of trimethylacetic acid (Fluka, AG) and heptanoc acid, reaction was carried out with sodium metal pieces in dry benzene till the evolution of hydrogen ceased. Sodium salt so formed was then filtered and dried.

Preparation of complexes

The complexes were prepared by mixing 0.1 *M* ferric nitrate with 0.6 *M* aqueous solution of the corresponding sodium carboxylate.

Trisodium tris(pyridine 2,6-dicarboxylato)ferrate(III) complex was prepared by reacting 0.81 g ferric nitrate with 1.13 g monosodium pyridine 2,6-carboxylate in 1:1 water-ethanol mixture.

Sodium salt of quinic acid could not be prepared and, hence, its complex was prepared by treating 0.056 g iron powder (electrolytic grade, S. Merck) with a warm aqueous solution of 1.92 g (3 m*M*) acid. The resultant solution was slowly evaporated on a water bath.

In all the cases coloured complexes separated out immediately and these were dried *in vacuo* over fused $CaCl_2$. C, H analyses (Table 1) were carried out at the analytical laboratories of Regional Sophisticated Instrumentation Centre, Lucknow. Fe was determined spectrophotometrically using 1,10-phenanthroline reagent.

Table 1 – Analytical data of various carboxylate complexes

Sl. No.	$Na_3[Fe(OCOR)_6]$ R =	Colour	Found (Calc) %		
			Fe	C	H
1	$(CH_3)_3C-$	Middle buff	7.23 (7.66)	48.65 (49.25)	7.50 (7.38)
2	$CH_3(CH_2)_5-$	Brick red	7.42 (7.13)	62.65 (63.24)	9.32 (9.88)
3	$CH_3(CH_2)_{10}-$	Middle buff	4.24 (4.20)	65.75 (65.50)	9.91 (10.46)
4	$2,5\text{-}Cl_2C_6H_3-$	Middle buff	5.02 (4.62)	33.75 (34.15)	1.82 (1.42)
5	$2,5\text{-}(CH_3)_2C_6H_3-$	Middle buff	5.89 (5.75)	64.20 (63.60)	5.30 (5.30)
6	$2\text{-}MeO\ C_6H_4-$	Golden yellow	5.85 (5.43)	55.65 (55.81)	4.30 (4.07)
7	$3\text{-}MeOC_6H_4-$	Brick red	5.12 (5.43)	55.35 (55.81)	4.54 (4.07)
8	$Na_3[Fe(R)_3]$ R = pyridine 2,6-dicarboxylic acid	Brown	7.80 (7.95)	35.37 (35.77)	1.75 (1.71)
9	$H_4[Fe(II)(C_7H_{10}O_6)_3]$ or $H_3[Fe(III)(C_7H_{10}O_6)_3]$	Grey	9.11 (8.88) (8.90)	39.75 (40.00) (40.06)	4.70 (5.39) (5.25)

Physical measurements

Mössbauer spectra were recorded using a constant acceleration transducer, driven Mössbauer spectrometer in conjunction with a PC based 1 K Multichannel Analyzer (Nucleonix, Hyderabad). A 5 mCi $^{57}Co(Rh)$ source (procured from the Isotope Group, BARC, Bombay) was used. All the spectra were recorded at room temperature and visually fitted with Lorentzian line shape. The spectrometer was calibrated using natural iron foil. Sodium nitroprusside dihydrate (SNP) was used as the standard.

Infrared spectra (4000-200 cm^{-1}) were recorded in KBr medium on a Perkin-Elmer-157 IR spectrophotometer. Thermogravimetric (TGA) and differential thermal gravimetric analyses (DTG) were carried out at a heating rate of 10°C per min using Perkin-Elmer Thermogravimetric Analyzer System Model TGS-2 and Thermal Analysis Data Station TADS 3600 of RSIC, Nagpur. Magnetic moments were determined from magnetic susceptibility measurements using Gouy's balance and $Hg[Co(SCN)_4]$ as the standard.

Reflectance spectra were recorded using a Shimadzu model UV-240 spectrophotometer employing MgO as the reference.

Results and Discussion

All the complexes are coloured solids and stable under atmospheric conditions. Fe(III) in an octahedral environment will be surrounded by six or three carboxylate ligands with central iron atom having an electronic configuration $t_{2g}^3 e_g^2$. Due to the large size of the carboxylate ligands, especially with long chain alkyl groups, geometry is likely to be distorted quite significantly.

All the complexes exhibit a well resolved quadrupole doublet except the quinic acid complex where a three line spectrum is observed. Mössbauer spectrum of quinic acid complex can be re-

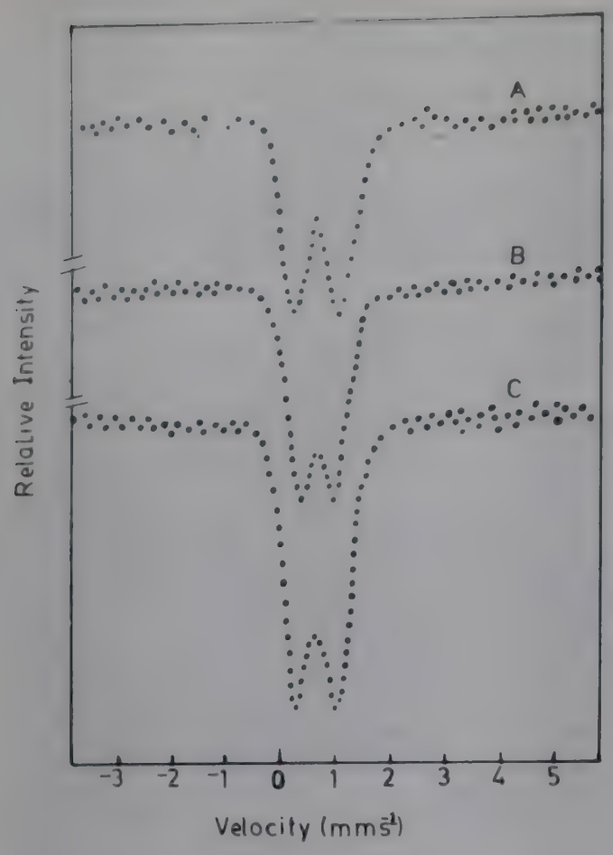

Fig. 1 – Mössbauer spectra of (A) 2,5-dichlorobenzoic acid, (B) 3-methoxybenzoic acid and (C) heptanoic acid complexes.

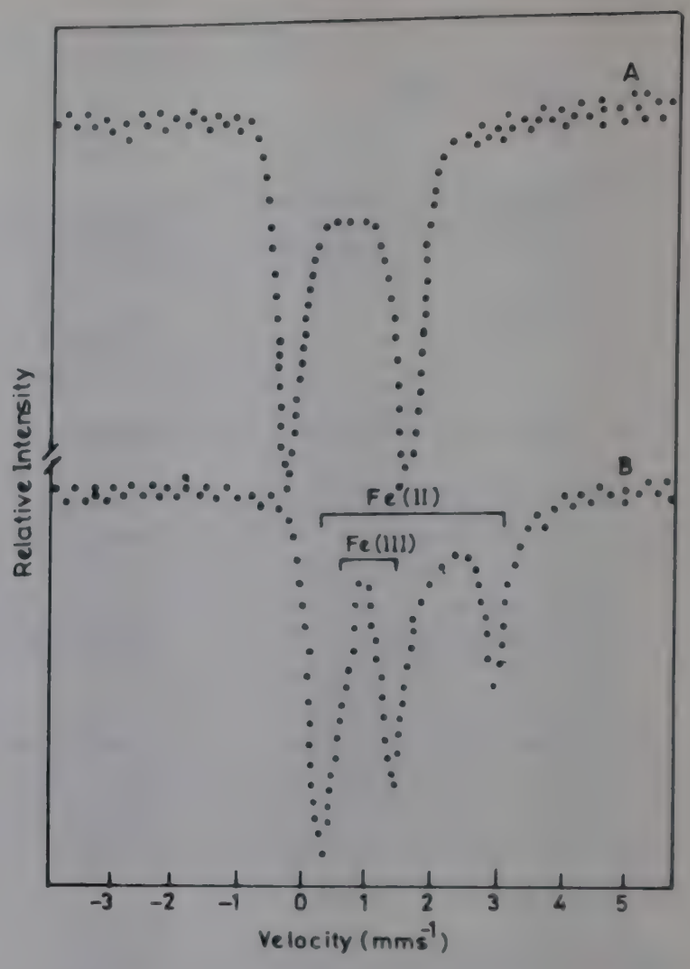

Fig. 2 – Mössbauer spectra of Fe complexes of (A) pyridine 2,6-dicarboxylic acid and (B) quinic acid at room temperature.

solved into two sets of doublets, one corresponding to Fe(II) and another more intense to Fe(III). Typical Mössbauer spectra of substituted benzoato and heptanoic acid complexes are shown in Fig. 1. Similarly, Mössbauer spectra of pyridine 2,6-dicarboxylic acid and quinic acid complexes are shown in Fig. 2. Isomer shift (δ), quadrupole splitting (ΔE_Q) along with magnetic moment and electronic spectral bands are given in Table 2.

Reflectance spectra of these complexes exhibit two bands (Table 2) of low intensity at 19,000 cm^{-1} and 25,000 cm^{-1} corresponding to spin forbidden $^6A_{1g} \rightarrow {}^4T_{1g}$ and $^6A_{1g} \rightarrow {}^4T_{2g}$ transitions respectively. These are in agreement with literature[12] assignments.

Magnetic moments

Magnetic moments of the carboxylate complexes are in the range of 5.29-6.23 B.M. indicating high spin state of Fe(III) with five unpaired electrons. High $\mu_{eff.}$ values in some cases may be attributed to (i) some contribution from the alkyl or aryl groups attached to the carboxylate, (ii) non-quenching of orbital[11] contribution, (iii) some other magnetic interactions including magnetically non-equivalent sites in a unit cell and (iv) large distortions in the geometry of the complexes. Even though there is no direct evidence the possibility of multiple centre bands cannot be ruled out.

Infrared spectra

Infrared spectra of a wide variety of carboxylates of different metal ions have been studied[13-18]. The most prominent features of infrared spectra of the carboxylate complexes are the sharp and well defined absorptions due to $\nu_{as}(OCO)$, $\nu_s(OCO)$ and $\delta(OCO)$ observed in the region as 1665-1470, 1430-1340 and 770-600 cm^{-1} respectively. Their positions and intensities are similar to those reported for other carboxylate complexes[8-10,19]. Another important band is due to $\nu(Fe-O)$[20] observed in the region 540-440 cm^{-1}. Other characteristic bands[21] such as $\nu(C-O)$, $\nu(C-C)$ and $\nu(C-H)$ were also observed in regions 1110-1000, 1290-1210 and 3250-2720 cm^{-1} respectively. It follows that in all carboxylate complexes studied here $\Delta\nu = [\nu_{as}(OCO) - \nu_s(OCO)]$ is in the range 180-295 cm^{-1} which is higher than that for the corresponding sodium salt in all the cases indicating unidentate character of the carboxylate ligands[13].

Table 2 – Mössbauer parameters†, magnetic moments and electronic spectral bands of various carboxylato complexes at room temperature (25°C)

Complex	Isomer shift* δ (mm s^{-1})	Quadrupole splitting ΔE_Q (mm s^{-1})	$\mu_{eff.}$ (B.M.)	Electronic spectral bands (cm^{-1})	
1	0.58	0.30	5.66	25,000	19,600
2	0.64	0.78	6.02	25,000	19,600
3	0.66	0.60	5.26	25,320	19,600
4	0.58	0.88	6.23	25,310	20,200
5	0.64	0.54	5.77	25,320	19,230
6	0.67	0.36	5.75	25,000	20,200
7	0.65	0.56	5.89	25,000	19,050
8	0.62	1.92	5.29	25,000	19,200
9	0.74 Fe(III)	1.11	6.36	25,000	–
	1.54 Fe(II)	2.71			

* w.r.t. sodium nitroprusside as a standard. † Standard deviations are ± 0.03 mm s^{-1}.

It has also been shown that the direction of shift of ν_{as}(OCO) mode in the coordinated unidentate carboxylate ligand is towards higher wavenumbers, whereas that of ν_s(OCO) is towards lower wavenumber compared to their respective positions in simple ionic carboxylates[16]. In the present study, ν_{as}(OCO) mode appears either at a higher or at the same wave number and ν_s(OCO) appears at a lower wavenumber with respect to the corresponding sodium salt of the acid. Therefore, both criteria, the magnitude of separation as well as the direction of shift, indicate a unidentate nature of carboxylate ligands[14–16].

The ν(Fe–O) mode in the complexes studied here appears in the region 540-440 cm^{-1} in accordance with that reported in the literature[20,21]. Bassi *et al.*[22] have also observed ν(Fe–O) for alkali tris(malonato)ferrates(III) in the range 560-530 cm^{-1}. In aliphatic carboxylates Fe–O stretching frequencies increase in the order $(CH_3)_3C- < CH_3(CH_2)_5- < CH_3(CH_2)_{10}-$. On the other hand, for substituted benzoato complexes ν(Fe–O) values are higher than those for aliphatic carboxylate complexes. This may be explained in terms of a partial double bond character for H_5C_6-C bond causing a partial change in polarity of the Fe–O bond.

For pyridine 2,6-dicarboxylic acid complex, additional bands at 1600 and 1430 cm^{-1} are observed corresponding to free uncoordinated carboxylic acid. It suggests only bidentate nature of pyridine 2,6-dicarboxylic acid. Also a characteristic band corresponding to Fe–N stretching vibration at 400 cm^{-1} is observed. Naik and Curran[23] have also confirmed bidentate nature of pyridine 2,6-dicarboxylic acid in its Sn(IV) complexes, thus leaving one –COOH free.

For quinic acid an unusual situation seems to exist where one COOH and four OH groups are present. Two bands at 1610 and 1420 cm^{-1} correspond to ν_{as}(OCO) and ν_s(OCO) respectively suggesting a unidentate coordination for the carboxylate. However, analytical and physical measurements suggest the ligand to be bidentate which is possible only if one of the –OH groups is also bonded. Besides, a band at 480 cm^{-1} due to ν(Fe–O) (from-COO) and another weak band at 360 cm^{-1} due to ν(Fe–N) confirm this suggestion[13]. Presence of other free OH groups is confirmed by a broad band at 3250 cm^{-1}.

Mössbauer studies

A perusal of Table 2 indicates that for aliphatic carboxylate complexes δ varies in the narrow range of 0.58-0.66 mm s^{-1} and increases in the order: $(CH_3)_3C- < CH_3(CH_2)_5- < CH_3(CH_2)_{10}-$. For substituted benzoato complexes also δ varies in the range 0.58-0.67 mm s^{-1} indicating only a small change in *s*-electron density at the iron nucleus. It may be attributed to π-resonance as a result of which some electronic charge may be donated to the *d*-orbitals of Fe resulting in variation

Table 3 – Thermogravimetric data of the carboxylate complexes

Complex	Starting dec. temp. (°C)	DTG peak (°C)	Dec. Process	Constant Wt. Temp. (°C)	Final wt (%)	Possible end product
1	120	320	(slow)	450	24.8	$3Na_2O.Fe_2O_3$
2	200	270	(fast)	480	27.0	$3Na_2O.Fe_2O_3$
3	150	260	(fast)	480	17.6	$3Na_2O.Fe_2O_3$
4	200	380	(fast)	460	22.2	$2NaCl.NaFeO_2$
5	150	450	(very slow)	550	19.17	$3Na_2O.Fe_2O_3$
6	100	220	(very slow in stages)	560	36.4	—
7	200	350 250	(slow in stages)	550	34.52	—
8	80	160 540	(very fast)	600	63.0	Loss of CO_2 at 160°C, later two ligands are lost.
9	180	240	(very fast)	400	47.7	Fe_2O_3

in δ values. Nature of electron donating or withdrawing groups at *o*- and/or *p*-position of the benzene ring may also affect the isomer shift[8,24]. This is because disubstitution in benzene ring may affect the nature of Fe–O bond to some extent. Similar variations have been observed in alkyl phosphine and phosphite substituted pentacyano ferrate complexes[25]. It is well known that δ values and metal-ligand stretching vibrations are affected by the substitution of alkyl or halide group in the ligand irrespective of low or high spin nature of iron(III) complex.

In case of point charges surrounding Fe(III) ion in octahedral geometry no quadrupole splitting is expected, because the 3*d*-electrons are equally populated. However, substituted carboxylate ligands are large enough to cause distortion and hence net electric field gradient (EFG) is generated due to ligand contribution giving rise to quadrupole splitting. In the present studies of alkyl and substituted benzoato complexes, ΔE_Q in the range of 0.30-0.88 mm s^{-1} is observed suggesting small but significant distortions in the octahedral geometry.

Amongst aliphatic carboxylate complexes, ΔE_Q increases from 0.30 for trimethylacetato complex to 0.78 mm s^{-1} for heptanoic acid complex. On further increase in chain length in dodecanoic acid, it is reduced to 0.60 mm s^{-1}. It means that with increasing chain length, first ΔE_Q increases and then subsides suggesting a decrease in distortion. Probably with increasing chain length, the chain coils causing a decrease in distortion and hence decrease in ΔE_Q. Almost a similar observation was made by us for dicarboxylate complexes[10].

It is further observed from Table 2 that within the series of substituted benzoato complexes, large variation in ΔE_Q is observed. 2,5-Dichlorobenzoato complex exhibits large ΔE_Q (0.88 mm s^{-1}) compared to 2,5-dimethylbenzoato complex (0.54 mm s^{-1}). Similarly, 3-methoxybenzoato complex gives larger $\Delta E_Q = 0.56$ mm s^{-1} compared to 2-methoxybenzoato complex (0.36 mm s^{-1}). These observations clearly suggest that not only the nature of substituent but also the position of substitution affects the distortion in geometry quite significantly.

In the case of pyridine 2,6-dicarboxylic acid complex the δ value (0.56 mm s^{-1}) lies within the range expected for typical iron(III) high spin complexes[6,7]. However, it exhibits quite a large $\Delta E_Q = 1.92$ mm s^{-1} suggesting a large distortion presumably due to free carboxylic acid group. Naik and Curran[23] have also observed large ΔE_Q for Sn(IV) complexes of this ligand.

In the case of quinic acid complex a three line spectrum (Fig. 2B) has been observed. It can be

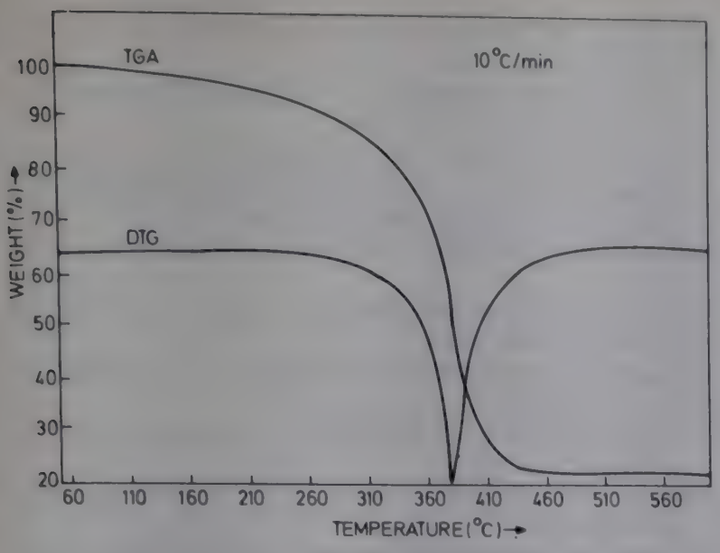

Fig. 3 – TGA and DTG plots of sodium hexa-2,5-dichlorobenzoatoferrate(III)

resolved into two doublets arising due to Fe(II) and Fe(III) states. It seems that besides the Fe(III) complex, Fe(II) complex is also formed. In that case larger ΔE_Q (= 2.71 mm s^{-1}) may be due to Fe(II) state while the smaller ΔE_Q (= 1.11 mm s^{-1}) may be due to Fe(III) complex. Such a large ΔE_Q in Fe(III) complex indicates large distortion because of cyclohexane ring. The observed δ values of 0.74 and 1.54 mm s^{-1} also correspond to Fe(III) and Fe(II) states respectively. As suggested in preceding section on IR, iron may be bound through carboxylate and hydroxyl groups at 1 and 5 positions respectively. At this stage it is difficult to say if it is a mixture of two complexes or both the states of iron exist in the same complex. Surprisingly, its magnetic moment is quite high.

Thermal decomposition studies

In most studies on thermal decomposition of carboxylate complexes, sodium ferrate $NaFeO_2$ has been identified as the end product[26-29]. Table 3 lists the thermal decomposition data. In all the cases no weight loss was observed around or below 100°C except in the case of pyridine 2,6-dicarboxylic acid complex. It indicates absence of water molecules in all the carboxylate complexes. For all the three aliphatic carboxylate complexes a constant weight was obtained at 450°C and this corresponds to Na_3FeO_3 or $3Na_2O.Fe_2O_3$. Formation of sodium ferrate is confirmed by the characteristic six line Mössbauer spectrum. When trimethylacetic acid complex was heated at 200°C for 4 hr, ΔE_Q increased from 0.30 to 0.62 mm s^{-1}. On further heating at 350°C for 4 hr, it gave a six line spectrum with $\delta = 0.70$ mm s^{-1} confirming the formation of Na_3FeO_3. In the case of 2,5-dimethylbenzoato complex also final weight corresponded to the same composition. For 2,5-dichlorobenzoato complex, decomposition was very fast as shown in Fig. 3, yielding a DTG peak at 380°C and a constant weight of 22.2% at 460°C. This may be assigned to the final product having the composition $2NaCl.NaFeO_2$. In the case of two methoxy benzoates and quinic acid complexes, all giving about 35-47% final weight, it is difficult to assign any possible composition for the final product.

For pyridine 2,6-dicarboxylic acid complex, a two stage decomposition is observed, similar to the case of malonic acid complexes[19]. Presumably in the first stage a CO_2 molecule belonging to the free carboxylic acid is knocked out at 160°C. Later two ligands seem to be lost, yielding simple iron complex with pyridine carboxylate. A similar observation has been made by Allan *et al.*[29] for pyridine 2,3-dicarboxylic acid complexes of Mn, Fe, Co and Ni which ultimately yield metal oxide.

When quinic acid complex was heated at 220°C for 4 hr, it gave a six line Mössbauer spectrum with $\delta = 0.72$ mm s^{-1} which corresponds to the formation of α-Fe_2O_3 as in other previously reported cases[26,29].

Acknowledgement

Grateful thanks are due to the CSIR, New Delhi, for financial assistance. Thanks are also due to the authorities of the Regional Sophisticated Instrumentation Centres, Lucknow, and Nagpur for elemental analysis, infrared spectra and thermal studies respectively.

References

1 Oldham C, *Progress in inorganic chemistry*, Vol. 10, edited by F A Cotton (Interscience, New York), 1968, 223.
2 Alcock N W, Tracy V M & Waddington T C, *J chem Soc*, (1976) 2243.
3 Mehrotra R C & Bohra R, *Metal carboxylates* (Academic Press, London) 1983, 396.
4 Jorgenson C K, *Inorganic complexes* (Academic Press, London) 1963, 94.
5 Bancroft G M, Maddock A G & Randl R P, *J chem Soc* (*A*), (1968) 338.
6 Hoy G R & Barrows F de S, *Phys Rev*, 139 (1965) 929.
7 Duncan J F, Kanekar C R & Mok K F, *J chem Soc* (*A*), (1969) 480.
8 Garg A N, Parwate D V & Raj D, *Indian J Chem*, 26A (1987) 304.
9 Garg A N, Shukla P N & Goel P S, *Inorg chim Acta*, 5 (1971) 520.
10 Lanjewar R B, Waditwar A M & Garg A N, *J radioanal nucl Chem*, 125 (1988) 75.
11 (a) Selwood P W, *Magnetochemistry* (Wiley Interscience, New York) 1965.
(b) Dutta R L & Syamal A, *Elements of magnetochemistry* (S Chand, New Delhi), 1982, 139.

12 Long G J, Robinson W T, Tappmeyer W P & Bridges D L, *J chem Soc Dalton Trans*, (1973) 573.
13 Nakamoto K, *Infrared spectra of inorganic and coordination compounds*, 4th Edn (Wiley Interscience, New York), 1986, 231.
14 Nakamoto K, Morimato Y & Martel A E, *J Am chem Soc*, 83 (1961) 4528.
15 Manhas B S & Trikha A K, *J Indian chem Soc*, 58 (1981) 284.
16 Deacon G B & Philips R J, *Aust J chem*, 31 (1978) 1709; Deacon G B, Huber F & Philips R J, *Inorg chim Acta*, 104 (1985) 41; *Coord Chem Rev*, 33 (1980) 227.
17 Tyagi A S & Srivastava C P, *J Indian chem Soc*, 58 (1981) 284; 59 (1982) 823.
18 Dziobkowski C T, Wrobleski J T & Brown D B, *Inorg Chem*, 20 (1981) 671, 679.
19 Lanjewar R B & Garg A N, *Indian J Chem* (MSS No. 6435). In Press.
20 Ferrao J R, Driver R, Walker W R & Wazniak W, *Inorg Chem*, 6 (1967) 1586.
21 Schemetz M J, Nakagawa I, Mizushima & Quagliano J V, *J Am chem Soc*, 81 (1959) 287.
22 Bassi P S, Randhawa B S & Kaur S, *Hyper Inter*, 28 (1986) 745.
23 Naik D V & Curran C, *Inorg Chem*, 10 (1971) 1017.
24 Gupta D C & Sharma N D, *Indian J Chem*, 16A (1978) 526.
25 Inoue H, Sasagawa M, Fluck E & Shirai T, *Bull chem Soc Japan*, 56 (1983) 3434.
26 Bassi P S, Randhawa B S & Bilaspuri G K, *J thermal Anal*, 31 (1986) 1007.
27 Music S, Ristic M & Popovic P, *J Radioanal nucl Chem articles*, 121 (1988) 21.
28 Bassi P S, Randhawa B S & Jain H S, *Thermochim Acta*, 62 (1983) 209.
29 Allan J R, Barron M & Werninck A R, *Thermochim Acta*, 116 (1987) 275.

Indian Journal of Chemistry
Vol. 30A, April 1991, pp. 357-362

Multidentate behaviour of 2-formylcyclohexanone schiff bases in the Co(II), Ni(II), Cu(II) and Zn(II) complexes

C Natarajan*, C D Sheela & P R Athappan
Department of Inorganic Chemistry, Madurai Kamaraj University, Madurai 625 021, India

Received 22 May 1990; revised 5 September 1990; accepted 10 December 1990

Metal(II) chelates of schiff bases derived from the condensation of 2-formylcyclohexanone with *o*-aminophenol (FCAP), *o*-aminothiophenol (FCAT) or *o*-aminobenzoic acid (FCAB) have been prepared and characterized. The complexes are of the type M(ONX)nB for M = Cu(II) and Zn(II), and $M(NX)_2nB$ for M = Co(II) and Ni(II) [X = phenolic oxygen, sulphur or carboxylic oxygen; B = H_2O, Py; n = 0, 1 and 2]. Conductivity data indicate non-ionic nature of the complexes. IR and PMR data show that while the free ligands exist in the ketamine form, in the complexes they exist in the enimine form. All the schiff bases behave as dibasic tridentate ligands in the Cu(II) and Zn(II) complexes and monobasic bidentate ligands in Ni(II) and Co(II) complexes. The subnormal magnetic moments of Cu(II) complexes are ascribed to antiferromagnetic interaction arising from dimerisation: Pyridine cleaves the dimers to afford square-planar monomers with pyridine occupying the fourth coordination site. Ni(II) and Co(II) complexes of FCAP and FCAT schiff bases are low-spin with square-planar structure while the corresponding FCAB schiff base complexes are high-spin with octahedral geometry.

Metal derivatives of schiff base ligands have been extensively studied[1-4]. In recent years considerable interest has been evinced in the chemistry of complexes with tridentate ligands. Such ligands, because of their ability to form mono and bis species, yield complexes with different structural features[5-11]. Further interest in this type of complexes stems from the proposed existence of similar bimetallic sites in several copper enzymes concerned with oxygen transport, storage and reactivity. A search for synthetic analogues of binuclear copper(II) system to mimic type III proteins resulted in the synthesis and study of a large number of systems[12-14]. Much attention has been paid to the metal complexes of *o*-hydroxyarylideneaminoacids[15] and hydrazones[16] which may provide a model for the mechanism of amineoxidase inhibition. Binuclear Pd(II) and Ni(II) complexes with NNS donor set have been reported recently[17]. Apart from the traditional tridentate ligands, Ni(II) complexes with the ligands having −O, O, O− sequence have also been reported[18]. In view of novelties in structures introduced by these ligands it was felt worthwhile to investigate the behaviour of tridentate schiff base ligands of 2-formylcyclohexanone. In this paper we report the synthesis and characterization of N-2-formylcyclohexylidene-*o*-aminophenol (FCAP), N-2-formylcyclohexylidene-*o*-aminothiophenol (FCAT) and N-2-formylcyclohexylidene-*o*-aminobenzoic acid (FCAB).

Materials and Methods

Metals were determined by incinerating the complexes with an excess of $(NH_4O_2C)_2.H_2O$. Elemental analyses were carried out at VHNSN College, Virudhunagar, India. Conductivity measurements in MeOH were made using a Toshniwal conductivity meter and the weight loss experiments were done in an air oven. Magnetic susceptibilities were measured at 8000 G in a Gouy balance calibrated against $Hg[Co(NCS)_4]$ at 302-304 K. Electronic spectra were recorded in $CHCl_3$ using Perkin-Elmer 402 UV-VIS spectrophotometer and Shimadzu UV-160 spectrophotometer. IR spectra (4000-200 cm^{-1}) were obtained in KBr phase on a Perkin-Elmer 577 grating spectrophotometer. PMR spectra were recorded in $CDCl_3$ or pyridine-d_5 with TMS as the internal standard on a Perkin-Elmer R32, 90 MHz spectrometer. Molecular weights were determined cryoscopically in diphenyl (71°C).

Syntheses of ligands

2-Formylcyclohexanone (FCH) was prepared by the Claisen condensation of cyclohexanone with

ethyl formate in the presence of metallic sodium as reported in the literature[19]. The schiff bases were prepared as follows:

N-2-Formylcyclohexylidene-o-aminophenol (FCAP)

Equimolar amounts (20 mmol) of FCH and *o*-aminophenol were dissolved in 30 cm^3 of hot EtOH and the mixture was kept below 20°C for 2 h. The precipitate that separated was recrystallised from EtOH to obtain yellow needles, m.p. 183°C [Found (calc.) % for $C_{13}H_{15}NO_2$: C, 71.83 (71.89); H, 6.57 (6.91); N, 6.24 (6.45)].

N-2-Formylcyclohexylidene-o-aminobenzoic acid (FCAB)

To 6.3 cm^3 (50 mmol) of FCH dissolved in EtOH (20 cm^3), 6.85 g (50 mmol) of *o*-aminobenzoic acid in 10 cm^3 of EtOH was added and the contents were heated on a water bath for 15 min, cooled and refrigerated overnight. The product obtained was recrystallised from EtOH to get orange-yellow needles, m.p. 197°C (lit.[20] m.p. 199°C).

The schiff base could not be isolated in the case of N-2-formylcyclohexylidene-*o*-aminothiophenol (FCAT).

Syntheses of complexes: Co(FCAP)$_2$, Ni(FCAP)$_2$, Cu(FCAP) and Zn(FCAP).H$_2$O

A solution of metal(II) acetate [10 mmol in the cases of Cu(II) and Zn(II) salts and 5 mmol in the cases of Co(II) and Ni(II) salts in H_2O (10 cm^3)] was mixed with FCAP (10 mmol) solution in hot EtOH (30 cm^3). A few drops of NaOH solution were added to make the solution neutral and the complex that separated was collected on a filter, washed with H_2O, aqueous EtOH and dried *in vacuo*.

Co(FCAT)$_2$, Ni(FCAT)$_2$, Cu(FCAT) and Zn(FCAT).H$_2$O (in situ)

A mixture of *o*-aminothiophenol (5 mmol) and FCH (5 mmol) was added to EtOH (20 cm^3) and stirred magnetically for 0.5 h. To this solution, 1 *M* aqueous NaOH (4 cm^3) was added followed by an ethanolic solution of metal(II) chloride [5 mmol for Cu(II) and Zn(II) salts and 2.5 mmol for Co(II) and Ni(II) salts]. The stirring was continued for an hour and the solid that formed was filtered, washed with water followed by EtOH:H_2O (1:1 v/v) and dried *in vacuo*.

Co(FCAB)$_2$.2H$_2$O, Ni(FCAB)$_2$.2H$_2$O, Cu(FCAB) and Zn(FCAB).H$_2$O

FCAB (10 mmol) in EtOH (30 cm^3) was added to the solution of appropriate metal(II) acetate [10 mmol for Cu(II) and Zn(II) salts and 5 mmol for Co(II) and Ni(II) salts] in H_2O (10 cm^3) with stirring. The copper complex that separated immediately was filtered, washed with H_2O and aqueous EtOH and dried *in vacuo*. In the case of Ni(II), Co(II) and Zn(II) complexes the *p*H was raised to 7 and contents diluted with water when the solid separated out. It was filtered, washed with aqueous EtOH and dried *in vacuo*.

Cu(FCAP).Py, Cu(FCAT).Py and Cu(FCAB).Py

The copper complex was dissolved in excess of pyridine and refluxed for 0.5 h. The excess pyridine was evaporated at room temperature when the monopyridinate separated in crystalline form. The crystals were filtered, washed with petroleum ether (b.p. 60-80°C) and dried *in vacuo*.

Results and Discussion

The analytical data of the complexes and their colours are given in Table 1. The data are consistent with formulae MLnB for Cu(II) and Zn(II) complexes and ML_2nB for Ni(II) and Co(II) complexes. All the chelates are soluble in organic solvents and insoluble in water. Weight loss experiments indicate loss of water in the case of zinc complexes, $Co(FCAB)_2(H_2O)_2$ and $Ni(FCAB)_2(H_2O)_2$ at 130°C. Conductance measurements in MeOH indicate that the complexes are non-electrolytes (Λ_M = 10-20 ohm^{-1} cm^2 mol^{-1}).

Infrared and PMR spectra

The ligands can exist in three tautomeric forms[21], viz., ketimine(I), enimine(II) and ketamine(III).

The IR spectra of FCAP, FCAB and its potassium salt show a broad absorption around 3300-3450 cm^{-1} which may be due to hydrogen bonded ν(OH) in structure(II) or ν(NH) in (III). The strong band appearing in the region 1630-1655 cm^{-1} has been assigned to perturbed ν(C=O), and the lowering from typical free carbonyl value may be ascribed to chelation and hydrogen bonding. The next intense band in the 1500-1520 cm^{-1} region has been assigned to NH deformation mode. All these data are indicative of ketamine structure(III)[21,22] for the ligands. A more definite evidence for the presence of acidic proton is adduced from the PMR studies. The ligands show a doublet around δ 10-12 ppm (exchangeable with D_2O) which may be due to NH or OH proton. But the large coupling constant (J = 13 cps) by which this signal is split, rules out the possibility of the hydroxylic proton in (II), since it is

Table 1 – Elemental analyses, colour and magnetic moments of complexes

Complex (colour)	Found (Calc.), %				$\mu_{eff.}$ (B.M.)
	M	C	H	N	
Cu(FCAP) (Green)	22.73 (22.81)	55.62 (56.01)	4.25 (4.67)	4.72 (5.03)	1.08
Cu(FCAP).Py (Dark green)	17.78 (17.77)	59.92 (60.41)	5.23 (5.03)	7.54 (7.83)	1.88
$Ni(FCAP)_2$ (Brown)	12.41 (11.96)	63.48 (63.58)	5.82 (5.71)	5.45 (5.71)	dia.
$Co(FCAP)_2$ (Brown)	11.87 (12.00)	63.21 (63.55)	5.31 (5.70)	5.42 (5.70)	2.59
$Zn(FCAP).H_2O$ (Yellow)	21.68 (21.91)	52.01 (52.28)	4.82 (5.03)	4.46 (4.69)	dia.
Cu(FCAT) (Green)	22.02 (21.57)	53.34 (52.96)	4.73 (4.41)	4.95 (4.75)	1.16
Cu(FCAT).Py (Brown)	16.69 (17.01)	58.40 (57.83)	4.35 (4.82)	7.84 (7.50)	1.71
$Ni(FCAT)_2$ (Brown)	11.15 (11.23)	60.05 (59.69)	5.16 (5.36)	5.05 (5.36)	1.23
$Co(FCAT)_2$ (Brown)	10.91 (11.27)	59.92 (59.66)	5.22 (5.35)	5.60 (5.35)	2.02
$Zn(FCAT).H_2O$ (Yellow)	20.48 (20.79)	50.01 (49.62)	5.13 (4.77)	4.35 (4.45)	dia.
Cu(FCAB) (Green)	20.58 (20.73)	54.39 (54.81)	4.04 (4.24)	4.47 (4.57)	1.90
Cu(FCAB).Py (Dark green)	16.07 (16.48)	59.65 (59.14)	4.92 (4.67)	6.91 (7.26)	1.78
$Ni(FCAB)_2.2H_2O$ (Cream)	9.84 (10.11)	57.32 (57.86)	5.20 (5.17)	4.45 (4.82)	2.75
$Co(FCAB)_2.2H_2O$ (Orange)	10.32 (10.14)	57.31 (57.84)	5.12 (5.16)	5.02 (4.82)	4.86
$Zn(FCAB).H_2O$ (White)	20.43 (20.03)	51.74 (51.48)	4.81 (4.60)	4.62 (4.29)	dia.

relatively far away from the methine proton than the NH proton in (III). The reported coupling constant of 12.8 cps for $H-N-C''$ by Dudek and Volpp[23] support the inference. The phenolic and carboxylic protons occur as singlets at δ 9.9 and 12.7 ppm respectively. Similar ketamine

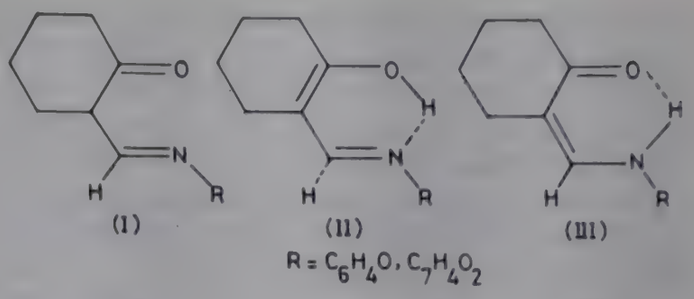

structures have been proposed for the schiff bases of 2-formylcyclohexanone[24] and other β-diketones[21,22].

In all the metal complexes of FCAP and FCAB, the bands due to ν(NH), ν(CO) and δ(NH) are conspicously absent. But an intense band in the 1590-1630 cm^{-1} region appears which is assigned to ν(C=N). In the PMR spectra of $Ni(FCAP)_2$, $Zn(FCAP).H_2O$ and $Zn(FCAB).H_2O$, the doublet due to NH disappears. These observations suggest that the ligands coordinate in the enimine form (II) involving coordination through C=N group.

In all the mono and bis complexes of FCAP, the νOH (phenolic) observed around 2580-2630 cm^{-1} in the ligand disappears indicating deprotonation. The ν(C–O) suffers a positive shift showing coordination through phenolic oxygen. ν(OH) observed at 3200 cm^{-1} in FCAB vanishes in all the metal chelates suggesting deprotonation of COOH group. In the potassium salt of the ligand, the ν_{as}(COO) and ν_s(COO) occur respectively at 1610 and 1375 cm^{-1}; these are lowered in the metal chelates. The separation (Δν 205-229 cm^{-1}) between these two bands for the Co(II), Ni(II) and Zn(II) complexes indicates unidentate carboxylate coordination[25] while that for the Cu(II) complex (Δν 172 cm^{-1}) is diagnostic of bridged carboxylate coordination[26]. In FCAT complexes a weak band in the range 645-662 cm^{-1}, characteristic of ν(C–S), appears[27] in addition to ν(C=N) in the 1610-1622 cm^{-1} range.

In relation to the parent compounds, the pyridine adducts Cu(FCAP).Py, Cu(FCAT).Py and Cu(FCAB).Py show a decrease in ν(C=N) (10-25 cm^{-1}). Further, Cu(FCAP).Py registers a lower value for ν(C–O) (3-9 cm^{-1}) and Cu(FCAT).Py a lower value for ν(C–S) (38 cm^{-1}). The decrease suggests that these bonds are weakened and this may be due to the σ-donor and π-acceptor properties of pyridine. In the Cu(FCAB).Py complex, ν_s(COO) manifests a decrease of 32 cm^{-1} causing the Δν value to increase to 204 cm^{-1}. This is characteristic of unidentate carboxylate[25] coordination which suggests that on pyridine addition, the binuclear structure of Cu(FCAB) involving carboxylate bridge has collapsed to give monom-

ers with pyridine occupying the fourth coordination site. The presence of pyridine in the adducts is indicated by a series of pyridine ring vibrations near 1000 cm^{-1} and also the characteristic bands[28] at 628 and 420 cm^{-1}.

The PMR spectra of Zn(II) complexes show no signals due to alicyclic OH. These complexes exhibit ν(OH) in the region 3200-3350 cm^{-1} due to coordinated water. In the IR spectra of Cu(FCAP), Cu(FCAT) and Cu(FCAB), the alicyclic ν(OH) is absent. These data indicate that these ligands behave as dibasic tridentate in the Cu(II) and Zn(II) complexes involving azomethine nitrogen, phenolic oxygen/sulphur/carboxylic oxygen and alicyclic OH group.

The PMR spectrum of $Ni(FCAP)_2$ manifests a peak at δ 9.7 ppm indicating alicyclic OH proton. In the IR spectra of Ni(II) and Co(II) complexes of FCAP and FCAT the νOH (alicyclic) appears in the region 3240-3360 cm^{-1}. The broad band around 3200 and 3360 cm^{-1} in the $Ni(FCAB)_2.2H_2O$ and $Co(FCAB)_2.2H_2O$ respectively has been ascribed to ν(OH) of the coordinated water and alicyclic OH. The data lend support to the monobasic bidentate behaviour of these ligands in the Ni(II) and Co(II) complexes involving C=N and OH/SH/COOH groups in coordination.

Magnetic moment and electronic spectra: Copper(II) complexes

The copper complexes of FCAP and FCAT have magnetic moments of 1.08 B.M. and 1.16 B.M. respectively. The subnormal magnetic moments indicate binuclear structure (IV) with two planar copper atoms side by side linked by two oxygen or sulphur atoms which will permit antiferromagnetic exchange interaction between copper atoms. The structure is similar to that postulated for acetylacetonemono(*o*-hydroxyanil)copper(II) by Barclay *et al.*[7] on the basis of X-ray studies. It is also quite likely that exchange interaction can occur through the oxygen or sulphur bridges by means of super exchange mechanism[29].

The copper(II) complex of FCAB shows a magnetic moment (1.90 B.M.) which is slightly higher than the spin-only value. In conformity with the bridged carboxylate group predicted by the IR spectra of this complex, a binuclear structure (V) similar to that of Cu(II) complex of 5-nitrosalicylalanthranilic acid[8] has been proposed.

The observed nuclearity of 1.9-2.2 for the Cu(II) complexes of FCAP, FCAT and FCAB in the molecular weight determination is consistent

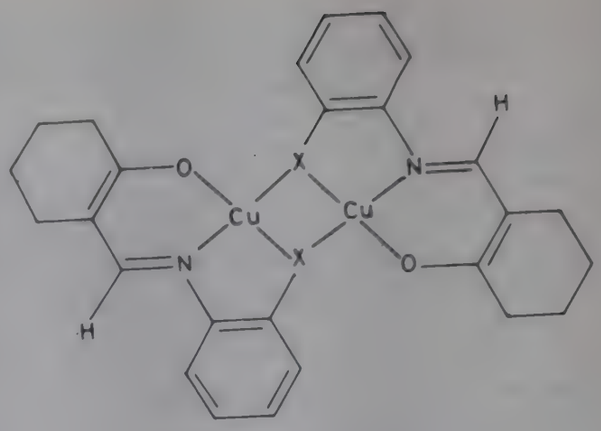

(IV)

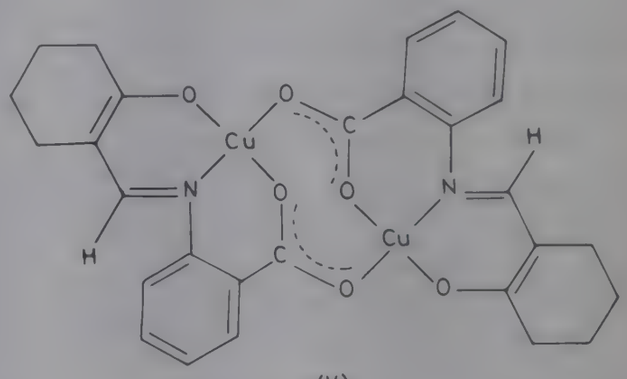

(V)

with a dimeric structure where the tri-coordinate copper achieves ligancy 4. A complexity of 2.0-2.2 has been reported for N-salicylidene-N'-*n*-palmitylhydrazinocopper(II)[30].

The pyridine derivatives obtained from dimeric Cu(FCAP), Cu(FCAT) and Cu(FCAB) have a normal magnetic moment in the 1.71-1.88 B.M. range, characteristic of square-planar monomeric arrangement. On dissolving in pyridine, the dimer molecules dissociate into monomer molecules with pyridine occupying the fourth coordination site[9].

The electronic spectra of Cu(II) complexes of FCAP and FCAT show a broad band in the 16670-19610 cm^{-1} region due to a combination of $^2B_{1g} \rightarrow {}^2A_{1g}$, ^2E_g transitions in a distorted square-plane. In Cu(FCAP).Py and Cu(FCAT).Py the band is shifted to lower frequency (15870-16400 cm^{-1}) indicating adduct formation and square-planar structure of the monomer. The Cu(FCAB) complex shows absorption bands at 13890, 25670 and 38020 cm^{-1}. The low energy ligand field band may be due to $^2B_{1g} \rightarrow {}^2A_{1g}$ transition. The high energy bands are due to the charge-transfer transitions (O→Cu), characteristic of copper carboxylate system[31]. The low energy ligand field band indicates lowering of symmetry due to non-planarity of the eight-membered and

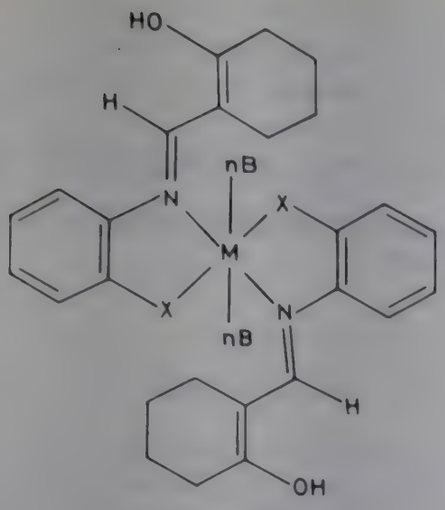

M = Ni(II), Co(II)
N = O, I
B = H_2O
X = O, S, COO
(VI)

six-membered rings in the binuclear structure[8]. In the pyridine adduct, the low energy band is shifted to 15750 cm^{-1}, characteristic of tetragonal Cu(II). This suggests that the non-planar square configuration in the binuclear structure changes to planar structure with six-membered rings only in the monomer[8].

Nickel complexes

The Ni(II) complex of FCAP is diamagnetic with square-planar structure. The Ni(II) complex of FCAT possesses a magnetic moment of 1.23 B.M. As this value is much lower than the spin-only value, a planar structure is proposed for this complex[32]. This is supported by the electronic spectra which are typical of planar complex[31], with the bands at 18660 and in the 22990-25510 cm^{-1} regions arising from $^1A_{1g} \rightarrow {}^1A_{2g}$ and $^1A_{1g} \rightarrow {}^1B_{1g}$ transitions, respectively. However, the Ni(II) complex of FCAB has $\mu_{eff.}$ value of 2.75 B.M. indicating hexacoordinated structure. The peaks in its electronic spectrum at 11720, 17480 and 26810 cm^{-1} may be assigned respectively to $^3A_{2g} \rightarrow {}^3T_{2g}$, $^3A_{2g} \rightarrow {}^3T_{1g}$ and $^3A_{2g} \rightarrow {}^3T_{1g}$ (P) transitions, characteristic of octahedral geometry (VI).

Cobalt complexes

The magnetic moments of Co(II) complexes of FCAP and FCAT are 2.59 and 2.02 B.M., respectively, which are indicative of low-spin Co(II) ion with one unpaired electron[33]. The electronic spectral bands in the 19720-21140 and 21140-25640 cm^{-1} regions are characteristic of square-planar geometry and are assigned to the transitions from lower filled orbitals to a_{1g} (d_{z^2}) orbital[31]. The cobalt-FCAB complex has a moment of 4.86 B.M. It has bands in the visible region at 17990 and 22930 cm^{-1}. The latter band is assigned to $^4T_{1g} \rightarrow {}^4T_{1g}(P)$ transition of Co(II) in an octahedral environment (VI). The other band may be due to a spin-forbidden transition to doublet states derived from free ion ^2H or ^2G terms[31].

Zinc complexes

The Zn(II) complexes are diamagnetic with no ligand field transition. They form 1:1 complexes with the fourth coordination site being occupied by a water molecule. They may presumably have a tetrahedral structure.

Acknowledgement

We thank the CSIR, New Delhi for the award of SRF to one of us (CDS). Our thanks are also due to USIC for providing instrumental facilities.

References

1 Sacconi L, *Coord Chem Rev*, 1 (1966) 126.
2 Yamada S & Takeuchi A, *Coord Chem Rev*, 43 (1982) 187.
3 Holm R H & O'Connor M J, *Prog inorg Chem*, 14 (1971) 241.
4 Cariati F, Ganadu M L, Zoroddu A, Marsani R & Quidacciola R, *Inorg Chem*, 24 (1985) 4030.
5 Casellato U & Vigato P A, *Coord Chem Rev*, 23 (1977) 31.
6 Muto Y, *Bull chem Soc Jpn*, 33 (1960) 1242.
7 Barclay G A, Haris C M, Kaskins B F & Kokot E, *Proc chem Soc*, (1961) 264.
8 Kishita M & Kubo M, *Bull chem Soc Jpn*, 35 (1962) 1241.
9 Kubo M, Kuroda Y, Kishita M & Muto Y, *Aust J Chem*, 16 (1963) 7.
10 Melnik M, *Coord Chem Rev*, 42 (1982) 259.
11 Syamal A, *Coord Chem Rev*, 16 (1975) 309.
12 Sorrell T N, Jamson D L & O'Connor C J, *Inorg Chem*, 23 (1984) 190.
13 Doedens R J, *Prog inorg Chem*, 21 (1976) 209.
14 Fackler J P Jr, *Prog inorg Chem*, 21 (1976) 55.
15 Mahood M R & El-Gyar S A, *Polyhedron*, 6 (1987) 1017.
16 Singh B, Singh R N & Aggarwal R C, *Polyhedron*, 4 (1985) 401.
17 Handa M, Mikurya M, Zhong Z J, Okawa H & Kida S, *Bull chem Soc Jpn*, 61 (1988) 3883.
18 Biradar N S, Patil B R & Kulkarani V H, *Inorg chim Acta*, 15 (1975) 33.
19 Platiner P A & Treadwell P, *Helv chim Acta*, 28 (1945) 771.
20 Petrow V A, *J chem Soc*, (1942) 693.
21 Holtzclaw (Jr) H E, Collman J P & Alire R M, *J Am chem Soc*, 80 (1958) 1100.
22 Dudek G O & Holm R H, *J Am chem Soc*, 83 (1961) 2099.
23 Dudek G O & Volpp G P, *J Am chem Soc*, 85 (1963) 2697.
24 Berde H V, Gogte V N, Jose C I & Tilak B D, *Indian J Chem*, 8 (1979) 493.

25 Carruthern J, Frait K & Rossotti F J C, *Acta Crystallogr*, B31 (1975) 2044.
26 Alcock N W, Tracy V M & Waddington T C, *J chem Soc Dalton*, (1976) 2243.
27 Colthup N B, Dey L H & Wiberly S E, *Introduction to infrared and Raman spectroscopy* (Academic Press, New York), 1964.
28 Percy G C & Thronton D A, *J inorg nucl Chem*, 35 (1973) 2719.
29 Kramers, *Physics*, 1 (1934) 182.
30 Ohto H, *Bull chem Soc Japan*, 33 (1960) 202.
31 Lever A B P, *Inorganic electronic spectroscopy* (Elsevier, Amsterdam), 1968.
32 Shukla P R, Singh V K & Jaiswal A M, *J Indian chem Soc*, 60 (1983) 321.
33 Kent Barefield E, Busch D H & Nelson S M, *Quart Rev*, 22 (1968) 458.

Indian Journal of Chemistry
Vol. 30A, April 1991, pp. 363-368

Formation constants of Mn(II), Cu(II), Co(II), Zn(II), Fe(II), Ni(II) and Pd(II) complexes of peonolphenylhydrazone

G Sreedhar Naidu & R Raghava Naidu*
Department of Chemistry, Sri Venkateswara University, Tirupati 517 502

Received 9 January 1990; revised 4 September 1990; accepted 6 November 1990

Thermal and solution-stabilities of peonolphenylhydrazone chelates of Mn(II), Cu(II), Co(II), Zn(II), Fe(II), Ni(II) and Pd(II) have been measured. Thermodynamic parameters of complex formation and kinetic parameters of complex decomposition have also been evaluated. The solution stabilities determined *p*H-metrically in 75% dioxane-water, acetone-water and ethoxyethanol-water mixtures are in fair agreement with the Irving-Williams series of stability. The results obtained are compared with the data available in the literature for structurally similar ligand complexes. Amongst the solvents employed, acetone-water shows abnormal behaviour. The order of solution stabilities is found to be: Fe > Cu > Pd > Ni > Co > Zn > Mn while that for thermal stabilities, on the other hand, is: Mn > Ni > Pd > Cu > Fe.

In view of the biochemical[1,2] and analytical importance[3-8] of phenylhydrazones, it was thought worthwhile to study the thermal and solution stabilities of the metal chelates of peonolphenylhydrazone (2-hydroxy-4-methoxyacetophenonephenylhydrazone).

Materials and Methods

The proton-ligand and metal-ligand formation constants were determined at different temperatures using Irving-Rossottii[9,10] *p*H titration technique. The titrations were performed using a double-walled beaker thermostated at 20 ± 0.5°C, 30 ± 0.5°C and 40 ± 0.5°C.

Peonolphenylhydrazone (m.p. 108°C) was prepared according to the literature method[11,12]. Its solutions (0.1 *M*) were prepared in various organic solvents. The metal salt solutions were prepared in doubly distilled water and standardised by appropriate standard methods[13]. Acetone, dioxane and ethoxyethanol were purified before use by usual procedures[12].

Cu(II), Ni(II), Pd(II), Fe(II) and Mn(II) complexes were prepared by adding to the metal ion solution (containing about 60 mg of the metal ion) at *p*H 5.0-6.0; 3.5-4.5; 4.5-6.0 and 7.5-8.5 respectively a slight excess of the ligand solution (1% in methanol) and precipitates were washed with hot water followed by methanol and dried *in vacuo*.

An Elico digital (LI-120-A) *p*H meter was used for *p*H-measurements. The experimental procedure involved the titrations of the following solutions (total volume 50 ml) against carbonate free standard sodium hydroxide (0.1 *M*) solution. The ionic strength of the solution was kept at 0.05 *M* (KNO_3).

(a) 5 ml of nitric acid (0.01 *M*)
+ 37.5 ml of organic solvent
+ 5 ml of KNO_3 solution (0.05 *M*)
+ 2.5 ml of water.

(b) 5 ml of nitric acid (0.01 *M*)
+ 36.5 ml of organic solvent
+ 5 ml of KNO_3 solution (0.05 *M*)
+ 2.5 ml of water
+ 1 ml of ligand solution (0.002 *M*).

(c) 5 ml of nitric acid (0.01 *M*)
+ 36.5 ml of organic solvent
+ 5 ml of KNO_3 solution (0.05 *M*)
+ 2 ml of water
+ 1 ml of ligand solution (0.002 *M*)
+ 0.5 ml of metal salt solution (0.01 *M*).

Thermal analysis was carried out at the Institute of Chemistry, KISHINEV, USSR with a MOM (Budapest, Hungary) derivatograph at a heating rate of 5°/min.

The *p*H meter readings were corrected for the non-aqueous medium following the procedure of Van-Uitert and Hass and others. The activity coefficient ($1/\gamma$) for the ionic strength (0.05 *M*) was calculated by interpolation from the data of Debye-Huckel[14] and Harned-Owen[15]. The values for log U_H, log $1/\gamma$ and log U_H° at different temperatures and for different solvents are given in Table 1.

The dissociation constant of the ligand was obtained from the formation curve of the proton-li-

gand system (Table 1). The proton-ligand formation curve was obtained by plotting pH versus $\bar{n}_A$. Metal-ligand formation curves were obtained by plotting $p\bar{L}$ versus $\bar{n}$ values. From the formation curve ($\bar{n}$ versus $p\bar{L}$) it was found that the log K_1 and K_2 values did not show any substantial difference; the values were corrected by the least squares method[10].

The thermodynamic parameters ΔG, ΔH, and ΔS were evaluated from the stability constants of the metal complexes determined at three different

Table 1A— Stepwise and overall stability constants of Fe, Co, Cu, Mn, Ni, Zn and Pd chelates of peonolphenylhydrazone in different aqueous organic solvents

[Temps. = 20°, 30°, 40°C; μ = 0.05 M (KNO_3)]

Temp.		Cu(II)	Pd(II)	Co(II)	Fe(II)	Zn(II)	Ni(II)	Mn(II)
				75% 1,4-Dioxane-water				
20°C	log K_1	13.43	13.27	12.78	13.58	12.18	12.93	11.43
	log β_2	26.25	26.05	23.96	26.76	23.10	24.74	21.26
	log K_2	12.82	12.78	11.18	13.18	10.92	11.81	9.83
30°C	log K_1	13.16	13.08	12.54	13.28	11.91	12.73	11.12
	log β_2	25.94	25.50	23.51	26.20	22.65	24.45	20.83
	log K_2	12.78	12.42	10.97	12.92	10.74	11.72	9.71
40°C	log K_1	13.02	12.92	12.32	13.15	11.73	12.62	10.92
	log β_2	25.39	25.30	23.01	25.68	22.11	24.09	20.05
	log K_2	12.37	12.38	10.69	12.53	10.38	11.47	9.12
				75% Acetone-water				
20°C	log K_1	12.98	12.48	11.73	13.16	10.93	12.18	10.87
	log β_2	25.10	24.19	22.56	25.44	20.99	23.46	20.75
	log K_2	12.12	11.71	10.83	12.28	10.06	12.28	9.88
30°C	log K_1	12.71	12.03	11.17	12.89	10.89	11.74	10.18
	log β_2	24.25	23.48	21.38	25.01	20.44	22.72	19.30
	log K_2	11.83	11.45	10.21	12.12	9.51	10.98	9.12
40°C	log K_1	12.36	11.82	11.10	12.57	10.31	11.62	10.27
	log β_2	23.83	22.85	21.27	24.24	19.74	22.30	19.32
	log K_2	11.47	11.03	10.17	11.67	9.43	10.68	9.25
				75% 2-Ethoxyethanol-water				
20°C	log K_1	12.21	11.89	10.83	12.58	10.47	11.18	10.03
	log β_2	23.54	23.05	20.91	24.56	19.80	21.84	18.90
	log K_2	11.33	11.16	10.08	11.98	9.33	10.66	8.87
30°C	log K_1	12.02	11.52	10.58	12.23	10.24	10.83	9.87
	log β_2	23.11	22.34	20.32	23.70	19.16	21.01	18.20
	log K_2	11.09	10.82	9.74	11.47	8.92	10.18	8.33
40°C	log K_1	11.81	11.40	10.18	12.10	9.98	10.58	9.63
	log β_2	22.69	22.02	19.51	23.58	18.81	20.59	18.00
	log K_2	10.88	10.62	9.33	11.48	8.83	10.01	8.37

Values corrected to ± 0.05 log K units using least squares method.

Table 1B—Ligand formation constants of peonolphenylhydrazone and log U_H°, log U_H and log $1/\gamma$ values in organic media at different temperatures (°C)

Value of	Dioxane-water			Acetone-water			Ethoxyethanol-water		
	20°	30°	40°	20°	30°	40°	20°	30°	40°
Ligand formation constant	12.70	12.65	12.60	12.15	12.05	11.90	11.55	11.45	11.30
log U_H°	0.3898	0.4341	0.4609	0.3029	0.3338	0.3596	0.2191	0.2509	0.2713
log U_H	0.16	0.18	0.19	0.13	0.15	0.16	0.08	0.10	0.11
log $1/\gamma$	0.2298	0.2541	0.2709	0.1729	0.1838	0.1996	0.1391	0.1509	0.1613

Table 2—Thermodynamic parameters of Co, Ni, Mn, Cu, Pd, Zn and Fe chelates of peonolphenylhydrazone in different aqueous organic solvents

[$\mu = 0.05\ M\ (KNO_3)$]

$M(C_{15}H_{15}O_2N_2)_2 \cdot 2H_2O$ M =	Dioxane-water medium			Acetone-water medium			Ethoxyethanol-water medium		
	$-\Delta G$	$-\Delta H$	$+\Delta S$	$-\Delta G$	$-\Delta H$	$+\Delta S$	$-\Delta G$	$-\Delta H$	$+\Delta S$
Cu(II)	35.195	18.045	58.522	33.653	26.647	23.910	30.903	17.725	45.312
Pd(II)	34.926	17.835	58.331	32.432	28.115	14.733	31.560	21.611	33.955
Fe(II)	35.878	22.660	45.112	34.108	25.178	30.479	32.928	20.562	42.204
Zn(II)	30.971	20.772	34.809	28.142	26.227	6.435	26.546	20.772	19.706
Co(II)	32.124	20.143	40.890	30.247	27.067	10.852	28.061	26.727	4.603
Ni(II)	33.170	13.639	66.661	31.453	24.348	24.279	29.281	26.227	10.423
Mn(II)	28.235	21.191	24.036	27.820	25.808	6.868	25.339	18.892	22.003

temperatures using the usual thermodynamic relationships[16]. From the thermal analysis data, the kinetic parameters associated with the complex decomposition reaction were evaluated using the Coats-Redfern[17] equation. Coats-Redfern equation (intergral method) may be written in the form

$$\log\left[\ln\frac{W_a/W_a - W}{T^2}\right] = \log\frac{ZR}{\phi E^*}(1 - 2RT/E^*) - \frac{E^*}{2.303\,RT}$$

where W_a = mass loss at the completion of the reaction, W = mass loss at time, t, Z = frequency factor, ϕ = linear rate of heating and E^* = activation energy of the reaction.

A plot of $\log\left(\ln\frac{W_a}{W_a - W}\Big/ T^2\right)$ versus $1/T$ showed a linear relationship with a slope of $-E^*/2.303\,RT$ from which the activation energy was calculated. The pre-exponential factor was found out from the intercept. The activation entropy ΔS^* was obtained by the relation,

$$\Delta S^* = 2.303\,R \log\frac{Zh}{kT_S}$$

where h is Planck's constnat, k is Boltzmann constant and T_S is the peak temperature from DTG. The free energy of activation G^* and the specific reaction rate constant K_r were calculated using the following equations,

$$G^* = E^* - T_S \Delta S^*$$

$$K_r = Z \exp(-E^*/RT_S)$$

Results and Discussion

Solution stabilities

Peonolphenylhydrazone showed a maximum at $\bar{n}_A = 1.0$ in the dioxane-water, 2-ethoxyethanol-water and acetone-water media indicating that the hydrazone behaves as a monobasic acid. The acid dissociation constant found in different solvent media followed the order, 2-ethoxyethanol < acetone < dioxane. A plot of pK_L versus $1/D$ was found to be linear (where D is the dielectric constant). However, in acetone-water medium, the dissociation constant of the ligand is lower than the expected value and it may be attributed to the non-ideal behaviour of acetone-water solvent. The order of stabilities (Table 1) of the metal chelates observed in all the three solvents was: Fe > Cu > Pd > Ni > Co > Zn > Mn. This almost follows [except Fe(II)] the Irving-Williams order[18].

Table 3—Analytical data of metal complexes

Complex	Found (Calc.), %			
	M	C	H	N
$[Cu(C_{15}H_{15}O_2N_2)_2 \cdot 2H_2O]$	10.59 (10.47)	59.18 (59.06)	5.62 (5.58)	9.09 (9.18)
$[Ni(C_{15}H_{15}O_2N_2)_2 \cdot 2H_2O]$	9.72 (9.68)	59.74 (59.68)	5.83 (5.80)	9.18 (9.25)
$[Fe(C_{15}H_{15}O_2N_2)_2 \cdot 2H_2O]$	9.30 (9.27)	60.06 (59.95)	5.58 (5.49)	9.36 (9.31)
$[Pd(C_{15}H_{15}O_2N_2)_2 \cdot 2H_2O]$	16.29 (16.20)	55.18 (55.09)	5.28 (5.19)	8.65 (8.56)
$[Mn(C_{15}H_{15}O_2N_2)_2 \cdot 2H_2O]$	9.17 (9.13)	59.98 (59.83)	5.69 (5.64)	9.38 (9.30)

Hence, the nature of chelation and the type of bonding may be similar in all the chelates. The higher values for Fe(II) chelates (Table 1) may be due to the resonance stabilities in the system[19,20]. The order of stabilities of the complexes with respect to the solvents is: dioxane > acetone > ethoxyethanol (Table 1). The dielectric constants for the pure as well as the mixed solvents are in the order: acetone > ethoxyethanol > dioxane. This also shows the abnormal behaviour of acetone-water mixture. Similar abnormalities were reported in the literature[21-23]. The enhanced stability of the metal chelates in acetone-water may be due to the weak interacting behaviour of acetone. A plot of log β_2 versus ionization potentials shows that the stabilities of the complexes can be better correlated with the second ionization potential rather than the first.

In general, for a given metal ion, if log K_1 is greater than log K_2 and the difference between them is large, then considerable steric hindrance would be expected during the addition of second ligand molecule. However, the data given in Table 1 show that the difference in the log K_1 and K_2 values is small and the ratio of log K_1/K_2 is positive in all the cases which indicate that there is no steric hindrance to the addition of second ligand molecule and the tendencies for the formation of complex species ML_2 and ML^+ are almost equal. Further, the maximum values obtained for $\bar{n}$ are < 2 confirming 1 : 2 metal-ligand stoichiometry.

A comparison of the data of the overall stability constants (log β_2) of peonolphenylhydrazone complexes with those of peonoloxime and 2-hydroxy-1-naphthaldoxime reveals that solution stabilities of peonolphenylhydrazone chelates are higher than those of peonoloxime[21] and 2-hydroxy-1-naphthaldoxime[24] chelates. This may be attributed to the introduction of $=N-NH-C_6H_5$ group in place of

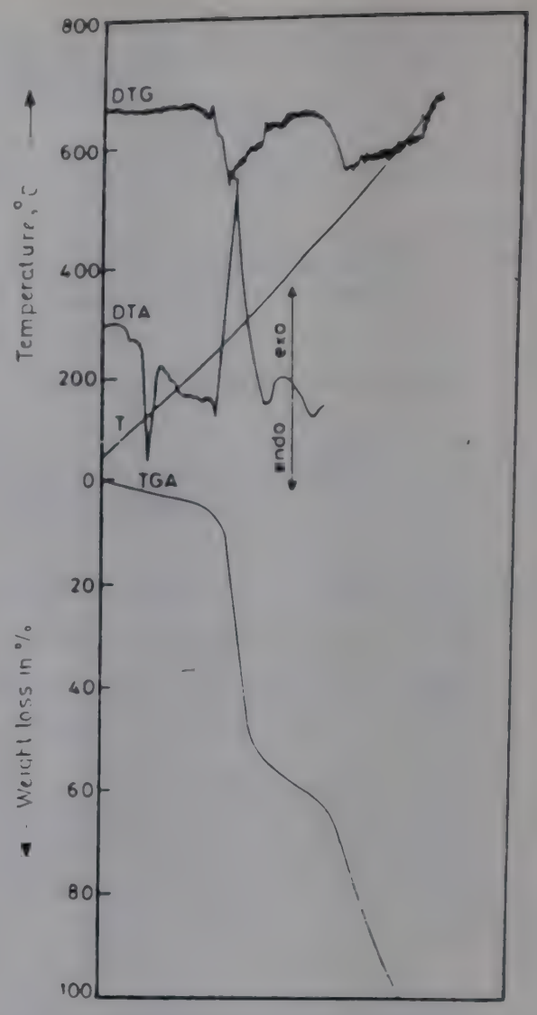

Fig. 1—TGA, DTA and DTG curves of peonolphenylhydrazone

$=N-OH$ group which tends to increase the stabilities of the complexes, due to increase in basic character of the ligand as well as electron density at reactive centre.

The thermodynamic parameters ΔG (Gibbs energy), ΔH (enthalpy) and ΔS (entropy) of peonolphenylhydrazone complexes (Table 2) and log β_2 values show decrease in stabilities with increase in temperature suggesting that the interaction of metal ions with the ligand is exothermic in nature[25]. Further, ΔH_1 values are found to be greater than ΔH_2 (values are not given in Table) indicating that the metal ion progressively loses water molecules[26] with the formation of ML_2 complexes.

Thermal behaviour of solid complexes

The copper(II), nickel(II), palladium(II), iron(II) and manganese(II) complexes are coloured powders, non-hygroscopic in nature and stable in air. None of the complexes sublimed upon heating. Elemental anlaysis data indicate that the complexes are dihydrated and show 1 : 2 (metal : ligand) stoichiometry (Table 3).

Peonolphenylhydrazone is stable upto 115°C (Fig. 1) whereas its metal chelates with Fe(II), Cu(II),

Table 4—Kinetic parameters of peonolphenylhydrazone complexes

Complex	Activation energy, E^* (kcal mol^{-1})	Frequency factor, Z (sec^{-1})	Activation entropy, ΔS^* (e.u)	Free energy of activation, G^* (kcal mol^{-1})	Specific reaction rate constant, K_r (S U^{-1})
$[Cu(PPH)_2 \cdot 2H_2O]$	+21.842	3.901×10^3	−43.839	+53.009	3.961×10^3
$[Ni(PPH)_2 \cdot 2H_2O]$	+14.640	4.933×10	−57.105	+54.213	4.985×10
$[Fe(PPH)_2 \cdot 2H_2O]$	+28.273	6.380×10^5	−33.711	+51.635	6.512×10^5
$[Pd(PPH)_2 \cdot 2H_2O]$	+14.928	1.093×10^3	−46.069	+43.168	1.106×10^3
$[Mn(PPH)_2 \cdot 2H_2O]$	+11.440	2.125×10	−58.988	+58.217	2.140×10

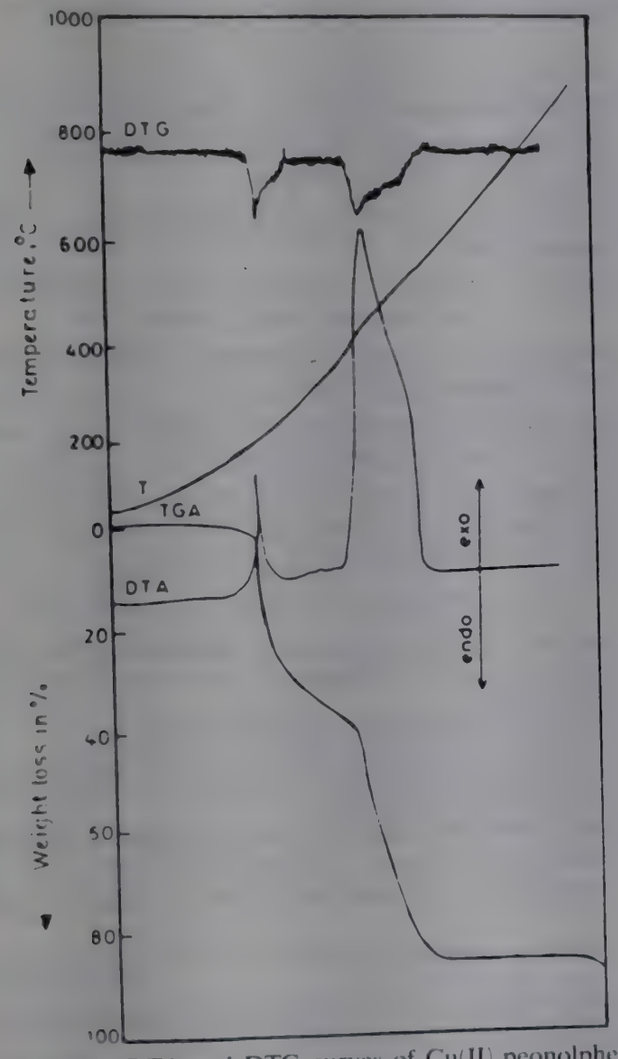

Fig. 2—TGA, DTA and DTG curves of Cu(II) peonolphenylhydrazone chelate

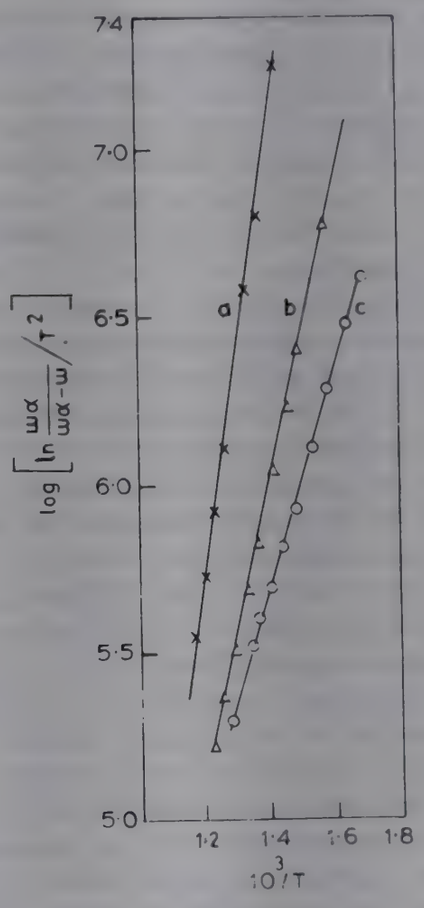

Fig. 3—Coats-Redfern plots of (a) peonolphenylhydrazone; (b) copper chelate and (c) nickel chelate

Pd(II), Ni(II) and Mn(II) are found to be stable upto 150°, 155°, 180° and 195°C respectively. The thermograms (Fig. 2) of these chelates indicate that they are dihydrated which is confirmed by infrared spectral data of the chelates (bands at 3480-3450, 850-835 & 790-755 cm^{-1}). The pyrolysis curves of the chelates show two distinct regions of decomposition, the first stage showing the loss of two water molecules and part of organic material ($-NHC_6H_5$) and the second stage indicating the loss of remaining organic material.

First stage:

$$M(C_{15}H_{15}N_2O_2)_2 \cdot 2H_2O \xrightarrow[\text{Ist stage}]{150\text{-}300^\circ C} M(C_9H_9NO_2)_2$$

Second stage:

$$M(C_9H_9O_2N)_2 \xrightarrow[\text{IInd stage}]{300\text{-}560^\circ C} M/MO$$

The DTG curves of the complexes also indicate two distinct peaks corresponding to the two maximum slopes observed in the TGA curves confirming

the two stages of decomposition of the complexes. The final pyrolysis product in palladium chelate is the metal, while metal oxides are the end products in all the other cases. The order of thermal stabilities is found to be Mn > Ni > Pd > Cu > Fe. Extrapolation of the fairly linear portions of the pyrolysis curves at high and low temperatures and taking the point of intersection as the decomposition temperature leads to the following thermal stability order: Mn > Ni > Pd > Cu > Fe.

The kinetic parameters of complex decomposition process evaluated by using Coats-Redfern equation (Fig. 3, Table 4) reveal that the activation energy values of the complexes are in the order: Fe > Cu > Pd > Ni > Mn. This trend in kinetic parameters is different from the trend in thermal stability. The negative values of entropy of activation (ΔS^*) for all the chelates suggest that the activated complex has a more ordered structure than the reactants and the low Z values indicate that the reactions are slower than normal.

A comparison of the initial decomposition temperatures and the overall stability constants indicates that the thermal stabilities of chelates are in the order: Mn > Ni > Pd > Cu > Fe while the solution stabilities are in the order: Fe > Cu > Pd > Ni > Mn. Iron complex was found to be more stable in solution than Cu, Ni, Pd and Mn chelates. The manganese chelate which is least stable in solution, on the other hand, decomposed at a much higher temperature than the copper, palladium, nickel and iron chelates. The solution and thermal stabilities of these complexes are opposed to each other[22,24,26]. The increase in strength of metal-ligand bond results, therefore, in a decrease in the thermal stability of the complexes. This may be explained by the fact that the thermal decomposition of the chelates investigated does not begin by the scission of the metal-ligand bond but by the cleavage of another bond in the chelate ring. An increase in strength of the coordinating metal-ligand bond results in a weakening of that bond of the chelate ring, which is first ruptured on heating[23,24,27,28].

Acknowledgement

The authors are thankful to Dr C I Turta, Institute of Chemistry, KISHINEV, USSR for help in recording the TGA, DTA and DTG of the metal complexes.

References

1 Kitaev Yu P, Buzykin B I & Troepolskaya T V, *Russion Chem Rev*, (1970) 441.
2 Moon M W, Friedman A R & Steinhards A, *J agr food Chem*, 20 (1972) 1187.
3 Umapathy P & Raju N A, *Indian J Chem*, 1 (1963)272.
4 Umapathy P & Raju N A, *Indian J Chem*, 2 (1964) 248.
5 Umapathy P, Venkata Reddy D & Raju N A, *Indian J Chem*, 3 (1965) 471.
6 Adinarayana Reddy K, Ph.D Thesis, Sri Venkateswara University, Tirupati, 1973.
7 Naik H B, Patel G B & Thakar V M J, *J Indian chem Soc*, 50 (1973) 12.
8 Ray H L, Garg B S & Singh R P, *Curr Sci*, 42 (1973) 852.
9 Calvin M & Melchior N C, *J Am chem Soc*, 70 (1948) 3270.
10 Irving H M & Rossottii H S, *J chem Soc*, (1954) 2904.
11 Adams, *J chem Soc*, 41 (1919) 260.
12 Vogel A I, *A text book of practical organic chemistry* (ELBS, London), 1968.
13 Vogel A I, *A text book of quantitative inorganic analysis*, 3rd Edn (ELBS and Longmans Green, London), 1961.
14 Maron S H & Prutton C F, *Principles of physical chemistry*, 4th Edn (Oxford & IBH) 1967.
15 Harned H S & Owen B B, *Physical chemistry of electrolytic solutions* (Reinhold, New York) 1950, 548.
16 Yalsimirakii K B & Vasilev V P, *Instability constants of complex compounds* (Pergaman Press, Oxford) 1960.
17 Coats A W & Redfern J P, *Nature*, 201 (1964) 68.
18 Irving H M & Williams R J P, *Nature*, 162 (1948) 746.
19 Kalavathi S V, Omprakash K L, Jagannadha Charyulu K, Chandhrapal A V & Reddy M L N, *Indian J Chem*, 27A (1988) 823.
20 Ratoury V G, *J inorg nucl Chem*, 41 (1979) 250.
21 Suresh Babu V, Ugandhar Raju D & Raghava Naidu R, *Indian J Chem*, 18A (1979) 87.
22 Grigoripopa, Constantine Luca & Vasile Mage, *Chem Abstr*, 63 (1965) 2438.
23 Seshagiri V & Brahmaji Rao S, *Aust J Chem*, 20 (1967) 2783.
24 Ramesh A, Seshadri Naidu R & Raghava Naidu R, *Indian J Chem*, 19A (1980) 1133.
25 Subba Reddy V V, Sethuram B & Navaneeth Rao T, *Indian J Chem*, 17 (1979) 200.
26 Bandoopadyay Anupkumar & Choudhury A K, *Indian J Chem*, 26 (1987) 853.
27 Seshagiri V & Brahmaji Rao S, *Z Anal Chem*, 262 (1972) 275.
28 Seshadri Naidu R & Raghava Naidu R, *Indian J Chem*, 15A (1977) 254.

Indian Journal of Chemistry
Vol. 30A, April 1991, pp. 369-371

Notes

Osmium(VIII) mediated vanadium(V) oxidation of arsenic(III) in aqueous sulphuric acid

M I Sambrani & J R Raju*

Chemistry Department, Karnatak University, Dharwad 580 003

Received 6 June 1990; revised 30 October 1990; accepted 30 November 1990

Osmium(VIII) mediated oxidation of As(III) by V(V) in aqueous sulphuric acid involves formation of an Os(VIII)-As(III) complex which interacts with V(V) resulting in a termolecular complex. The latter then yields As(V). The probable active species are discussed.

Osmium(VIII) catalysed Ce(IV) oxidation of As(III) in acid medium has been shown to proceed via a multistep mechanism involving different intermediate oxidation states of Os(VIII)[1] like Os(VII), Os(VI) and Os(V); the key elementary step is the Os(VIII)-As(III) interaction leading to the formation of one mole each of As(V) and Os(VI) with rate constant $k_a = 1.45 \times 10^5$ dm^3 mol^{-1} s^{-1} at 25°C. This key Os(VIII)-As(III) interaction seems to be common in the oxidation of As(III) by one equivalent oxidants in acid medium[2]. In view of our interest in the key step, Os(VIII)-As(III) reaction and the catalytic role generally displayed by Os(VIII), we have studied the title reaction and the results are presented here.

Experimental

Reagent grade chemicals and doubly distilled water were used throughout. Arsenic(III), As(V) and Os(VIII) solutions were prepared as described elsewhere[3]. The stock solution of V(V) was prepared by dissolving NH_4VO_3 in 0.50 mol dm^{-3} H_2SO_4 and standardised. Ionic strength, calculated from the *in situ* $[H^+]$, $[HSO_4^-]$ and $[SO_4^{2-}]$ obtained from the acid sulphate equilibrium constant and dissolved $[SO_4^{2-}]$, was maintained using Na_2SO_4. Temperature was constant within ±0.05°C.

Kinetics

Thermally equilibrated solutions containing the required amounts of Os(VIII), H_2SO_4 and Na_2SO_4 were mixed and the reaction was followed spectrophotometrically by measuring the absorbance of V(V) in the reaction solution at 360 nm using a Bausch and Lomb Spectronic 2000 instrument. Under the reaction conditions, V(V) solutions followed Beer's law at 360 nm with $\varepsilon = 100$ dm^3 mol^{-1} cm^{-1} (±1%) in the concentration range of 5.0×10^{-4} to 8.0×10^{-3} mol dm^{-3} and Os(VIII) did not interfere. When [As(III)] was greater than [V(V)], the reaction was followed titrimetrically upto 90% as, beyond this stage, Os(VIII) was likely to be reduced to Os(IV) in the presence of excess [As(III)], and Os(IV) also absorbs at 360 nm. Rates were reproducible within ±5%.

Stoichiometry

Reaction mixtures containing varying concentrations of reactants and a fixed amount of Os(VIII) (8.0×10^{-5} mol dm^{-3}) in 4.0 mol dm^{-3} sulphuric acid-sulphate medium were kept over 24 hr at 25°C and the amounts of V(V), As(III) and V(IV) were found by measuring absorbance at 360 nm ([V(V)] > [As(III)]), titration with BrO_3^- and measuring the absorbance at 765 nm ($\varepsilon = 19.7 \pm 1$ dm^3 mol^{-1} cm^{-1}) respectively. Under the conditions, [As(III)] > [V(V)], [V(IV)] and [As(III)] were found as before and As(V) was determined titrimetrically. Osmium(VIII) was analysed by extraction into chloroform and measuring the absorbance[4] of the solution at 282 nm ($\varepsilon = 1870$ dm^3 mol^{-1} cm^{-1}). The [Os(VIII)] was found to have decreased slightly, a result also found in earlier work[5] of Os(VIII) catalysis. The results showed that two moles of V(V) reacted with one mole of As(III) to give V(IV) and As(V): 2V(V) + As(III) = 2V(IV) + As(V).

Results

In view of the complexity of the reaction, the order of the reaction was found under different conditions extending from excess [V(V)] over [As(III)] through [V(V)] ~ [As(III)] to [V(V)] much less compared to [As(III)]. The order in Os(VIII) is nearly unity when [V(V)] is greater or comparable to [As(III)] and slightly less than unity when [V(V)] is much less than [As(III)] (Tables 1 and 2). In calculating the order in [Os(VIII)], the direct reaction of V(V) with As(III) occurring to a small extent has also been taken into account. At fixed [Os(VIII)] (8.0×10^{-5} mol dm^{-3}), orders in As(III) and V(V) were found from log-log plots of initial rates versus concentration while keeping all other

Table 1 – Effect of [V(V)], [As(III)] and [Os(VIII)] on Os(VIII) mediated V(V)-As(III) reaction in 4.0 mol dm^{-3} H_2SO_4 at 25°C

[V(V)] > [As(III)]; I = 4.3 mol dm^{-3}

$[V(V)] \times 10^3$ (mol dm^{-3})	$[As(III)] \times 10^4$ (mol dm^{-3})	$[OS(VIII)] \times 10^5$ (mol dm^{-3})	10^7 (Initial rate) (mol dm^{-3} s^{-1})
4.0	4.0	0	0.17
4.0	4.0	4.0	0.83
4.0	4.0	8.0	1.52
4.0	4.0	12	2.22
4.0	4.0	16	3.30
4.0	4.0	24	4.55
4.0	4.0	8.0	1.58
6.0	4.0	8.0	1.48
8.0	4.0	8.0	1.47
10	4.0	8.0	1.53
4.0	2.0	8.0	1.01
4.0	6.0	8.0	2.22
4.0	8.0	8.0	2.94
4.0	10	8.0	3.82
4.0	20	8.0	6.93

conditions identical. At constant [V(V)], order in As(III) is unity at [V(V)] > > [As(III)]; the order in As(III) gradually decreases more and more from unity when [As(III)] relative to the fixed [V(V)] is increased. A similar trend in the order in V(V) is also noticed. As the [V(V)]/[As(III)] ratio, at fixed [As(III)], increases from a small fraction through unity to a much higher value, the order in V(V) is unity at first and then decreases with increase in relative [V(V)]; at [V(V)] > > [As(III)], the order in V(V) is almost zero (Tables 1 and 2). The log [V(V)] versus time plots are also linear in the initial stages upto 50% ([As(III)] > > [V(V)]), the deviation from linearity beyond this stage being presumably due to the interference of the Os(VIII)-As(III) direct reaction, the Os(VIII) tending to be reduced by the excess As(III) as the [V(V)] is much decreased. First order rate constants obtained from the initial linear portions are as follows. At [V(V)] of 7.5×10^{-4}, 1.0×10^{-3}, 1.5×10^{-3}, 2.0×10^{-3}, 4.0×10^{-3}, 6.0×10^{-3} and 8.0×10^{-3} mol dm^{-3}, the pseudo-first order constants are 7.9×10^{-3}, 4.4×10^{-3}, 1.0×10^{-3}, 5.1×10^{-4}, 3.8×10^{-4}, 3.1×10^{-4} and 2.9×10^{-4} s^{-1} respectively ([As(III)] = 2.0×10^{-2}, [Os(VIII)] = 8.0×10^{-5}, [H_2SO_4] = 4.0, I = 4.3 mol dm^{-3}; temp. 25°C).

The activation parameters were evaluated in the case of the catalysed as well as the uncatalysed

Table 2 – Effect of [V(V)], [As(III)] and [Os(VIII)] on Os(VIII) mediated V(V)-As(III) reaction in 4.0 mol dm^{-3} H_2SO_4 at 25°C

[As(III)] > [V(V)]; I = 4.3 mol dm^{-3}

$[V(V)] \times 10^2$ (mol dm^{-3})	$[As(III)] \times 10^2$ (mol dm^{-3})	$[OS(VIII)] \times 10^5$ (mol dm^{-3})	$10^6 \times$ (Initial rate) (mol dm^{-3} s^{-1})
0.40	2.0	0.0	0.094
0.40	2.0	4.0	1.47
0.40	2.0	8.0	2.92
0.40	2.0	12	4.39
0.40	2.0	16	5.28
0.40	2.0	20	7.42
0.40	2.0	24	8.33
0.40	2.0	28	9.25
0.40	2.0	36	11.9
0.30	1.0	8.0	0.80
0.40	1.0	8.0	1.36
0.70	1.0	8.0	1.60
1.0	1.0	8.0	1.93
1.4	1.0	8.0	2.66
1.7	1.0	8.0	3.06
2.0	1.0	8.0	3.22
4.0	1.0	8.0	3.76
6.0	1.0	8.0	3.70
8.0	1.0	8.0	3.61
10	1.0	8.0	3.52
0.40	1.3	8.0	1.90
0.40	1.6	8.0	2.17
0.40	2.4	8.0	3.25
0.40	2.8	8.0	3.30
0.40	3.2	8.0	3.36
0.40	5.0	8.0	3.60

reaction from the dependence of rate constants on temperature. $\Delta H^{\neq}$ and $\Delta S^{\neq}$ for the catalysed reaction were 28.2 ± 2 kJ mol^{-1} and -50 ± 10 JK^{-1} (k_1 at 25°, 30°, 35°, 40° and 45°C: 5.1×10^{-4}, 6.2×10^{-4}, 7.7×10^{-4}, 9.9×10^{-4} and 1.0×10^{-3} s^{-1} respectively). The activation data for the uncatalysed reaction were: $\Delta H^{\neq} = 66.7 \pm 5$ kJ mol^{-1} and $\Delta S^{\neq} = -25 \pm 5$ JK^{-1}.

Discussion

The Os(VIII) catalysed V(V)-As(III) reaction in acid medium displays a complex rate law as shown in Eq. (1). While the Os(VIII) order remains almost constant throughout the wide range of relative concentration variation of the react-

ants, the orders in the two reactants vary as shown

$$\text{Rate} = A[V(V)]^x [Os(VIII)][As(III)]^y \quad \ldots (1)$$

($x \to 0$ as $[V(V)] \to 8[As(III)]$ or higher;
$y \to 0$ as $[As(III)] \to 8[V(V)]$ or higher)

in Eq. (1). Such results may be accounted for in terms of Scheme 1 or Scheme 2. Scheme 1 involves the key Os(VIII)-As(III)

$$As(III) + Os(VIII) \xrightarrow{k_a} As(V) + Os(VI)$$

$$Ce(IV) + Os(VI) \xrightarrow{k_b} Ce(III) + Os(VII)$$

$$Ce(IV) + Os(VII) \xrightarrow{k_c} Ce(III) + Os(VIII)$$

$$As(III) + Os(VI) \xrightarrow{k_d} As(V) + Os(IV)$$

$$Ce(IV) + Os(IV) \xrightarrow{k_e} Ce(III) + Os(V)$$

$$Ce(IV) + Os(V) \xrightarrow{k_f} Ce(III) + Os(VI)$$

Scheme 1

step, as shown in the Os(VIII) catalysed Ce(IV)-As(III) reaction, characterised by a very high rate constant[1]. The direct Os(VIII)-As(III) reaction has a very much lower rate constant[2]. The present study also is not in agreement with Scheme 1 and a more satisfactory mechanism is seen in Scheme 2 which involves the formation of an Os(VIII)-As(III) complex. This complex (C_1) is also understood to form in the direct Os(VIII)-As(III) reaction and interacts with V(V) in further steps leading to As(V) formation (Scheme 2). Other fast steps follow and regenerate the catalyst. Scheme 2

$$Os(VIII) + As(III) \overset{K_1}{\rightleftharpoons} C_1$$

$$C_1 + V(V) \overset{K_2}{\rightleftharpoons} C_2$$

$$C_1 \xrightarrow{k_r} As(V) + V(IV) + Os(VIII)$$

followed by fast steps

Scheme 2

leads to rate law (2) which is in agreement with the complexity of the reaction orders which depend on the proportion of the reactant concentrations. Neglecting the higher order terms which are shown to be rather small in comparison to unity leads to Eq. (3) where the second and third terms shown after unity in the denominator are more important than others. According to Eq. (3), plots of $[Os(VIII)][V(V)]/(\text{rate})$ versus $1/[As(III)]$ and $[Os(VIII)][As(III)]/(\text{rate})$ versus $1/[V(V)]$ should be linear and this is verified in Fig. 1. The

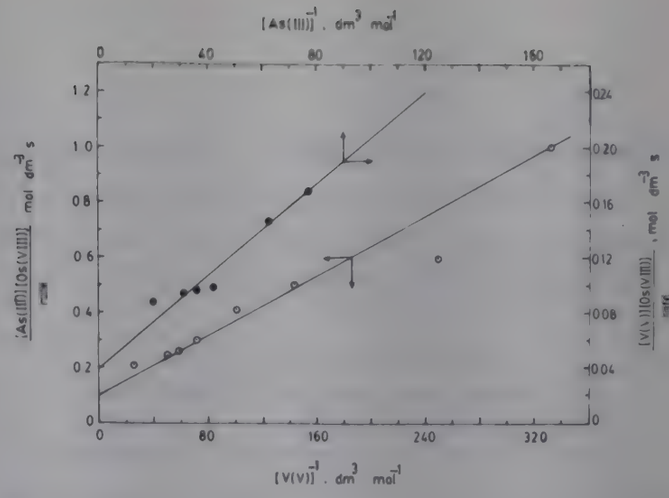

Fig. 1 – Verification of rate law (3) (conditions as in Table 2)

$$\text{Rate} = \frac{k_r K_1 K_2 [V(V)]_T [Os(VIII)]_T [As(III)]_T}{(1+K_1K_2[Os(VIII)][As(III)])(1+K_1[As(III)]+K_1K_2[As(III)][V(V)])} \times$$

$$(1+K_1[Os(VIII)]+K_1K_2[Os(VIII)][V(V)])^{-1} \quad (2)$$

$$\text{Rate} = \frac{k_r K_1 K_2 [V(V)]_T [Os(VIII)]_T [As(III)]_T}{(1+K_1[As(III)]+K_1K_2[As(III)][V(V)]+(K_1K_2+K_1^2)[Os(VIII)][As(III)]+K_1[Os(VIII)])} \quad (3)$$

values of the product, $K_1K_2k_r$, is 640 ± 200 s^{-1} which cannot be unambiguously split into values of K_1, K_2 and k_r. If K_1 may be borrowed from earlier work[2], rates for several experimental conditions may be calculated and are found to be of the correct order of magnitude.

The Os(VIII) species in acid solutions as encountered earlier may be in the form of H_2OsO_5 largely undissociated[6] like the As(III) species of H_3AsO_3 having a very low dissociation constant[7]. Vanadium(V) may be present[8] as $VO(OSO_3H)_3^{2+}$ or $V(OH)_3HSO_4^+$ and the absence of acidity effect might be due to the presence of more than one such species being active in the oxidation. The activation data generally support such conclusions.

References

1 Robert L H, Harry L P & James B W, *Anal Chem*, 39 (1967) 600.

2 Tuwar S M, Nandibewoor S T & Raju J R, *Transition metal Chem*, (in press).

3 Kampli S R, Nandibewoor S T & Raju J R, *J molecular Cat*, communicated.

4 Goldstein G, Manning D L & Oscar Menis, *Talanta*, 7 (1961) 296.

5 Sandell E B, *Colorimetric determination of traces of metals*, (Interscience, New York) 1959, p. 702.

6 Mehrotra U S & Mushran S P, *Canad J Chem*, 48 (1970) 1148.

7 Smith J D, *The chemistry of arsenic, antimony and bismuth*, Vol. 2, (Pergamon press, Oxford) 1975, p. 608.

8 Pal B B, Mukerjee D C & Sengupta K K, *J inorg nucl Chem*, 34 (1972) 3433.

Indian Journal of Chemistry
Vol. 30A, April 1991, pp. 372-374

Physicochemical studies of 4-trifluoroacetyl and 4-trichloroacetyl derivatives of 3-methyl-1-phenylpyrazol-5-one and their U(VI), Fe(III) and Ca(II) complexes

Bieluonwu Augustus Uzoukwu
Coordination and Analytical Chemistry Unit,
Department of Pure and Industrial Chemistry,
University of Port Harcourt, Port Harcourt, Nigeria

Received 3 July 1990; revised and accepted 28 November 1990

The pK_a values of the 4-trifluoroacetyl (2.76 ± 0.13) and 4-trichloroacetyl (3.02 ± 0.05) derivatives of 3-methyl-1-phenylpyrazol-5-one have been determined. Their U(VI), Fe(III) and Ca(II) complexes have been isolated and characterized using UV-visible, IR (4000-200 cm^{-1}), ^1H, ^{13}C and ^{19}F NMR spectral studies.

4-Acylpyrazolones[1-5] have been shown to be good extraction reagents for metals in acidic solutions. Akama *et al.*[6,7] in their systematic study of alkyl substituted 4-acyl derivatives of 3-methyl-1-phenyl-pyrazol-5-one showed that due to its slightly lower pK_a value, the 4-benzoyl derivative (HPMBP) proved to be more efficient in the extraction of metal ions than the other 4-acylpyrazolones studied[6,7]. The pK_a values of the corresponding 4-trifluoroacetyl (HPMTFP) and 4-trichloroacetyl (HPMTCP) derivatives (structure I) have been determined. These low values indicate that HPMTFP and HPMTCP

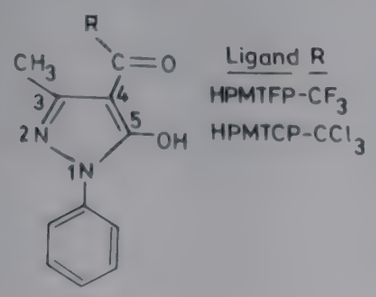

Ligand	R
HPMTFP	$-CF_3$
HPMTCP	$-CCl_3$

(I)

may prove to be even more efficient reagents for metal extraction. The interaction of these ligands with metal ions in an aqueous solution has been studied and the solid complexes isolated have been characterized.

Experimental

Electronic spectral measurements were made with a Pye Unicam PU8700 series UV-visible spectrophotometer. Measurements of *p*H of solutions were made with a Corning *p*H meter. Conductance measurements were made with a Philips PW 9506 conductivity meter. Magnetic susceptibility measurements were made by the Gouy method using a Johnson-Matthey Chemical balance. Perkin Elmer 598 spectrophotometer was used for obtaining the IR spectra of the compounds in nujol mull and CsI discs. The ^1H and ^{19}F NMR spectra were obtained using BRUKER DATA WPAT 80 while the ^{13}C NMR spectra were obtained using the WUM 360 model, both models were on FT mode. Acetone-d_6 was used as the solvent.

The 4-trihaloacetylpyrazolones were prepared by methods described elsewhere[1] and twice recrystallized from aqueous ethanol. Stock solutions of 10^{-3} *M* HPMTFP and 10^{-3} *M* HPMTCP were prepared in dioxane. Ionic strengths (0.1 *M*) of solutions were maintained by 1 *M* $NaClO_4$. Nitrate or acetate salt of metals were used for preparing the complexes in the solid state. All the chemicals used were of analytical reagent grade.

Procedure

Determination of acid dissociation constants of ligands

Ligand solutions of equal concentrations in various 10 mL flasks were prepared in 20% (v/v) dioxane-water medium at 20°C. The ionic strength of solution was maintained at 0.1 *M* with $NaClO_4$. The *p*H of the solution was varied by adding NaOH or $HClO_4$. The changes in the absorption spectra of both the ligands with *p*H were recorded. The pK_a values were calculated using the relation $pK_a = pH - \log (A - A_{min})/(A_{max} - A)$ where A_{max} is asymptotic absorbance at high *p*H and A_{min} is asymptotic absorbance at low *p*H while A is absorbance at a given *p*H. The values were refined using the method of least squares.

Preparation of metal complexes

The metal salt (5 mmol) was dissolved with warming in 75 mL of water. This was added slowly with stirring to a warm solution of 10 mmol of ligand in 75 mL ethanol. The reaction stoichiometry of metal-ligand mole ratio was 1:2. In the case of Fe(III), 5 mmol of the Fe(III) ion was added to 15 mmol of the ligand as described above. The metal-ligand mole ratio was 1:3. The precipitate separated immediately

Table 1—Physical and microanalytical data for ligands and their U(VI), Fe(III) and Ca(II) complexes

Compound (colour)	Melting point (°C)	Found (Calc.), %			λ_1 (nm) (ε_1^*)	λ_2 (nm) (ε_2^*)	λ_3 (nm) (ε_3^*)	Methyl moiety		Molar conductance (S mol^{-1} cm^2)
		C	H	N				δ(H)**	δ(C)**	
HPMTFP	139	53.11	3.88	10.25	252	294		2.45(s)	14.89	—
(Pink)		(53.34)	(3.36)	(10.37)	(0.14)	(1.32)				
$UO_2(PMTFP)_2.2H_2O$	306	34.31	2.83	6.20	251	290		2.50(s)	16.29	13.8
(Orange)	(dec.)	(34.14)	(2.39)	(6.63)	(1.64)	(3.66)		2.66(s)	18.83	
$Fe(PMTFP)_3$	184	49.76	2.92	9.62	253	295	469	—	—	18.4
(Wine-red)		(50.07)	(2.80)	(9.73)	(1.19)	(3.54)	(0.56)			
$Ca(PMTFP)_2$	144	50.11	3.05	10.01	252	297		2.39(s)	16.22	1.5
(White)		(49.83)	(2.79)	(9.68)	(0.51)	(3.22)		2.86(s)	18.93	
HPMTCP	136	45.10	2.94	8.52	251	295		2.60(s)	17.35	—
(Pink)		(45.11)	(2.84)	(8.77)	(0.27)	(1.31)				
$UO_2(PMTCP)_2.2H_2O$	222	30.31	2.34	6.18	251	302		2.80(s)	19.72	13.8
(Orange)	(dec.)	(30.56)	(2.14)	(5.96)	(0.99)	(1.72)				
$Fe(PMTCP)_3$	120	42.68	2.83	8.28	252	293	469	—	—	15.9
(Wine-red)		(42.76)	(2.39)	(8.31)	(1.39)	(3.42)	(0.48)			
$Ca(PMTCP)_2$	150	42.78	2.62	8.00	252	293		2.55(s)	18.84	5.0
(Orange)		(42.58)	(2.38)	(8.28)	(0.51)	(1.74)				

s, singlet; *values × 10^{-4} l^{-1}.mol.cm; **values in ppm

and was washed with aqueous ethanol (1:1) solution and filtered. The products were recrystallized from aqueous ethanol (1:4), filtered, dried in air and stored over fused $CaCl_2$ in a desiccator.

The elemental analyses for C, H and N of the compounds were carried out at the School of Chemistry and Molecular Sciences, University of Sussex, England.

Results and discussion

The pK_a values obtained for HPMTFP (2.76±0.13) and HPMTCP (3.02±0.05) are lower than those reported[6,7] for other 4-acylpyrazolones, including the widely used HPMBP, indicating that these two ligands may prove to be more powerful reagents for the extraction of metal ions from acidic solutions. The sequence of the pK_a values, 2.76 (HPMTFP) < 3.02 (HPMTCP), can be explained on the basis of the electron withdrawing power of the substituents CF_3 and CCl_3 (structure I) since the electronegativities of these groups follow the order: $CF_3 > CCl_3$.

The analytical data given in Table 1 indicate a general molecular formula MA_nxH_2O (M, n, x = UO_2, 2, 2; Ca, 2, 0; Fe, 3, 0; A = 4-acylpyrazolone anion). Conductance measurements of the metal complexes in DMF gave negligible molar conductances showing that all the metal complexes are non-ionic.

Electronic and vibrational spectral analyses

The electronic spectral data of the ligands and their metal complexes given in Table 1 show that the absorption maxima values λ_1 and λ_2 of both the ligands and their metal complexes are identical. Both absorptions in these compounds have been ascribed to intraligand $\pi \rightarrow \pi^*$ transitions. The broad absorption between 430 and 510 nm, with centre at 469 nm, observed for the Fe(III) complexes has been ascribed to ligand to metal charge-transfer.

On comparison with previous reports on the IR spectra of 4-acylpyrazolones[8-11], the broad band near 3600 cm^{-1} in the IR spectra of the U(VI) complexes is ascribed to νOH of coordinated water. The broad bands at 3400 cm^{-1} (HPMTFP) and 3100 cm^{-1} (HPMTCP) assigned to νOH of the enolic form of the ligand, are absent in the spectra of the metal complexes suggesting coordination through deprotonated OH group. OH bending or deformation modes are observed at 1672 cm^{-1} (HPMTFP), 1678 cm^{-1} (HPMTCP), 1640 cm^{-1} (UO_2-PMTFP) and 1625 cm^{-1} (UO_2-PMTCP). The involvement of CO group of the ligand in the chelation process is indicated by the shift of νC=O from 1625 cm^{-1} (HPMTFP) and 1637 cm^{-1} (HPMTCP) to the region 1600-1638 cm^{-1} in the IR spectra of the metal complexes. $\nu_{as}O=U=O$ in both U(VI) complexes occurs near 930 cm^{-1}. The absorption bands at 264 cm^{-1} (U), 280 cm^{-1} (Fe) and

360 cm^{-1} (Ca) for metal complexes of HPMTFP and those at 270 cm^{-1} (U), 260 cm^{-1} (Fe) and 391 cm^{-1} (Ca) for metal complexes of HPMTCP have been assigned νM − O. They follow the trend U < Fe < Ca, which is the order of decrease in atomic mass of metal M.

NMR spectral analyses

^{1}H NMR spectral results show that the hydroxyl proton signal [δ, 7.13 (s) for HPMTFP; 3.60 (s) for HPMTCP] observed in the ligands is absent in all the metal complexes confirming deprotonation of OH group of each of the ligands on bonding. It is interesting to note from Table 1 that the methyl protons experience upfield shift in the Ca(II) complexes (apart from the signal at 2.86 ppm for Ca-PMTFP) and downfield shift in the U(VI) complexes. The two singlets observed for the methyl protons in the spectra of U(VI) and Ca(II) complexes of HPMTFP suggest that the ligand moieties in the complexes are perhaps stereochemically different. The phenyl proton resonances appear in the region δ 7.11-8.66 ppm as broad multiplets. The signals in the case of Fe(III) complexes appear to be broadened due to paramagnetic shift. The following magnetic moments (Fe-PMTFP): $\mu_{eff.} = 6.13$ B.M. and (Fe-PMTCP): $\mu_{eff.} = 5.80$ B.M. have been obtained for the Fe(III) complexes. The deviation of the $\mu_{eff.}$ values obtained for these Fe(III) complexes from the calculated value (5.92 B.M.) may be an indication of the degree of distortion from the regular O_h symmetry in these complexes.

The ^{13}C NMR spectral data given in Table 1 show that the methyl carbon atom resonates downfield in the metal complexes relative to its position in the spectra of the ligands. This trend agrees with the trend shown by methyl protons of the U(VI) complexes but is in contrast to that observed in the case of the Ca(II) complexes. Two singlets have been observed for the methyl carbon atom of the Ca-PMTFP and the UO_2-PMTFP complexes. Other ^{13}C NMR spectral results show that C(4) and C(5) carbon atoms resonate slightly downfield in the U(VI) and Ca(II) complexes indicating that both carbon atoms are deshielded in these complexes. This may be due to the involvement of both carbon atoms in electron delocalization of the chelate ring. C = O carbon atom of UO_2-PMTCP is also deshielded for the same reason. However, the C = O carbon atoms of UO_2-PMTFP, Ca-PMTFP and Ca-PMTCP resonate upfield relative to those of the respective ligands, indicating that these atoms are shielded in these complexes which may be due to a greater part of the electron pair donated by C = O to the metal ion residing on C = O.

In the ^{19}F NMR spectral studies the chemical shifts recorded relative to $CFCl_3$ reveal single fluorine resonance peaks at −71.0 ppm (HPMTFP), −65.6 ppm (UO_2-PMTFP) and −74.1 ppm (Ca-PMTFP).

Acknowledgement

The author wishes to thank Prof. E.C. Okafor and Dr J.D. Smith for their assistance and the British Caledonian Airways for financial support.

References

1 Jensen B S, *Acta chem scand*, 13 (1959) 1668.
2 Zolotov Y A, Chmutova M K & Palei P N, *Zh anal Khim*, 21 (1966) 1217.
3 Zolotov Y A, Chmutova M K & Palei P N, *J anal Chem USSR*, 23 (1968) 1298.
4 Karalova Z K & Pyzhova Z I, *J anal Chem USSR*, 23 (1968) 1381.
5 Moseev L I & Monakhov B V, *Radiokhimiya*, 10 (1968) 309.
6 Akama Y, Sato K, Ukaji M & Kawata T, *Polyhedron*, 4 (1985) 59.
7 Akama Y, Yokota H, Sato K & Nakai T, *Talanta*, 33 (1986) 288.
8 Okafor E C, *Polyhedron*, 2 (1983) 309.
9 Okafor E C, *Spectrochim Acta*, 37A (1981) 951.
10 Okafor E C, *Spectrochim Acta*, 37A (1981) 939.
11 Okafor E C, *Spectrochim Acta*, 38A (1982) 981.

Indian Journal of Chemistry
Vol. 30A, April 1991, pp. 375-378

Studies on cobalt (II), nickel (II), copper (II) and zinc (II) complexes with glyoxal bis(2-pyrazinoyl hydrazone)

G S Sanyal* & S Garai

Department of Chemistry, University of Kalyani, Kalyani 741 235

Received 26 April 1990; revised 18 September 1990; accepted 6 December 1990

Complexes of Co(II), Ni(II), Cu(II) and Zn(II) with glyoxal bis(2-pyrazinoyl hydrazone) have been prepared and characterized on the basis of analytical data and various physicochemical studies. A square-planar structure for the Ni(II) complex and distorted octahedral structures for Co(II) and Cu(II) complexes have been proposed.

In recent years hydrazones have been actively investigated as donors because of their varied ligational behaviour towards different metal ions and manifestation of novel structural features in the metal complexes[1-7]. Much work has been done with the schiff bases containing pyridine ring system[8]. Pyrazine with an additional ring nitrogen is a weaker base[9], but it often forms many structurally important complexes[10-12]. The present investigation was undertaken to study the interaction of the schiff base derived from glyoxal and pyrazine-2-carboxylic acid hydrazide with Co(II), Ni(II), Cu(II) and Zn(II) ions.

Experimental

The ligand, glyoxal bis(2-pyrazinoyl hydrazone), was prepared by heating a mixture containing a solution of disodium glyoxal bisulphite (0.01 mol) in water (50 ml) and pyrazine-2-carboxylic acid hydrazide (0.02 mol) {prepared beforehand according to published procedure[13]} in water (100 ml), on a steambath for 30 min, cooling and filtering the contents followed by washing (with water) of the precipitate formed [yield ~70%, m.p. 190°C; Found: C, 47.72; H, 3.35; N, 36.23%. Calc. for ($C_{14}H_{12}N_6O_2$); C, 48.30; H, 3.35; N, 37.58%].

Preparation of the complexes

The complexes $CoLCl_2.2H_2O$ and $Cu_3(L\text{-}2H)Cl_4.4H_2O$ were prepared by adding an excess (~1.0 g) of solid hydrated cobalt (II)/copper (II) chloride to a refluxing suspension of the ligand (200 mg) in methanol (60-70 ml) on a steambath when the ligand dissolved completely. On further refluxing the solution (4-5 hr) after filtering, the complex precipitated. It was filtered, washed with hot methanol and dried over fused $CaCl_2$. The complexes $Co_3Cl_4(L\text{-}2H).3H_2O$ and Ni(L-2H) were similarly prepared from their hydrated metal (II) chloride (~ 0.7 mmol) and the ligand (~ 0.7 mmol); the cobalt (II) complex precipitated upon concentrating and cooling the filtered reaction mixture, and the nickel complex precipitated on pouring the solution into water; the precipitates were washed with methanol (cobalt)/water (nickel) and dried as above, yield ~ 60%.

$Cu(L\text{-}2H).4H_2O$ and Zn(L-2H) were prepared by adding the powdered ligand (0.5 mmol) into an aqueous ammoniacal solution (25 ml) of the metal chloride ($CuCl_2.2H_2O$ or anhydrous $ZnCl_2$) (0.5 mmol) and stirring the contents at room temperature for an hour. The metal complexes precipitated were filtered, washed with very dilute ammonia followed by water and dried, yield ~ 70%.

The complexes devoid of anions were insoluble in most solvents; other complexes were generally soluble in DMSO. The complexes $M_3(L\text{-}2H)Cl_3.xH_2O$ {M = Cu(II), x = 4; M = Co(II), x = 3} were highly soluble in water; the solution did not produce immediately any characteristic precipitate with silver nitrate.

Infrared spectra were recorded in KBr (400-4000 cm^{-1}) using a Perkin Elmer spectrophotometer, Model 1330. IR spectral measurements in the range 200-4000 cm^{-1} and elemental analyses were carried out at CDRI, Lucknow. Cu(II) and Zn(II) were analysed[14] gravimetrically as quinaldinates, Ni(II) as dimethylglyoximate and Co(II) electrogravimetrically as metallic cobalt. Electronic spectra were recorded on a Hitachi spectrophotometer model 200-20 in nujol. EPR spectra were recorded at RSIC, Madras. Magnetic moment and conductivity measurements were made as described elsewhere[15].

Results and discussion

Molar conductance values of 10^{-3} *M* solutions of the complexes in DMSO (36.8-54.2 ohm^{-1} cm^2 mol^{-1})/water (101.0-120.4 $ohm^{-1}cm^2mol^{-1}$) indicated[16] the complexes to be nonelectrolytes, although some solvolysis occurred.

Table 1-Analytical, magnetic moment and electronic spectral data of the complexes

Complex (Colour)	Magnetic moment (B.M.)†	Found (Calc), %					Electronic spectra‡ ν_{max} (kK)
		Metal	C	H	N	Anion	
$CoLCl_2.2H_2O$	5.38	12.75	30.52	2.75	24.31	16.50	26.3
(Brown)		(12.85)	(30.90)	(3.00)	(24.03)	(15.24)	19.4
							18.9
							11.5
Zn(L-2H)	—	18.15	39.24	2.12	29.88	—	
(Yellow)		(18.00)	(39.88)	(2.21)	(31.02)		
Ni(L-2H)	—	16.2	40.60	2.05	31.92	—	25.6
(Red)		(16.5)	(40.59)	(2.25)	(31.57)		17.5 br
							11.6 sh
$Cu_3(L\text{-}2H)Cl_4.4H_2O$	1.20	27.40	20.58	0.97	15.93	21.48	22.7
(Brown)		(27.20)	(20.57)	(1.14)	(16.00)	(20.30)	11.7
$Cu(L\text{-}2H).4H_2O$	1.56	14.55	33.11	3.62	25.41	—	23.3
(Snuff)		(14.70)	(33.36)	(3.70)	(25.95)		13.7 w br
							11.5 sh
$Co_3(L\text{-}2H)Cl_4.3H_2O$	2.68	26.20	21.60	1.84	16.90	20.79	18.50
(Orange red)		(26.35)	(21.55)	(2.09)	(16.76)	(21.25)	14.80

†Per metal atom, ‡in nujol mull

IR spectrum of the ligand, glyoxal bis(2-pyrazinoyl hydrazone) [structure I], shows bands at 3500 (m, br), 3270 (s, sh); 1700 (s); 1520 (s) and 1000-1060 cm^{-1} tentatively assigned to ν_{NH}, amide-I ($\nu_{C=O}$), amide-II [$\delta_{(NH)} + \nu_{(CN)}$] and ν_{N-N} (plus ring breathing modes) respectively[1,17]. In the Co(II) complex, $CoLCl_2.2H_2O$, the amide I band remains at the same position as in the free ligand indicating that keto oxygen is not coordinated. Upward shift of the ν_{N-N} band suggests[18,19]

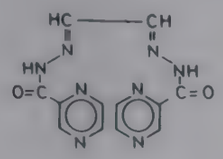

I

coordination through nitrogen of the azomethine group ($-CH=N-$). The pyrazine ring out-of-plane bending vibration at 385, 430 cm^{-1} moves to ~ 400, 460 cm^{-1} indicating that the ring nitrogen is coordinated. A new band at 1640 cm^{-1} (m) (absent in the free ligand) may be assigned to $H-O-H$ bending mode[20]; bands typical of coordinated water are not discernible from the spectrum[20-22]. Isothermal (~ 150°C) mass loss, generally indicative of coordinated water, is not conclusive in view of some previous reports[23].

In the complexes containing deprotonated ligand, $Cu(L\text{-}2H).4H_2O$, $Zn(L\text{-}2H)$, $Cu_3(L\text{-}2H)Cl_4.4H_2O$ and $Co_3(L\text{-}2H)Cl_4.3H_2O$, the amide-II band is split/displaced upwards/gets reduced in intensity; the amide-I band is substantially lowered ($\Delta\nu \sim 50\text{-}80$ cm^{-1}) relative to the free ligand value, which suggests coordination through the deprotonated enolised oxygen; the resulting ν_{NCO} band manifests in the 1360-1330 cm^{-1} region. Upward shift of ν_{N-N} or its splitting (1020-1100 cm^{-1}) indicates coordination of azomethine nitrogen. Presence of water is apparent from the characteristic broad contour around 3500 cm^{-1} and bending $H-O-H$ mode in the region 1640-1650 cm^{-1}, although these cannot be used to determine whether the water is coordinated or not. Isothermal (120°C) mass loss (16.8, 6.7 and 7.5% respectively) for the above complexes indicates that water may be at least partly crystalline; bands in the region 520-560 cm^{-1} assignable[24] to coordinated water are absent in the $Cu(L\text{-}2H).4H_2O$ complex but are present in others. New bands in the region 1060-1000 cm^{-1} due to ring breathing mode suggest coordination through pyrazine ring nitrogen in $Cu_3(L\text{-}2H)\ Cl_4.4H_2O$ and $Co_3(L\text{-}2H)\ Cl_4.3H_2O$. A band at ~ 300 cm^{-1} (m) may be assigned to ν_{Cu-Cl}. The two complexes have an overall spectral similarity; new band (s) in the region 820-870 cm^{-1} which may be attributed[25] to vibration of are apparent in their spectra.

Spectral profile of the nickel (II) complex, Ni(L-2H) is different from that of $Cu(L\text{-}2H).4H_2O$ or $Zn(L\text{-}2H)$ in respect of multiplicity of bands and

suggests a different mode of bonding. The amide-I band remains almost at the same position as in the free ligand and indicates that the keto oxygen is not coordinated. The ν_{NH} band (3260 cm^{-1}) disappears in the nickel (II) complex suggesting coordination through its deprotonated nitrogen. Splitting (425, 450 cm^{-1}) of the pyrazine ring out-of-plane bending vibration (430 cm^{-1}) alongwith the appearance of a new band in the region 1000-1060 cm^{-1} suggests coordination of the ring nitrogen.

The μ_{eff} value of the $CoLCl_2.2H_2O$ complex (5.38 B.M.) is suggestive[26] of distorted octahedral stereochemistry. The nickel (II) complex is diamagnetic and hence square planar. Subnormal values in respect of octahedral stereochemistry are observed for Co_3(L-2H) $Cl_4.3H_2O$ and the Cu(II) complexes. A number of factors may be responsible[27,28] for this but in the absence of low temperature magnetic data it is difficult to discuss the significance of such behaviour.

EPR spectrum of Cu_3(L-2H) $Cl_4.4H_2O$ in the polycrystalline state showed a single g-value at room temperature ($g = 2.19$) as well as at liquid nitrogen temperature ($g = 2.17$): little structural information could be gained from this. The spectrum of Cu(L-2H).$4H_2O$ was reversed axial with $g_\perp$ (2.18) > $g_\parallel$ (2.05). The complex would thus have an essentially d_{z^2} ground state which can occur with either a compressed tetragonal, a trigonal bipyramidal, a cis-octahedral or a rhombically distorted octahedral structure[29,30]. The spectrum of the same complex is apparently rhombic at liquid nitrogen temperature.

Electronic spectra (Table 1) of the complexes were recorded in nujol mull. The spectrum of the nickel (II) complex is typical of planar Ni(II) and consistent with ν_{max} normally observed[31,32] in the regions 16.5-21.0 kK (ν_2), 22.0-25.0 kK (ν_3) [and 12.0 kK (ν_1, vw)] assignable to $^1A_{1g} \rightarrow {}^1A_{2g}$ and $^1A_{1g} \rightarrow {}^1E_{1g}$ transitions respectively. The brown coloured $CoLCl_2.2H_2O$ complex as well as the red coloured Co_3(L-2H)$Cl_4.3H_2O$) exhibited bands in the region 18.5-19.8 kK tentatively assigned to $^4T_{1g}(F) \rightarrow {}^4T_{1g}(P)$ (ν_3) transition in an octahedral environment[31]. Observed band positions in the copper (II) complexes suggest distorted octahedral structures[31].

On the basis of magnetic moment and spectral data, a square planar structure for Ni(L-2H) complex may be tentatively proposed (structure II). Octahedral structures for other complexes are probable because of the tetradentate ligand chelation, coordinated halogen (e.g. $CoLCl_2.2H_2O$, structure III) or coordinated halogen and water (e.g. Cu_3(L-2H) $Cl_4.4H_2O$, structure IV) or coordinated pyrazine ring nitrogen [Cu(L-2H).$4H_2O$, structure V].

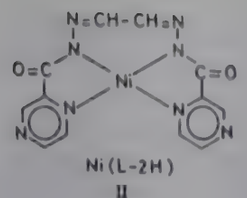

II

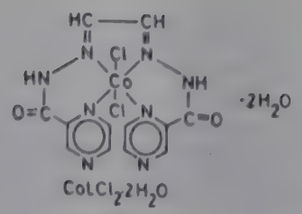

III

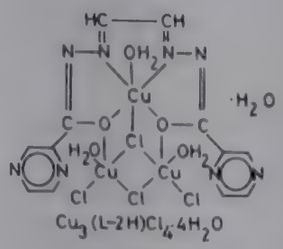

IV

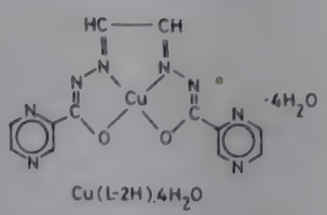

V

References

1 Pelizzi C, Pelizzi G & Vitali F, *J chem Soc Dalton Trans*, (1987) 177.

2 Mangia A, Pelizzi C & Pelizzi G, *Acta Crystallogr*, 30B (1974) 2146.

3 Pelizzi C, Pelizzi G, Predieri G & Resola S, *J chem Soc Dalton Trans*, (1982) 1349.

4 Hursthouse M B, Amarasiri S, Jayaweera A & Andrew Quick, *J chem Soc Dalton Trans*, (1979) 279.

5 Haran R, Gairin J & Commenges G, *Inorg chim Acta*, 46 (1980) 63.

6 Murphy T B, Jahnson D K, Rose N J, Aruffo A & Schomaker V, *Inorg chim Acta*, 66 (1982) L-67.

7 Amminabhavi T M, Biradar N S & Rudziuki W E, *Inorg chim Acta*, 78 (1983) 107.

8 Dutta R L & Hossain M M, *J scient ind Res*, 44 (1985) 635.

9 Albert A, Goldacre R & Phillips J, *J chem Soc*, (1948) 2240.

10 Flescher E B, Jeter D & Flortan R, *Inorg Chem*, 13 (1974) 1042.

11 Clein C L, Stevens E D, O'Connor C J, Majestes R J & Trefonas L M, *Inorg chim Acta*, 70 (1983) 151.

12 Fleischer E B & Lawson M B, *Inorg Chem*, 11 (1972) 2772.

13 Merck F E, *Chem Abstr*, 30 (1936) 6994.

14 Vogel A I, *A text book of quantitative inorganic analysis* (ELBS, London) 1962.

15 Sanyal G S, Modak A B & Mudi A, *Indian J Chem*, 20A (1981) 510.

16 Geary W J, *Coord Chem Rev*, 7 (1971) 81.

17 Burger K, Ruff I & Ruff F, *J inorg nucl Chem*, 27 (1965) 179.

18 Pelizzi C & Pelizzi G, *Inorg chim Acta*, 18 (1976) 39.

19 Aggarwal R C, Singh N K & Singh R P, *Inorg Chem*, 20 (1981) 2794.

20 Gamo I, *Bull chem Soc Japan*, 34 (1961) 1430.

21 Fujito J, Nakamoto K & Kobayashi M, *J Am chem Soc*, 78 (1956) 3963.

22 Ferraro J R & Walkar A, *J chem Phys*, 42 (1965) 1278.

23 Nuttal R H & Slalkar D M, *J inorg nucl Chem*, 40 (1978) 39.

24 Nakamoto K, *Infrared spectra of inorganic and coordination compounds*, 2nd Edn (Wiley, New York) 1970.

25 Hewkin D J & Griffith W P, *J chem Soc (A)*, (1966) 472.
26 Niswander R H, St Clair A K, Edmondson S R & Taylor L T, *Inorg Chem*, 14 (1975) 478.
27 Stoufer R C, Smith D W, Clevenger E A & Norris T E, *Inorg Chem*, 5 (1966) 1167, 1825.
28 Kato M, Jonassen H B & Fanning J C, *Chem Rev*, 64 (1964) 99.
29 McGregar K T & Halfield W E, *J chem Soc Dalton Trans*, (1974) 2448.
30 Estes W E, Govel D P, Halfield W E & Hodgson D J, *Inorg Chem*, 17 (1978) 1415.
31 Lever A B P, *Inorganic electronic spectroscopy* (Elsevier Amsterdam) 1968.
32 Lever A B P, Lewis J & Nyholm R S, *J chem Soc*, (1963) 2552.

Indian Journal of Chemistry
Vol. 30A, April 1991, pp. 379-381

Reactions of dithizone with transition metal complexes of acetylacetone and oxine

A A M Aly* & A H Osman

Chemistry Department, Faculty of Science, Assiut University, Assiut, Egypt

Received 16 April 1990; revised and accepted 20 September 1990

Synthesis of mixed acetylacetonato-dithizonato complexes of VO^{2+}, Cr^{3+}, Fe^{3+} and Co^{3+} as well as dithizonato-oxinato complexes of Co^{2+} and Ni^{2+} is described. On the basis of electronic spectral data, the mixed acetyl-acetonato complexes are assigned octahedral and the mixed oxine complexes tetrahedral geometry. Photolysis of the complexes in chloroform solution is also investigated. Photooxidation through a reactive excited state of the charge transfer to solvent (CTTS) type is suggested. Thermal behaviour of the complexes has been also discussed.

Although dithizone has wide applications as an analytical reagent in the photometric analysis of metals, and it forms binary complexes with many metals[1,2], reports are scarce on its mixed ligand complexes[3]. Further, among mixed ligand complexes of acetylacetone and of oxine, complexes with sulphur donors are scarce[4-8]. We report here the preparation and characterisation of mixed ligand transition metal complexes containing dithizonate and acetylacetonate/oxinate as co-ligands.

Experimental

All the chemicals used were of analytical reagent grade. Dithizone (E. Merck) was used without further purification. The acetyl-acetonato and oxinato metal complexes, i.e., $VO(acac)_2$, $Cr(acac)_3$, $Fe(acac)_3$, $Co(acac)_3$, $Co(ox)_2$ and $Ni(ox)_2$ were prepared following recommended methods[9,10].

(Acetylacetonato)(dithizonato)oxovanadium(IV) and bis(acetylacetonato)(dithizonato)chromium(III)/iron(III)/Co(III)

A chloroform solution (10 ml) of dithizone (2.0 mmol) was added dropwise with continuous stirring to a chloroform solution (15 ml) of the metal acetylacetonate (2.0 mmol). After stirring overnight, the solution was evaporated to about one-third the original volume, followed by the addition of petrolium ether. The precipitated complex was filtered, washed with a little chloroform and dried over P_4O_{10}.

(Acetylacetonato)bis(dithizonato)chromium(III)/iron(III)/Co(III)

These complexes were prepared by the above mentioned procedure using a 2:1 ratio of dithizone: metal acetylacetonate.

(Dithizonato)(oxinato)cobalt(II)/nickel(II)

A suspension of bis(oxinato)metal(II) (3.0 mmol) in 10 ml chloroform was mixed with a chloroform solution (10 ml) of dithizone (3.0 mmol), and the mixture refluxed for three hours. Precipitation was caused by adding petrolium ether. The product was filtered, washed with a little chloroform and dried over P_4O_{10}.

The instruments used in the present work were: Perkin-Elmer 599 B recording spectrophotometer for IR spectra (KBr), Shimadzu UV-200 S spectrophotometer for UV spectra, Rayonet photochemical chamber reactor Modell RPR-100 for irradiation, and a thermobalance consisting of an electric balance of the type Sartorius 2003 MP, a small furnace and a sample holder.

Results and discussion

The complexes were soluble in most of the organic solvents. Analytical data of the complexes are recorded in Table 1.

Table 1—Analytical data and colours of the complexes

Complex (colour)	Found(Calc.)		
	C%	H%	N%
[VO(acac)(HDz)] (Brick red)	51.10 (51.31)	4.50 (4.30)	13.40 (13.29)
[$Cr(acac)_2$(HDz)] (Black)	54.55 (54.64)	4.82 (4.98)	11.12 (11.08)
[Cr(acac)$(HDz)_2$] (Brown)	56.33 (56.26)	4.45 (4.41)	16.81 (16.93)
[$Fe(acac)_2$(HDz)] (Brown)	54.02 (54.23)	4.81 (4.94)	11.20 (10.99)
[Fe(acac)$(HDz)_2$] (Brown)	55.79 (55.94)	4.21 (4.39)	16.77 (16.83)
[$Co(acac)_2$(HDz)] (Dark violet)	53.88 (53.90)	4.99 (4.91)	10.90 (10.93)
[Co(acac)$(HDz)_2$] (Black)	55.55 (55.68)	4.25 (4.37)	16.86 (16.75)
[Co(ox)(HDz)] (Dark violet)	57.77 (57.64)	3.91 (3.73)	15.33 (15.27)
[Ni(ox)(HDz)] (Black)	57.51 (57.67)	3.82 (3.73)	15.31 (15.28)

The IR spectra of the complexes exhibit the characteristic bands of the ligands involved in the mixed ligand complexes. For the acetylacetonato-dithizonato mixed ligand complexes, it is inferred from the IR spectra that the bidentate coordination of acetylacetonate is not altered upon further reaction with dithizonate since characteristic bands for $\nu C \doteq O$ and $\nu C \doteq C$ appear at 1575-1590 and 1520-1535 cm^{-1}, and no band for free carbonyl is observed above 1600 cm^{-1} (ref. 11).

In the spectrum of VO(acac)(HDz), $\nu V=O$ is observed at 1015 cm^{-1} indicating that the five coordinate geometry around V(IV) is retained as in the parent $VO(acac)_2$[12].

The two complexes of oxine, viz., Co(ox)(HDz) and Ni(ox)(HDz) display $\nu C=N$ and $\nu C-O$ at 1540 and 1120 cm^{-1}, respectively.

Chelation of the dithizonate moiety is evidenced by the appearance of νNH at 3220-3300 cm^{-1} and $\nu C=S$ at 840-850 cm^{-1}, typical of dithizonate coordination through S and N[3c,13]. A band located at 1320-1350 cm^{-1} is attributed to $\nu N-C$ of N – Ph bond.

The electronic spectra (chloroform solutions) of all the present complexes display an intense absorption band due to dithizonate moiety in the region 18000-19000 cm^{-1} (refs 2, 3a). In the spectrum of VO (acac) (HDz) a band occurring at 20833 cm^{-1} may be attributed to the dithizonate part. No *d-d* bands could be observed for this complex. The two bands appearing at 23255 and 37735 cm^{-1} are probably due to CT and intraligand (acetylacetonate) transitions, respectively.

The $Cr(acac)_2(HDz)$ and $Cr(acac)(HDz)_2$ complexes show a band at ~ 16000 cm^{-1} ($^4A_{2g} \rightarrow {}^4T_{2g}$). The transition $^4A_{2g} \rightarrow {}^4T_{1g}$ occurs at 21739 cm^{-1} for $Cr(acac)_2(HDz)$, and at 23255 cm^{-1} for $Cr(acac)(HDz)_2$. These two transitions are compatible with the expected pseudooctahedral geometry around Cr(III). A band located at 37037 and 38461 cm^{-1} for $Cr(acac)_2(HDz)$ and $Cr(acac)(HDz)_2$, respectively, seems to correlate with a π-π^* transition of acac[14]. The $Cr(acac)_2(HDz)$ complex exhibits, in addition, a CT band at 30303 cm^{-1}, usually found in acetylacetonate complexes[14].

The two iron(III) complexes, $Fe(acac)_2(HDz)$ and $Fe(acac)(HDz)_2$, display a broad structured dithizonate band at ~ 19000 cm^{-1}, which obscures the *d-d* bands. In addition, the two iron complexes show a band of high intensity at 37735-38461 cm^{-1} (π-π^* on $acac^-$)[14].

The spectra of the Co(III) complexes show the transition $^1A_{1g} \rightarrow {}^1T_{2g}$, typical of octahedral Co(III) complexes. It appears at 22222 and 23809 cm^{-1} for $Co(acac)_2(HDz)$ and $Co(acac)(HDz)_2$, respectively. The two complexes show bands of medium intensity in the regions 32258-33333 cm^{-1} and 38461-41666 cm^{-1}, which are presumably due to intraligand transition of $acac^-$ and HDz^-, respectively.

For the Co(ox)(HDz) complex, the dithizonate band at 18867 cm^{-1} obscures the *d-d* bands of Co(II). The two bands at 23255 and 38461 cm^{-1} are assigned to CT and intraligand transitions, respectively.

The band at 14925 cm^{-1} in the Ni(ox)(HDz) complex is ascribed to the transition $^3T_1(F) \rightarrow {}^3T_1(P)(\nu_3)$ which is indicative of a tetrahedral coordination around Ni(II). The two bands at 29411 and 35713 cm^{-1} are correlated with CT and intraligand transitions.

Photochemistry

The spectral changes associated with photolysis of the complexes in chloroform solution at 300 nm show that the most prominent features in the absorption spectra decrease in intensity. By analogy with other photooxidations in halocarbon solvents, where solvent molecules act as electron acceptors[15-18], it is presumed that the complex becomes cationic; and chloride, abstracted from the solvent, acts as the counter anion. Such cations formed in the primary step by charge transfer to solvent (CTTS) are unstable and undergo further decomposition[16,18]. Vogler *et al.*[19] assumed a similar mechanism for the photooxidation of 1,2-dithiolene complexes of Ni(II), Pd(II) and Pt(II) in chloroform.

Irradiation of chloroform solutions of the present complexes at 365 nm gives rise to similar results, but the rate of conversion is low in comparison to that for irradiation at 300 nm. This behaviour seems to be characteristic of the reactivity of CTTS excited states.

Thermal analysis

TGA analyses (heating rate 7°C/min) of the following complexes were carried out in the temperature range 100-400°C: VO(acac)(HDz), $Cr(acac)_2(HDz)$, $Fe(acac)_2(HDz)$, $Co(acac)_2(HDz)$, and Co(ox)(HDz). The thermograms consisted of three decomposition steps. For the complexes VO(acac)(HDz), and Co(ox)(HDz) it was difficult to correlate the individual steps with decomposition products of reasonable constitution. However, the first mass losses of the complexes $Cr(acac)_2(HDz)$ (190°C), $Fe(acac)_2(HDz)$ (140°C) and $Co(acac)_2(HDz)$ (170°C) were found to be commensurate with the elimination of one acetylacetone molecule and an azo group (N_2) (from the dithizonate moiety).

It is suggested that the mechanism of decomposi-

tion involves the initial loss of a proton from dithizonate to one of the two acetylacetones, which leaves as a neutral acetylacetone molecule; the primary dithizonate is thus transformed into a secondary dithizonate[20]. Assuming elimination of the azo group, a 4-coordinate complex can be visualised at this stage.

References

1 Rosinkin A, *Photometric analysis* (Mir Publishers, Moscow) 1971.

2 Irving H & Cox J J, *J chem Soc*, (1961) 1470.

3 (a) Math K S & Freiser H, *Anal Chem*, 41 (1969) 1682. (b) Perpinan M F, Ballester L, Santos A, Monge A, Ruizvolero C & Puebla E G, *Polyhedron*, 6 (1987) 1523. (c) Aly A A M, Kamal M M, El-Meligy M S & El-Said A I, *Z Naturforsch*, 42b (1987) 1447.

4 Misra M K & Ramanrao D V, *J Indian chem Soc*, 50 (1973) 460.

5 Tembe G L, Kokatnur S B & Murty Q S R, *Proc Indian Acad Sci*, 97 (1986) 19.

6 Murty R N, Dash R N & Ramana D V, *J Indian chem Soc*, LXI (1948) 943.

7 Aly A A M, El-Meligy M S & Zidan A S A, *Trans Met Chem*, 14 (1989) 366.

8 Aly A A M & El-Said A I, *Z Naturforsch*, 44b (1989) 323.

9 Fernelius W C & Bryant B E, *Inorg Synth*, 5 (1957) 105.

10 Vogel A I, *Quantitative inorganic analysis*, 2nd edition, (Longmans, Green and Co., New York) 1955.

11 Behnke G T & Nokamoto K, *Inorg Chem*, 6 (1967) 443.

12 Slbin J, *Chem Rev*, 65 (1976) 153.

13 Fabretti A C & Peyronel G, *J inorg nucl Chem*, 37 (1975) 37.

14 Adamson A W & Fleischauer P D, *Concepts of inorganic photochemistry* (Wiley, New York) 1975.

15 Vogler A & Kunkely H, *Angew Chem Int Edn (Engl)*, 19 (1980) 221.

16 Vogler A & Kunkely H, *J Am chem Soc*, 103 (1981) 1559.

17 Bock C R & Wrighton M S, *Inorg Chem*, 76 (1977) 1309.

18 Vogler A & Kunkely H, *Angew Chem Int Edn (Engl)*, 20 (1981) 386.

19 Vogler A & Kunkely H, *Inorg Chem*, 21 (1982) 1172.

20 Kemula W & Gauko T, *J chem Soc Chem Commun*, (1971) 1063.

Indian Journal of Chemistry
Vol. 30A, April 1991, pp. 382-384

Some lanthanide (III) nitrate complexes of N-(4′-benzoylidene-3′-methyl-1′-phenyl-pyrazol-5′-one)isonicotinylhydrazine

P Indrasenan* & K R Sarojini

Department of Chemistry, University of Kerala
Trivandrum 695 034, India

Received 23 April 1990; revised and accepted 1 October 1990

Nine new complexes of lanthanide (III) nitrates with N-(4′-benzoylidene-3′-methyl-1′- phenylpyrazol-5′-one) isonicotinylhydrazine (BMPIH) have been synthesised. All these complexes have the general formula $[Ln(BMPIH)_2(NO_3)_3]$ where Ln = La, Pr, Nd, Sm, Eu, Gd, Tb, Dy and Y. In these complexes BMPIH acts as a neutral bidentate ligand utilizing the azomethine nitrogen and the ring carbonyl oxygen as the donor atoms. The nitrate groups coordinate in a unidentate fashion and, hence, a coordination number of 7 is assigned to the central metal ion.

Lanthanide (III) ions form two types of complexes with 4-benzoyl-3-methyl-1-phenylpyrazol-5-one (BMPP)[1,2] under different experimental conditions. In the first type BMPP acts as a univalent bidentate ligand[1] and in the other type it acts as a neutral bidentate ligand [2]. In view of the dependence of the bonding behaviours of BMPP on the experimental conditions, it was thought of interest to study the coordination behaviour of a schiff base derived from BMPP. We report here the synthesis and characterisation of nine lanthanide (III) nitrate complexes of the schiff base derived from BMPP and issonicotinylhydrazine, viz., N-(4′-benzoylidene-3′-methyl-1′-phenylpyrazol- 5′-one)-isonicotinylhydrazine (BMPIH) (structure I).

Experimental

Nitrates of La(III), Pr(III), Nd(III), Sm(III), Eu(III), Gd(III), Tb(III), Dy(III) and Y(III) were prepared from their respective oxides (99.9% pure) as reported earlier[3]. BMPP was prepared by benzoylating 3-methyl-1-phenyl-pyrazol-5-one (MPP) by the Jensen method[2,4]. The schiff base, BMPIH, was prepared by condensing equimolar amounts of BMPP (27.8 g) and isonicotinylhydrazine (13.7 g) in ethanol (200 ml each) on a water bath for about 4h. Then the reaction mixture was concentrated to 100 ml, from which on cooling BMPIH crystallized out as red crystals. These crystals were filtered, washed with the minimum quantity of cold ethanol (10 ml) and recrystallized from hot ethanol. The purity of the sample was checked by elemental analysis, IR spectrum, and melting point (230°C).

All the nine complexes were prepared by the following general procedure. Solutions of lanthanide (III) nitrate (0.5 g in 25 ml C_2H_5OH) and BMPIH (1.0 g in 75 ml C_2H_5OH) were mixed together and the resulting solution was kept under reflux on a water bath for 4h. Then the reaction mixture was concentrated when a viscous mass was obtained. It was washed repeatedly with hot benzene (10 ml each) to remove excess ligand. The solid complex was dissolved in hot ethanol (25 ml and the clear solution was stirred after adding diethyl ether (75 ml) when the complex precipitated. The complexes so separated were collected and dried *in vacuo* over phosphorus (V) oxide (yield = ~92%).

Molar conductivities of the complexes at room temperature (28±2°C) were measured in acetonitrile, methanol and nitrobenzene (~10^{-3} *M* solutions) using an Elico conductivity bridge type M82T equipped with a dip type cell having platinum electrodes (cell constant of 1.64 cm^{-1}). Magnetic susceptibilities of the complexes were determined at room temperature by the Gouy method[5]. Electronic spectra of the ligand (BMPIH) and the lanthanide complexes in methanol (~10^{-4} *M* solutions) were recorded on a Hitachi 220A double beam uv-visible spectrophotometer in the range 185-900 nm. The IR spectra of the ligand and the complexes were recorded in KBr using a Perkin-Elmer 397 IR

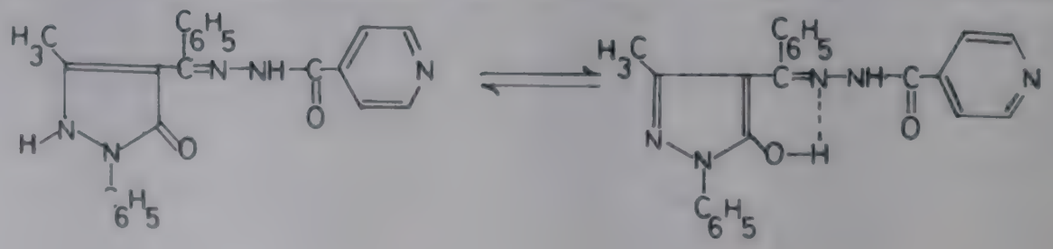

keto form (I) enol form

spectrophotometer. The lanthanide contents of the complexes were determined by the oxalate-oxide method[6] and the nitrate contents by the nitron method[7]. The carbon, hydrogen and nitrogen analyses of the ligand and the complexes were carried out at the Regional Sophisticated Instrumentation Center, CDRI, Lucknow. Molecular weights of the complexes were determined by the Rast method using biphenyl as the solvent[8].

Results and discussion

All the complexes are non-hygroscopic solids, which are moderately soluble in acetonitrile, ethanol, methanol and nitrobenzene, and insoluble in benzene, carbon tetrachloride, chloroform, diethyl ether, and petroleum ether. From the elemental analysis, molecular weight and molar conductance data (Table 1), all the complexes can be formulated as $[Ln(BMPIH)_2(NO_3)_3]$, where Ln = La, Pr, Nd, Sm, Eu, Gd, Tb, Dy and Y. Molar conductivity values of the complexes in acetonitrile (52-82 $ohm^{-1}cm^2mol^{-1}$) and in methanol (172-219 $ohm^{-1}cm^2mol^{-1}$) indicate considerable solvolysis. However, values in nitrobenzene (1.3-1.9 $ohm^{-1}cm^2mol^{-1}$) indicate non-electrolytic behaviour. Therefore, molar conductivity data suggest that the nitrate ions are within the coordination sphere in these complexes. The room temperature magnetic moments of the complexes are in agreement with the theoretical values calculated by the Van Vleck formula[10]. Thus, the La and Y complexes are diamagnetic, whereas all the other complexes are paramagnetic in nature.

The electronic spectrum of the ligand exhibits two bands in the UV region at 40.0 and 47.6 kK. These two bands are present in the spectrum of the complexes also, which are assigned to $n \rightarrow \pi^*$ and $\pi \rightarrow \pi^*$ transitions, respectively. There is no absorption in the visible region for the ligand and the complexes. However, the spectra of the complexes show an additional broad band at 27.7 kK in the UV region. This broad band is attributed to strong L→M charge-transfer transitions.

The IR spectrum of the ligand (BMPIH) exhibits a medium band at 3300 cm^{-1}, which is assigned to νNH mode. This band is present in the spectra of the complexes also in the same region suggesting that both the imino nitrogen atoms do not participate in coordination. The spectrum of the ligand also exhibits broad band at 2560 cm^{-1} and a strong sharp band at 1630 cm^{-1}. The broad band is attributed to νOH mode of the enol form of the ligand, in which the OH group is strongly hydrogen bonded as shown in (I). The sharp band at 1630 cm^{-1} is assigned to νC=O of the ring carbonyl group present in the keto form. Therefore, BMPIH exhibits keto-enol tautomerism

Table 1—Analytical and molecular weight data of lanthanide (III) nitrate complexes with BMPIH

Complex (colour)	Found (Calc.)					
	Metal (%)	Carbon (%)	Hydrogen (%)	Nitrogen (%)	Nitrate (%)	Molecular wt.
$[La(BMPIH)_2(NO_3)_3]$ (Orange)	12.37 (12.40)	49.10 (49.28)	3.28 (3.39)	16.18 (16.25)	17.10 (16.62)	1066 (1120)
$[Pr(BMPIH)_2(NO_3)_3]$ (Orange)	12.50 (12.60)	49.32 (49.24)	3.42 (3.39)	16.28 (16.24)	16.60 (16.59)	1036 (1121)
$[Nd(BMPIH)_2(NO_3)_3]$ (Orange)	12.60 (12.80)	49.02 (49.11)	3.36 (3.38)	16.18 (16.20)	16.32 (16.54)	1183 (1124)
$[Sm(BMPIH)_2(NO_3)_3]$ (Orange)	13.20 (13.30)	48.68 (48.85)	3.34 (3.36)	16.20 (16.10)	16.54 (16.45)	1119 (1130)
$[Eu(BMPIH)_2(NO_3)_3]$ (Orange)	13.49 (13.42)	48.50 (48.76)	3.28 (3.35)	16.14 (16.08)	16.48 (16.43)	1120 (1132)
$[Gd(BMPIH)_2(NO_3)_3]$ (Orange-Yellow)	13.74 (13.82)	48.66 (48.55)	3.40 (3.34)	15.96 (16.00)	16.58 (16.35)	1197 (1137)
$[Tb(BMPIH)_2(NO_3)_3]$ (Yellow)	13.94 (13.95)	48.54 (48.46)	3.28 (3.33)	16.02 (15.97)	16.50 (16.33)	1198 (1139)
$[Dy(BMPIH)_2(NO_3)_3]$ (Yellow)	14.19 (14.22)	48.32 (48.29)	3.29 (3.32)	15.84 (15.92)	16.36 (16.28)	1165 (1143)
$[Y(BMPIH)_2(NO_3)_3]$ (Yellow)	8.34 (8.32)	51.45 (51.64)	3.62 (3.55)	16.98 (17.03)	17.54 (17.40)	1009 (1069)

when it is free. However, in the spectra of the complexes the broad band corresponding to νOH disappears and the band corresponding to νC=O of the ring carbonyl is shifted to 1610 cm^{-1}. These changes indicate that the ligand exists exclusively in the keto form in the complexes bonding through the ring carbonyl oxygen.

A strong sharp band observed at 1680 cm^{-1} in the spectra of the ligand and complexes is attributed to νC=O of the side chain carbonyl group attached to the hydrazine part. Since there is no change in the frequency of νC=O (side chain) on complexation it is suggested that this carbonyl group does not take part in coordination in the present series of complexes. The IR spectrum of BMPIH exhibits two strong bands at 1600 and 1580 cm^{-1}, which are assigned to νC=C and νC=N, respectively. The pyridine ring stretching vibrations appear at 1550 and 1470 cm^{-1} and the out-of-plane bending of CH of the pyridine ring at 830 cm^{-1} in the spectrum of the ligand. In the spectra of the complexes the band due to band due to νC=C and the two bands at 1470 and 830 cm^{-1} due to the pyridine ring remain unaltered, whereas the νC=N mode is shifted to 1560 cm^{-1}. The band at 1550 cm^{-1} of the ligand is shifted to 1540 cm^{-1}. The shift of νC=N mode indicates that the azomethine nitrogen takes part in complex formation. Since the positions of the bands due to the pyridine ring do not change appreciably in the spectra of the complexes, it is suggested that the pyridine nitrogen does not take part in coordination and hence BMPIH acts as a neutral bidentate ligand coordinating through the ring carbonyl oxygen and azomethine nitrogen.

In the spectra of the complexes five new bands appear at 1430, 1320, 1020, 540 and 480 cm^{-1}. The first three bands are assigned to ν_4, ν_1 and ν_2 modes respectively, of the coordinated nitrate ion. Since the separation between ν_4 and ν_1 is of the order of ~ 110 cm^{-1}, the nitrate ions are suggested to be coordinated unidentately in these complexes[11]. The bands at 540 and 480 cm^{-1} are attributed to νM − N and νM − O, respectively[12], nitrogen having a smaller mass than oxygen.

From the foregoing discussion it is concluded that BMPIH acts as a neutral bidentate ligand coordinating through the ring carbonyl oxygen and the azomethine nitrogen. In these complexes the nitrate ions are coordinated unidentately and hence, a coordination number of 7 is assigned to the lanthanide ions.

Acknowledgement

The authors express their sincere thanks to the UGC, New Delhi for awarding a teacher-fellowship to one of them (KRS) under the FIP scheme.

References

1 Okafor E C, *J inorg nucl Chem*, 42 (1980) 1155.
2 Kunchandy Sam & Indrasenan P, *Polyhedron*, 9 (1990) 795.
3 Jayasankar H & Indrasenan P, *J less-comm Met*, 132 (1987) 43.
4 Jenson B S, *Acta chem scand*, 13 (1959) 1668.
5 Lewis J & Wilkins R G, *Modern coordination chemistry* (Interscience, New York) 1960, p 409.
6 Kolthoff I M & Elving P S, *Treatise on analytical chemistry*, Vol 8, Part 2 (Interscience, New York) 1963, p 34 & 51.
7 Vogel A I, *A text-book of quantitative inorganic analysis*, 4th Edn (Longmans, London), 1978, p 131.
8 Palmer W G, *Experimental physical chemistry* (Cambridge University Press, Cambridge) 1954, p 119.
9 Geary W J, *Coord Chem Rev*, 7 (1971) 81.
10 Van Vleck J H & Frank N, *Phys Rev*, 34 (1929) 1494.
11 Curtis N F & Curtis Y M, *Inorg Chem*, 4 (1964) 804.
12 Karayannis N M, Mikulski C M, Strako M J, Pytlewoki L L & Labes M M, *J inorg nucl Chem*, 32 (1970) 2629.

Indian Journal of Chemistry
Vol. 30A, April 1991, pp. 385-386

Formation constants of binary and ternary complexes of Cu(II) with ninhydrin and some O, O; N, O and N, N donor ligands in aqueous medium

Ch Venkata Ramana Reddy, Ch Sarala Devi &
M G Ram Reddy*

Department of Chemistry, Osmania University,
Hyderabad 500 007

Received 23 July 1990; revised 19 September 1990; accepted 28 November 1990

The formation constants of 1:1 and 1:2 binary chelates of Cu(II) with ninhydrin (1,2,3-triketohydrindene hydrate or 2,2-dihydroxy-1,3-indanedione) and the corresponding 1:1:1 ternary chelates involving oxalic acid, catechol, α-alanine, valine, ethylenediamine and 2,2-bipyridyl as primary ligands have been determined *p*H metrically at 20°, 30°, 40° and 50°C at 0.1 *M* (KNO_3) ionic strength. The effect of change in ionic strength has also been studied at 30°C. The order of stabilities of ternary complexes has been discussed in terms of Δlog *K*, basicity of the ligands, nature of donor sites and thermodynamic parameters.

The synthesis, characterisation and biological activities of Co(II), Ni(II) and Zn(II) complexes of schiff base of ninhydrin and glycine have been reported earlier[1]. The present work was undertaken to study the nature of Cu(II) complexes formed in solution by ninhydrin (nin) in the presence of other donors like alanine (ala), valine (val), oxalic acid (oxa), catechol (cat), ethylenediamine (en) and 2,2-bipyridyl (bipy) under different conditions.

Experimental

All the chemicals used were of AR grade. The following sets of solutions (volume 50 ml) were prepared in doubly distilled water and titrated potentiometrically against 0.1 *M* carbonate free standard KOH under N_2 atmosphere.
1. HNO_3 (4×10^{-3} *M*); 2. HNO_3 (4×10^{-3} *M*) + A (primary ligand) (2×10^{-3} *M*); 3. HNO_3 (4×10^{-3} *M*) + L (secondary ligand) (2×10^{-3} *M*); 4. HNO_3 (4×10^{-3} *M*) + A (2×10^{-3} *M*) + Cu(II) (2×10^{-3} *M*); 5. HNO_3 (4×10^{-3} *M*) + L (2×10^{-3} *M*) + Cu(II) (2×10^{-3} *M*); 6. HNO_3 (4×10^{-3} *M*) + A (2×10^{-3} *M*) + L (2×10^{-3} *M*) + Cu(II) (2×10^{-3} *M*).

For the [Cu(II)-A-L] ternary system, where A = catechol, the concentrations used were [Cu(II)] = [A] = [L] = 1×10^{-3} *M* in all the sets. An ionic strength of 0.1 *M* (KNO_3) was maintained in all the sets, while studying temperature effect and a temperature of 30°C was maintained while studying the effect of ionic strength. For the binary systems, a metal-ligand ratio of 1:5 was maintained.

The proton-ligand dissociation constant (pK_a) of ninhydrin (secondary ligand) and the formation constants of metal-ninhydrin binary systems have been evaluated by analysing the titration curves using the methods of Irving and Rossotti[2]. The formation constants of ternary chelates were determined using the method of Santhappa and Ramamoorthy[3]. The results have been presented in Table 1. The thermodynamic parameters ΔH (enthalpy), ΔS (entropy) and ΔG (free energy) have been calculated using the standard equations.

Results and discussion

The $\bar{n}$ values (0.1 to 1.9) for the binary systems indicate the formation of 1:1 (Cu-L) and 1:2 (Cu-L_2) complexes. The ligand (nin) starts coordinating to Cu(II) at $\approx$ *p*H 5.6. The standard deviations for proton-ligand and metal-ligand and ternary formation constants are within $\pm$ 0.06 log units.

In all the ternary systems studied, the mixed ligand curves closely follow the 1:1 [Cu(II)-A] where A = oxa, cat, ala, val, en and bipy binary curves in the lower *p*H region until the protons of primary ligands are neutralised, indicating the formation of binary [Cu(II)-A] complexes in this region. The divergence of the ternary curves from those of the binary [Cu(II)-A] system, above this *p*H region confirms the formation of ternary complexes of the type [Cu(II)-A-L] in two step equilibria.

The proton-ligand dissociation constant (pK_a) of ninhydrin, formation constants of binary complexes (1:1 and 1:2 binary) as well as those of mixed ligand complexes (1:1:1) were found to decrease with increase in ionic strength of the medium. To find out whether the ligands coordinate in dissociated or undissociated form and also to know the mechanism of complexation equilibria, the stability constants (log *K*) obtained at different ionic strengths were plotted against $\sqrt{\mu}$. The plots gave straight line. The slope values ranging from -0.45 to -0.78 obtained in all the cases were far less than the expected values[4,5]. The shapes of the formation curves were also similar at different ionic strengths indicating similar type of interaction. From these observations, it was evident that the ninhydrin reacts with [CuA] primary complex both in dissociated and undissociated forms.

Table 1 — Stability constants and thermodynamic parameters of Cu(II) binary and ternary complexes in aqueous medium [Temp. = 30°C; $\mu = 0.1$ *M* (KNO_3)]

System	$\log K^{CuA}_{CuAL}$	$\Delta \log K$	ΔH (kJ mol^{-1})	ΔG (kJ mol^{-1})	ΔS (J mol^{-1}K^{-1})
Cu(II)-nin			16.1	32.7	54.8
Cu(II)-oxa-nin	5.01	−0.63	9.9	29.1	63.3
Cu(II)-cat-nin	5.21	−0.43	10.4	30.2	65.4
Cu(II)-en-nin	5.26	−0.38	10.6	30.5	65.8
Cu(II)-bipy-nin	5.32	−0.32	10.7	30.9	66.6
Cu(II)-ala-nin	5.24	−0.40	10.5	30.4	65.6
Cu(II)-val-nin	5.22	−0.42	10.5	30.3	65.4

$\log K^{Cu}_{CuL} = 5.64$ (1:1)
$\log K^{Cu}_{CuL_2} = 5.15$ (1:2)
pK_a of ninhydrin = 8.81
$-\Delta H$ and $-\Delta G$ are accurate within ± 0.5-1.5 kJ mol^{-1}
ΔS accurate within ± 1.5 J mol^{-1}K^{-1}.

It can be seen that the binary complexes are more stable than the ternary complexes, resulting in negative $\Delta \log K$ values for all the ternary systems. Such a lowering of stabilities in the case of ternary complexes compared to those of binary chelates may be due to the availability of lesser number of coordination sites for ninhydrin on the metal in the primary complex [CuA] as compared to the free metal ion.

The order of overall stabilities of the [CuAL] ternary systems is bipy > en > ala > val ≥ cat > oxa. This sequence of stabilities is in accordance with the basicities, nature of donor atoms and $\Delta \log K$ values of the ligands. From these studies it is observed that, though schiff base formation is established in the synthesis of metal complexes of ninhydrin and amino acids, no such condensation takes place between ninhydrin and amino acids in aqueous medium in the presence of metal ions and instead ternary complex formation takes place.

The decrease in $\log K$ values with increase in temperature and negative ΔG values shows that all the reactions are exothermic and spontaneous. The negative ΔH (enthalpy) and positive ΔS (entropy) values (Table 1) are the major driving forces for the spontaneity of binary and ternary complex formation. The higher $\log K$ value for [Cu(II)-nin] binary complex may be due to its greater ΔH value compared to that of ternary complexes. The ΔS values for the formation of [CuAL] ternary complexes are higher than those for [Cu(II)-nin] binary system. Thus the entropy factor appears to be responsible for the observed trend in $\log K^{Cu}_{CuL}$ and $\log K^{CuA}_{CuAL}$ values. This could be due to the greater destabilisation of ternary chelates caused by enthalpy changes as compared to the stabilisation induced by the entropy changes. Hence, it can be concluded that a number of factors such as $\Delta \log K$ [$\log K^{CuA}_{CuAL} - \log K^{Cu}_{CuL}$], basicity, nature of donor atoms, enthalpy, entropy etc affect the stabilities of these chelates.

References

1 Koteswara Rao N S R R M M & Ram Reddy M G, *Biology of metals* (In Press, 1990).

2 Irving H M & Rossotti H S, *J chem Soc*, (1954) 2904.

3 Ramamoorthy S & Santhappa M, *Indian J Chem*, 9 (1971) 381.

4 Robinson R A & Strokes R M, *Electrolyte solutions* (Butterworths, London) 1955, 229.

5 Harned H S & Owen B B, *The physical chemistry of electrolyte solutions*, 2nd Edn (Reinhold, New York) 1950, 547.

Indian Journal of Chemistry
Vol. 30A, April 1991, pp. 387-389

An extractive spectrophotometric method for the determination of vanadium as V(II)-8-hydroxyquinoline complex into acetylacetone-chloroform

R S Chauhan & L R Kakkar*
Department of Chemistry, Kurukshetra University, Kurukshetra 132 119

Received 28 May 1990; revised 4 September 1990; accepted 1 November 1990

A simple and rapid extractive spectrophotometric method of determination of vanadium is developed by reduction of the metal ion with Zn/Hg in presence of 8-hydroxyquinoline under acidic conditions employing acetylacetone-chloroform as extractant. No interference is shown by W(VI), Cr(VI, III), U(VI), Mo(VI), Fe(II), Co(II), Ni(II), Cu(II) and several other elements of interest. The applicability of the method is tested by analysis of a large number of different samples. The method is highly reproducible with a standard deviation of 0.0065 and Sandell's sensitivity 8.6956×10^{-2} μg V/cm^2. Stoichiometry of the complex is also studied.

Most of the photometric procedures available for microdetermination of vanadium in its different oxidation states, particularly V and IV, using various organic ligands[1-10] suffer seriously from the interference of several metal ions which, therefore, require prior separations. Though V(III) and V(II) are not stable, the former has been stabilized by complexation[11,12] with a view to develop methods for determination of vanadium in trace amounts. But there is hardly any information on the similar use of V(II). In the present work, a highly selective and sensitive analytical method has been developed based on the reaction of V(II) with 8-hydroxyquinoline using acetylacetone in chloroform as extractant.

Experimental

A stock solution of vanadium was prepared by dissolving accurately weighed amount of sodium metavanadate (Reachim) in distilled water. Working solutions containing 100 μg V/ml and 10 μg V/ml were prepared by appropriate dilutions. A solution of 8-hydroxyquinoline (E. Merck), 0.5% (w/v), was prepared in ethanol; acetylacetone (SRL, AR) and chloroform (GR) of high purity were used. Zinc amalgam (2%, w/w) was prepared[13] from zinc metal (AR) and pure mercury (AR). Solutions of other ions were prepared in water or dilute acids. Synthetic samples were prepared by mixing vanadium with other metal ions in suitable amounts as shown in Table 1. High speed steel Super Rapid Extra 500 was brought into solution by aqua regia[14]. Reverberatory flue dust samples from copper manufacture, containing no vanadium, were mixed with a solution of known vanadium content and dried in an oven. After fusion of the flue dust with sodium peroxide (8 times the weight of sample), the leach was neutralized with conc. sulphuric acid and made slightly alkaline. It was boiled, the hydroxide precipitate was filtered and washed well with distilled water. The *p*H of the filtrate was adjusted to 7 and vanadium determined as described below in the procedure.

Procedure

To a sample solution containing 400 μg of vanadium in a 125 ml separatory funnel were added 3 ml of 5 *M* sulphuric acid, 2 ml (0.5%) of

Table 1—Analysis of different samples by the proposed method

Sl No.	Composition of sample		V, found (μg)
	Matrix*	V, added (μg)	
1	W(0.5)	40	39.5, 40.0
2	U(0.2)	80	78.5
3	W(0.2) U(0.5)	300	298.5, 299.0
4	W(0.5) Cr(0.5)	250	249.0
5	W(0.5) U(0.2), Cr(0.2)	200	198.0
6	Ni(0.5) Cu(0.5) Co(0.5)	450	448.0
7	Ni(2), Cu(2) Co(2) Fe(1)†	400	400.5
8	Mn(1) Al(2) Ce(1)	500	498.0
9	Zn(0.5) Zr(0.5) Cd(0.5) Ti(0.5) Re(0.2)	450	447.5
10	[Ni(0.6) Pt(0.2) Pd(0.2)]†	100	98.0
11	[Al(20) Zn(3.5) Cu(1.25) Fe(0.175)]†	50	48.5
12	[Fe(2.5) Ni(1.15) Cr(1) Mn(0.05)]†	50	52.0
13	Reverberatory flue dust (200)	100	96.0
	Reverberatory flue dust (250)	150	147.0
14	High speed steel super Rapid extra 500	1.0%‡	0.95%, 0.97%

*Numbers in brackets indicate mg of element/sample in aliquot.
†In presence of EDTA (Sample Nos 10-12, correspond to palau, V-alloy and nichroloy, respectively).
‡Reported value (Fe was removed first as hydroxide).

8-hydroxyquinoline solution, and enough distilled water to make the volume 10 ml. It was shaken gently with 0.5 ml of 2% zinc amalgam for 35-45 sec. To minimize the contact with the air, the aqueous layer was immediately covered with 10 ml of 1:4 acac:$CHCl_3$ and the amalgam was then drained off. The contents were equilibrated for 3 min to transfer the brownish red metal complex to the organic layer, while taking care to release the pressure occasionally through the stop cock. The coloured solvent was filtered into a 10 ml volumetric flask using Whatman filter paper No. 41. The volume was finally made upto the mark with the pure solvent. The absorbance of the complex was measured at 455 nm against a similarly treated reagent blank on a UV-visible spectrophotometer (Shimadzu UV-140-02) and the amount of vanadium present was determined from a standard curve drawn earlier by plotting absorbance values against varying vanadium concentrations in the range 5-100 μg V/ml.

Results and discussion

V(II) obtained on reduction of V(V) with zinc-amalgam in 1-2 *M* H_2SO_4/HCl formed a brownish red species with 8-hydroxyquinoline which could be quantitatively extracted into 1:4 acetylacetone: chloroform. The V(II) complex exhibited an absorption maximum at 455 nm, where the absorbance of the reagent blank was negligibly small and hence all the absorbance measurements were carried out at 455 nm. Beer's law was found to hold good in the range 5-100 μg V/ml and the molar absorptivity, specific absorptivity and Sandell's sensitivity were 585.8156 $l\,mol^{-1}\,cm^{-1}$, 0.0015 $mol\,g^{-1}\,cm^{-1}$ and 8.6956×10^{-2} μg V/cm^2, respectively.

The complex was though not extractable into several organic solvents, namely, isoamyl alcohol, *n*-butyl alcohol, amyl acetate, isobutyl methyl ketone, ethyl methyl ketone, tribenzylamine-chloroform, benzene, carbon tetrachloride, etc., but it was found to be extractable with acetylacetone in chloroform. The absorbance remained unaffected when 1:1, 1:2 or 1:4 acetylacetone:chloroform mixtures were used as extractant. For the sake of economy, 1:4 acetylacetone:chloroform mixture was preferred.

The effect of various parameters like reduction time, acid concentration, equilibration time, etc., on the absorbance of the V(II) complex was studied. It was found that for 400 μg V, the optimum conditions are: 1-2 *M* H_2SO_4, 1-2.5 ml (0.5%) oxine reagent, reduction with 0.5-1.5 ml 2% Zn/Hg for 35-45 sec in 10 ml aqueous volume and extraction with an equal volume of 1:4 acetylacetone:chloroform mixture for 3 min.

Acetylacetone in combination with V(II)-8-hydroxyquinoline forms a neutral extractable species which in absence of the former, is not extractable into pure chloroform. The ratio of vanadium, 8-hydroxyquinoline and acetylacetone in the extracted species was found to be 1:2:4 by Job's method of continuous variations[15] as modified by Vosburgh and Cooper[16] by using equimolar solutions in each set (namely 7.83×10^{-3} *M*, 3.92×10^{-3} *M*). The stoichiometry was further confirmed by the mole ratio method[17].

Under the chosen conditions, W(VI), U(VI), Cr(VI, III), Zr(IV), Ce(IV), Al(III), Bi(III), Sb(III), Fe(II), Co(II), Ni(II), Cu(II), Zn(II), Pb(II), Cd(II), Mn(II), Mg(II), Ba(II), Hg(II), Ca(II), Be(II) (2 mg/ml); Ag(I) (1 mg/ml); Se(IV), Ti(IV) (0.5 mg/ml); and Rh(III), Ru(III), Re(VII) (0.05 mg/ml) did not interfere (higher amounts were not tested). Fe(III) (0.25 mg/ml); Pd(II) (0.05 mg/ml) (in presence of EDTA) had no effect.

Chloride (150), nitrate (200), sulphate (300), phosphate (150), acetate (500), fluoride (200), EDTA (150), citrate (50), tartrate (100) and oxalate (50) also did not affect the determination. The figures shown in parentheses indicate the mg amount of sodium salt of the anion.

Application

The proposed method for the spectrophotometric determination of vanadium makes use of complexation of V(II) with oxine, for the first time. It is free from the interference of a large number of elements of great analytical importance which seriously affect the various methods of determination of vanadium. The complex is stable for about 35 min and the results obtained are reproducible with a standard deviation of 0.0065. The validity of the method was further tested by its application to the analysis of a variety of samples including reverberatory flue dust and high speed steel. The results obtained are in good agreement with the amount of vanadium initially added to the sample (Table 1). The method is highly selective and sensitive and compares favourably with the existing methods often used for the determination of vanadium.

Acknowledgement

Our sincere thanks are due to the CSIR, New Delhi for financial support and the Chairman, Department of Chemistry, Kurukshetra University, Kurukshetra, for providing laboratory facilities.

References

1 Capitan-Vallvey L F, Molina-Diaz A & Pascual-Reguera M I, *Analusis*, 17 (1989) 280.

2 Jimin Yu, Guanghui Wu, Xiangxi Fan & Huamin Hou, *Fenxi Huaxue*, 16 (1988) 1030.
3 Singh R & Mishra R K, *J Indian chem Soc*, 65 (1988) 816.
4 Marcazenko Z & Lobinski R, *Talanta*, 35 (1988) 1001.
5 Gowda H S & Rekha G K, *Indian J Chem*, 26A (1987) 984.
6 Lorenzo Ferreira, Rosa A, Casais Laino, Maria del Carcon & Bermejo Martinez F, *Rev Port Quim*, 27 (1985) 511.
7 Verdizade N A & Ragimova Z B, *Azerb Khim Zh*, 3 (1985) 109.
8 Gordeeva M N & Antonova M S, *Vestn Leningr Univ, Fiz Khim*, 3 (1981) 53.
9 Valero Jose, *An Quim, Ser B*, 81 (1985) 372.
10 Shaoqing Li, Toing-zhang Guo & Wengging Hu, *Fenxi Huaxue*, 14 (1986) 129.
11 Arya S P & Yatirajam V, *Acta Cienc Indica Chem*, 12 (1986) 67.
12 Yatirajam V & Arya S P, *Anal Chim Acta*, 86 (1976) 209.
13 Palmer W G, *Experimental inorganic chemistry* (Cambridge University Press, London), 1959, 419.
14 Charlot G & Bezier D, *Quantitative inorganic analysis* (Methuen, London), 1957, 305.
15 Job P, *Ann Chim*, 9 (1928) 113.
16 Vosburgh W C & Cooper G R, *J Am chem Soc*, 63 (1941) 437.
17 Yoe J H & Jones A L, *Ind Engng Chem, Anal Ed*, 16 (1944) 111.

Indian Journal of Chemistry
Vol. 30A, April 1991, p. 390

Comments on the paper "Synthesis and characterisation of model compounds: Part II—Complexes of iron(II), iron(III), cobalt(II), cobalt(III), nickel(II) and copper(II) with *o*-vanillin oxime"

Sir,

Our attention was drawn to a recent paper published in your journal by K. Hussain Reddy, *Indian J Chem*, **29A** (1990) 497. In this paper Reddy[1] has synthesised and characterised iron(II), iron(III), cobalt(II), cobalt(III), nickel(II) and copper(II) complexes of *o*-vanillin oxime. However, Reddy has erroneously taken *o*-vanillin oxime to be 3-hydroxysalicylaldoxime instead of 3-methoxysalicylaldoxime. Thus, the assigned structures of the schiff base as well as of the metal complexes are not correct. Reddy's analytical data (C, H and Cl%) do not fit our calculated values (see Table 1) for the complexes considering 3-methoxysalicylaldoxime and, hence, his analytical data are in error. Even the calculated N% (for all the complexes) and H Ni(II) and Cu(II) complexes) values repor Reddy considering 3-hydroxysalicylaldoxim incorrect. His analytical data (N% and H%) complexes do not even fit the calculated valu sidering 3-hydroxysalicylaldoxime.

Table 1—Calculated analytical data of *o*-vanillin oxime complexes

Complex/Stoichiometry	Calc.[a]%			
	C	H	N	Cl
$[FeL_2(H_2O)_2]$ $FeC_{16}O_8N_2H_{20}$	45.30	4.72	6.61	
$[FeL_2(H_2O)_2]Cl$ $FeC_{16}O_8N_2H_{20}Cl$	41.80	4.35	6.10	7.72
$[CoL_2(H_2O)_2]$ $CoC_{16}O_8N_2H_{20}$	44.97	4.68	6.56	
$[CoL_2(H_2O)_2]Cl$ $CoC_{16}O_8N_2H_{20}Cl$	41.52	4.32	6.05	7.68
$[NiL_2]$ $NiC_{16}O_6H_{16}N_2$	49.14	4.09	7.17	
$[Cu_2L_4]$ $CuC_{16}O_6H_{16}N_2$	48.54	4.04	7.08	

[a]Calculated using the following atomic weight values: Fe = 55.85, Co = 58.93, Ni = 58.69, Cu = 63.54, C = 12.00, H = 1.00 and N = 14.00.

Reddy has indicated that "the bands due phenolic OH and NOH groups are also obs these complexes". But the complexes in re *not have* any free phenolic OH group.

Further, Reddy has assigned the ν(and $\nu(M-O)$ in the following $\nu(M-N) > \nu(M-O)$ [viz. $\nu(Fe-N)$, ~ 545 $\nu(Fe-O)$, 400 cm^{-1}; $\nu(Co-N)$, 540(570) $\nu(Co-O)$, 370 cm^{-1}; $\nu(Ni-N)$, 545 $\nu(Ni-O)$, 380 cm^{-1}; $\nu(Cu-N)$, 540(570) $\nu(Cu-O)$, 385 cm^{-1}] without indicating th are non-ligand bands. The $\nu(M-O)$ band i broad and strong while the $\nu(M-N)$ is usual and strong as a larger dipole moment char volved in the vibration of the M−O bond parison with that in the M−N bond, and is expected to occur at higher ener $\nu(M-N)$[2,3]. Although some authors stil $\nu(M-O) < \nu(M-N)$, which is erroneous; generally believed that $\nu(M-O)$ should higher energy than $\nu(M-N)$ as per the exp Thus, the $\nu(M-N)$ and $\nu(M-O)$ assign Reddy should be reversed. The assignmen bands each at 540 and 570 cm^{-1} to ν(Cu $\nu(Co-N)$ by Reddy[1] are also erroneous as not expect two such bands since the electr ronment of the M−N bonds in the compl same.

28 September 1990

A. Syar

Department of Ch
Regional Engineeri
Kurukshetra 13211

References

1 Hussain Reddy K, *Indian J Chem*, 29A (1990) 4
2 Ferraro J R, *Low-frequency vibrations of inorg nation compounds* (Plenum Press, New York),
3 Syamal A & Maurya M R, *Indian J Chem*, 24 and references therein.

ABLE

वैज्ञानिक तथा औद्योगिक अनुसंधान परिषद
SCIENTIFIC & RESEARCH LIBRARY
Accession No ...
- 4 APR 1991
सी.एफ.टी.आर.आई. क्षेत्रीय केन्द्र
C. F. T. R. I. REGIONAL CENTRE, LUDHIANA

BIRDS

Indian subcontinent is home to a takingly vast range of Bird species besides ost to a large number of migratory birds. n the hot, dry open plains in the west and pical rainforests of the east, between the ad alpine peaks of the Himalayas in the ınd the ocean washed Land's end in the ıre to be found bird species which are ly different from one another. Each ıas its own species which may or may not ıd in other regions. Of the World's ed total of 8600 species of Birds, India has 1200 species, apart from seasonal visitors. ›ird species range from the largest sized rane and the Himalayan Bearded Vulture nallest thumb-sized flower-pecker, from ›urful pheasants to the dull coloured ›arrows; from the sweet-voiced golden ıd koel to the raucous house crows and s, from the rarest Mountain Quail to the . myna and sparrow.

described as "feathered bipeds", the ce of birds in literature, art, sport, cation, religion as well as an article of ıot be over-emphasized.

Such a vast wealth of avifauna has naturally given rise to a large number of publications dealing with different aspects of India's Birds such as distribution, taxonomy and classification. However, a single compilation highlighting all their economically important aspects is perhaps non-existent.

The present publication lays emphasis on the economic aspects of Indian Birds. The volume covers all aspects of the life of Birds and their interaction with man. The different chapters deal with game, song and plumage birds, birds as pets and for game, role of birds in agriculture, horticulture, forestry and medicine, bird migration, aviation hazards due to birds, management of birds, their control as also conservation. The classification of birds, their inter-relationships and their description are given in great detail. The different indexes—Latin, English and Vernacular names—should be of help to users of the volume.

The volume is well illustrated with colour plates and priced moderately so as to be within the reach of students as well as others.

ISBN. 81-85038-90-2
PP 157 + xii; Price: Rs 125.00; $ 45.00; £ 30.00

o order copy please send Rs 125.00 (+ Rs 10.00 as postage charges) by Demand raft or cheque drawn in favour of Publications & Information Directorate, New elhi-110 012 (INDIA) to:-

Senior Sales & Distribution Officer
Publications & Information Directorate (CSIR)
Hillside Road, NEW DELHI-110012 (INDIA)

NOW AVAILABLE

PLANTS FOR RECLAMATION OF WASTELANDS

Approximately one-half of the arable land in the tropics is unproductive, of which about 175-million ha lie in India. Phased and scientific reclamation of these lands may not only improve the soil but meet the requirement of food, fodder, fuel, timber, etc. of the country.

Plants for Reclamation of Wastelands, a contribution from the Publications & Information Directorate to the National Mission on Wastelands Development, describes briefly various types of wastelands in India, their characteristics, causes for degradation of land, importance of topsoil and green cover and the role of grasses, herbs, shrubs, trees, and nitrogen-fixing and energy-plants. A small account on the development of mined wastelands is also given.

Major portion of the book is devoted to approximately 1000 selected economic plants, mostly indigenous or naturalized, suitable for reclamation of various wastelands, and which provide timber, fuel, fodder and other vegetable products.

Emphasis is laid on the correct scientific names, vernacular names, morphology, distribution, ecology and cultivation of the plants dealt with classifed lists of these plants suitable for various wastelands are appended for easy reference.

The book is well illustrated with coloured plates, halftones and line-drawings. An in dispensable guide and source-book for ecologists, environmentalists, researchers, foresters, and to those concerned with the development of wastelands.

ISBN 81-85038-89-9

Price: Rs.325.00; $110.00; £65.00

Order for the book should be accompanied by a Cheque or a Demand Draft made payable to Publications & Information Directorate and sent to

Senior Sales and Distribution Officer

PUBLICATIONS & INFORMATION DIRECTORATE

Dr. K.S. Krishnan Marg

New Delhi-110012

Printed & Published by Dr. G. P. Phondke, Director, Publications & Information Directorate (PID)
Hillside Road, New Delhi 110 012, at PID Photocomposition Unit

D(W) 103

RN 7090/63